

Design of Heavy-duty Pavements Incorporating a Granular Interlayer

by

Imtiaz Ahmed

(B.Sc. Civil Engg., M.Sc. Civil Engg.)

Department of Civil Engineering

Thesis submitted to the University of Nottingham for the degree of Doctor of Philosophy

May 2020

Design of Heavy-duty Pavements Incorporating a Granular Interlayer

by

Imtiaz Ahmed

(B.Sc. Civil Engg., M.Sc. Civil Engg.)

Supervised By

Dr. Nick Thom (Assistant Professor)

Mr. Andrew Dawson (Associate Professor)

NOTTINGHAM TRANSPORTATION ENGINEERING CENTRE **(NTEC)**

DEPARTMENT OF CIVIL ENGINEERING

FACULTY OF ENGINEERING

UNIVERSITY OF NOTTINGHAM, UK

May 2020

Abstract

Pavements have been used to transport goods and people from one place to another over the years. Pavement construction technologies have been continuously evolving starting from compacted ground to brick roads and modern hot mix asphalt roads capable of speed, safety, durability and comfort. The advancing construction technologies have led to heavy-duty pavements (Inverted Pavements) in South Africa to accomodate heavy loads in warm climates. Inverted Pavements are types of pavement in which the layer arrangement is different from that of a conventional flexible pavement. In an inverted pavement, the unbound granular base layer is constructed just under the hot mix asphalt surfacing and another granular layer modified with cement is constructed underneath it. This current project involves designing inverted pavements based on laboratory testing. The project is divided into different phases which are summarised here.

As a low stiffness unbound layer is constructed in a sandwich between stiffer layers, its performance becomes one of the determining factors relating to the pavement's resistance to failure. Therefore, extensive laboratory testing has been performed in the current project to study unbound material performance under different influencing factors including moisture, fines content, number of load applications and stress conditions. The results show that the selected unbound granular material (UGM) gradations based on South African base specifications performed significantly well under these influencing factors. The resilient and permanent deformation performance of unbound granular materials is presented in detail in this thesis.

The second phase of the project involved testing different inverted pavement combinations in the laboratory to establish the effect of layer thickness on performance under given loading and environmental conditions. Permanent deformation and reflective cracking were the criteria to assess the pavement performance under load. Different laboratory testing matrices were developed for permanent deformation and reflective cracking. The testing was performed at different temperatures under the same load to evaluate the pavement's resistance to both failure criteria in

a wheel tracking device. A conventional mould was used for evaluating permanent deformation while a new mould was designed and manufactured for studying crack initiation and propagation. The results showed that the different thickness combinations within an inverted pavement performed differently with some of the thickness variations affecting the performance significantly.

The third phase of the project involved the prediction of permanent deformation and crack propagation in inverted pavements. Different techniques were combined to develop a methodology to predict the permanent deformation in a full-depth inverted pavement. The predicted permanent deformation values were compared with the measured ones and very close correspondance was observed. Similarly, crack initiation and propagation were also predicted by developing a mechanics-based methodology calculating the forces and hence bending in asphalt surfacing leading to calculation of tensile strains. The calculated strains were used to develop a fatigue characteristic. The methodology developed was applied to a real pavement and promising results were obtained.

Acknowledgement

First of all, I would like to thank Allah Almighty for giving me this beautiful life full of blessings and so many amazing, caring and loving people. I am also very grateful to Almighty for this wonderful opportunity to study at one of the most amazing places with amazing folk around. Secondly, my gratitude goes towards my supervisors, Dr Nick Thom and Mr Andrew Dawson for always being there for me. My special acknowledgements go to Nick for his continuous technical and professional support, guidance, availability and fruitful discussions on and off the subject. His valuable and critical comments have resulted in the current shape of the thesis. Although I did not visit Andrew as frequently as Nick, I considered all his comments and really appreciate his efforts in making this PhD thesis what it is today.

This is also a right platform to thank my sponsors, Mirpur University of Science & Technology (MUST) AJK, Pakistan, and University of Nottingham, UK for their financial assistance towards this project.

Great gratitude goes towards the technical staff at Nottingham Transportation Engineering Centre (NTEC) for their continuous and professional support. It would be very unjust not to mention Jon Watson, Richard Blakemore, Martyn Barrett, Lawrence Pont, Margaret, Laura, Mat and Anthony. This project would not be possible without their technical support. I really thank all these wonderful people.

My colleagues at NTEC have always been a source of inspiration for me throughout the study period. I would like to thank Bilal Bhai, Waqas, Waleed, Ahmed Abed, Rami, Tahseen, Juan, Taqia, Chris, Charles, Monketh, Gustavo, Raza, Adeel, Ayesha, Saira and Sanaa for supporting and motivating me towards my goal and making my stay in Nottingham full of memories.

My friends in Nottingham have, probably, been the best part of my life in the city for the past four years. Ibrar, Usman, Shani, Ehtisham, Hassan, Umer Bhai, Aqib, Yasam Bhai, Rizwan, Nasir and so many others, you guys have left so many memories in my mind that it would be very difficult to go back home. I will miss you guys. How can I not mention the hospitality and

care from Ibrar's family members? You really made me feel at home. Thank you so much.

I really thank God for having my sisters here in the United Kingdom. How can I even think of thanking you for everything you did for me during my stay in the UK? I still remember the first day when I came here and Manha's reaction. I am thankful to Bajo Noreen, Bajo Misbah, Bhai Ashfaq, Yasir, Alisha and Manha for giving me so much love, care and encouragement during my stay in the UK. I am going to miss you guys a lot.

Lastly, I would like to thank my parents and family members for their patience during my studies. It is a great blessing to have you guys as family, I love you so much. Sana, I missed you; I wish you were here too. It would have been great fun if you were here. I would especially like to thank my Taya Abu Ji for his guidance and support throughout my life. I would not be sitting and writing this if you had not persuaded me to change my educational path when I was fed up of not getting admission in any medical university. I dedicate my successes to you. Thank you for supporting me every day of my life.

Most importantly, I would like to thank my wife and my cute, charming and adorable daughter Ahdia for their support and patience during my studies. If it was not for those video calls with Ahdia every day, I would have been stressed out. Her smile, in fact laughter, took all the loads of the PhD away and gave me strength and motivation to keep on working hard for my success. I love you my dear. I love you so much.

Imtiaz

May 2020

Dedication

Dedicated to

my family who always supported me

my teachers who inspired and encouraged me

and specially

my daughter “Ahdia Ahmed” whose smile is my life

Declaration

This is to declare that the contents of this thesis are my own work under the supervision of Dr Nick Thom and Mr Andrew Dawson and were performed at the University of Nottingham from 2016 to 2019. This thesis has not been submitted to any other institution for another degree. The same is also declared by my supervisors.

Imtiaz Ahmed
Nottingham, May 2020
Email: Imtiaz.ahmed@nottingham.ac.uk, imtiaz674@gmail.com, Imtiaz.ce@must.edu.pk,

Dr. Nick Thom
Assistant Professor
NTEC, Faculty of Engineering
The University of Nottingham, UK
NG7 2RD
Email: nicholas.thom@nottingham.ac.uk

Mr. Andrew Dawson
Associate Professor
NTEC, Faculty of Engineering
The University of Nottingham, UK
NG7 2RD
Email: andrew.dawson@nottingham.ac.uk

Table of Contents

1 Introduction 1

1.1 Introduction to the road network in the UK 1

1.2 Pavement Structure 2

1.3 Motivation and background 2

1.4 Aim 4

1.4.1 Objectives 4

1.5 Methodology 5

1.6 Chapter Organization 7

2 Literature Review 8

2.1 Inverted Pavement; an Introduction 8

2.2 Permanent deformation in Unbound Granular Materials 10

2.2.1 Shakedown Theory 11

2.2.1.1 Historical Perspective of Shakedown Concept 13

2.2.2 Aggregate Anisotropic Characterization 15

2.2.2.1 Historical perspective of anisotropic consideration 18

2.2.3 Factors Affecting Permanent Deformation Of UGMs 27

2.2.3.1 Effect of Stress 28

2.2.3.2 Effect of Number of Load Applications 29

2.2.3.3 Effect of Moisture Content 30

2.2.3.3.1 The concept of suction and its measurement 32

2.2.3.4 Effect of Stress History 35

2.2.3.5 Effect of Density 36

2.2.3.6 Effect of Grading, Fines Content, and Aggregate Type 37

2.2.3.7 Effect of Variable and Constant Confining Pressure 39

2.2.3.8 Effect of Principal Stress Rotation 39

2.2.4 UGM Permanent deformation models 41

2.3 Resilinet behaviour of Unbound Granular Materials 46
2.3.1 Resilient response modelling 47
2.4 Permanent Deformation in Asphalt Pavements 52
2.4.1 Permanent Deformation Prediction Models 53
2.4.2 Three-stage Rutting Development 57
2.4.3 Rutting prediction model types 58
2.4.4 Approaches to Predict Rutting 59
2.5 Cracking in HMA Pavements 62
2.5.1 Mechanism of reflective cracking 63
2.5.2 Development of reflective cracking 64
2.6 Inverted Pavement 68
2.6.1 A brief history of Inverted Pavements 69
2.6.2 Slushing 71
2.6.3 Design methodology in South Africa 72
2.6.3.1 Material Characterization 73
2.6.3.2 Structural Analysis 78
2.6.3.3 Pavement Life Prediction 78
2.6.4 Comparison of Inverted and Conventional 81
2.6.4.1 Cracking 86
2.6.4.2 Aggregate Base Stiffness 87
2.6.4.3 Economic Benefits of inverted pavements 88
2.6.5 Simulations of Inverted Pavements 90
2.7 Conclusions 93
2.8 Summary 94
3 Materials and Methods 95
3.1 Introduction 95
3.2 Materials 95

3.2.1 Bitumen..... 95
3.2.2 Aggregates..... 96
3.2.3 Cement 97
3.3 Experimental Programme..... 97
3.3.1 Component Level Testing..... 98
3.3.1.1 Aggregate Testing..... 99
3.3.1.1.1 Density/Moisture by Vibratory Compactor..... 99
3.3.1.1.2 PUMA Testing.....102
3.3.1.1.2.1 PUMA specimen: description, preparation and testing 103
3.3.1.2 Bitumen Mixes.....106
3.3.1.2.1 Stiffness Test for HMA.....107
3.3.1.2.2 Repeated Load Axial Test (RLAT).....107
3.3.1.3 Compressive Strength of Concrete used for Cement Treated Base 109
3.3.2 Structure Level Testing 109
3.3.2.1 Wheel Tracking for Permanent Deformation.....110
3.3.2.2 Wheel Tracking for Cracking 114
3.3.2.2.1 Wheel Tracker mould for Cracking test setup 115
3.3.3 Predictive Analysis.....117
3.3.3.1 Predictive Analysis for Permanent Deformation 117
3.3.3.1.1 Prediction in AC.....117
3.3.3.1.2 Prediction in UGM 120
3.3.3.2 Predictive Analysis for Cracking 124
3.3.4 Summary.....125
4 Unbound Granular Materials Characterization in an Inverted Pavement.....126
4.1 Introduction.....126

4.2 Materials and testing program 127
4.3 UGM stiffness by PUMA 129
4.3.1 PUMA test summary 133
4.3.2 Effect of Moisture content on Unbound Base Performance ..134
4.3.3 Effect of Fines content on Unbound Base Performance 137
4.4 Permanent Deformation from the PUMA 141
4.4.1 PUMA test summary at each Stress Stage 144
4.4.2 Effect of moisture on UGM permanent deformation 145
4.4.3 Effect of Fines Content on UGM permanent deformation 147
4.5 Correlating PUMA data to Triaxial developed stress strain model 153
4.6 Conclusions 159
5 Simulative Testing of Inverted Pavements 160
5.1 Introduction.....160
5.2 Permanent Deformation (Rutting) in Inverted Pavement 160
5.2.1 Materials and Testing Program 161
5.2.1.1 Materials 162
5.2.1.2 Testing Program 162
5.2.1.3 Wheel Tracking Mould and Specimen preparation 164
5.2.1.4 The Wheel Tracking Machine.....168
5.2.1.5 Effect of layer thickness on the performance of an inverted pavement in a simulative testing environment 170
5.2.1.5.1 Base layer as an indicator of inverted pavement performance 171
5.2.1.5.2 Effect of asphalt on pavement performance 173
5.3 Reflective Cracking in Inverted Pavements.....178
5.3.1 Materials and Testing Matrix.....179
5.3.2 Wheel Tracking Mould parts and description 180

5.3.3 Specimen Preparation 184
5.3.4 The Wheel Tracking Machine 185
5.3.5 Cracking test results and discussion 189
5.4 Conclusions 193
6 Predicting Permanent Deformation in Inverted Pavement ...195
6.1 Introduction.....195
6.2 Linear Viscous Approach 195
6.3 Methodology 197
6.3.1 Pseudo-Viscosity in Asphalt Mixtures 197
6.3.2 Pseudo-Viscosity in Unbound Granular Base Layer 201
6.4 Permanent Deformation Prediction in Inverted Pavement 203
6.4.1 Assumptions.....206
6.4.2 Results 206
6.5 Conclusions 213
7 Predicting Fatigue Life in Inverted Pavements 214
7.1 Introduction.....214
7.2 Analysis of Wheel Tracker tests.....214
7.3 Results 221
7.4 Application to Real Pavements 224
7.5 Conclusions 227
8 Design Guide for Inverted Pavements 228
8.1 Introduction.....228
8.2 Design approach.....228
8.3 Summary 229
9 Conclusions and Recommendations.....230
9.1 Conclusions 230
9.1.1 Characterization of Unbound Granular Materials 230
9.1.2 Simulative Testing.....231

9.1.3 Predicting Rutting in inverted pavements 233
9.1.4 Predicting Fatigue life in inverted pavements 233
9.2 Recommendations 234
10 References 236

List of Figures

Figure 1.1: Flow diagram for methodology 6

Figure 2.1: A typical inverted pavement 9

Figure 2.2: Shakedown ranges 11

Figure 2.3: Permanent deformation behaviour of UGMs based on shakedown theory 12

Figure 2.4: Stratified cross-anisotropic material under axial symmetry (after Tutumluer 2008) 18

Figure 2.5: Horizontal stiffness ratio (M_R^h/M_R^v) distribution throughout the base in the presence of 20.7 kPa horizontal residual stresses (after Tutumluer and Thompson, 1997b) 20

Figure 2.6: Typical variations of vertical and horizontal moduli with deviator stress for crushed limestone (after Tutumluer and Seyhan, 1999) 21

Figure 2.7: Modulus variations in horizontal and vertical directions (after Allen 1973) 22

Figure 2.8: Relationship between stiffness anisotropy and stress ratio (after Tutumluer 1997) 23

Figure 2.9: Comparative radial stresses through unbound layer (After Tutumluer and Thompson 1997) 23

Figure 2.10: Cross-Anisotropy of Pavement Layers (After Tarefder et al. 2016) 25

Figure 2.11: Strains in granular materials during one cycle of load application 27

Figure 2.12: The definition of Stress path in p-q space 29

Figure 2.13: Influence of Drainage on Permanent Deformation Development (Dawson 1990) 31

Figure 2.14: Concept of suction (after Thom 2014) 33

Figure 2.15: Effect of Stress History on Permanent Strain (Brown and Hyde 1975) 36

Figure 2.16: Effect of Grading and Compaction on Plastic Strain (Thom and Brown 1988) 38

Figure 2.17: Grading parameter "n" definition (After Thom 1988) 38

Figure 2.18: Effect of principal stress rotation on the accumulation of permanent strain (after Thom and Dawson, 1996) 40

Figure 2.19: Demonstration of the time-hardening approach (After Rahman and Erlingsson 2015) 46

Figure 2.20: Stages of Permanent Deformation (after Khodaii and Mehran 2009) 57

Figure 2.21: Comparison of the measured and predicted rutting (mm) at different air void contents (%) (After Nahi et al. 2014) 62

Figure 2.22: Schematic of reflective cracking mechanisms: (a) temperature variation and (b) traffic loading (after Baek 2010 thesis) 64

Figure 2.23: Reflective cracking paths observed in: (a) HMA/HMA structure with glass-grid interlayer (Jayawickrama et al., 1987) and (b) HMA/PCC structure with geo-grid interlayer (Kuo and Hsu, 2003) 65

Figure 2.24: Reflective crack locations: (a) primary and secondary crack (after de Bondt, 1998) and (b) sequence of double crack (after Zhou and Sun, 2002) 67

Figure 2.25: Fracture modes of reflective cracking 68

Figure 2.26: Design approach (After Theyse et al 1996) 72

Figure 2.27: Fatigue crack initiation transfer functions for thin asphalt surfacing layers (continuous graded) 79

Figure 2.28: Fatigue crack initiation transfer functions for thin asphalt surfacing layers (gap graded) 79

Figure 2.29: Stress evolution in the granular base along the wheel path. Stress ratio q/p (left column), and intermediate stress ratio b= (σ2 -σ3) / (σ1 - σ3) (right column) along the centreline for different asphalt thicknesses. In all cases, tGAB = 150mm and tCTB=300mm. The blue, red and yellow lines correspond to the top, half-depth and bottom of the GAB, respectively 91

Figure 2.30: Stiffness contours (MPa) within the granular base under the applied wheel load q=650 kPa for different thicknesses of the granular base. In all cases, tAC = 50mm and tCTB = 300mm 92

Figure 2.31: GAB stiffness anisotropy contours within the granular base for tGAB = 150mm and tCTB = 300 mm 93

Figure 3.1: Mineral composition of granite using MLA analysis (Zhang et al. 2015) 97

Figure 3.2: Laboratory testing matrix/plan..... 98

Figure 3.3: Aggregate gradations selected for the study + South African G1 limits..... 99

Figure 3.4: Suction temperature 100

Figure 3.5: Proctor Test results.....101

Figure 3.6: PUMA mould and its components.....103

Figure 3.7: PUMA test in progress 104

Figure 3.8: Screen shot of an on-going PUMA test at 5th loading stage 105

Figure 3.9: PUMA samples after testing.....106

Figure 3.10: Granite gradation for 0-14mm dense graded mix 106

Figure 3.11: An ongoing ITSM test 107

Figure 3.12: Repeated load axial test for AC permanent deformation ...108

Figure 3.13: RLAT tested samples 108
Figure 3.14: Compressive strength of CTB 109
Figure 3.15: Aggregate gradation for simulative testing with the maximum particle size of 14mm 111
Figure 3.16: Wheel Tracker tested specimen 113
Figure 3.17: Wheel tracking device 114
Figure 3.18: Viscosity vs Strain (Stages) 118
Figure 3.19: Methodology for AC rutting prediction 120
Figure 3.20: Time Hardening approach (After Rahman and Erlingsson 2015) 122
Figure 4.1: UGM (Granite) gradations for PUMA and Triaxial (South African specification) 127
Figure 4.2: Resilient modulus definition (after Sadrossadat et al. 2018)130
Figure 4.3: Stiffness at different moisture contents for 4.1% fines unbound granular base material 130
Figure 4.4: Stiffness at different moisture contents for 6.7% fines unbound granular base material 131
Figure 4.5: Stiffness at different moisture contents for 13.5% fines unbound granular base material 131
Figure 4.6: Stiffness at different moisture contents for 7.4% fines unbound granular base material 132
Figure 4.7: Stiffness summary at different moisture contents 133
Figure 4.8: Stress ratio applied during PUMA test 134
Figure 4.9: Stiffness summary for 4.1% fines content at different moisture contents at end of 1000 cycle each.....135
Figure 4.10: Stiffness summary for 6.7% fines content at different moisture contents at end of 1000 cycle each.....136
Figure 4.11: Stiffness summary for 13.5% fines content at different moisture contents at end of 1000 cycle each.....136
Figure 4.12: Stiffness summary for 7.4% fines content at different moisture contents at end of 1000 cycle each.....137
Figure 4.13: Stiffness summary for specimen with different fines contents tested at suction 138
Figure 4.14: Stiffness summary for specimen with different fines contents tested at 3% moisture.....138
Figure 4.15: Stiffness summary for specimen with different fines contents tested at 5% moisture.....139
Figure 4.16: Stiffness summary for specimen with different fines contents tested at optimum moisture 139
Figure 4.17: Permanent Deformation at different moisture contents for 4.1% fines unbound granular base material 141

Figure 4.18: Permanent Deformation at different moisture contents for 6.7% fines unbound granular base material 141

Figure 4.19: Permanent Deformation at different moisture contents for 13.5% fines unbound granular base material 142

Figure 4.20: Permanent Deformation at different moisture contents for 7.4% fines unbound granular base material 142

Figure 4.21: Permanent Deformation summary 144

Figure 4.22: Permanent Deformation at different moisture contents for 4.1% fines material at the end of each stress stage 145

Figure 4.23: Permanent Deformation at different moisture contents for 6.7% fines material at the end of each stress stage 145

Figure 4.24: Permanent Deformation at different moisture contents for 13.5% fines material at the end of each stress stage 146

Figure 4.25: Permanent Deformation at different moisture contents for 7.4% fines material at the end of each stress stage 146

Figure 4.26: Permanent Deformation for different materials at suction .148

Figure 4.27: Permanent Deformation for different materials at 3% moisture 148

Figure 4.28: Permanent Deformation for different materials at 5% moisture 149

Figure 4.29: Permanent Deformation for different materials at optimum moisture 149

Figure 4.30: Effect of moisture contents on permanent strain of UGMs with different fines contents.....150

Figure 4.31: Effect of moisture contents on resilient modulus of UGMs with different fines contents.....150

Figure 4.32: Effect of fines contents on permanent strain of UGMs tested at different moisture contents 151

Figure 4.33: Effect of fines contents on resilient modulus of UGMs tested at different moisture contents 151

Figure 4.34: Permanent strain vs rate of permanent strain at various axial stresses for UGM having 6.7% tested at suction 152

Figure 4.35: Permanent strain vs rate of permanent strain at various axial stresses for UGM having 13.5% tested at 3% moisture.....152

Figure 4.36: Permanent strain vs rate of permanent strain at various axial stresses for UGM having 7.4% tested at OMC.....153

Figure 4.37: Permanent deformation measured and predicted for 4.1% fines at suction moisture content.....156

Figure 4.38: Measured vs predicted strains (%) 156

Figure 4.39: Permanent deformation measured and predicted for 6.7% fines at 5% moisture 158

Figure 4.40: Permanent deformation measured and predicted for 13.5% fines at 3% moisture.....158

Figure 4.41: Permanent deformation measured and predicted for 7.4% fines at 5% moisture.....159

Figure 5.1: Granite gradation for 0-14mm dense graded asphalt mix...162

Figure 5.2: Unbound layer gradation for simulative testing.....163

Figure 5.3: A) Aggregate mixed with water and (B) Prepared cemented slab 165

Figure 5.4: Mixing water at OMC into unbound granular materials 166

Figure 5.5: A depiction of a wheel tracking specimen with 20mm AC, 50mm UGM, 30mm CTB, 12mm rubber as SG and 18mm wooden filler.....168

Figure 5.6: Wheel tracking equipment a) with hanging loads b) Zoomed to wheel 169

Figure 5.7: Methods for rutting manual calculation a) Depth Gauge with steel plate and b) Profilometer.....170

Figure 5.8: Wheel tracking specimen (untested vs tested).....170

Figure 5.9: Summary of simulative wheel tracking test results.....171

Figure 5.10: Permanent deformation of inverted pavements with 15mm thick AC.....172

Figure 5.11: Permanent deformation of inverted pavements with 20mm thick AC.....173

Figure 5.12: Permanent deformation of inverted pavements with 25mm thick AC.....173

Figure 5.13: Permanent deformation of inverted pavements with 20mm thick UGM 175

Figure 5.14: Permanent deformation of inverted pavements with 35mm thick UGM 175

Figure 5.15: Permanent deformation of inverted pavements with 50mm thick UGM 176

Figure 5.16: Permanent deformation of inverted pavements with 60mm thick UGM 176

Figure 5.17: New assembled mould for cracking tests 182

Figure 5.18: 40mm and 50mm high longitudinal side walls with welded angle sections.....182

Figure 5.19: Mould parts a) 10mm high longitudinal side walls and b) 40*40 angle sections for lateral support 183

Figure 5.20: Explaining the function of top steel plate and angle sections (unbolted).....184

Figure 5.21: Cement treated slab for cracking test a) marked for cutting into beams and b) cracked in a prepared specimen 185

Figure 5.22: Wheel tracking specimen for cracking test a) bitumen emulsion on top of UGM and fully prepared multiple specimen 185

Figure 5.23: Wheel tracking setup to study the crack propagation in an inverted pavement 186

Figure 5.24: Side and end views of the wheel tracking equipment 187

Figure 5.25: Wheel tracking specimen after testing 187

Figure 5.26: Progression of a crack in wheel tracker specimen 188

Figure 5.27: Random specimens during test 188

Figure 5.28: Cycle to initiate cracking in wheel tracking specimen 189

Figure 5.29: Effect of individual layers to initiate the cracks 191

Figure 5.30: Cycles to end the test on visual inspection 193

Figure 6.1: Cores taken from slab 198

Figure 6.2: Viscosity vs Strain (Stages).....199

Figure 6.3: RLAT plot for 15mm AC 200

Figure 6.4: RLAT plot for 20mm AC 200

Figure 6.5: RLAT plot for 25mm AC 201

Figure 6.6: Flow chart for permanent deformation prediction 205

Figure 6.7: Measured vs Prediction Deformation in specimens having 15mm AC and 20mm UGM 207

Figure 6.8: Measured vs Prediction Deformation in specimens having 15mm AC and 35mm UGM 207

Figure 6.9: Measured vs Prediction Deformation in specimens having 15mm AC and 50mm UGM 208

Figure 6.10: Measured vs Prediction Deformation in specimens having 15mm AC and 60mm UGM.....208

Figure 6.11: Measured vs Prediction Deformation in specimens having 20mm AC and 20mm UGM.....209

Figure 6.12: Measured vs Prediction Deformation in specimens having 20mm AC and 35mm UGM.....209

Figure 6.13: Measured vs Prediction Deformation in specimens having 20mm AC and 50mm UGM.....210

Figure 6.14: Measured vs Prediction Deformation in specimens having 20mm AC and 60mm UGM.....210

Figure 6.15: Measured vs Prediction Deformation in specimens having 25mm AC and 20mm UGM.....211

Figure 6.16: Measured vs Prediction Deformation in specimens having 25mm AC and 35mm UGM.....211

Figure 6.17: Measured vs Prediction Deformation in specimens having 25mm AC and 50mm UGM.....212

Figure 6.18: Measured vs Prediction Deformation in specimens having 25mm AC and 60mm UGM 212
Figure 7.1: A typical inverted pavement with cracks in CTB under load.215
Figure 7.2: A pavement structure without unbound granular layer 215
Figure 7.3: Pavement deformed shape under load showing forces and deflection 216
Figure 7.4: Inverted pavement deformed shape under load 217
Figure 7.5: Explanation of effective length 220
Figure 7.6: Fatigue characteristic 222
Figure 7.7: Fatigue life prediction with and without unbound granular layer 223
Figure 7.8: Measured and predicted number of cycles with and without UGM layer 224
Figure 7.9: Effect of UGM thickness on strains calculated 225
Figure 7.10: Strains calculated for different thickness combinations 225
Figure 7.11: Number of predicted cycles to failure (TRRL) 226

List of Tables

Table 2.1: Permanent deformation predictive models history in UGMs ... 42

Table 2.2: Permanent deformation predictive models history in ACs..... 55

Table 2.3: Inverted base pavements tested by the Heavy Vehicle Simulator (Data and original references in Theyse 2002, and Jooste and Sampson, 2005) 70

Table 2.4: Inverted base pavement case histories in the US 71

Table 2.5: Road Categories and Approximate Design Reliabilities Used in South Africa 73

Table 2.6: South African Road-Building Materials with Material Codes (After Theyse et al 1996)..... 74

Table 2.7: South African Road-Building Materials with Material Codes (After Theyse et al 1996)..... 75

Table 2.8: Suggested Elastic modulus for HMA 76

Table 2.9: Suggested Elastic modulus for CTB..... 77

Table 2.10: Suggested Elastic modulus for UGM 77

Table 2.11: The granular material parametric values suggested by South African specification 81

Table 2.12: Permanent deformation form Benkelman Beam (After Papadopoulos, data extracted from Johnson, 1961) 82

Table 2.13: Pavement Performance data from Mississippi (Barker et al 1973) 83

Table 2.14: Performance data on Georgia Tech laboratory study (Barksdale and Todres 1984; Tutumluer and Barksdale 1995)..... 84

Table 2.15: Performance data on Louisiana field test study (Titi et al. 2003) 85

Table 2.16: Pavement performance data in Morgan County quarry (Terrell et al. 2002; Lewis 2012)..... 86

Table 3.1: Properties of Bitumen used in the study 96

Table 3.2: Aggregate particle densities 96

Table 3.3: Compaction test summary 101

Table 3.4: Testing matrix for Wheel Tracking test 112

Table 4.1: Stress sequence for preliminary PUMA testing 128

Table 4.2: Testing matrix.....129

Table 4.3: Predictive analysis parameters.....157
Table 5.1: Simulative testing matrix.....164
Table 5.2: Rutting in individual layers.....177
Table 5.3: Shakedown Range in UGM.....178
Table 5.4: Testing Matrix for cracking tests.....180
Table 7.1: Calculations from the prediction exercise.....221

1 Introduction

1.1 Introduction to the road network in the UK

There are many modes of transport in the United Kingdom namely roads, railways, airways and waterways. The roads are considered to be most critical due to their usage and easy access for everyone. According to a statistical release by the Department of Transport (2018), there were 31,800 miles of major road in Great Britain, consisting of 2,300 miles of motorway (99% trunk, 1% principal), 29,400 miles of 'A' road (18% trunk, 82% principal) and 214,900 miles of minor road consisting of 18,800 miles of 'B' road, 53,400 miles of 'C' road and 142,700 miles of 'U' road. In 2018-19, a total of £3.8 billion to operate, maintain and enhance the strategic road network was spent by Highways England (Highways England, 2019). The huge budgets and network, therefore, indicate that the industry carries the multi-million GBP responsibility.

Engineers throughout the world have been striving very hard over hundreds and thousands of years to improve the means of transport of goods and people from one place to another in an efficient and comfortable way. This has led to the evolution of roads from the natural compacted ground to brick and paved roads in recent centuries. The advancements in science and technology have benefited pavement engineering in developing new and more durable pavements having longer service lives. One such advancement was the development of the inverted pavement which has historically been used in South Africa for carrying heavy traffic in a warm climate. Its excellent performance has resulted in the design methodology coming to the USA in the last few decades where multiple test sections have been constructed and are under monitoring. The current project would be first of its kind in the United Kingdom. Using this new type of design methodology in constructing roads in the UK may be one of the solutions for future durable pavements carrying heavier loads.

1.2 Pavement Structure

A typical pavement is constructed by arranging different layers having decreasing stiffness with depth. The stiff hot mix asphalt surfacing is capable of taking the wheel load and distributing it over a wider area underneath to maintain the durability of the pavement.

In a typical pavement, flexible or rigid, the aggregate layer is considered to be weak and vulnerable to failure due to traffic-induced loading and it needs to be protected by the asphalt concrete layer in flexible pavements or cement concrete layer in rigid pavements. The vast and ever-spreading road networks worldwide have contributed to the uncontrolled usage of natural materials like bitumen, cement and aggregates. The extensive use of these materials has made engineers and researchers strive to look for alternatives. The studies thus conducted have shown various new materials to be used as alternatives. Another solution to the problem can be found by improving the performance of pavements by more efficient and cost-effective designs. One of the alternatives can be an inverted pavement which has been used in South Africa for a few decades with very good performances (Cortes 2010)

1.3 Motivation and background

The layers are arranged in an inverted pavement resulting in a less stiff aggregate base constructed in between the stiff asphalt and cement treated base layers. The proximity of the aggregate base layer to the traffic load in an inverted pavement makes it more critical to the overall performance of the pavement. An inverted pavement relies on the performance of the unbound aggregate base layer for the overall mechanical response of the pavement, unlike conventional pavements in which the stiffer top layers distribute the load to the less stiff bottom layers over a broader area. The performance of this pavement type in South Africa over the years and recent studies on test sections in the USA prove its worth as an efficient alternative to conventional pavements (Theyse 2011). This project focusses on the design of heavy-duty pavements (inverted pavements) in the United Kingdom for the prevailing environmental and loading conditions.

Pavements have been designed by empirical methods over the years, developed from long term experience without considering the actual material response under different loading and environmental conditions. These design methods are limited to the type of pavements, materials and construction practices. The performance expectation of aggregate base layer in an inverted pavement is very different from conventional pavements either flexible or rigid. Therefore, the empirical design methods developed cannot be applied to design such pavement. To account for the actual response of the pavement under traffic loading and overcome the limitations of the empirical methods, researchers have developed different simulative testing techniques in the laboratory considering a mechanistic design approach. The pavement is treated as a structure in this method while numerical/analytical tools from mechanics are applied to study its mechanical behaviour under loading conditions.

Mechanistic design is based on understanding the profound behaviour of the materials in a pavement's response to loading. The unbound aggregates in a pavement display stress-dependent non-linear elastic behaviour under cyclic loading (Morgan 1966; Monismith et al. 1967; Hicks and Monismith 1971; Allen and Thompson 1974; Barksdale 1984; Adu-Osei 2000; Lekarp et al. 2000). The presence of a very thin asphalt layer accompanied by the stiff cement-treated foundation in an inverted pavement develops extensive stresses in an unbound aggregate base under traffic loading. Larger fluctuations in the state of stress intensify the non-linear response of the unbound aggregate base in an inverted structure (Cortes 2010). The mechanical response of an unbound aggregate layer in a pavement under compaction and during service loading is, therefore, the most important parameter to be thoroughly considered and evidently understood before the design methods for this type of pavements can develop.

The shifting towards better pavement performance, depleting natural resources, cost-efficient solutions, budget issues and energy efficiency have diverted the attention of researchers worldwide to alternate pavements. The use of inverted pavements in the UK has probably been hindered by the lack of field trial section construction and laboratory-based research to

study the mechanical response and performance of such a pavement under prevailing environmental conditions.

The present work, therefore, is an attempt to focus on studying the mechanical behaviour of the unbound aggregate base layer under traffic and loading conditions. The stress-dependent resilient and permanent deformation behaviour of the materials was thoroughly characterized under a newly developed testing device named the Precision Unbound Material Analyser (PUMA). The results from the PUMA were then correlated with the conventional and widely adopted triaxial apparatus by fitting a triaxial model to the PUMA data. The behaviour of the thin hot mix asphalt (HMA) layer was also investigated in this project by testing different thicknesses of layers by simulative testing in a wheel tracking device. The effect of different layer thickness combinations on permanent deformation and reflective cracking in inverted pavements was part of the simulative study in the wheel tracking device. Finally, a new methodology was developed to predict the permanent deformation within an inverted pavement using a linear viscous approach. Linear viscosity of asphaltic materials from the Repeated Load Axial Test (RLAT) and an already developed stress-dependent permanent deformation model for unbound granular materials (UGMs) was adopted in this approach and satisfactory results were reported. Similarly, a methodology was developed to predict the initiation and propagation of reflective cracking in the simulative inverted pavements.

1.4 Aim

The project was aimed at the design of heavy-duty pavements (inverted pavements) with the ability to withstand heavy traffic loads at high temperatures without failure. It was targeted to be constructed with conventional materials with a better performing design for the unbound aggregate base layer.

1.4.1 Objectives

The current study focused on the following objectives;

1. Comprehensive literature survey regarding the resilient and permanent behaviour of unbound granular materials in pavements. The permanent deformation and reflective cracking behaviour in

asphaltic materials was a part of the literature review. The behaviour of inverted pavements was also investigated in the literature.

2. Studying the behaviour of a less stiff base layer of UGMs in between stiffer layers.
3. Studying unbound granular material behaviour under different axial stresses applied.
4. Evaluating the effect of moisture and fines contents on resilient and permanent deformation of unbound granular materials in the PUMA.
5. Developing a methodology to study inverted pavements behaviour under load in the laboratory.
6. Assessing the effect of different layers on inverted pavement performance under load.
7. Studying the effect of thickness combinations of asphaltic materials and unbound granular layer on permanent deformation performance in a simulative testing environment.
8. Designing and acquiring a new mould to study reflective cracking initiation and propagation in inverted pavements.
9. Studying the effect of thickness combinations of asphaltic materials and unbound granular layer on reflective cracking resistance in a simulative testing environment.
10. Developing a methodology to predict the permanent deformation within an inverted pavement by adopting a linear viscous approach. Different methodologies were adopted to calculate the viscosities of asphaltic and unbound materials respectively.
11. To develop an approach to represent the reflective crack initiation and propagation within an inverted pavement due to the presence of the brittle cemented layer underneath.

1.5 Methodology

The flow diagram shows the methodology adopted for the research project.

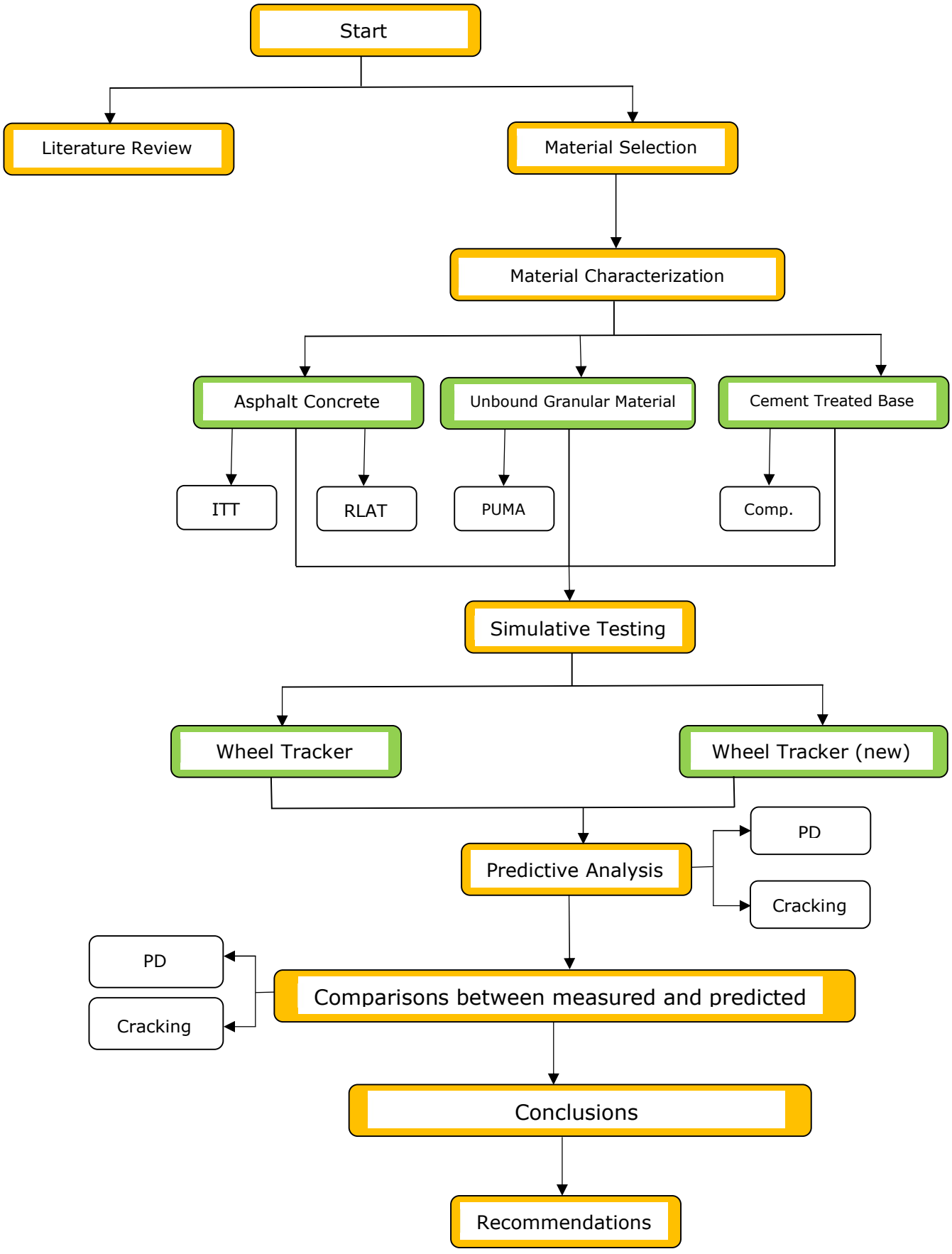


Figure 1.1: Flow diagram for methodology

1.6 Chapter Organization

Chapter one has introduced the research project by giving the problem statement, aims and objectives to the study. The methodology to be adopted to study inverted pavement behaviour is also represented in a flow diagram. The content summary of all the chapters is represented too.

An ample literature review is carried out in Chapter 2. The literature review covers the unbound granular materials behaviour under loading; different theories to characterize the permanent deformation behaviour of UGMs are also summarised; the permanent deformation and cracking within the pavements is mentioned as well; finally, a detailed representation of the literature regarding the in-situ performance of the inverted pavements is cited.

Chapter 3 encompasses the materials and methods adopted during the study. All the materials used, their properties and the testing methods followed during the research are documented.

Chapter 4 states the findings from the PUMA test regarding the resilient and permanent deformation behaviour of the UGMs. The effect of axial stresses, moisture and fines contents on these properties is also documented in detail. The methodology established to fit an already developed model from triaxial test to the PUMA data is described.

Chapter 5 comprises the findings from the simulative testing of inverted pavements. The effect of layer thicknesses on permanent deformation and reflective cracking resistance of the inverted pavement is shown and discussed. The design of the newly acquired mould to study reflective cracking is also mentioned.

Chapter 6 describes the permanent deformation prediction methodology developed during the research. The predictions are compared with the laboratory results and significant similarity was observed.

Chapter 7 represents the approach developed to predict crack initiation and propagation within an inverted pavement.

Chapter 8 documents all the conclusions from the project. Recommendations for future research are also mentioned.

2 Literature Review

The Inverted Pavement (IP) is an inventive highway pavement design where the lower supporting cemented layer is more rigid than the upper structural unbound granular material (UGM) layer. The design was developed in South Africa in the early 1970s where it has been given different names including G1-Base, Inverted Base, Sandwich Pavement, and Upside-Down Pavement. Since then, South African highway engineers and authorities have been using this design as a major pavement design for almost all types of roads in the country. Pavement engineers in the United States of America (USA) have also been trying to successfully use variants of IP on different road networks in the country including rural, state and interstate highway systems (Buchanan 2011; Rasoulian 2004). The United Kingdom is yet to start using this innovative pavement construction technology. This project would be the first step towards a more durable and economical replacement of the conventional pavements in the region.

The literature review is distributed into the following disciplines and sub-disciplines.

Inverted Pavement-an introduction, Unbound Granular Materials (UGM) and factors affecting Permanent Deformation in UGM, Prediction of Permanent Deformation in UGM, Failure modes in Pavements- Rutting and cracking, Rutting in asphalt pavements, Cracking in asphalt pavements, Historical perspective of IP.

2.1 Inverted Pavement; an Introduction

A pavement is generally designed and constructed by selecting the optimum combination of layer thicknesses along with the material properties which are based on strength, availability, anticipated loading conditions, durability and economic analysis. Pavements constructed based on the above parameters are expected to carry the anticipated loads in different environmental conditions throughout their lives. The current mechanistic-empirical (ME) design approach involves prediction of the material responses under different loading and environmental conditions in a typical

pavement. Performance prediction can also be valuable for maintenance and rehabilitation as well as the life cycle cost-benefit analysis of pavements.

A typical IP, Figure 2.1, ranges from 812-1220 mm thick depending upon traffic and environmental conditions (Lewis et al. 2012). Inverted pavements are constructed by constructing a less stiff unbound granular material (UGM) sandwiched between stiffer asphalt concrete (AC) at the top and cement-treated base (CTB) at the bottom. The subgrade is provided underneath as in a conventional flexible pavement for ultimate load bearing. As the top asphalt layer in an inverted pavement is a thin layer, the unbound granular base layer (UGBL) acts as a main structural component of the structure rather than being a load transferring layer as in conventional flexible pavements. The permanent deformation characteristics, therefore, of UGMs are very important for evaluating the pavement performance under loading.

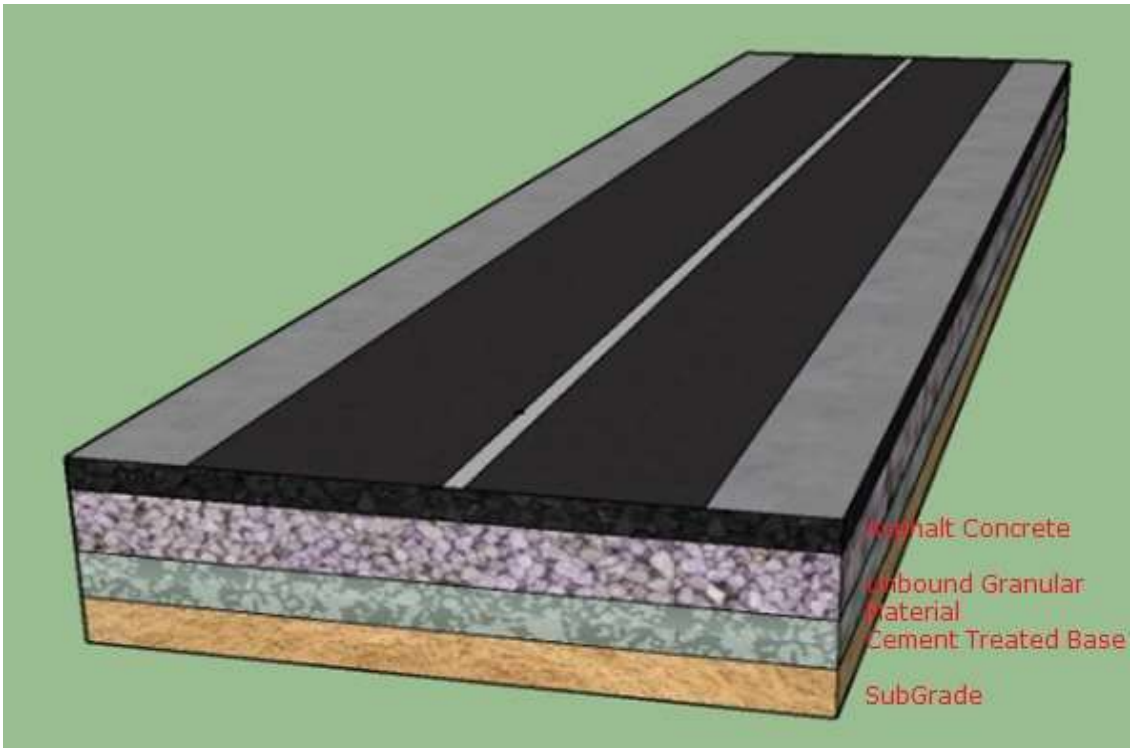


Figure 2.1: A typical inverted pavement

2.2 Permanent deformation in Unbound Granular Materials

Pavements are built in layers constructed with different materials at different levels. The materials used for constructing the pavements include hot mix asphalt (HMA) concrete, cement-treated aggregates, unbound granular materials (UGMs) and compacted subgrade soils. In a typical pavement, the stiff asphalt and cemented layers are provided to take the load from the tyre of the vehicle and distribute it over the wider sub-grade via an unbound granular layer. The UGMs are usually provided in the conventional pavements as the load-distributing component taking the load from HMA to the ultimate load-bearing sub-grade. The layer arrangement in an inverted pavement, though, makes the UGM as a structurally important layer within the pavement. As the UGM layer is constructed just beneath the thin HMA layer in an inverted pavement, the structural reliability of this layer becomes a requisite for the design engineer. The following section summarizes the performance of UGM in pavements; it also includes the factors affecting the permanent deformation (PD) performance of the UGM as well as a summary of the PD predicting models developed by researchers.

The moving wheels from the traffic impose cyclic stresses on the UGM in the pavement and they act as varying magnitudes of vertical, horizontal and shear stresses, including rotation of the principal stresses (Lekarp 1999). The resulting amount of permanent deformation in the UGM is dependent on the magnitude of the stresses and accumulates with each cycle of loading (Sharp and Booker 1984, Lekarp 1999, Gidel et al. 2001). Besides stress levels, the amount of permanent deformation is influenced by various other factors such as stress history, moisture content, density, fines content, aggregate type and principal stress rotation (Lekarp 1999).

Permanent deformation development is considered to consist of two phases. Initially, the permanent deformation in unbound granular materials increases rapidly with each load application. This phase is termed as post-compaction where material densifies, pore volume reduces and volumetric changes in material occur (Werkmeister et al. 2004, El-Basyouny et al.

2005). The deformation rate becomes nearly constant in the second phase and only volume changes occur in material although shear deformation rises at an increasing rate (Werkmeister et al. 2004). At failure, only shear strain occurs, and no volume change (EL-Basyouny et al. 2005). According to Tholen (1980), permanent deformation is caused by compaction, crushing and material migration. Permanent deformation in unbound granular materials is believed to be better explained by two theories named as shakedown theory and anisotropic concept. The following is a brief introduction to both the philosophies.

2.2.1 Shakedown Theory

Sharp and Booker (1984) and Sharp (1985) introduced a new concept to characterize the performance of unbound granular materials under loading called shakedown theory. The shakedown theory has since proven in many studies to be capable to characterize the different responses of unbound granular materials under traffic loading (Arnold 2004, Werkmeister et al. 2004, Werkmeister 2006, Tao et al. 2010). The accumulation of permanent deformation with the applications of a number of load cycles can be of three different types according to different studies (Dawson and Wellner (1999) and Werkmeister et al. (2001). The shakedown ranges are shown in Figure 2.2 and Figure 2.3.

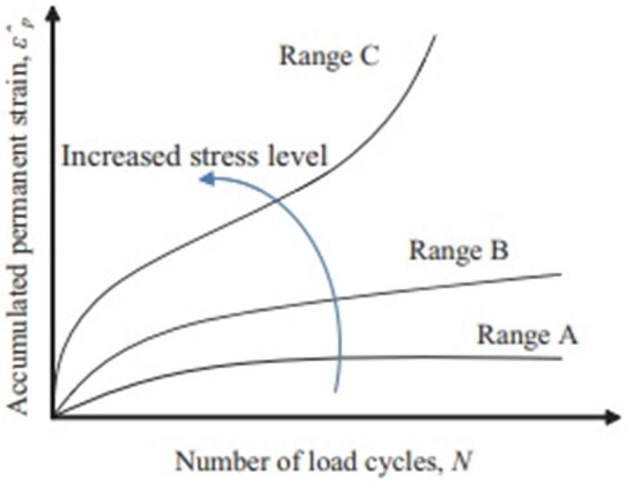


Figure 2.2: Shakedown ranges

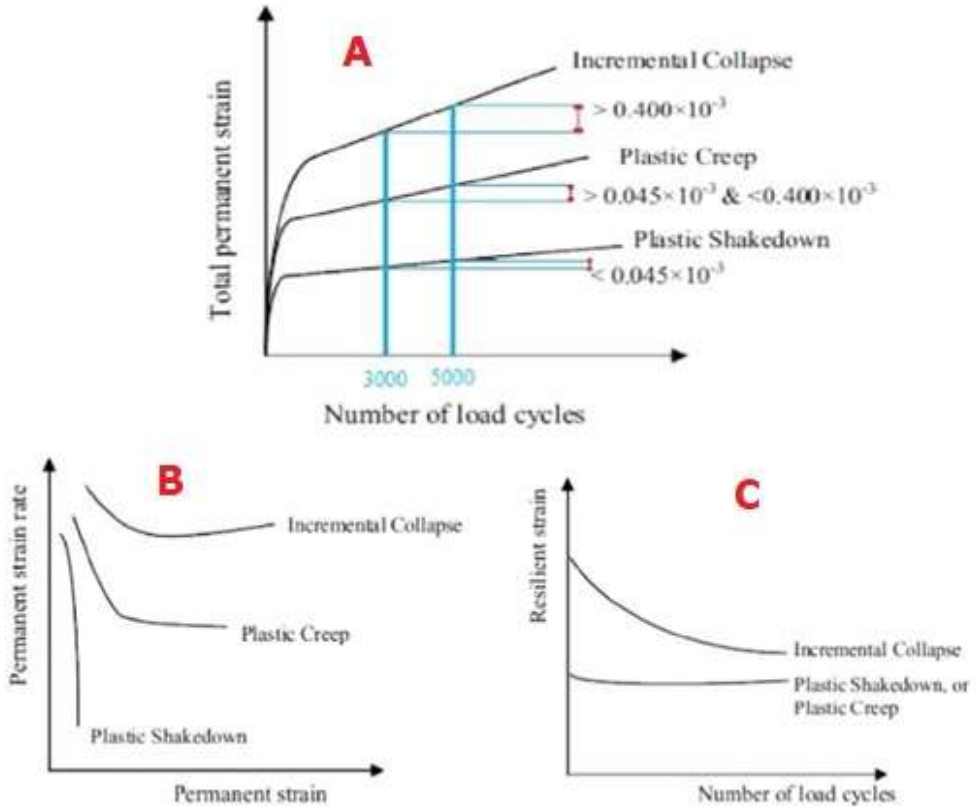


Figure 2.3: Permanent deformation behaviour of UGMs based on shakedown theory

Range A – plastic shakedown range: Up to a certain stress level, the post-compaction is completed after a finite number of load applications and the material stabilises with no further permanent strain. Then, the response becomes entirely resilient.

Range B – intermediate response (plastic creep): For a stress level higher than that for range A but lower than a certain level the permanent strain rate (per cycle) decreases from high to a low and nearly constant level during the first several load cycles. Then, the permanent strains continue to accumulate at a very slow rate.

Range C – incremental collapse: For stress levels higher than for range B, the permanent strain rate decreases very slowly compared with ranges A or B or not at all. Accumulation of permanent strain continues with load applications, leading to failure.

To define the shakedown boundaries, Werkmeister (2003) suggested the following criteria based on Repeated Load Triaxial Test (RLTT) results

performed on crushed Granodiorite aggregates by applying a range of confining pressure (70,140,210 and 280 kPa) with additional deviatoric stress ranging from 105 to 840kPa at a frequency of 5Hz. These have also been adopted in the European Standard EN-13286-7 (CEN 2004a):

$$Range - A: \left(\hat{\varepsilon}_p^{5000} - \hat{\varepsilon}_p^{3000}\right) < 0.045 \times 10^{-3}$$

$$Range - B: 0.045 \times 10^{-3} < \left(\hat{\varepsilon}_p^{5000} - \hat{\varepsilon}_p^{3000}\right) < 0.4 \times 10^{-3}$$

$$Range - C: \left(\hat{\varepsilon}_p^{5000} - \hat{\varepsilon}_p^{3000}\right) > 0.4 \times 10^{-3}$$

where ε_{p3000} and ε_{p5000} are accumulated permanent strains at the 3000th and 5000th load cycles, respectively, in an RLTT. According to Werkmeister et al. (2001), Range A behaviour is permitted in the pavement, Range B behaviour may be permitted for a certain maximum number of load cycles, whereas Range C behaviour should not appear in a well-designed pavement.

2.2.1.1 Historical Perspective of Shakedown Concept

Historically, permanent deformation behaviour of unbound granular materials is studied and modelled using analytical models (Lekarp and Dawson 1998), plasticity theory-based models (Bonaquist and Witczak 1997; Desai 2002; Chazallon et al. 2006) and the shakedown theory (Cerni et al., 2012). In the newest developed models, the shakedown concept is applied to pavements (Collins et al 1993) and leads to calculating either the shakedown load (Nguyen et al. 2008; Boulbibane et al. 2005; Richard and Booker 1984) or the plastic strains and the inelastic displacements (Habiballah and Chazallon (2005).

The behaviour of unbound granular materials subjected to repeated loads remains not fully understood and is currently the subject of interesting research worldwide. Advanced laboratory testing techniques are specifically developed to understand and characterize soil response to repeated loads (Zhao et al. 2008). In the case that applied load exceeds the yield criterion of the UGM, the response of the granular material may change according to the cycles of loading. To study this phenomenon the shakedown theory was developed (Zarka and Casier, 1979). This theory was applied through limit analysis in flexible pavement layers by Sharp and Booker (1984) and Sharp 1985). According to Zhao et al. (2008), when the applied cyclic load is

above the yield limit but lower than a critical load limit, termed as the shakedown limit, the structure may exhibit some initial plastic deformation; however, after a number of load cycles, the structure ceases to experience any further plastic strain and responds purely elastically to the subsequent load. Other approaches to calculating the analytical shakedown limit in a layered flexible pavement subjected to tyre pressure can be via the upper-bound solution (Collins and Boulbibane, 1998) or the lower-bound solution (Yu and Hossain, 1998). Researchers have also tried to investigate the shakedown limits of UGM in laboratory experiments (Barksdale, 1972; Siripun et al., 2010; Cerni et al., 2012). The experimental approaches usually are conducted through long-run triaxial dynamic loading tests performed in various stress ratios for a large number of loading cycles. In recent years, attempts have been made to consider the effects of shakedown in pseudo-dynamic finite element simulation of pavement structures (Habiballah and Chazallon, 2005; Allou et al., 2009; Chazallon et al., 2009; Ghadimi et al., 2014). The advantage of using the shakedown theorems is that detailed stress and strain history are not required during calculation. Numerical tools as well are adapted to this particular problem, to solve complex multi-physics equation systems (Yu and Hossain 1998; Werkmeister et al. 2004; Wang and Yu 2013; Sharp and Booker 1984).

A model has been developed based on the shakedown theory by Allou et al. (2007) to predict the permanent deformation in the unbound granular base layer in low traffic pavements. Chazallon et al (2009) modelled the rutting in two flexible pavements using a finite element program by incorporating a shakedown theory-based permanent deformation model for unbound granular materials. Rahman and Erlingsson (2016) performed triaxial tests to study the moisture dependent permanent deformation behaviour of unbound granular materials using the shakedown concept. Gu et al (2017) characterized and predicted the permanent deformation behaviour of unbound granular materials for pavement ME design. They evaluated the permanent deformation behaviour of the unbound granular materials based on shakedown theory and developed a prediction model. Saberian et al. (2019) studied the permanent deformation behaviour of recycled concrete aggregates and crushed rocks containing crumb rubber and crushed glass

in a series of repeated load triaxial tests. The permanent deformation behaviour was evaluated by following Werkmeister's shakedown criteria. The results indicated the suitability of recycled concrete aggregates as a base and sub-base layer in the pavement. In another study, Saberian and Li (2019) studied the suitability of recycled concrete aggregates in the pavement sub-layers by applying the shakedown limits.

2.2.2 Aggregate Anisotropic Characterization

The load in a conventional flexible pavement base layer is distributed to the underlying layers by aggregate interlock. This is achieved by the compression and shear forces between the aggregate particles which are oriented in a chainlike manner (Tutumluer and Thompson 1997). As tensile forces cannot be transferred in such a manner, the horizontal application of such forces affects the behaviour of the aggregate base layer depending on the directional dependency of material stiffnesses which can only be considered in an anisotropic approach rather than isotropic. A more realistic and accurate determination of the stresses, strains and deformations can be made possible with a basic understanding and application of anisotropic behaviour of the aggregates in a base layer. Currently available mechanistic pavement design methods are based on linear elastic programs for predicting the load-induced stresses, strains and deformations in a pavement. The conventional linear elastic programs neither consider the horizontal stiffness of the material nor the residual stresses induced by the compaction in the layer. It has also been well demonstrated that the pavement response to wheel induced load is typically non-linear (Tutumluer, 1995; Brown and Pappin 1981; Thompson and Elliott 1985). Further, the linear elastic response does not consider the compaction and applied loading induced anisotropic behaviour of the granular materials.

During the application of the wheel loads on the pavement, most of the deformations are recoverable and considered as elastic. The elastic response of the aggregates can generally be determined in small strain range under static unloading conditions. The other instrument for determining the elastic response of granular materials can be the repeated load triaxial test conducted for the resilient response (Tutumluer, 2008). The elastic stiffness of a granular medium has customarily been shown by

resilient modulus (M_R). It is defined as repeatedly applied vertical stress (deviator stress), applied usually in the triaxial test setup, divided by the recoverable axial strain in the specimen. Different studies have shown that the resilient response of pavement materials is non-linearly elastic making resilient modulus dependent upon the stress state (Tutumluer 2008; Uzan et al. 1992; Uzan 1985; Boyce 1980).

The performance of unbound granular materials depends upon the arrangement of the particles at any instant which is characterized by the UGM physical properties, construction equipment, method and loading and environmental conditions. In a typical base layer of flexible pavement, an apparent (directional) anisotropy is induced during the construction by the preferential directional placement of particles which is further aided by the loading from compaction equipment and traffic. With the increase in the aggregate stiffness, the deformability in the vertical direction decreases resulting in a high elastic modulus achieved in this direction. This load transfer is achieved by the compression and shear forces between the aggregate particles which are oriented in a chainlike manner (Dobry et al. 1989). The grain to grain transfer mechanism, however, cannot accommodate tensile forces. With the horizontal application of such tensile forces, the behaviour of the granular materials is affected by the material stiffness's dependency on direction. An anisotropic consideration for analysis can arguably accommodate such direction-dependent (anisotropic) stiffness of the granular particles (Tutumluer 2008; Tutumluer 1998; Tutumluer 1995). The unbound granular materials exhibit an exceptional anisotropy, called cross-anisotropy, under the application of compaction and wheel induced loadings.

The resilient modulus M_R is used to describe the stiffness of the pavement layers (Hicks and Monismith 1971). Researchers have developed many different laboratory test methods over the years to measure resilient modulus (FHWA 1996; Tutumluer and Seyhan 1999; NCHRP 2002; Puppala 2008). The tests have been developed to simulate the traffic loading and compaction of the pavement similar to the field conditions. However, studies and experience have shown that laboratory compaction cannot perfectly simulate the actual roller compaction and the complexity of the

stresses in-situ is very difficult to be meet in laboratory tests (Kim and Tutumluer 2005). Furthermore, most of these tests don't consider the anisotropy, inherent as well as stress-induced, of the granular material which has a considerable effect on the pavement response under given loading conditions (Kim et al. 2005; Al-Qadi et al. 2010; Wang and Al-Qadi 2013). Many techniques have also been developed by researchers to measure granular material stiffness in-situ (Fleming et al. 2000). A few types of equipment including the Falling Weight Deflectometer (FWD), Lightweight Deflectometer (LWD) and seismic Pavement Analyser (SPA) are also commercially available for in-situ stiffness measurement for UGMs (Nazarian et al. 1993; Fleming et al. 2007; NCHRP 2008). Surface deflections under impulse loading are measured in the first two methods whereas the third method uses a wave propagation technique to measure the stiffness. It can be seen from recent findings by the researchers that a good correlation exists between the laboratory and field measured stiffness using wave propagation and the in-field resilient modulus of the granular materials (William and Nazarian 2007; Schuettpelz et al. 2010).

The material's resilient properties are considered to be the same in all directions in isotropic representation while the anisotropic approach has different elastic modulus and Poisson's Ratio in horizontal and vertical directions. There are usually five material properties which are needed for an anisotropic representation of the material; resilient moduli values in vertical and horizontal (radial) direction (M_R^z and M_R^r), shear modulus in the vertical direction G_R, Poisson's ratio for strain in the vertical direction due to horizontal direct stress v_z, Poisson's ratio for strain in any horizontal direction due to horizontal direct stress v_z (Zienkiewicz and Taylor 1989). The variables, n and m, represent the ratio of modulus in the horizontal direction to modulus in the vertical direction and shear modulus in the z-direction to modulus in the vertical direction respectively. All these parameters are shown in Figure 2.4 (Tutumluer 2008).

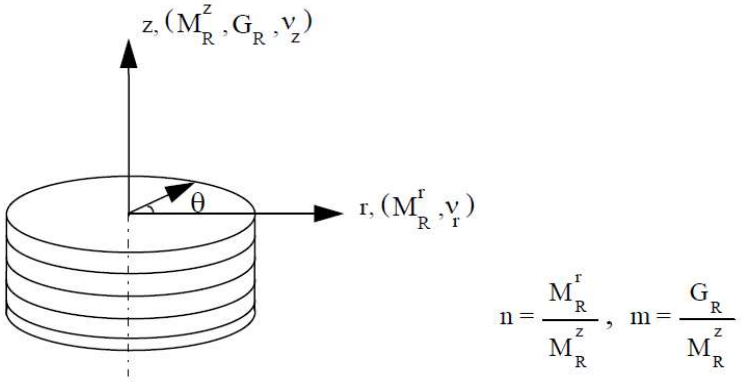


Figure 2.4: Stratified cross-anisotropic material under axial symmetry (after Tutumluer 2008)

Many types of equipment have been used for determining the anisotropy of unbound granular materials with advantages and disadvantages. One of the most used tests to find the anisotropy of granular materials is the repeated load triaxial test. The main advantage associated with the triaxial test is its ability to capture the axial as well as radial deformation on a specimen comparatively easily. Generally, some additional arrangement is required to capture the lateral strain of the specimen. There have been many different additions made in the past for finding specimen lateral strain including Bison coils attached to the membrane (Allen 1973), radial strain gauges attached to the specimen at mid-height (Hicks 1970) and three radial non-contact transducers placed 120 degrees apart around the specimen (Crockford et al. 1990).

2.2.2.1 Historical perspective of anisotropic consideration

The anisotropic approach for aggregate characterization in the pavement has been considered previously at Georgia Institute of Technology and University of Illinois (Tutumluer 1995; Tutumluer and Thompson 1997a). This approach enabled researchers to determine the stiffness modulus in the horizontal and shear direction in addition to the conventional vertical direction. The modulus in horizontal and shear directions was found to be a fraction of the modulus in the vertical direction (Tutumluer 1995; Tutumluer and Thompson 1997a). Unlike the isotropic approach, the horizontal stiffness was found to be much lower than the vertical stiffness under anisotropic consideration. These stiffnesses were not assumed, rather

predicted by the non-linear stress-dependent models based on triaxial test specimen data. It has been documented that the researchers used a cross-anisotropic approach to model both important parameters of the granular materials, i.e. direction-dependent stiffness and dilative behaviour (Tutumluer 1995; Tutumluer and Thompson 1997a).

A conventional flexible pavement was modelled by Tutumluer and Thompson (1997b) by using the GT-PAVE finite element program. It was attempted for the first time to use three stress-dependent M_R models in a cross-anisotropic base to entirely define the resilient behaviour of granular material in vertical, horizontal and shear planes.

$$M_R = K_A\, p_a\, (I_1 / p_a)^{KB}\, (\tau_{oct} / p_a)^{KC}$$

where M_R is resilient modulus, $I_1 = \sigma_1 + \sigma_2 + \sigma_3 = \theta$ = first stress invariant or bulk stress, $\tau_{oct} = 1/3\{(\sigma_1-\sigma_2)^2 + (\sigma_1-\sigma_3)^2 + (\sigma_2-\sigma_3)^2\}^{1/2}$ = octohedral shear stress or for triaxial conditions ($\sigma_2=\sigma_3$), $\tau_{oct} = 0.471\sigma_d$ ($\sigma_d = \sigma_1-\sigma_3$ = deviator stress), pa = atmospheric pressure (100 kPa or 14.7 psi) and KA, KB, KC = material constants obtained from repeated load triaxial tests. The three cross-anisotropic moduli, each modelled by the same stress dependent functional form similar to the models proposed by Lade and Nelson (1987) Uzan (1985) and Uzan et al. (1992), have following model parameters;

		I_1	τ_{oct}
	Co-Efficient	Exponent	Exponent
Horizontal Resilient Modulus M_R^h	K_1	K_2	K_3
Vertical Resilient Modulus M_R^v	K_4	K_5	K_6
Shear Resilient Modulus G_R	K_7	K_8	K_9

where K_1-K_9 are the parameters for models which can easily be obtained from the triaxial test data. The researchers also reported the horizontal and shear stiffness to be in the range of 3-21% and 18-35% of the vertical stiffness for certain types of aggregates (Tutumluer 2008). They also reported the lower values of horizontal stiffness ratio (M_R^h / M_R^v) under the wheel load which increased radially away from the centreline reaching up

to approximate value of 1 which is a condition for isotropic material behaviour as shown in Figure 2.5.

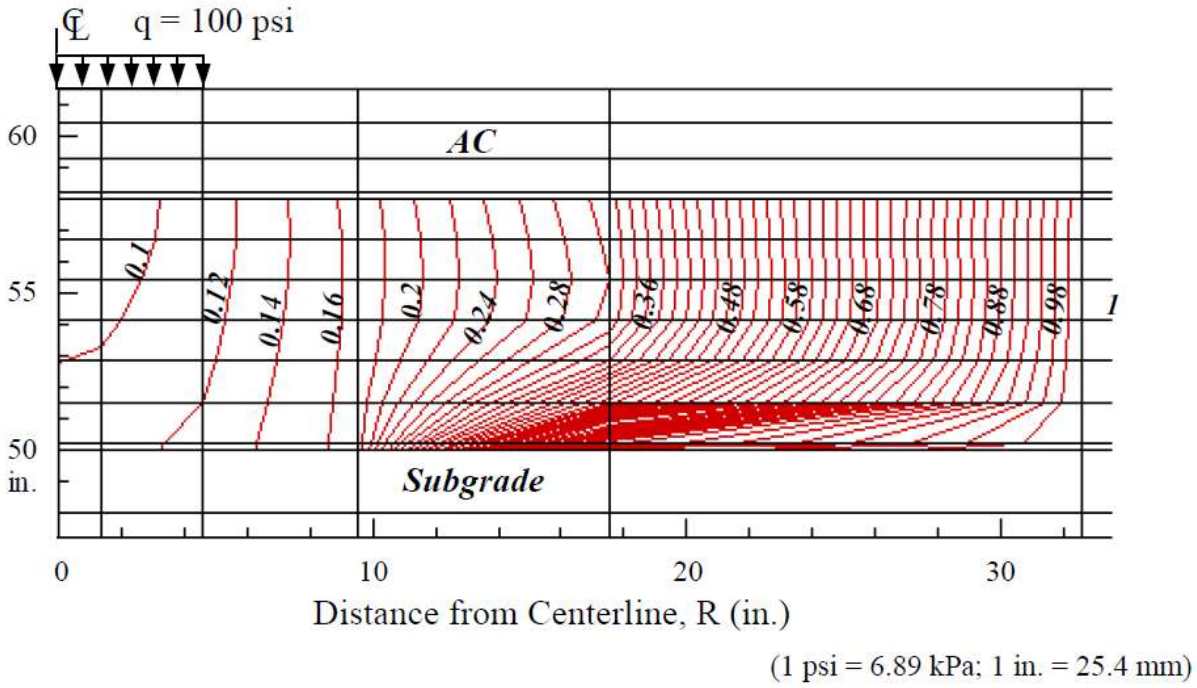


Figure 2.5: Horizontal stiffness ratio (M_R^h/M_R^v) distribution throughout the base in the presence of 20.7 kPa horizontal residual stresses (after Tutumluer and Thompson, 1997b)

It has also been mentioned that residual stresses induced have a significant effect on granular material behaviour, especially horizontal stiffnesses calculations. These stresses offset any lower magnitude tensile stress while providing confinement radially away from the centreline (Garg et al. 1998; Tutumluer and Thompson 1997a-b; Tutumluer 2008).

The lack of equipment for determining anisotropic properties has been one of the hindrances in adopting the anisotropic approach for granular material characterization. Standard triaxial tests applying repeated loads on the specimen in the laboratory are not capable of applying the most damaging field loading conditions to calculate the deformations, permanent and resilient, of the unbound granular base layer under the moving loads. Researchers have attempted to modify the triaxial test apparatus for capturing the field conditions as much as possible in the laboratory. One such equipment for the purpose was reported by Tutumluer and Seyhan (1999). An advanced triaxial machine, named University of Illinois FastCell

(UI-FC) was reported to be capable of determining the resilient anisotropic properties of granular materials in the laboratory. The equipment, being able to independently cycle stresses in horizontal and vertical directions, was ideal to simulate the dynamic stresses on the sample and thus characterize the granular materials using a stress-dependent anisotropic approach. The concept of directional dependency (anisotropy) of granular material stiffness was well supported by the initial results obtained from the tests conducted on four different types of aggregates. The stiffness modulus calculated using stress-strain equations varied significantly in horizontal and vertical directions under applied stress states. The application of the same set of stress states in the same testing procedure on a synthetic material having isotropic properties in all directions revealed the same stiffness modulus in all the directions. The Figure 2.6 shows the higher resilient modulus in vertical directions at all stress states for crushed limestone.

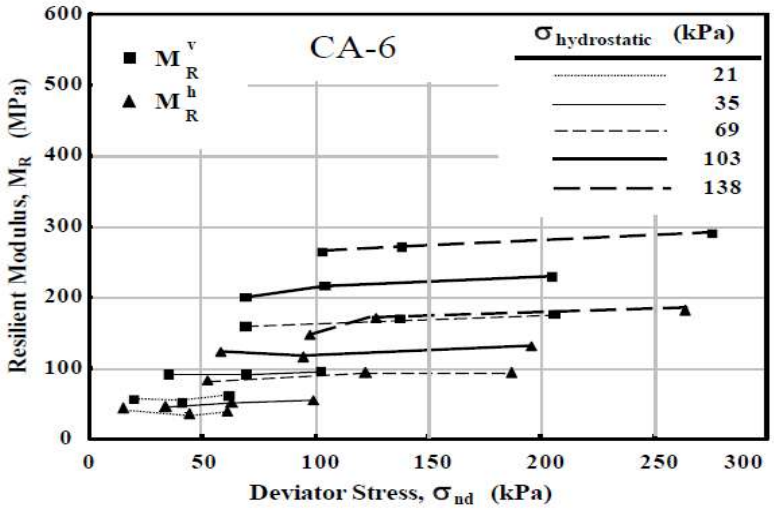


Figure 2.6: Typical variations of vertical and horizontal moduli with deviator stress for crushed limestone (after Tutumluer and Seyhan, 1999)

Similar trends were observed by Allen (1973). The modulus calculated for the crushed stone was found to be greater in the vertical direction compared to the horizontal counterpart as shown in Figure 2.7.

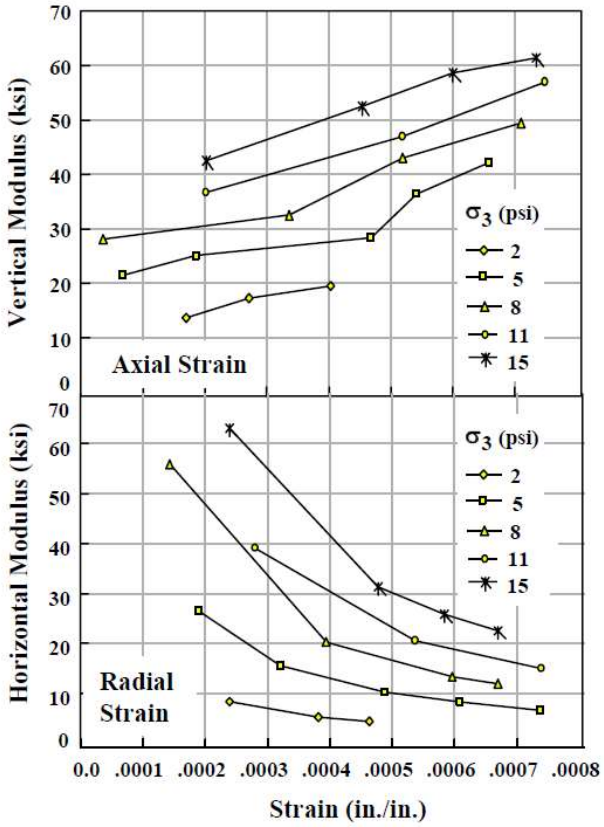


Figure 2.7: Modulus variations in horizontal and vertical directions (after Allen 1973)

Moreover, the relationship between the anisotropy and the stress ratio (σ_1/σ_3) was also studied. The stiffness anisotropy of granular materials tends to increases with the stress ratio (Tutumluer 1997). The Figure 2.8 shows the relationship between anisotropy and stress ratio. Similar trends were also observed by Lo and Lee (1990) and Konishi (1978). Konishi also commented on the increase in vertical stiffness as compensation for the reduction in horizontal stiffness resulting in the same volumetric stiffness.

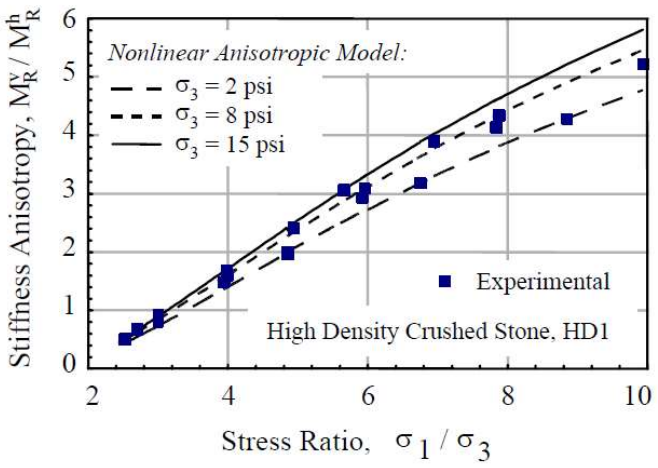


Figure 2.8: Relationship between stiffness anisotropy and stress ratio (after Tutumluer 1997)

The research was further extended to compare the radial stresses predicted by the non-linear anisotropic model with the linear elastic programs. By using the constant modulus value of 152 MPa (22 ksi), calculated by the non-linear approach, in the granular layer, the isotropic linear elastic approach was adopted for analysis. The comparative results are shown in Figure 2.9. The effect of compaction induced compressive residual stress 21 MPa (3 ksi) incorporated in the non-linear analysis is also shown in Figure 2.9.

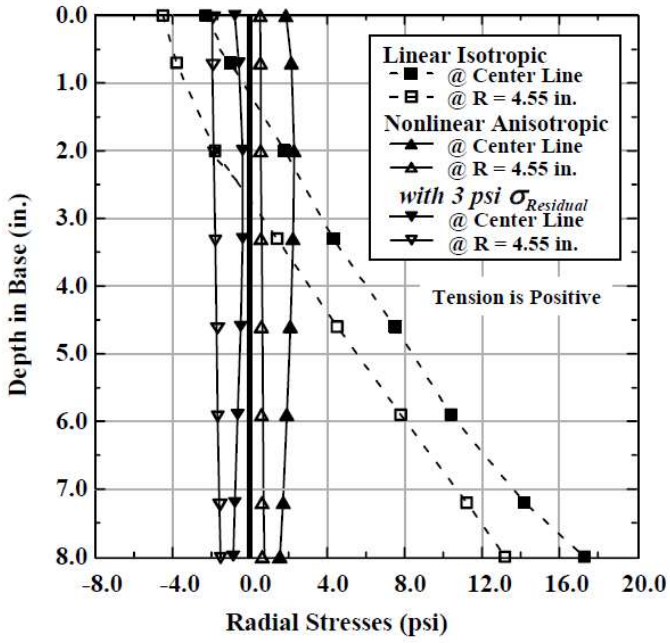


Figure 2.9: Comparative radial stresses through unbound layer (After Tutumluer and Thompson 1997)

The research team at the International Centre for Aggregate Research (ICAR), USA developed predictive models for resilient and permanent deformation of the unbound aggregate layer in a pavement structure. The research team also worked on the development of a testing protocol for determining the stiffness modulus of aggregates. The protocol developed is not as complicated as the advanced triaxial testing procedure. The stress sensitivity and anisotropic behaviour are evaluated by applying three different stress regimes to the specimen where each regime has ten different stress levels. It was found from the test results that non-linear and anisotropic stress sensitivity best describe the aggregate behaviour within a pavement under loading. More realistic stress distribution within the granular layer can be achieved by adopting anisotropic considerations (Tutumluer 2008). Seyhan et al. (2005) conducted a stress excursion analysis to study granular material under different stress paths. Crushed aggregates triaxial specimen were prepared and tested under five different stress paths which were believed to be representative of wheel load-induced compression and extension type stress states. Generally, larger modulus values in the vertical direction were observed. Some critically low values of modulus in the vertical direction were also observed at some extension states (Seyhan et al. 2005).

The concept of the anisotropy has long been related and studied for characterizing unbound granular materials (Al-Qadi et al. 2010). Attention to the presence of anisotropy in other layers was commenced by Masad et al. (2002). They conducted extensive laboratory testing on AC specimen to study the anisotropy. They reported 30% more stiffness modulus in the horizontal direction than the vertical stiffness modulus. They also noted a decrease in stiffness anisotropy with the decrease in mixture temperature (Masad et al. 2002). The next step towards anisotropic considerations for AC was taken by Wang et al. (2005). Laboratory tests performed on 4-inch (100mm) AC specimen in a servo-controlled triaxial cell indicated the existence of anisotropy, i.e. different stiffness moduli were observed in horizontal and vertical directions. Motola and Uzan (2007) also reported as much as 40% anisotropy in AC by conducting dynamic modulus testing on AC specimens.

In a recent study, the stress-strain response of the pavement was evaluated by considering the anisotropic approach in all the layers, i.e. AC, base and subbase (Tarefder et al. 2016). An actual field pavement section was studied to understand the effect of directional (anisotropy) and stress dependency of layers on the pavement performance under loading. Falling Weight Deflectometer (FWD) measured deflection and strain values at the test section were used in the Finite element program, ABAQUS, to validate the selected model. Anisotropic effects were then studied by subjecting this model to actual dynamic traffic loading. The research study concluded that the horizontal tensile strain at the bottom of AC and vertical strains on top of all layers decrease when the horizontal stiffness modulus increases. Therefore, the decrease in horizontal stiffness modulus increases the chances for fatigue damage and permanent deformation. Furthermore, the unbound subgrade was observed to be less sensitive to cross-anisotropy as compared to other layers as shown in Figure 2.10.

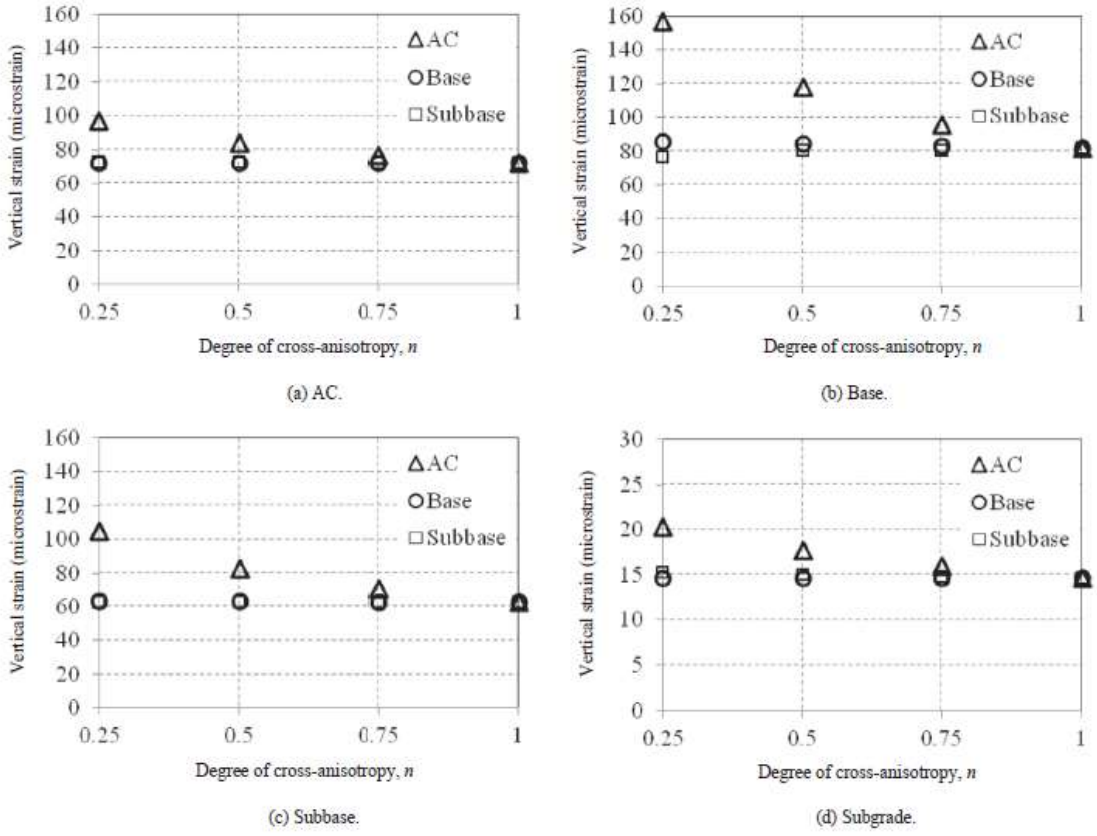


Figure 2.10: Cross-Anisotropy of Pavement Layers (After Tarefder et al. 2016)

The materials used in constructing pavements have been characterized by well-equipped pavement laboratories as well as by field studies. These studies, therefore, help researchers to constitute the mathematical predictive models to be used in mechanistic-empirical pavement design approaches. For the characterization of different pavement materials, different specialised pieces of pavement testing equipment are used, for example, unbound granular materials have historically been studied in triaxial equipment (Lekarp 1999, Uthus 2007). This test carries significance in characterizing the unbound granular materials due to its ability to apply cyclic stresses, similar to the stress conditions in a pavement under load, to a pre-compacted cylindrical specimen and measure the corresponding deformations under applied stresses (Wood 1990, Gidel et al. 2001). The test data enables researchers to characterise the deformation of unbound granular materials and permanent deformation due to each load application. The triaxial test, though, is usually performed by applying a single-stage (SS) stress level where a constant amplitude cyclic stress is applied. Therefore, several test specimens have to be prepared to study the effect of different stress levels on unbound granular material performance in a SS repeated load triaxial test. Different stress magnitudes can be applied to the same Triaxial specimen in a multi-stage (MS) repeated load triaxial test (Gidel et al. 2001, CEN 2004a). The MS test has its benefits in being a better representation of a range of stresses applied to unbound layer of a pavement. It also enables researchers to consider the stress history effect on the specimen as well as being able to reduce the time, effort and finances to test several specimens as in case of SS Triaxial test. The complexity of performing triaxial tests in the laboratory has always led researchers to look for alternative ways to characterize the unbound layers. Cooper Technology developed an instrument to apply multistage stress on a specimen in the laboratory which can be a good alternative to the rather complex Triaxial for simulating in-situ stress conditions on unbound granular material. The instrument is called Precision Unbound Material Analyzer (PUMA). Another advantage of PUMA is that the horizontal stresses cycle as well as the vertical, which gives a much more realistic stress condition.

2.2.3 Factors Affecting Permanent Deformation Of UGMs

Rutting or accumulated permanent deformation (PD) is the primary distress for unbound aggregate bases in flexible pavements. Accordingly, understanding the PD behaviour of an unbound granular material (UGM) plays a significant role in the accurate evaluation and prediction of the performance of an unbound base layer (Epps et al. 2014).

The unbound granular base is a structural component of an inverted pavement. The performance of an unbound granular material (UGM) in a pavement is stress-dependent and usually characterized by its permanent deformation. Under traffic loading, the unbound granular materials undergo complex deformation behaviour. The larger part of the behaviour is resilient or recoverable and a small part of deformation under each load cycle is permanent (Lekarp 1999, Erlingsson and Magnusdottir 2002, Huang 2004). The behaviour is also shown in Figure 2.11. The accumulation of deformation under each load cycle in a pavement leads to the rutting (Lekarp 1999, Hornych and Absamad 2004, Uzan 2004, Cerni et al. 2012).

The permanent deformation of the layer is affected by a number of different factors. Of all the factors, stresses have probably the most significant effect on permanent deformation behaviour of UGM. Other factors include but are not limited to the number of load cycles, compaction density, moisture content of UGM, percentage of fines content in a UGM sample, gradation and aggregate type. In the current research, the effect of factors like stresses, number of load applications, fines content and moisture content has been studied in the laboratory.

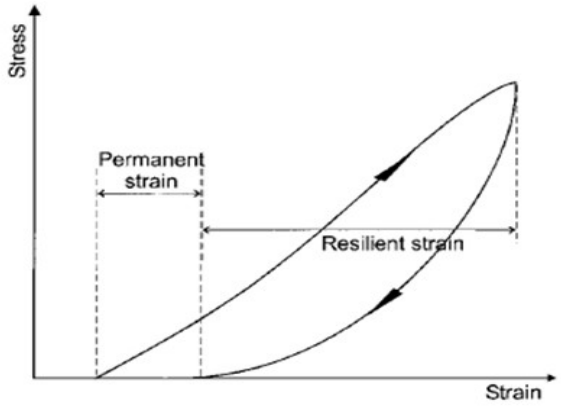


Figure 2.11: Strains in granular materials during one cycle of load application

2.2.3.1 Effect of Stress

There has been a great number of studies in which researchers have attempted to relate the stresses with the accumulation of permanent deformation in UGMs. The literature history goes to as far back as 1966 when Morgan (Morgan 1966) studied the effect of confining and deviatoric stresses on UGM in repeated load Triaxial (RLT) tests. He found an increase in accumulation of axial permanent deformation by increasing the deviatoric stresses at a constant confining stress and by decreasing the confining stress at constant deviatoric stress. The research led towards the fact that both these stresses affect the permanent deformation behaviour of UGMs in the form of some stress ratio and various researchers have studied the issue in the laboratory under different conditions including (Lashine et al. 1971; Barksdale, 1972; Pappin, 1979; Paute et al., 1996; Lekarp and Dawson, 1998).

Lashine et al. (1971) performed a few triaxial tests on a crushed rock in a partially saturated and drained environment and reported the settling of permanent deformation values to almost a constant value, related to a ratio of deviatoric stress to confining pressure. Brown and Hyde (1975) also reported similar results by studying crushed rock under constant confinement in a triaxial environment. They further described that similar results can also be obtained in a varying confining pressure test if the analyses are performed by taking the mean value of the confining stresses. Another aspect in the literature has been to study the shear strength effect on permanent deformation accumulation. This aspect has been studied by (Raymond and Williams 1978; Pappin 1979; Thom 1988; Paute et al. 1996) and many more. The concept is to consider the shear failure line as a boundary to the permanent deformation under repeated loading. The concept has been questioned by researchers like (Lekarp and Dawson 1998) who argue that the incremental nature of permanent deformation in UGMs can’t be studied under sudden collapse concept as in case of static failures tests. So, shear strength and stress levels which cause a sudden failure cannot be of great interest in the case of permanent deformation accumulation in UGMs which is a gradual process. Lekarp and Dawson

(1998) also showed that an increase in stress path length in *p-q* space, Figure 2.12, increased the magnitude of permanent strain.

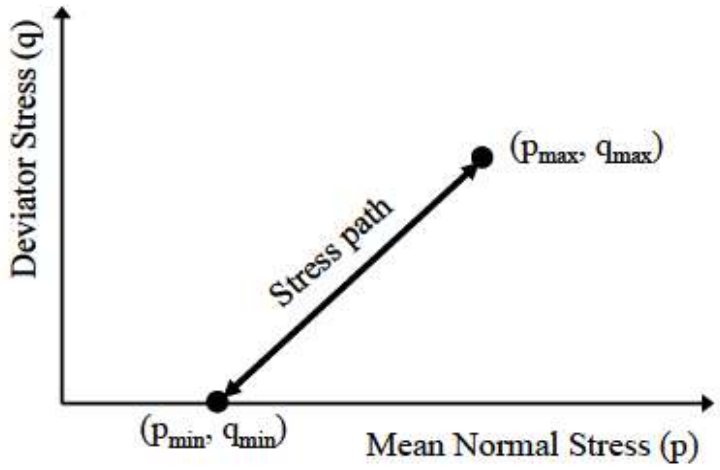


Figure 2.12: The definition of Stress path in p-q space

2.2.3.2 Effect of Number of Load Applications

The accumulation of permanent deformation in UGMs is a gradual process where every application of load contributes to it. So, the number of load applications becomes one of the most influential factors in the accumulation of permanent deformation. The effect of the number of load application on PD behaviour of UGMs has been studied historically by various researchers including (Morgan, 1966; Barksdale, 1972; Sweere, 1990; Paute et al 1996; Theyse 2002; Lekarp and Dawson 1998; Kolisoja 1998) and many more. Researchers like Morgan (1966) showed that the permanent deformation continues to increase with the number of load applications. He went on to apply as many as 2,000,000 cycles of load application and found that the PD was still increasing. Barksdale in 1972 performed triaxial tests on UGMs and reported a linear increase in permanent deformation with the logarithm of the number of load applications. He further reported that the rate of PD accumulation may increase suddenly after a relatively large number of load applications. Similar results were also reported by Maree (1978) cited in Theyse (2002). He reported a constant increase in strain rate at high-stress levels which eventually changed into an exponential increase between 5000 and 10,000 load cycles leading to failure. But, it was reported by Paute et al (1996) that permanent deformation rate in UGMs decreases constantly with the increasing number of load cycles to such a value which may be

used to define the limit value of permanent deformation accumulation. Lekarp (1997) and Lekarp and Dawson (1998) responded from tests conducted on different materials under different stress conditions that the stability in UGMs where permanent deformation rate decreases with applied load applications can only be achieved at low-stress levels whereas the rate of permanent deformation would continue to increase continuously with load applications at higher stress levels. Another study (Kolisoja 1998) conducted under a very high number of load applications revealed that the rate of permanent deformation accumulation might not be expressible as a simple function. The argument in support was the observation of a material, which was appearing to reach stable conditions, becoming unstable under further loading.

Three distinct types of behaviour of the development of permanent strain after the first 10,000 load cycles are observed from the range of literature (although researchers may have only observed one type of behaviour depending on the stress levels used):

A. decreasing permanent strain rate with increasing load cycles to a possible limiting permanent strain value
B. linear increase in permanent strain with increasing load cycles; and
C. exponential increase in permanent strain and failure with increasing load cycles.

2.2.3.3 Effect of Moisture Content

The presence of moisture has a significant effect on the permanent deformation behaviour of unbound granular materials; the presence of adequate moisture contributes towards the enhanced strength and stiffness properties of unbound granular materials. But with the increase in moisture content and approaching the saturation condition, the application of load causes positive pore water pressure which decreases the permanent deformation resistance of unbound materials. During the extensive research being carried out on unbound materials in the last few decades, researchers have attempted to study the moisture effect on permanent deformation performance under loading in the laboratory and in the field. These studies have resulted in the unanimous finding that a combination of a high degree of saturation and low permeability, due to poor drainage, leads to high pore

pressure, low effective stress, and consequently, low stiffness and low deformation resistance (Haynes and Yoder 1963; Barksdale 1972; Maree et al. 1982; Thom and Brown 1987; Dawson et al. 1996). Haynes and Yoder (1963) reported, in their research study, a 100% increase in the total axial permanent strain when the saturation was increased from 60% to 80%. Similarly, 68% greater permanent axial strain was observed in soaked samples by Barksdale (1972) as compared to those in partially saturated conditions. A relatively small increase in moisture can trigger a dramatic increase in permanent deformation rate, as stated by Thom and Brown (1987). They further stated the possibility of large permanent strain occurring without generating excessive pore water pressure in unbound material, the permanent strain apparently being due to the lubricating effect of the water on the granular assembly. Analysing RLT permanent strain tests, Dodds et al. (1999) found that aggregate contaminated with 10% clay fines did not survive for 100,000 loading cycles when saturated, while aggregate free from clay fines did survive. Maree et al (1982) conducted in-situ trials by using a heavy vehicle simulator and reported an increase in the rutting potential of granular materials due to wetting.

The stress-strain behaviour of soils and granular materials can be improved significantly by draining the system. An example of the positive effect of drainage on permanent strain development in granular materials is illustrated in Figure 2.13 for Triaxial tests with different drainage conditions.

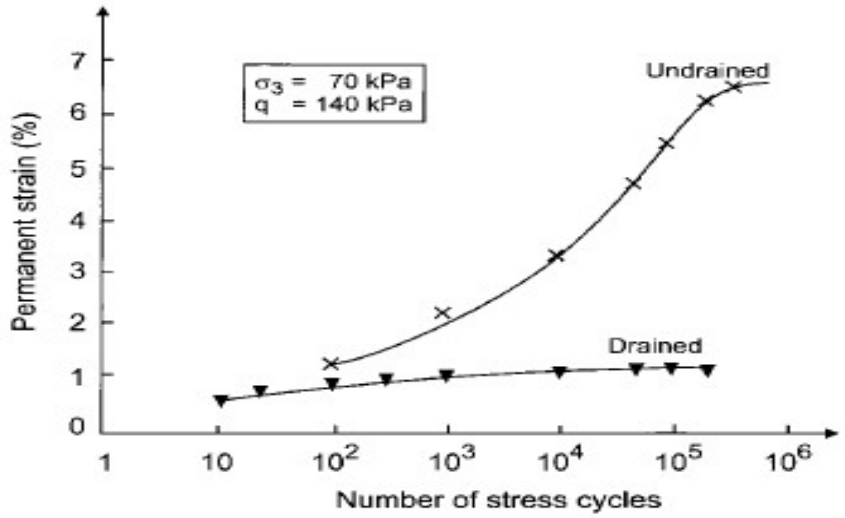


Figure 2.13: Influence of Drainage on Permanent Deformation Development (Dawson 1990)

The effect of moisture content can also be related to its effect on soil suction and thus effective stress. Excess water in aggregates increases the pore water pressure through a reduction in the amount of suction (i.e. suction moving closer to zero) which in turn decreases the effective stress.

$$p' = p - u$$

where p'= effective stress, p= total mean normal stress and u=pore water pressure

This will reduce the shear strength and result in local permanent deformation transpiring as ruts in the surface. If the aggregate becomes saturated then suction that pulls particles/stones together reduces to zero and can become negative which results in de-compaction and the development of shallow shear and potholes. If the subgrade soil is an expansive clay and water is allowed to enter the foundation, the deterioration of the pavement may be exacerbated by damaging subgrade volume changes and differential heaving. Other signs of damage due to water infiltration are the pumping of water and fines through cracks and distress associated with frost heave.

2.2.3.3.1 The concept of suction and its measurement

Water is held in the soil matrix by absorption and surface tension forces at a pressure less than atmospheric (Croney 1977). Soil moisture suction, or suction, is a measure of the pressure required to abstract water from a sample of soil which is free from external loading. Suction is expressed on the pF scale, which is the common logarithm of the height in centimetres of an equivalent column of water.

Krahn and Fredlund (1972) define the total suction as the negative gauge pressure relative to the external gas pressure on the soil water to which a pool of pore water must be subjected in order to be in equilibrium through a semi permeable membrane with the soil water. The total suction was proposed as the sum of the osmotic suction and the matrix suction and the relationship was proved by measurements of all three parameters on a variety of soils. The osmotic suction is due to the different salts which may be dissolved in the pore water and which affect the surface tension. The

matrix suction is due to the size and shape of pores in the soil skeleton and the clay particle surface absorption.

Figure 2.14 shows schematically the influence of water content on the dry density achieved (i.e. the density of the aggregate alone) during compaction; the optimum water content is the condition in which compaction is easiest and the highest densities are reached. At even higher water contents there is simply no room for all the water in the mixture without a reduction in density.

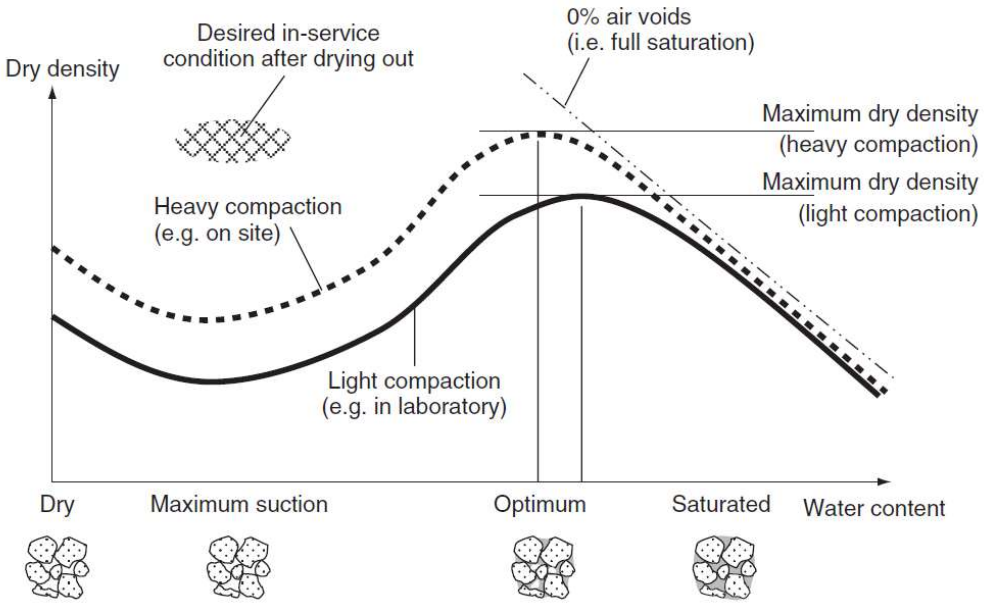


Figure 2.14: Concept of suction (after Thom 2014)

A proper appreciation of these water-related effects is crucial if a high-quality granular layer is to be achieved, and it means that the following procedure is needed.

- Mix material at optimum water content (or slightly above to allow for evaporation during handling).
- Compact at optimum water content.

A specialised instrument called a psychrometer is used for measuring the total suction in any given soil sample. The instrument uses thermocouples which measure the humidity of the air surrounding the soil sample under study. Measurements of the electrical conductivity can be used to calculate the osmotic suction. All types of suction apparatus which involve allowing the sample to reach moisture equilibrium across a porous stone or

membrane measure the matrix suction as the stones are permeable to salts dissolved in the pore water.

It was reported by Krahn and Fredlund (1972) that the changes in total suction with moisture content in any given soil sample was mainly affected by the changes in matrix section because the osmotic suction was almost constant. They also reported the dependence of the matrix suction, and hence total suction in the sample, on the specimen moisture content whereas the dry density didn't affect these properties making them independent of it. It was also reported by Shackel (1973) that the suction in soil samples was primarily influenced by the degree of saturation whereas dry density had a small affect as well. In another research by Croney et al. (1958), it was reported that in heavy clays the suction was affected to a smaller degree by the dry density. They also reported the effect of dry density on the relationship between suction and moisture content to be below approximately 2 on the pF scale for silty and sandy clays.

The dependence of suction on water content and surcharge was reported by Snethen and Johnson (1977) who showed matrix suction to be dependent while osmotic suction was independent of both. The relationship between suction and moisture content for clays was reported to have three distinct regions by Russell and Mickle (1970) where the liquid limit and the plastic limit almost represented points of inflection. They reported an approximate suction value of 3.7 on the pF scale for heavy clays as compared to the corresponding 3.2 for silty clays. It is also to be noted that a pF value of approximately 3.0 represents a vacuum.

The relationship between suction and moisture content was reported to exhibit a kind of hysteresis by Croney et al (1958) by using a pressure plate apparatus. The hysteresis was exhibited in such a way that the measured suction at any given value of moisture content depended on the moisture condition whether the sample was initially wet and then dried or was wetted from a dry state. They related it to the fact of having different suction values for emptying and filling the pores. They also found that continuously disturbed soils exhibit a unique curve showing the relationship between suction and moisture content.

These findings were not supported when varying the equipment used. For example, the use of a psychrometer by Snethen and Johnson (1977) to establish the relationship between suction and moisture content for four different soils with plasticity indices between 13 and 68 showed no hysteresis between the curves for the wetting and drying processes. They suggested the type of equipment to be the reason for the lag reported by studies involving the pressure plate apparatus.

The suction value on the pF scale was reported to be directly proportional to the log of the moisture content by Shackel (1973) ranging from pF 0.6 to pF 1.8 whereas the dry density and degree of saturation affected the relationship constants. Similar results were also documented by Croney (1977) by plotting the moisture content versus plasticity index. He reported almost linear contours of suction for the range of pF 2.0 to pF 3.0. Another study by Snethen and Johnson (1977) reported a direct linear relationship, over a range of pF 2 to pF 4.7, between suction values on the pF scale and the moisture content.

The effect of compaction technique was also reported by Mou and Cha (1981) who performed different tests on clays having a plasticity index of 19. They reported different curves for suction and moisture content for kneading and static compaction. Another finding was higher values of suction for static compaction as compared to the kneading for each sample.

2.2.3.4 Effect of Stress History

The performance of unbound granular materials in terms of permanent strain resistance at any moment depends on stress history i.e. the order of application of loads. It was shown by Brown and Hyde (1975) that the permanent strain was considerably greater under application of a single stage higher stress (50-650) as compared to strain due to the sequential increase in stresses (the rest) applied as shown in Figure 2.15. The stress values in the figure (e.g. 50-250) correspond to the major and minor principal effective stresses respectively where all the stresses were applied in incremented type of loading except 50-650 which was applied as a single stage stress.

Accelerated pavement tests (Arnold et al., 2003) showed that if the load increased, an initial sharp increase in surface deformation occurred despite

the fact that prior to this increase the rate of permanent strain was minimal and either constant or decreasing with increasing load cycles. After the initial sharp rise in surface deformation with the larger wheel load the permanent strain rate stabilised to a constant or decreasing value.

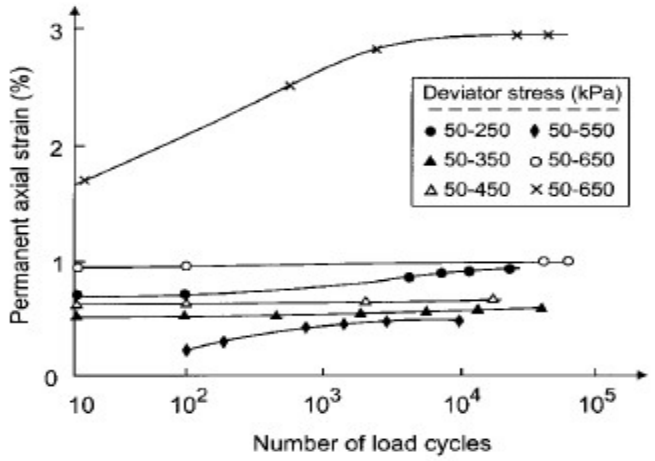


Figure 2.15: Effect of Stress History on Permanent Strain (Brown and Hyde 1975)

When repetitive loads are applied, the effect of stress history appears as a result of gradual material stiffening by each load application, causing a reduction in the proportion of permanent to resilient strains during subsequent loading cycles. Even though the effect of stress history on permanent deformation behaviour has been recognized, very limited research appears to have been done to study this effect. In laboratory permanent deformation tests, the effect of stress history is normally eliminated by using a new specimen for each stress path applied. Because of stress history effects, it is usually recommended that a new sample be used for RLT permanent strain tests at different stress levels. However, this is not always practical as a large number of tests are required to cover the full spectra of stress states that may occur within the pavement.

2.2.3.5 Effect of Density

One of the major factors affecting the long term permanent strain behaviour of unbound materials is the degree of compaction designated by density. The effect of density has been studied extensively in previous studies (Holubec 1969; Barksdale 1972, 1991; Allen 1973; Marek 1977; Thom and Brown 1988; Dodds et al. 1999). The studies have shown significant

improvement in resistance to permanent strain under loading by increasing the density of granular materials. An increase of approximately 185% in axial permanent strain was reported by Barsdale (1972) when the specimen was compacted to 95% of maximum density rather than 100%. Dodds et al. (1999) performed Repeated Load Triaxial tests on unbound materials and noted significant reduction in axial permanent strain when specimens were compacted at a lower density of 90% as compared to specimens compacted to 95% density. Allen (1973) studied the effect of density on permanent strain behaviour of crushed limestone and gravel. He reported a reduction of 80% permanent axial strain in crushed limestone and 22% in gravel from Proctor to Modified Proctor density. Another research by Holubec (1969) studied the effect of density on different aggregate shapes. They reported a significant reduction in permanent strain with increased density for angular particles in the case of no accompanying increase in the transient pore pressure during repetitive loading. No significant reduction in permanent strains by increasing density was reported for round-shaped aggregate particles, the reason being the higher initial density for rounded aggregate compared to that of angular under the same compaction effort.

2.2.3.6 Effect of Grading, Fines Content, and Aggregate Type

The effect of density on axial permanent strain performance of unbound granular materials was reported in the previous section which in turn depends on grading, fines content and type of aggregates. Dunlop (1966) found a decrease in axial permanent strain if the density is increased by a change in grading and keeping the compaction effort the same. Thom and Brown (1988) conducted RLT permanent strain tests on crushed dolomitic limestone at a range of gradings and compaction level, Figure 2.16. They reported the least axial permanent strain in uniformly graded materials under un-compacted condition. When the specimen was heavily compacted, the resistance to axial permanent strain was similar at all the gradings. The grading parameter "n" was adopted in the study to achieve a good spreading of the material gradation as shown in Figure 2.17.

Another study was conducted by Dawson et al. (1996) who found the effect of grading on permanent deformation to be more significant than the degree of compaction; they reported the maximum resistance to permanent strain

for the densest mix. The same behaviours were also observed by Kamal et al. (1993). The difference between the findings of Thom and Brown and the other researchers may be due to the fact that a very wide range of gradings and densities were adopted in the study by Thom and Brown which were very different and exceeded the range likely to be experienced in a pavement under loading. Another possible reason for this difference could be the fact that they performed their experiments on 100% dry materials as opposed to the most of the other studies.

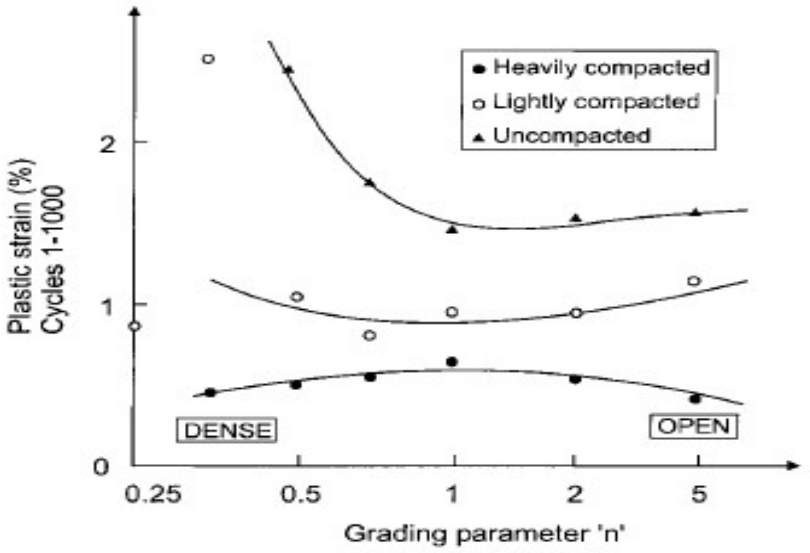


Figure 2.16: Effect of Grading and Compaction on Plastic Strain (Thom and Brown 1988)

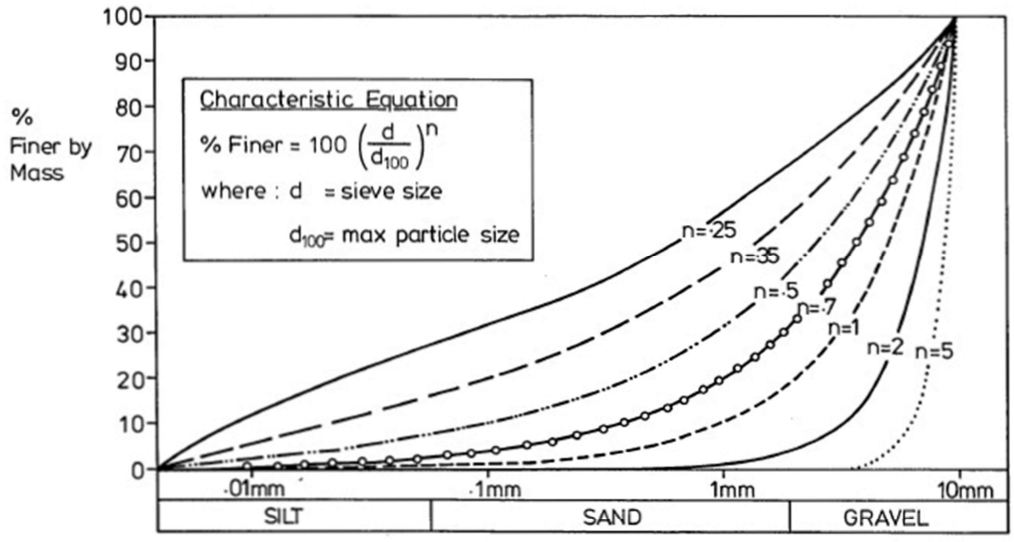


Figure 2.17: Grading parameter "n" definition (After Thom 1988)

It was discovered in Repeated Load Triaxial tests by (Barksdale, 1972, 1991; Thom and Brown, 1988) that the permanent axial deformations increase with an increase in fines contents of the materials used. The same hypothesis was also supported by Dodds et al. (1999) who found the highest deformations with the addition of 10% fines content. He observed the development of higher pore water pressure for the granular materials with higher fines content. The excessive pore water pressure reduced the effective stress thereby reducing the beneficial level of confinement.

The effect of surface characteristics of the different aggregate types of the same density on permanent strains was studied by Allen (1973). He found less permanent strains in angular materials like crushed stone as compared to rounded aggregates particles like gravel. The better behaviour of angular materials is attributed to the higher angle of shear resistance in these materials due to better particle interlock. Barksdale and Itani (1989) investigated the influence of aggregate shape and surface characteristics on aggregate rutting. They concluded that a blade-shaped crushed aggregate is slightly more susceptible to rutting than other types of crushed aggregate. Moreover, cube-shaped, smooth rounded river gravel was almost two times more susceptible to rutting than crushed aggregates.

2.2.3.7 Effect of Variable and Constant Confining Pressure

The RLT test conditions in terms of variable confining pressure (VCP) or constant confining pressure (CCP) also affect the magnitude of permanent strain. Variable confining pressure best matches conditions in the field but is more difficult to test in the laboratory. Therefore, CCP conditions are commonly used in the RLT apparatus as done by Sweere (1990). This was justified by Sweere who reported that there is a correlation between testing at VCP and CCP. Apparently, the result from testing at CCP is the same as testing at VCP, provided the CCP is half the maximum confining pressure in the VCP test, which is the average value.

2.2.3.8 Effect of Principal Stress Rotation

Reorientation of principal stresses during shear is a feature of the induced stresses associated with many field loading situations. The influence of reorientation on soil strength and stress-strain response needs to be considered for a reliable prediction of in-situ behaviour. The effect of

principal stress reorientation on permanent strain is not yet fully understood. This is probably due to the constraint of the triaxial test, the most commonly used laboratory test for reproducing in-situ loading conditions in the laboratory, not to be able to provide continuous change in principal stress orientation.

Nevertheless, the literature available indicates that principal stress reorientation in granular materials under vehicular loading results in larger permanent strains than those predicted by cyclic triaxial testing. Youd (1972) investigated the behaviour of sands in a cyclic shear box and noted a marked increase in density as a result of the rotation of the principal stress axes. The density increase was then shown to be directly related to the magnitude of the observed cyclic shear. Similar observations were reported by Ansell and Brown (1978) for crushed limestone.

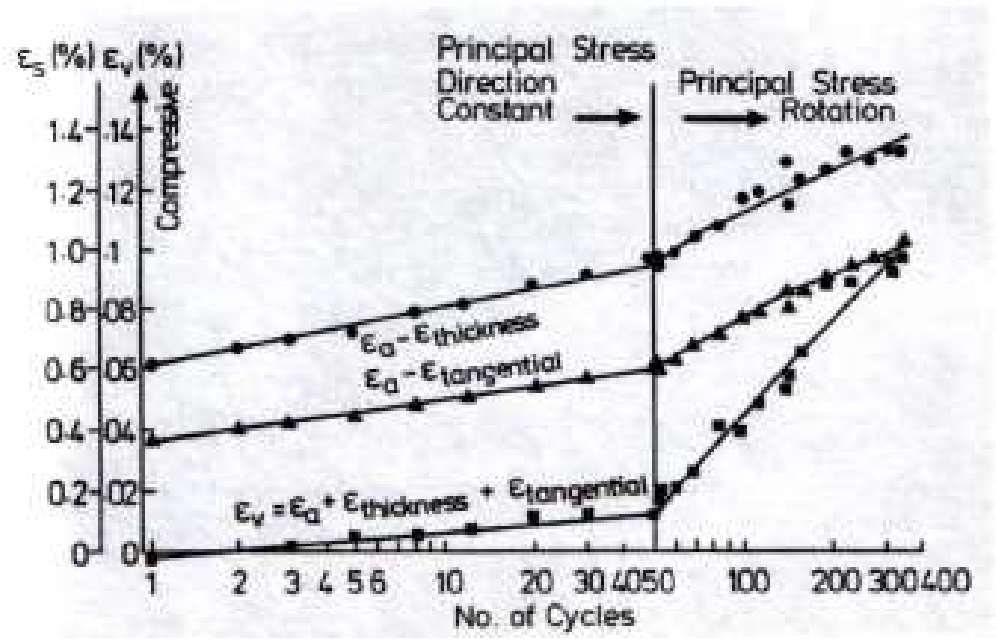


Figure 2.18: Effect of principal stress rotation on the accumulation of permanent strain (after Thom and Dawson, 1996)

Chan (1990) observed the effect of shear stress reversal on permanent strain in hollow cylinder tests on crushed limestone both with and without the application of shear stress. The tests with shear stress reversal showed much higher permanent strain than tests with no shear stress. Higher permanent strains were also obtained from bi-directional compared with uni-directional shear reversal. Uni-directional shear reversal simulates the stress condition under a wheel load moving in one direction. It follows that

bi-directional is the case where the wheel load moves forward and backwards over the same position. It was also found that the higher the ratio of shear stress to normal stress the higher the permanent strains.
Other tests by Thom and Dawson (1996) with the hollow cylinder apparatus found similar results to Chan (1990). Figure 2.18 (Thom and Dawson, 1996) shows that the permanent strain increased significantly when stress cycling was accompanied by principal stress rotation. Taking the points on Figure 2.18 it is clear that there is a significant increase in the rate of permanent strain development due to the effect of introducing principal stress rotation.

2.2.4 UGM Permanent deformation models

Predicting the accumulation of permanent deformation in UGM using mathematical models requires taking into account the various factors that affect permanent deformation. The models available in the literature mostly consider the accumulation of permanent deformation either as a function of the number of load applications or as a function of stress level. Some of the models combine the influence of the number of load cycles with the stress level. However, these models do not explicitly consider the other factors mentioned earlier. Lekarp (1999) and Hornych and Absamad (2004) have summarised the available permanent deformation models as relationships describing the influence of the number of load applications and relationships describing the influence of applied stresses.

Historically, researchers have developed various permanent deformation models based on one or more factors affecting the behaviour under loading. The prediction model development goes as back as to the 1960s when Booker worked on various projects to study the permanent deformation of unbound granular materials. A model was developed by Tseng and Lytton in 1989 which relates stress level to permanent deformation, assuming a linear relationship between the two parameters, and also combines the effect of the number of load applications. This model is also used in the Mechanistic-Empirical Pavement Design Guide (MEPDG) (ARA 2004) and is expressed as;

$$\hat{\varepsilon}_p\,(N) = \varepsilon_r \varepsilon_0\, e^{-(\rho/N)^{\beta}}$$

Table 2.1: Permanent deformation predictive models history in UGMs

Sr. No.	Model	Authors	Year	Supporting Equations	Parameters
1	$\varepsilon_p = a + b\log N$	Barksdale	1972		a and b are regression parameters
2	$\varepsilon_p = aN^b$	Monismith et al	1975		a and b are regression parameters
3	$\hat{\varepsilon}_p(N) = \varepsilon_r \varepsilon_0 \, e^{-(\rho/N)^\beta}$	Tseng and Lytton	1989	$\log\beta = -0.61119 - 0.017638\, W_c$	ε_0, β, ρ= regression parameters W_c = gravimetric moisture content
4	$\varepsilon_p = a\, N^b$	Sweere	1990		a and b are regression parameters
5	$\varepsilon_p = (AN + B)(1 - e^{-CN})$	Wolff	1992		
6	$\varepsilon_p = (mN + a)(1 - e^{-bN})$	Wolff and Visser	1994		a, b and m are regression parameters
7	$\hat{\varepsilon}_p = a\left[1 - \left(\frac{N}{100}\right)^{-b}\right]$	Paute et al	1996		a and b are regression parameters
8	$\varepsilon_p = AN + \frac{BN}{\left[1 + \left(\frac{BN}{C}\right)^D\right]^{1/D}}$	Theyse	2000		A,B,C and D material parameters
9	$\varepsilon_p = AN + B(1 - e^{-CN})$	Theyse	2000		A,B and C material parameters

10	$\hat{\varepsilon}_p(N) = \varepsilon^0 \left[1 - \left(\frac{N}{100}\right)^{-B}\right]$ $X \left(\frac{L_{max}}{p_a}\right)^u \left(m + \frac{s}{p_{max}} - \frac{q_{max}}{p_{max}}\right)^{-1}$	Gidel et al.	2001	$L_{max} = \sqrt{p_{max}^2 + q_{max}^2}$	ε^0 , B , u= material parameters, p_a is a reference stress taken as 100 kPa, n triaxial tests, p = $\sigma_1 + 2\sigma_3$ and q = $\sigma_1 - \sigma_3$ where σ_1 is the total axial stress and σ_3 is the confining pressure, m is the slope, and s is the intercept of the Mohr–Coulomb failure line in p–q space
11	$\hat{\varepsilon}_p(N) = CN^b \frac{R}{A-R}$	Korkiala-Tanttu	2005	$R = \frac{q}{q_f}$, $q_f = mp + s$	C and b are material parameters. R is the shear stress ratio, q is the deviator stress and q_f is the deviator stress at failure, p is the hydrostatic stress
12	$\varepsilon_p = \beta_s \left(\frac{\varepsilon_0}{\varepsilon_r}\right) e^{-\left(\frac{\rho}{N}\right)^\beta} \varepsilon_v$	Modeified Tseng-Lytton by AASHTO	2008		β_s is a global calibration coefficient; ε_r is the resilient strain imposed in the laboratory test; and ε_v is the average vertical resilient strain in the base layer of a flexible pavement
13	$\left(\frac{\varepsilon_0}{\varepsilon_r}\right) = \frac{\left(e^{\rho^\beta} \times 0.15\right) + \left(e^{\left(\frac{\rho}{10^9}\right)^\beta} \times 20\right)}{2}$	AASHTO	2008	$\log\beta = -0.61119 - 0.017638\, W_c$ $\rho = 10^9 \times \left(\frac{-4.89285}{[1 - (10^9)^\beta]}\right)^{\frac{1}{\beta}}$	ε_0 , β, ρ= permanent deformation properties, β = shape factor, ρ = scale factor, W_c = gravimetric moisture content
14	$\varepsilon_p = AN^B + (CN + D)(1 - e^{-EN})$	Perez and Gallego	2010		A,B,C,D and E material parameters

15	$\varepsilon_p = A + B.N$	Cerni et al	2012		A and B are regression parameters
16	$\varepsilon_p = AN^B \sigma_d^C \left(\frac{\tau_f}{\tau_{max}}\right)^D$	Chow et al.	2014		τ_f =shear stress, τ_{max} =shear strength, σ_d=deviatoric shear stress, A, B, C, and D are regression coefficients
17	$\varepsilon_p = \varepsilon_0 \, e^{-(\rho/N)^\beta} \left(\sqrt{J_2}\right)^m (\alpha I_1 + K)^n$	Gu et al.	2016	$\alpha = \frac{2 \sin \Phi}{\sqrt{3}(3 - \sin \Phi)}$ $K = \frac{c \cdot 6 \cos \Phi}{\sqrt{3}(3 - \sin \Phi)}$	J_2 = second invariant of the deviatoric stress tensor; I_1 =first invariant of the stress tensor, ε_0, β, ρ, m and n = model co-efficient. C and Φ cohesion and friction angle.
18	$\left(\frac{\varepsilon_0}{\varepsilon_r}\right) = -2511.78 + 156.40 \ln(\gamma_d) + 9.65\, w - 2.70 pfc + 225.54 \ln(AI) - 30.86 SI - 53.77 \ln(TI)$	Gu et al.	2017	$\ln(\rho) = 42.83 - 4.56 \ln(\gamma_d) - 0.19w + 0.038 pfc$ $\beta = 0.29 - 0.52 \ln(\gamma_d) - 0.0058w - 0.0036 pfc + 0.56 \ln(AI) + 0.037 SI - 0.148 \ln(TI) + 0.0039 \lambda_G$	SI=shape index, TI=texture index, AI= angularity index, pfc = percent fine content, γ_d = dry density (kg/m^3), w= water content (%)
19	$\hat{\varepsilon}_p(N) = a\, N^{bS_f} S_f$ $\hat{\varepsilon}_p(N) = a\,(N - N_{i-1} + N_i^{eq})^{b(S_f)_i} (S_f)_i$	Rahman & Erlinggson	2015	$S_f = \frac{(q/p_a)}{(p/p_a)^\alpha}$	Pa=100kPa, $\alpha = 0.75$

There are several mathematical models available in the literature to predict the permanent deformation behaviour of unbound granular materials as shown in Table. The majority of these predictive models are based on single-stage (SS) triaxial tests considering one stress amplitude only. Erlingsson and Rahman (2013), though, introduced the time-hardening approach to extend these models to be used on multi-stage (MS) triaxial test data. It gives a better evaluation of performance enabling the efficient prediction of permanent deformation of unbound granular materials, nearing reality. Because most of the prediction models were developed based on SS loading conditions, the time-hardening formulation (Erlingsson and Rahman 2013) has been applied in order to use them for MS RLTTs. The time-hardening approach, Figure 2.19, calculates the equivalent number of load cycles (N^{eq}_i) for a certain stress path (i) in an MS loading condition that is required for that stress path (i) alone to attain the same amount of deformation that accumulated from all the previous stress paths. Then, the total number of load cycles N from the beginning of the loading is replaced by the effective number of load cycles as ($N - N_{i-1} + N^{eq}_i$), where N_{i-1} is the total number of load cycles at the end of the $(i-1)^{th}$ stress path (Figure 2.19). Accumulation of permanent strain during the current stress path is calculated using this effective number of load cycles. If the calculated N^{eq}_i approaches infinity, the inference is that no further permanent strain will occur for this stress path. Thus, this approach incorporates the effect of stress history on the material. The following equation shows the Rahman-Erlingsson model;

$$\hat{\varepsilon}_p\,(N) = a\,N^{bS_f}\,S_f$$

The equation above defines the Rahman-Erlingsson (R-E) model to predict permanent strain on the basis of stress ratio and number of load applications. where $\hat{\varepsilon}_p\,(N)$ is the accumulated permanent strain after N load cycles and a and b are regression parameters related to the material. The term S_f describes the effect of stress condition on the development of PD which is expressed as

$$S_f = \frac{(q/p_a)}{(p/p_a)^{\alpha}}$$

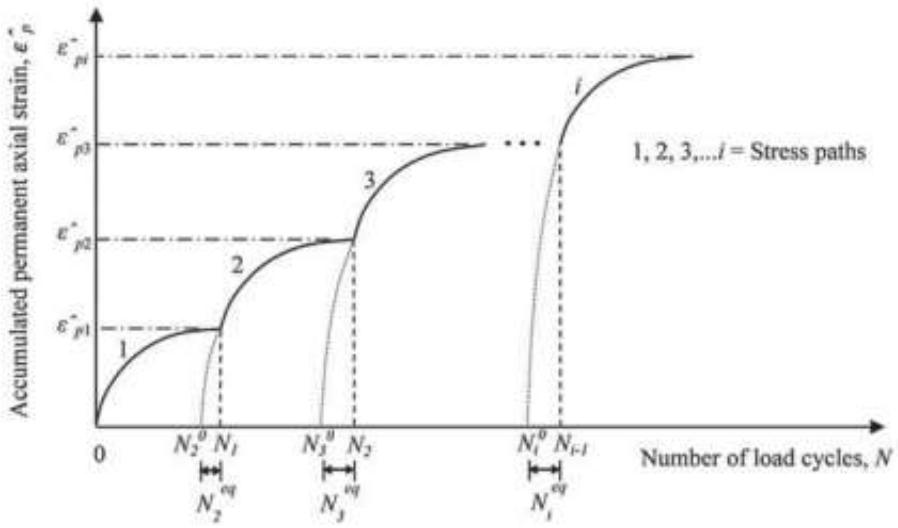


Figure 2.19: Demonstration of the time-hardening approach (After Rahman and Erlingsson 2015)

The equation can be modified to consider the time/strain hardening approach and is shown below;

$$\hat{\varepsilon}_p\,(N) = a\,(N - N_{i-1} + N_i^{eq})^{b(S_f)_i}\,(S_f)_i$$

where

$$N_i^{eq} = \left[\frac{\hat{\varepsilon}_{p_{i-1}}}{a\,(S_f)_i}\right]^{b^{-1}\,(S_f)_i^{-1}}$$

2.3 Resilinet behaviour of Unbound Granular Materials

The resilient deformation behaviour along with permanent deformation of unbound granular materials effectively characterize the material in a pavement structure and this has been studied and reported by many researchers over the last few decades. As it is a well-established reality that unbound granular materials behave as non-linear stress dependent materials under traffic loading exhibiting a time-dependent elastoplastic response, the traditional theories of elasticity could not be used to characterize it. Instead, the granular material's resilient response is characterized/defined by resilient modulus and Poisson's ratio. The shear and bulk moduli can also be used for this purpose. From the literature it is very clear that like permanent deformation, the resilient behaviour of granular materials is also affected, in varying degrees of importance, by

numerous factors including stress, moisture content, number of load cycles and stress history, fines content and maximum grain size, grading and density, load duration, aggregate type and particle shape, load frequency, and load sequence.

2.3.1 Resilient response modelling

The traditional theories of elasticity define the elastic properties of a material by the modulus of elasticity *E* and Poisson's ratio ν, which are material constants. Granular materials have widely been defined by a similar approach worldwide with the difference being the use of the resilient modulus instead of modulus of elasticity to account for the non-linearity of the material under loading. For repeated load triaxial tests with constant confining pressure, the resilient modulus and Poisson's ratio are defined, respectively, by

$$M_r = \frac{\Delta(\sigma_1 - \sigma_3)}{\varepsilon_{1,r}}; \quad \nu = -\frac{\varepsilon_{3,r}}{\varepsilon_{1,r}}$$

in which M_r = resilient modulus; ν = resilient Poisson's ratio; Δ indicates "change in"; and σ_1, σ_3, $\varepsilon_{1,r}$, and $\varepsilon_{3,r}$ = major and minor principal stress and recoverable axial and horizontal strain, respectively. The method calculates the resilient properties of the material similar to the methods applied to linear elastic isotropic material subjected to uni-axial stresses.

When cyclic confining pressure is applied, the generalized Hooke's law is employed for 3D stress-strain relationships of an isotropic, linear-elastic material. The resilient modulus and Poisson's ratio are then derived, respectively, from

$$M_r = \frac{\Delta(\sigma_1 - \sigma_3)\Delta(\sigma_1 + 2\sigma_3)}{\varepsilon_{1,r}\Delta(\sigma_1 + \sigma_3) - 2\varepsilon_{3,r}\Delta\sigma_3}; \quad \nu = \frac{\Delta\sigma_1\varepsilon_{3,r} - \Delta\sigma_3\varepsilon_{1,r}}{2\Delta\sigma_3\varepsilon_{3,r} - \varepsilon_{1,r}\Delta(\sigma_1 + \sigma_3)}$$

Various stress variables have been used by researchers over the years to develop analytical and mathematical procedures to describe the resilient modulus' stress dependence. Of these methods, quite a few are based on universally agreed simple curve fitting practices, and laboratory triaxial test data is generally used for it. Many researchers including Dunlap (1963) and

Monismith et al. (1967) showed resilient modulus' linear relationship with confining pressure. They also found a resilient modulus sensibly unaffected by magnitude of the repeated deviatoric stress with the condition that it does not result in excessive permanent deformation. Hence, they came up with the following equation depending on confining pressure alone. The p_0 in the equation represents atmospheric pressure.

$$M_r = k_1\sigma_3^{k2} \quad \text{or} \quad M_r = k_1\left(\frac{\sigma_3^{k2}}{p_0}\right)$$

A deviatoric stress function inclusion was thought necessary by some researchers including Pezo (1993) and Garg and Thompson (1997) in their analysis and they proposed following equations. The term q represents the deviatoric stress.

$$M_r = N_1 q^{N2}\sigma_3^{N3}$$

Some other researchers went a step further and included a stress ratio in their models as is routinely used in pavement design and analysis. An example is the model developed by Tam and Brown (1988).

$$M_r = k_1\left(\frac{p}{q}\right)^{k2}$$

Johnson et al. (1986), however, showed that the resilient modulus is dependent on both the first invariant of stress and the stress ratio, and suggested a model as follows: J_2 and τ_{oct} *represent the second stress variant and octahedral shear stresses respectively.*

$$M_r = k_1\left(\frac{J_2}{\tau_{\text{oct}}}\right)^{k2}$$

There is another widespread approach to the subject which represents the resilient modulus as a function of the sum of the principal stresses or bulk stresses. This led to the development of the universally acknowledged simple hyperbolic model by Seed et al. (1967), Brown and Pell (1967), and Hicks (1970). The model is commonly known as the *K*-θ model:

$$M_r = k_1\theta^{k2} \quad \text{or} \quad M_r = k_1\left(\frac{\theta}{p_0}\right)^{k2}$$

It has been accepted, used and acknowledged worldwide to study material stiffness dependence on stress due to its extreme simplicity. The simplicity represents various drawbacks which has encouraged researchers throughout the world to incorporate modifications in the model which could be found in the literature. For example, the constant Poisson's ratio value used in the model to find radial strain is not in line with the lately developed concept of varying Poisson's ratio under the applied stresses as shown by (Hicks 1970; Hicks and Monismith 1971; Brown and Hyde 1975; Boyce 1980; Sweere 1990; Kolisoja 1997). For example, reasonable axial strains were predicted by Sweere (1990) with a constant Poisson's ratio but this also resulted in rather weak volumetric and radial strain prediction. This model has also faced scrutiny by only considering the sum of the principal stresses as the influencing stress on resilient modulus which has been proven wrong in various studies, resulting in the need for additional stress parametric considerations to be made. For example, the dependence of resilient modulus of granular materials on the magnitude of the shear strain, induced mainly by shear or deviatoric stress, along with the bulk stress was shown by May and Witczak (1981). The inclusion of deviatoric stress by Uzan (1985) gave the *K*-θ model the following form.

$$M_r = k_1 p_0\left(\frac{\theta}{p_0}\right)^{k2}\left(\frac{q}{p_0}\right)^{k3} \qquad M_r = k_1 p_0\left(\frac{\theta}{p_0}\right)^{k2}\left(\frac{\tau_{oct}}{p_0}\right)^{k3}$$

In the 3D case, the deviator stress in the Uzan model is replaced by the octahedral stress. The inclusions of these stresses made the Uzan model an advanced and more routinely used model for resilient modulus computation, quite evident in various studies including (Lade and Nelson 1987; Witczak and Uzan 1988; Kolisoja 1997).

The model was then applied for repeated deviatoric stresses beyond and below the static failure criteria by Elliot and Lourdesnathan (1989). It was found that the model represented the data efficiently at stresses below

failure but this was not the case for stresses greater than the failure envelope, as increasing resilient modulus values were predicted by increasing the bulk modulus, which was opposite to the measured values. Incorporating a failure criterion/term into the model was, therefore, suggested by them with the condition that it has little to no effect until approaching the failure. The modified model, known as the stress ratio model, is expressed as

$$M_r = k_1 \frac{\theta^{k2}}{10^{A1}}$$

Later on, the effect of the density of the granular material was incorporated in *K*-θ and Uzan models by Kolisoja (1997) which resulted in the following expressions.

$$M_r = A(n_{\max} - n)p_0 \left(\frac{\theta}{p_0}\right)^{0.5}$$

$$M_r = B(n_{\max} - n)p_0 \left(\frac{\theta}{p_0}\right)^{0.7} \left(\frac{q}{p_0}\right)^{-0.2}$$

where density is accounted for by porosity of the aggregate. He also focussed on the need for a relatively large stress range series of the laboratory triaxial tests on given density specimens before applying these models reliably in practice. This could be used to find a reasonably accurate value for one of the material parameters which would subsequently result in resilient modulus values being computed from the equations for any given density and stress state combinations.

Constant confining pressure triaxial tests resulted in all of the above-mentioned resilient modulus predictive models. The need for studying the effect of both constant and varying confining pressures on resilient modulus led researchers to perform laboratory tests with both conditions. One such attempt was made by Karasahin (1993) who conducted triaxial tests with both constant and variable confining pressure and then used the following expression to calculate the resilient modulus:

$$M_r = A\left(\frac{p_m}{p_u}\right)^B \left(\frac{p_u}{\delta p}\right)^C$$

Satisfactory predictions resulted in both the cases in the study. Confinement types have also been varied by researchers like Nataatmadja and Parkin (1989) and Nataatmadja (1992). The results showed differences in stress dependence of the resilient modulus due to the type of confining pressure, and separate formulations were suggested as follows:

$$M_r = \frac{\theta}{q}(A + Bq) \quad \text{(CCP)}; \quad M_r = \frac{\theta}{\sigma_1}(C + Dq) \quad \text{(VCP)}$$

Nataatmadja demonstrated that the material parameters used were sensitive to changes in grading, maximum particle size, moisture content, and plasticity and concluded that these models are suitable for ranking material performance. Although many studies have been conducted to characterize the resilient modulus of granular materials, only a few have attempted this for resilient Poisson's ratio. This probably has been due to the greater difficulties in accurate measurement of the radial strains, as compared to the axial strains, which is required for determination of Poisson's ratio. Therefore, a rather constant value of Poisson's ratio is assumed in analysis which is typically 0.35 for granular materials. In reality though, Poisson's ratio values for sand were found to vary between 0.2 and 0.4 by Morgan (1966) who measured both strains, axial as well radial. Many researchers have also stated that resilient Poisson's ratio values for granular materials are a function of various factors including inherent physical properties and especially applied loading and stress conditions. A linear relationship of Poisson's ratio with increasing repeated deviatoric stress and an inverse relationship with confining pressure is also reported by many researchers. This was used by Hicks and Monismith (1971), who approximated the variation of Poisson's ratio with stresses by a third-degree polynomial expression given by

$$\nu_r = A + B\left(\frac{\sigma_1}{\sigma_3}\right) + C\left(\frac{\sigma_1}{\sigma_3}\right)^2 + D\left(\frac{\sigma_1}{\sigma_3}\right)^3$$

After performing triaxial tests with both constant and variable confining pressures, Karasahin (1993) also suggested the need to take the anisotropy effect into account for Poisson's ratio measurement at variable confinement. So, he proposed another mathematical equation to define the stress dependence of Poisson's ratio based on the type of confining stress which is shown as follows.

$$\nu_r = A \left(\frac{q_m}{p_u}\right)^B \left(\frac{p_u}{p_m}\right)^C \left(\frac{p_u}{\delta p}\right)^D$$

The variable confining pressure triaxial tests incorporating isotropy, though, resulted in very complex expressions. Some researchers including Sweere (1990) and Karasahin (1993) have stated Poisson's ratio values sometimes to be more than 0.5. This contradiction of basic Thermodynamics probably resulted from the fact that the analysis assumes a continual formulation of a mass of elements which are in reality discrete and basically unconnected. When Poisson's ratio exceeds 0.5, this indicates resilient dilatation; that is, the material transiently occupies more volume during the stress pulse.

2.4 Permanent Deformation in Asphalt Pavements

Pavements undergo different types of failure under loads with cracking and permanent deformation being amongst the most critical ones. Many researchers have examined these failure modes under different environmental and loading conditions over the years to explain the material and layer behaviour within the pavement both in the laboratory and in-situ. This section summarizes the development in scientific awareness related to pavement performance for resisting rutting and reflective cracking under loading in different laboratory and in-situ methodologies.

Longitudinal depressions along the length of the pavement are called permanent deformation or rutting. This mode of pavement failure usually occurs in hot areas due to dependency of asphalt mix performance on temperature. The road segments most affected by rutting are slow traffic areas such as intersections and bus stop etc. Rutting is generally of two types namely surface and structural rutting. Surface rutting occurs in the

Hot Mix Asphalt (HMA) wearing course probably due to poor asphalt mix design, construction or poor compaction. This type of rutting doesn't extend to the lower layers thereby providing an opportunity for an economical overlay or inlay to extend service life. Structural rutting occurs with deformation in the subgrade layer thereby causing failure in the top layers. The reason for structural rutting may be poor compaction or settlement of the subgrade layer. This type of rutting requires a full or nearly full-depth re-construction of the pavement thereby increasing life-cycle costs.

With the increase in traffic volumes and heavier loads, rutting or permanent deformation continues to be a critical issue for asphalt pavements (Cheng et al. 2002). Early rutting compromises ride comfort and reduces the life of hot-mix asphalt (HMA) pavements, consequently increasing economic costs. There are many factors that can contribute to the permanent deformation of HMA pavements including asphalt binder type, aggregate characteristics, mix design, production, construction, climate, and other related factors (Lu and Harvey 2006).

2.4.1 Permanent Deformation Prediction Models

Permanent deformation of hot mix asphalt (HMA) is one of the most critical distress types that affect the serviceability of asphalt pavements (Al-Khateeb and Basheer 2009; Javilla et al. 2017) and is caused by the accumulation of unrecovered deformation that occurs especially in summer under the repeated application of vehicle loads (Goh et al. 2011; Zhao and Zhang 2009; Khodaii and Mehran 2009). Generally, it is well known that the response of an asphaltic mixture depends on loading time and temperature. Asphalt concrete mixtures behave as linear visco-elastic materials under low-temperature conditions (or short loading times), while they behave as non-linear elasto-viscoplastic materials under high-temperature conditions (or long loading times) (Quintus 1994). When asphaltic mixtures behave as linear visco-elastic materials, they can be modelled using one of the physical models in which the model components are arranged as springs and dashpots either in parallel or in series to best fit test results. Other factors causing rutting include temperature, moisture, loading speed, wheel wandering and mixture shear strength (Mirzahossein et al. 2011; Park et al. 2017; Gladkikh et al. 2016; Sousa et al. 1991).

The two primary mechanisms of rutting have been identified as shear failure (lateral movement) and densification (volume reduction). Shear failure (lateral movement) of the HMA courses occurs in the top 100 mm of the pavement surface (Yildirim et al. 2007). However, if the material is substandard, shear failure can occur deeper. Permanent Deformation in the pavement is usually created gradually with increasing numbers of load applications. Typically, it appears as longitudinal depressions in the wheel paths and sometimes occurs in conjunction with upheavals on the sides. It is caused by a combination of densification (decrease in volume and, hence, increase in density) and shear deformation and can occur in any one or more of the HMA layers as well as in the unbound materials underneath the HMA. Lu and Harvey (2006) and Eisenmann and Hilmer (1987) found that rutting was mainly caused by deformation flow rather than volume change. Testing methods commonly used for rutting investigation include wheel tracking testing, static loading testing and uniaxial repeated loading testing (Domingos et al 2017; Bastos et al. 2017). Laboratory wheel-tracking devices are the most common type of equipment used to run simulative tests that measure pavement rutting performance by rolling a small loaded wheel device repeatedly across a prepared specimen. The test data are further used to predict the pavement performance in terms of rutting, fatigue, moisture susceptibility and stripping. In general, these wheel tracking devices have the potential for rut measurements based on the requisite laboratory conditions (e.g., load, number of wheel passes, temperature) that produce consistent and accurate correlations with field performance.

Historically, many studies have been conducted by researchers throughout the world to study pavement performance in different wheel tracking devices. The device's worth is proved by the effective results obtained for studying pavement performance in a simulative environment and thus designing a pavement (Cheng et al. 2002; Lu and Harvey 2006; Yildirim et al. 2007). Table 2.2 summarizes rut prediction methods developed over the years.

Table 2.2: Permanent deformation predictive models history in ACs

Sr. No	Model Name	Reference	Equation	Parameters
1	Semi-logarithmic	Barksdale et al. 1972	$\varepsilon_p = a + b\log N$	ε_p = permanent strain, N = number of passes, a,b=model parameters
2	Monismith mode	Monismith et al 1975	$\varepsilon_p = aN^b$	ε_p = permanent strain, N=No of load applications, a,b=model parameters
3	(VESYS Model)	Kenis 1977	$\varepsilon_p = \mu\,\varepsilon_r N^{-\alpha}$	ε_p = permanent strain, ε_r= resilient strain, N = number of passes, a, μ= regression parameter
4	Francken model	Francken 1977	$\varepsilon_p = \alpha_1 N^{\alpha_2} + \alpha_3(e^{\alpha_4 \times N} - 1)$	α_i= regression coefficients; N = number of passes; ε_p =vertical deformation/rut depth
5	Superpave model	McLean and Lytton (1993)	$\varepsilon_p = \varepsilon_p(1)\, N^S$	ε_p = permanent strain, $\varepsilon_p(1)$= permanent strain at the first load cycle, N = number of passes, S = regression parameter
6	Quintus model	Quintus et al. 1994	$RD_j = \sum_{i=1}^{j} \Delta RD_i = \sum_{i=1}^{j} \sum_{k=1}^{n} \varepsilon_{ik}^p\, h_k$	ΔRD_i = rut depth in season i, RD_j = rut depth accumulated up to season j, ε_{ik}^p= permanent strain during season i in element k, h_k = thickness of element k
7	AASHTO model	AASHTO 2002	$\frac{\varepsilon_p}{\varepsilon_r} = aT^b N^c$	ε_p = permanent strain, ε_r= resilient strain, N = number of passes, a,b,c = regression parameter
8		Al-Khateeb, Basheer 2009	$RD = aN^3 + bN^2 + cN$	RD = rut depth, N = number of wheel passes, and a, b, and c = model coefficients
9			$\varepsilon_p^N = \varepsilon_{Rve}^N + \varepsilon_{vp}^N$	

		Zhang et al. 2012	$\dot{\varepsilon_{vp}} = \frac{B\sigma^n}{\eta_{vp}} = \frac{B\sigma^n}{A\varepsilon_{vp}^p}$	ε_p^N =*permanent strain after the Nth loading cycle*, ε_{Rve}^N= residual viscoelastic strain after Nth loading cycle, ε_{vp}^N= viscous strain after Nth loading cycle, ε_{vp}^p, $\dot{\varepsilon_{vp}}$= viscous strain and viscous strain rate, respectively, η_{vp}= viscosity of the modified dashpot, σ = loading stress, A, B, n, p = material parameters
10		Nur Hossain et al 2013	$Rut_i = Rut_{i-1} + 2.49 \times 10^{-6} \left(N_{si}^{1.54\times10^2\varepsilon_{si}} + N_{ti}^{3.56\times10^2\varepsilon_{ti}}\right)$	Rut_i= Rut at time "i" from field measurements, Rut_{i-1}= Rut at time "i-1" from field measurements, N_{si}= Total No of steering axle passes at time "i", N_{ti}= Total No of Tandem axle passes at time "i"
11		Xie et al. 2017	$S_z = C_T \frac{1}{m(T_j)+1} \int_0^1 \int_0^h A(T_j) q^{n(T_j)} t^{m(T_j)+1} dz dt$ $C_T = 4.923 \times 10^{11} e^{-0.4858} + 142.5 e^{-0.0911}$ $t = \frac{NS}{Bv}$	S_z is the accumulated deformation in the depth z; C_T is the dynamic correction factor of temperature, which is regressed from test results in Matlab, $n(T_j)$, $A(T_j)$ and $m(T_j)$ are the creep parameter of the j^{th} sublayer at T temperature; t is the accumulated loading time and when the contact area and width are known, it can be determined by the vehicle speed v, where N is the times of loading; S is the contact area; B is the contact width; v is the vehicle speed
12		Kim et al. (2017)	$\varepsilon_p = 2.9895 \times 10^{-3} e^{6.2807\times10^{-6}N} e^{3.6723\frac{\tau}{\tau_f}N^{0.1032}} t^{0.4224}$ $\frac{\tau}{\tau_f} = \frac{(\sigma_1 - \sigma_3)(\tan\phi \sin\phi + \cos\phi - \tan\phi)}{2(c + \sigma_3 \tan\phi}$	ε_p = permanent strain, τ= shear stress (kPa), τ_f = shear strength (kPa), N = number of load cycles, t = load duration of each cycles (second), σ_1 = actual major principle stress under the given loading condition (kPa), σ_3 = actual minor principle stress under the given loading condition (kPa), c = cohesion (kPa), and ϕ = friction angle (^{0})

2.4.2 Three-stage Rutting Development

It is evident from the literature that rutting development occurs in three different phases and is termed as three-stage rutting development as shown in Figure 2.20. Three-stage models enable accurate simulation of rutting development and the identification of the transitional points of the rutting phases; in the primary phase the strain rate rapidly decreases with loading cycles; in the secondary phase the strain rate is almost constant; and in the tertiary phase the strain rate rapidly increases with loading cycles (Zhao and Zhang 2009; Khodaii and Mehran 2009; Witzcak 2002; Moghaddam et al. 2014).

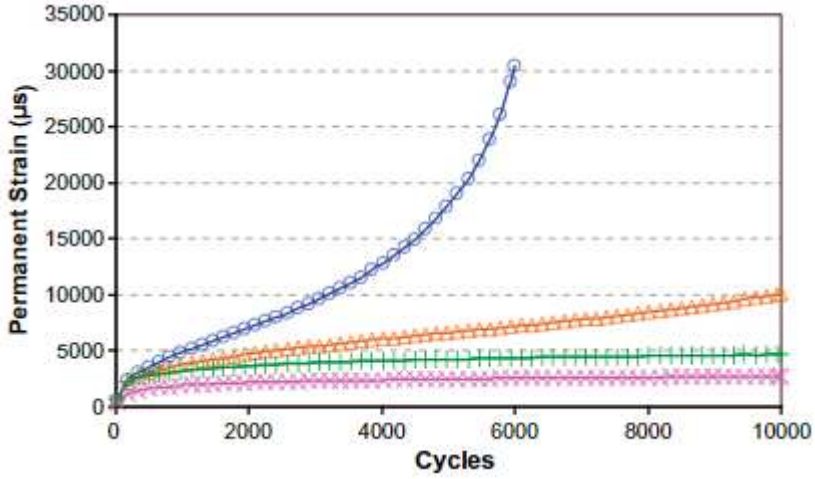


Figure 2.20: Stages of Permanent Deformation (after Khodaii and Mehran 2009)

The primary, secondary and tertiary phases of rutting development in asphalt mixtures could be related to densification, shear flow and shear failure of the mixtures respectively. According to literature, the primary phase is caused by the initial densification or compaction. The secondary phase is characterized by a relatively constant strain rate, and it could be related to the shear flow of mixtures, while the tertiary phase could be related to the shear failure of the mixtures (Zhang et al. 2016). In practice, most asphalt pavements are rehabilitated prior to reaching the tertiary rutting phase so as to minimize the structural damage, and to avoid unsafe trafficking conditions (Carvalho 2012). The number of cycles at which tertiary rutting begins (often referred to as the flow number) and the strain rate of the secondary phase have been popularly used as indicators for screening mixtures. Three-phase model parameters with high coefficients

of correlation to rutting development could make predictions of rutting and mixture characterisation easier to determine analytically (Carvalho 2012; Tarefder et al. 2003; Kim 2009; Tarefder 2003; Zhu and Fwa 2006). Among the various developed rutting prediction models, those which could simulate three-phase rutting included the Huurman model, Francken model, Zhang et al. model, Ye et al. model, Zhao-Zhang model, Zeng et al. model, Zhang-Pei-Zhang model and Ghazi-Imad model (Al-Khateeb and Basheer 2009; Zhao and Zhang 2009; Francken 1977; Huurman 1997; Zhang et al. 2016; Rushing and Little 2014; Ye et al. 2009; Zeng et al. 2014; Zhang et al. 2012).

2.4.3 Rutting prediction model types

At the First International Conference on the Structural Design of Asphalt Pavements in 1962, SHELL (Dormon, 1962) presented the first pavement design method that explicitly considered both fatigue and rutting. Since then, a series of rutting prediction models or calculation methods have been proposed. These proposed models have included empirical or semi-mechanistic models, mechanistic-empirical models and fully mechanistic models (Oscarsson 2011).

Empirical models are based on the data from laboratory or field tests. The representative empirical models include the Finn model (Finn et al., 1977), Wijeratne model (Wijeratne & Sargious, 1987), Archilla model (Archilla & Medanat, 2000), and Zheng model (Zheng, Niu, & Xu, 2009). Empirical models have strong pertinence and high reliability. However, they are dependent on specific materials, structures, and environments, so empirical models may not be accurate under different conditions.

For mechanistic models, the stress or displacement of a pavement structure is calculated on the basis of elastic or viscoelastic layer theory. Accordingly, the relationship between permanent deformation and stress or strain is established, and pavement rutting is then predicted. Representative models include the Uzan model (Uzan, 1983), SHELL model (Van de Loo, 1976), Zhang model (Zhang & Li, 1995), and shift model (Choi & Kim, 2013), which facilitate the easy and convenient prediction of pavement rutting. However, mechanistic models can only predict the permanent deformation of asphalt

mixture, whereas the effect of the pavement structure is neglected. Thus, the predicted rutting depth and the actual measured value usually differ considerably.

Both theoretically calculated stress or displacement and statistically established relationships are considered in the mechanistic–empirical model. Representative models include the Transport and Road Research Laboratory model (Whiffin & Lister, 1962), Majidzadeh model (Majidzadeh et al. 1978), VESYS1 model (Kenis, 1978; Kenis & Wang, 1997), Rauhut model (Rauhut, 1980), Strategic Highway Research Program model (Monismith et al., 1994), Wes Track model (Hand, Epps, & Sebaaly, 1999), Mechanistic-Empirical Pavement Design Guide (MEPDG) model (ARA, 2004; Von Quintus et al., 2012), and the Sun model (Lu & Sun, 2007). Mechanistic–empirical models are widely used in rutting prediction at present.

2.4.4 Approaches to Predict Rutting

There are two main approaches for predicting asphalt mixture rutting: the layer-strain method and the visco-elastic approach (Sousa et al. 1991). The layer-strain method can predict the life until rutting failure in asphalt mixtures by assuming a linear or non-linear relationship between the elastic stress field and vertical permanent deformation in each selected layer. This approach is only dependent on the elastic properties of the mixture and does not directly use the material viscosity (Khanzada 2000).

Romain (1972) developed a computer programme for the prediction of permanent deformation based on the layer-strain method. The layers of the pavement were divided into sublayers, and the produced model elements were sufficiently thin to be considered as homogeneous in terms of the vertical stress state. The stresses in each element were calculated by elastic theory and were then used with experimental stress-strain data to calculate the deformation in each element by applying a number of vehicle passages. The elemental deformation was summed up to produce the total surface deformation.

Morris et al. (1974) developed a rutting model for the asphaltic layers where the characteristics of permanent deformation were determined from triaxial tests. Tension and compression stress modes were applied to the samples

to evaluate the behaviour of the bituminous material. Comparison of the predicted rut depths with real measured values from Brampton Test Road in Canada was carried out by plotting a relationship between the total yearly permanent deformations over a period of 7 years. The model predicted that the permanent deformation occurred in the tension zone due to the lateral distortion of the material, which was the same as in the test section. Based on their model prediction they concluded that if tensile stresses exist in the field the mechanism of rutting is due to lateral distortion in the tension zone and the resistance to the stresses is provided by the binder only. Monismith et al. (1977) developed a model to predict the rut depth in asphalt mixtures under repeated traffic loading. The triaxial compression test was used to derive a constitutive relationship. It was found that the time of loading in the triaxial test was a very sensitive factor affecting rut prediction. The stresses and strains were computed by using the elastic multi-layer system ELSYM (computer programme) and the total rut depth was calculated by summing up strains from each layer.

Prediction models based on the visco-elastic approach invariably include a time-dependent response to the wheel load (Khanzada 2000). This type of rutting prediction model assumes that the ruts accumulate mainly from the shear flow of the pavement material. The viscoelastic approach is, unlike the layer-strain approach, purely dependent on the viscous characteristics of the asphalt and independent of the elastic properties. The viscoelastic properties of asphalt mixtures are, typically, measured from confined or unconfined creep testing. The method of linear viscoelastic asphalt material simulation and rutting prediction of asphalt concrete mixtures has been investigated by several researchers (Battiato et al. 1977; Collop and Cebon 1995; Monismith and Secor 1962; Moavenzadeh and Carnaghi 1966; Nunn 1986; Pagen 1972; Thrower 1977). The asphalt mixtures are assumed to behave as linear visco-elastic materials in this type of model, and this is considered as the main drawback of the approach. In reality, asphalt mixtures behave non-linearly at high temperatures and stress levels. However, the implementation of the non-linear properties of asphalt mixtures in modelling demands a more advanced tool.

A two-layer viscoelastic model was proposed by Battiato et al. (1977) to predict permanent deformation in asphalt mixtures. It was assumed that the subgrade is elastic and the asphaltic layers were simulated with a Maxwell model (spring and dashpot in series). The Unconfined Creep Test was used to find the material properties to fit the model. The ridge formed adjacent to the wheel path can be accounted for in this model. Their results showed that the assumption of elastic behaviour of the subgrade led to the permanent deformation due to the passage of a single wheel being independent of the stiffness of the subgrade.

Finite element techniques have successfully been used during the past 20 years to model the performance of asphalt pavements. Although finite element techniques have their added complexity, they usually give good simulation results and performance prediction for asphalt mixtures. Hua (2000) proposed a finite element model to relate the test results from Accelerated Pavement Testing facilities for asphalt mixtures and to predict the in-service performance of the flexible pavement. Different factors were considered as parameters affecting rutting magnitude such as pavement geometry, loading and test condition. The finite element analysis results showed that the model developed could predict material behaviour through a reasonable approximation of the factors. Al-Khateeb et al. (2011) developed a 2D finite element model to study the effect of static repeated wheel load on the formation of rutting in an asphalt pavement. A linear-elastic-plastic model was used to represent the pavement materials. The results were compared with actual field measurements and they showed a reasonable relationship. Wang et al. (2017) built a 3D finite element model to predict the rutting in asphalt mixtures and evaluated the different truck parameters including the axle load, speed and tyre pressure. The model performed well for predicting the rutting and reasonable results were obtained for all the truck parameters. Nahi et al. (2014) developed a finite element model for predicting rutting in asphalt mixtures with various air void contents. They observed 4-7% variation between measured and predicted rutting in the asphalt mixtures for different void contents as shown in the Figure 2.21.

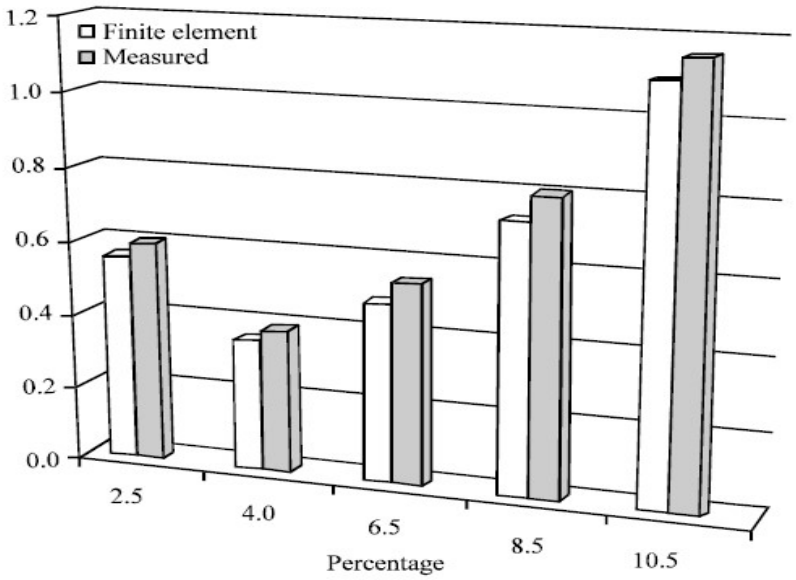


Figure 2.21: Comparison of the measured and predicted rutting (mm) at different air void contents (%) (After Nahi et al. 2014)

Abdullah (2019) developed a 3D finite element model to predict rutting in marl stabilized asphalt mixtures. The developed model was compared with wheel tracking test data and the reasonable correlation was observed.

Artificial neural networking (ANN) has also been utilized by researchers to predict the permanent deformation in asphalt mixtures and pavements over the years. The use of neural networking for the prediction of rutting in the pavement was initiated by Simpson et al. (1995). They developed a rutting prediction model on the basis of neural networks and compared with a linear regression model finding significantly improved predictions. Similarly, various other studies have been carried out in the last two decades to predict the permanent deformation in pavements for different materials, layers and loading combinations. A few examples include Tapkın et al. (2009), Shafabakhsh et al. (2015) and Gong et al. (2018).

2.5 Cracking in HMA Pavements

Along with rutting, cracking is one of the major and critical distress types witnessed in pavements under loading. Out of the various types of cracking patterns observed in the pavements, reflective cracking is the most severe conceptually for inverted pavements which contain a brittle lower layer constructed of cemented aggregates susceptible to cracking under loading

and temperature effects. The thin asphalt and presence of an unbound granular material in between makes it very vulnerable to propagation of reflective cracks in HMA. The following sections discuss the mechanism and development of reflective cracks in pavements.

2.5.1 Mechanism of reflective cracking

Reflective cracking is one of the critical failure types in pavement structures. It is generally observed in HMA layers above an incoherence, for example a joint in a Jointed Concrete Pavement (JCP). The thermal and mechanical loading cause excessive movements at the joints in jointed pavements contrasting with the continuous HMA layer. Substantial magnitude stresses result from such movements causing reflective cracks in the HMA layer when these stresses exceed the HMA strength. So, the development of reflective cracking depends on the type of loading applied.

Reflective cracking related to temperature loading is caused by horizontal movements in HMA and concrete slabs as shown in Figure 2.22. As it is evident that pavement temperature varies periodically and with depth, these variations cause repeated contraction and expansion. A uniform tensile stress is caused in the HMA layer due to contraction. The accumulated horizontal movements at the JCP joint result in additional tensile stresses in the HMA region, especially at the bottom of the HMA layer. The temperature in the HMA layer varies with pavement depth and this results in varying thermal stresses at the top and bottom of the HMA layer. Reflective cracks caused by thermal loading/stresses may develop either from the top or the bottom of the HMA layer (Nunn, 1989; Sha, 1993; Castell et al., 2000; Nesnas and Nunn, 2004; Song et al., 2006).

Both types of the movement, vertical and horizontal, are induced at the joint by the traffic load. Figure 2.22 shows different bending (tensile) and shear stresses at the bottom of the HMA layer corresponding to the tyre positions at points A, B and C respectively (Jayawickrama et al., 1989). Additionally, the magnitude of the subsequent bending and shear stresses are influenced by the support conditions of the underlying JCP. Therefore, it can be seen that either the bending stress, shear stress or both may govern the development of reflective cracking depending on the pavement

structure and traffic loading conditions. Traffic induced stresses, unlike thermal stresses, may occur more frequently and be more damaging as residual stresses accumulate within the HMA due to its inability to relax. As the HMA behaves relatively more brittle at low temperatures and relaxes slowly, the probability of developing a crack increases many fold compared to intermediate and high temperature at which HMA behaves less brittle, and relaxes more quickly.

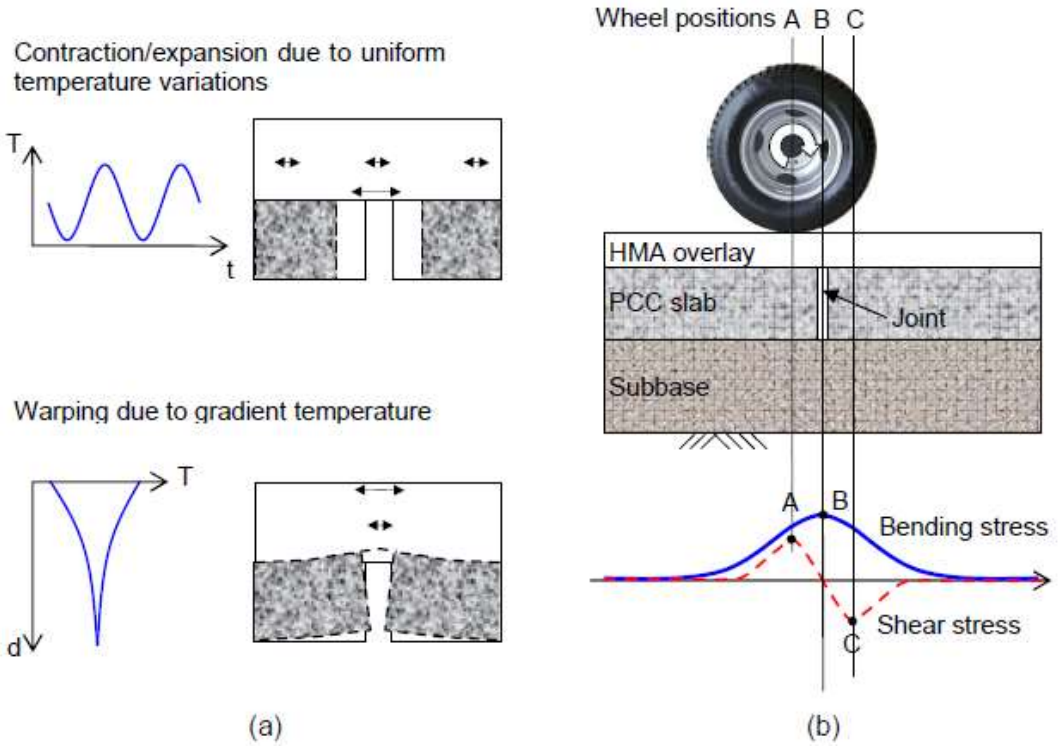


Figure 2.22: Schematic of reflective cracking mechanisms: (a) temperature variation and (b) traffic loading (after Baek 2010 thesis)

2.5.2 Development of reflective cracking

There have been many studies conducted to evaluate the development of reflective cracking in pavements. Many studies involving forensic investigation, laboratory testing and numerical simulations have found a variety of reflective cracking patterns although generally it is considered as a bottom-up cracking occurrence. Three different types of reflective crackings were observed by Jayawickrama et al. (1987) who applied horizontal loading in laboratory tests on a pavement consisting of two HMA layers jointed by glass-grid interlayer, as shown in Figure 2.23 (a). The three types of the cracking pattern observed are shown in Figure 2.23 (a)

and are; Type I, crack initiated at the bottom of the lower layer and propagated upward to the top of the upper layer, Type II, crack initiated at the bottom of the lower layer, propagated up to the interface of the layers and then followed the interface and type III, two cracks initiated at the top of the upper layer and bottom of the lower layer and headed towards the interface.

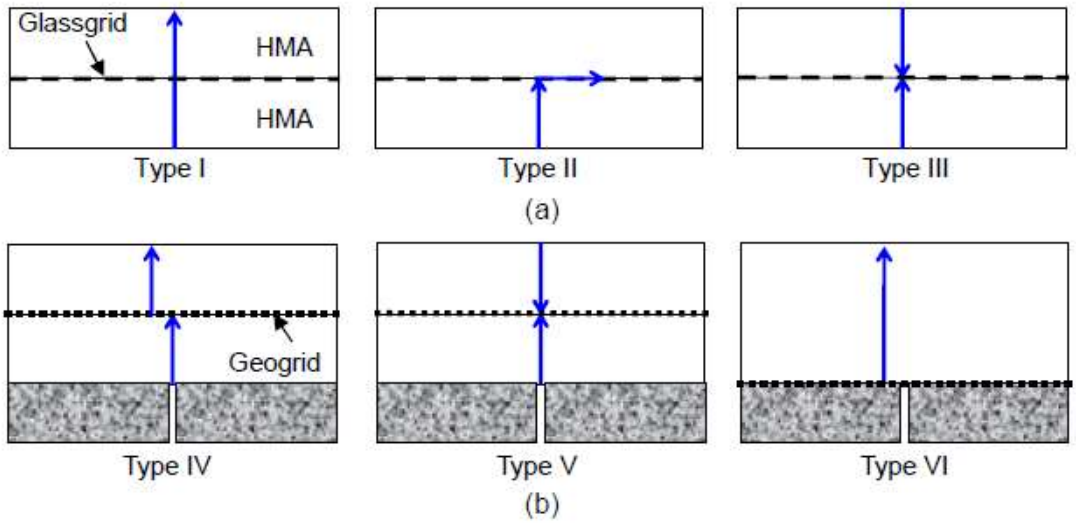


Figure 2.23: Reflective cracking paths observed in: (a) HMA/HMA structure with glass-grid interlayer (Jayawickrama et al., 1987) and (b) HMA/PCC structure with geo-grid interlayer (Kuo and Hsu, 2003)

Kuo and Hsu studied reflective crack patterns for an HMA overlay over a JCP reinforced with geo-grid interlayer. They observed three more crack propagation patterns as shown in Figure 2.23 (b) on the basis of various finite element analysis cases by varying geo-grid position, overlay thickness and asphalt concrete stiffness etc. The results indicated the development of reflective cracking at the bottom of the lower asphalt concrete layer propagating towards the interface and in the upper asphalt layer when the interface between the lower HMA layer and geo-grid was debonded (Type IV). They observed a cracking pattern similar to type III; the simultaneous development of bottom-up and top-down reflective cracking was observed when the interface bonding was broken. They termed it as type V reflective cracking pattern. In one of the analysis variations, they placed the geo-grid at the bottom of the lower HMA layer and debonded the interface between the HMA and underlying JCP layer, bottom-up cracking was observed and

termed as type VI. Researchers have reported the more likely occurrence of top-down reflective cracking with the condition of relatively low overlay stiffness, thick overlay or at high temperatures.

Sha (1993) reported top-down reflective cracking observed in forensic investigations in the field. In the majority of cores, Sha found top-down reflective cracking in relatively thick (38–82 mm) HMA overlays, while the entire HMA overlay was cracked in relatively thin (28–38 mm) HMA overlays. He concluded that surface-initiated thermal cracking was the main distress in thick HMA overlays, and bottom-up reflective cracking occurred in thin HMA overlays. The phenomenon of top-down cracking for thick HMA overlays was also confirmed by Nesnas and Nunn (2004) who performed field observations as well as numerical analyses of the various cracking situations in the pavements. Song (2006) performed a series of fracture-based finite element (FE) analyses and reported the traffic and temperature induced stresses to be the cause of development of bottom-up and top-down reflective cracking respectively.

The chances of bottom-up reflective cracking could be decreased by existing PCC pavements with higher load transfer efficiency (LTE) as reported by Kuo and Hsu (2003). The reason for reduction in chances of reflective cracks was described to be the lower stress concentration at the crack tip due to higher LTE. But, it could also be associated with the increased chances of top-down cracking.

Reflective cracking is generally instigated directly over the joint in a typical JCP, but it may initiate away from the joint. It may also occur at multiple points along the study area. De Bondt (1998), after performing finite element analysis, reported the initiation of a secondary reflective after the development of the primary reflective crack. The secondary crack was initiated, though, away from the joint. The interface around a crack tip can be debonded between the HMA overlay and the underlying layer due to double flexural deformation of a cracked overlay, as illustrated in Figure 2.24 (a). Researchers have reported twice as fast propagation of the primary reflective cracks as the secondary reflective crack at low bonding stiffness. The primary reflective crack propagated more slowly with the decline in bonding stiffness.

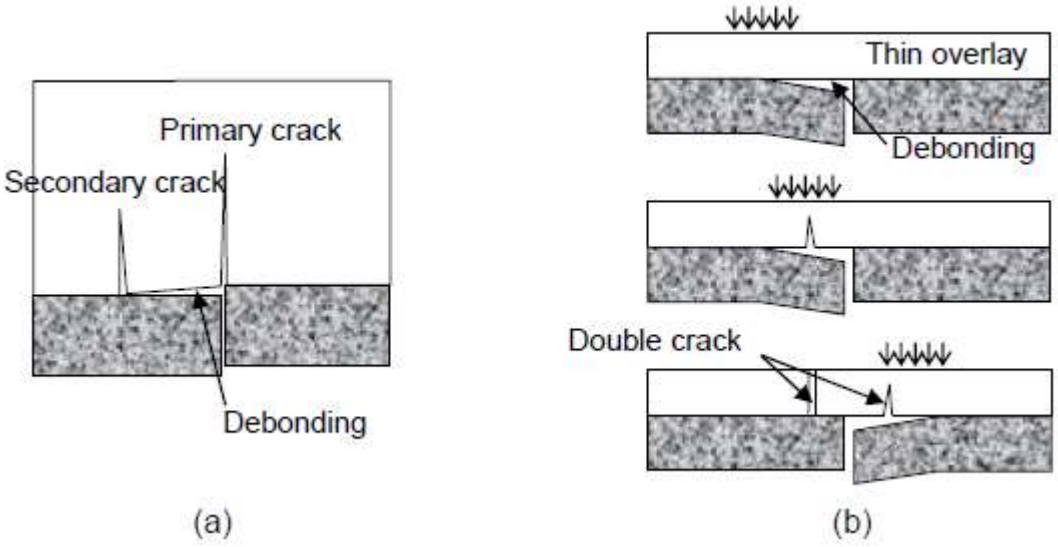


Figure 2.24: Reflective crack locations: (a) primary and secondary crack (after de Bondt, 1998) and (b) sequence of double crack (after Zhou and Sun, 2002)

Single and double reflective cracking was also observed by Zhou and Sun (2002) who performed accelerated pavement testing (APT) in the laboratory and gathered cracking data from field surveys. Debonding of up to 200-300mm extent was witnessed at the HMA/PCC interface near a joint in APT. They reported crack initiation at 40-60mm from the joint and that it propagated vertically towards the overlay surface. They also observed some cracks across joints and termed those as secondary reflective cracks as shown in Figure 2.24 (b). The field survey data analysis showed the occurrence of reflective cracking at a remarkable 90% (473 out of 525) of joints of which a majority (97%) had double cracks. Hence, the researchers concluded that double reflective cracking was a major type of reflective cracking in thin HMA overlays.

In fracture mechanics, cracks are classified in accordance with three loading modes (Anderson, 1994). Mode I is termed as opening mode in which the loading is applied normal to the crack plane and cracks propagate perpendicular to the crack plane. In Modes II and III, cracks occur in in-plane shear direction and the out-of-plane shear direction, respectively, when loading is applied parallel to a crack plane. Any of these ideal fracture modes can be mixed. For an HMA overlay on a JCP, fracture modes of reflective cracking are illustrated in Figure 2.25.

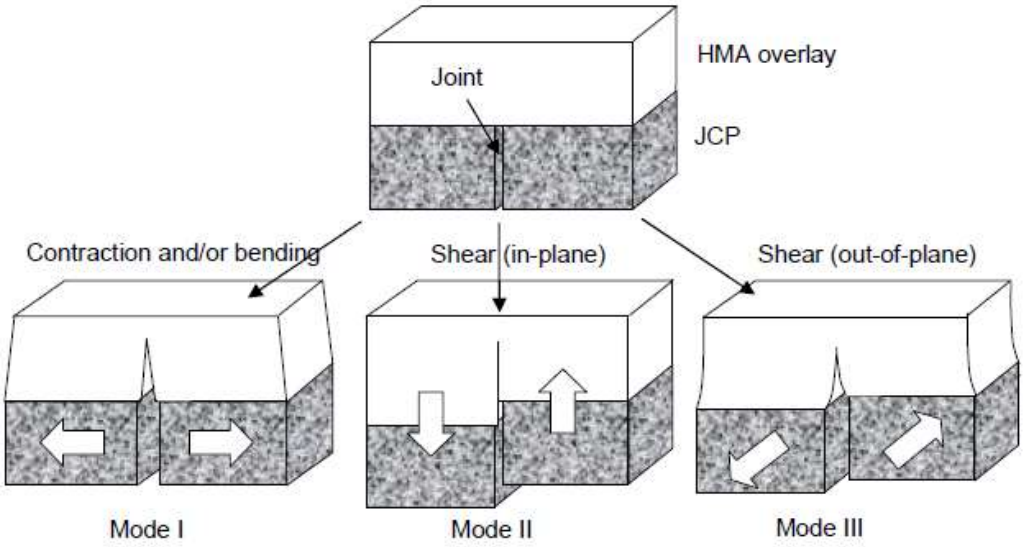


Figure 2.25: Fracture modes of reflective cracking

Generally, Mode I loading can result from both temperature and traffic. A tyre directly over the joint initiates bending in the HMA overlay which, along with temperature variations, causes horizontal movements of the PCC slabs resulting in accumulation of horizontal strain in the HMA overlay. The differential vertical (shear) movement of PCC slabs induced by the traffic loading can also result in Mode II fractures. Mode III fracture may be induced by lateral (longitudinal) movement of concrete slabs, but it is rarely observed in HMA overlays (Lytton, 1989; Mukhtar and Dempsey, 1996). Temperature and traffic loadings are usually applied together in HMA overlays, so that reflective cracking may develop in a mixed mode.

2.6 Inverted Pavement

Inverted pavements are flexible pavement structures where a relatively less stiff unbound aggregate layer is placed between the stiffer cement-treated base and asphaltic concrete layers. This type of structural arrangement in a pavement reduces its dependency on asphalt layer thickness alone without sacrificing the structural reliability by providing the required quality design. This can be achieved by utilizing the unbound aggregate base layer as a major structural component in this type of pavement (Tutumluer 2013).

South Africa is known to have used Inverted Base Pavements to support heavy traffic for many decades with considerably good results. The French pavement design guide also recommends inverted pavements to reduce

reflective cracking between cohesive layers (Corte and Goux, 1996). The USA has also initiated a few experiments in Inverted Pavements since the 1990s. In this context, a delegate of FHWA representatives visited South Africa in 1995 to assess the potential of Inverted Pavements in the USA (Horne et al. 1997). Consequently, two test sections at LaGrange and Morgan were constructed in the 2000s to monitor the performance of Inverted Pavements in the USA.

2.6.1 A brief history of Inverted Pavements

Inverted pavements are believed to have originated from South Africa as an economical alternative to rigid pavements in that country. The design faced early and quite hard scrutiny as it was thought that this pavement's performance could not match other types being used in the country, i.e. full-depth asphalt or rigid pavements. The improvements in aggregate properties and extensive construction experience eventually paved a way for Inverted Pavements to be South Africa's primary design for all highly loaded road networks (Freeme et al. 1980). The development of pavement testing facilities like Accelerated Pavement Testing (APT) and the Heavy Vehicle Simulator (HVS) has played a vital role in the progress of Inverted Pavements in South Africa (Du Plessis et al. 2006, Freeme et al. 1982, Theyse et al. 2011) as shown in Table 2.3.

Table 2.4 summarizes the reported inverted pavement constructions in the USA. The rehabilitation of a rigid pavement section in New Mexico is reported to be the first case of inverted pavements in the USA. There have been a few more cases of inverted pavements in the USA. A few of them have been documented by (Johnson 1961; Ahlvin et al. 1971; Barker et al. 1973; Grau 1973; Barksdale 1984; Barksdale and Todres 1983; Metacalf et al. 1999; Rasoulian et al. 2000; Titi et al. 2003). There have been two inverted pavements test sections constructed in the last twenty years in the USA at Morgan county and LaGrange County in Georgia (Terrell et al. 2003; Cortes 2010; Papadopoulas et al. 2016). Another inverted pavement test section has been constructed at Bull Run, Virginia USA without any published data yet. The Departments of Transportation (DoTs) from different states like New Mexico and Tennessee are considering to construct test sections of inverted pavements (Buchanan 2010; Tutumluer 2013).

Table 2.3: Inverted base pavements tested by the Heavy Vehicle Simulator (Data and original references in Theyse 2002, and Jooste and Sampson, 2005)

Location	S12 Cloverdene C17	P157/1 Olifantsfontein	P157/2 Jan Smuts	N3, Mooi River, Kwazulu-Natal
Layer Thicknesses (mm)	Gap-graded asphalt (70)	Semi-gap asphalt (30)	Semi-gap asphalt (35)	Gap-graded asphalt (50)
	G1 (320)	G2 (140)	G1 (140)	G1 (200)
	Lightly Cemented Base (280)	Lightly cemented subbase (100)	cemented Gravel (255	Lime stabilized subbase (155)
	Natural Gravel (100)	Natural Gravel (200)	Natural Gravel (125)	
Year	1978	1980	1980	1982
Location	TR86, Macleantown, Eastern Cape (303A2)	N2-23 Umkomaas, KawZulu-Natal, (327A3)	Road 2388, Cullinan, Gauteng, (398A4)	
Layer Thicknesses (mm)	Asphalt (40)	Asphalt (80)	Asphalt (30)	
	G2 (150)	G1 (160)	G3 (100)	
	Drainage Layer (150)	C3 (140)	C3 (150)	
	C4 (200)	C4 (120)		
	C5 (140)			
	G6 Subgrade			
Year	1986	1988	1997	

The earlier inverted pavements in South Africa were constructed by using gravel and different forms of Macadam for the unbound granular base layer (Jooste and Sampson 2005). The increasing trend of constructing inverted pavements in high traffic sections in the country increased the demand for structural integrity and performance from the unbound material. This led to the use of Crushed Stone material as unbound aggregate materials in the pavement. A different technique of compaction called Slushing was also developed to achieve high density, stable and superior base called G1 in South Africa.

Table 2.4: Inverted base pavement case histories in the US

Location	I-010-1 Road, Forks East, Mexico		F-51-1 Santa Fe New Mexico	US Army Corps Vicksburg, MS	Georgia Tech Atlanta, GA
Layer Thickness (mm)	AC (38)	AC (76)	AC (76)	AC (76)	AC (89)
	UAB (152)	UAB (152)	UAB (152)	UAB (152)	UAB (203)
	CTB (152)	CTB (152)	CTB (152)	stabilised clay subbase (152)	CTB (152)
Year	1960		1960	1971	1980
Reference	Johnson, 1961			Ahlvin et al. 1971 Barker et al. 1973	Barksdale 1984 Barksdale and Todres 1983
Location	Louisiana		Morgan County, GA	Lagrange, GA	Bull Run, VA
Layer Thickness (mm)	AC (89)		AC (76)	AC (89)	AC (127)
	UAB (102)		UAB (152)	UAB (152)	UAB (152)
	Soil-cement (152)		CTB (203)	CTB (254)	CTB (254)
			Filler (51)	Stabilized subgrade (152)	Prepared Subgrade
			Prepared Subgrade (CBR 15)		
Year	1991		1999	2008	2010
Reference	Metcalf et al. 1999 Rasoulian et al. 2000 Titi et al. 2003		Lewis et al. 2012 Terrell et al. 2003	Cortes 2010	Weingart, 2010

2.6.2 Slushing

Slushing is a technique to improve the density and hence performance of the unbound aggregate layer in a pavement contributing to the service life of the pavement. After the base layer is compacted with the standard

vibratory compactor at the optimum moisture content (OMC), Slushing is applied to the unbound granular base. In this technique, the base is flooded and compacted using static rollers causing isolated fines at the top which are washed away. The procedure results in the formation of a tightly interlocked matrix of aggregates. Kleyn (Kleyn 2012) documented the details of the procedure. Some researchers (Jooste and Sampson 2005) have reported a 3-4% increase in density due to the Slushing procedure.

Morgan county test section observed an entirely different scenario. The slushing technique in the USA did not result in any substantial improvement in density or stiffness as opposed to South African experience (Terrell et al. 2003). The noteworthy observation was a very high density in both the test section in the USA without using the slushing technique; the researchers attributed it to the rigid support provided by the Cement Treated Base (CTB) underneath.

The performance of an inverted pavement is also dependent on the aggregate quality and properties. The South African standards impose very strict limitations on aggregate origin, shape, fines and mechanical properties (Kleyn 2012, Theyse 2002).

2.6.3 Design methodology in South Africa

The South African inverted pavement design comprises the steps shown in Figure 2.26.

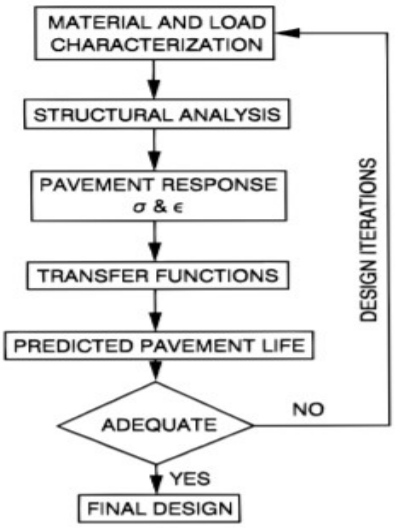


Figure 2.26: Design approach (After Theyse et al 1996)

The different types of highway and their approximate design reliability as per South African design is represented in Table 2.5.

Table 2.5: Road Categories and Approximate Design Reliabilities Used in South Africa

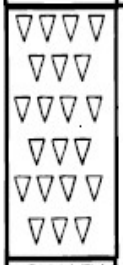
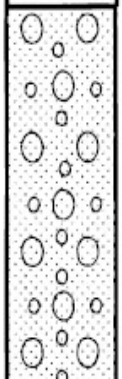
Road Category	Description	Approximate design reliability (%)
A	Interurban freeways and major interurban roads	95
B	Interurban collectors and major rural roads	90
C	Rural roads	80
D	Lightly trafficked rural roads	50

A very brief description of the various steps with the suggested material values are given as a brief guide to what has been used in South Africa over the years.

2.6.3.1 Material Characterization

The design of the pavement starts with characterizing the materials as in the case of a conventional flexible pavement. The Table 2.6 - Table 2.7 represent different parameter values suggested by the South African Mechanistic Design method (SAMDM) to be used for inverted pavement sections.

Table 2.6: South African Road-Building Materials with Material Codes (After Theyse et al 1996)

SYMBOL	CODE	MATERIAL	ABBREVIATED SPECIFICATIONS
	G1	Graded crushed stone	Dense - graded unweathered crushed stone ; Max size 37,5mm; 88% apparent relative density; fines PI < 4.0 (min 6 tests)
	G2	Graded crushed stone	Dense - graded crushed stone ; Max size 37,5 mm ; 100 - 102% mod. AASHTO or 85% bulk relative density; fines PI < 6 (min 6 tests)
	G3	Graded crushed stone	Dense - graded stone and soil binder ; max size 37,5 mm, 98 - 100% mod. AASHTO ; fines PI < 6
	G4	Natural gravel	CBR* ≮ 80 ; max size 53mm ; 98 - 100% mod. AASHTO ; PI < 6 Swell 0,2 @ 100% mod. AASHTO.
	G5	Natural gravel	CBR* ≮ 45 ; max size 63mm ; or $\frac{2}{3}$ layer thickness , density as per prescribed layer of usage , PI < 10 ; Swell 0,5 @ 100% mod. AASHTO.
	G6	Natural gravel	CBR* ≮ 25 ; max size 63mm ; or $\frac{2}{3}$ layer thickness , density as per prescribed layer of usage , PI < 12 ; Swell 1,0 @ 100% mod. AASHTO.
	G7	Gravel-soil	CBR* ≮ 15 ; max size $\frac{2}{3}$ layer thickness , density as per prescribed layer of usage , PI < 12 or 2 GM + 10 ; Swell 1,5 @ 100% mod. AASHTO.
	G8	Gravel-soil	CBR ≮ 10 ; at insitu density ; max size $\frac{2}{3}$ layer thickness , density as per layer of usage , PI < 12 or 2 GM + 10 ; Swell 1,5 @ 100% mod. AASHTO.
	G9	Gravel-soil	CBR ≮ 7 ; at insitu density ; max size $\frac{2}{3}$ layer thickness , density as per layer of usage , PI < 12 or 2 GM + 10 ; Swell 1,5 @ 100% mod. AASHTO.
	G10	Gravel-soil	CBR ≮ 3 ; at insitu density ; max size $\frac{2}{3}$ layer thickness , density as per layer of usage , or 90% mod. AASHTO.

* CBR at field compaction density

Table 2.7: South African Road-Building Materials with Material Codes (After Theyse et al 1996)

SYMBOL	CODE	MATERIAL	ABBREVIATED SPECIFICATIONS
	C1	Cemented crushed stone or gravel	UCS 6 to 12 MPa at 100 % mod AASHTO ; spec. at least G2 before treatment ; dense - graded
	C2	Cemented crushed stone or gravel	UCS 3 to 6 MPa at 100 % mod. AASHTO ; spec. generally G2 or G4 before treatment ; dense - graded
	C3	Cemented natural gravel	UCS 1,5 to 3,0 MPa and ITS ≥ 250 kPa at 100 % mod. AASHTO ; max. size 63 mm ; fines PI ≤ 6 after stabilization.
	C4	Cemented natural gravel	UCS 0,75 to 1,5 MPa and ITS ≥ 200 kPa at 100 % mod. AASHTO ; max. size 63 mm ; fines PI ≤ 6 after stabilization.
	EBM	Bitumen Emulsion Modified gravel	0,6% - 1,5% residual bitumen
	EBS	Bitumen Emulsion Stabilised gravel	1,5% - 5,0% residual bitumen
	BC1	Hot - mix asphalt	Continuously - graded ; max. size 53 mm
	BC2	Hot - mix asphalt	Continuously - graded ; max. size 37,5 mm
	BC3	Hot - mix asphalt	Continuously - graded ; max. size 26,5 mm
	BS	Hot - mix asphalt	Semi - gap - graded ; max. size 37,5 mm
	PCC	Portland cement Concrete	Modulus of rupture ≮ 4,5 MPa ; max size ≯ 75 mm
	AG	Asphalt surfacing	Gap graded
	AC	Asphalt surfacing	Continuously graded
	AS	Asphalt surfacing	Semi-gap graded
	AO	Asphalt surfacing	Open graded
	AP	Asphalt surfacing	Porous (Drainage) Asphalt
	S1	Surface seal	Single seal
	S2	Surface seal	Multiple seal
	S3	Surface seal	Sand seal
	S4	Surface seal	Cape seal
	S5	Slurry	Fine grading
	S6	Slurry	Medium grading
	S7	Slurry	Coarse grading
	S8	Surface renewal	Rejuvenator
	S9	Surface renewal	Diluted emulsion
	WM1	Waterbound macadam	Max. size 75 mm, PI of fines ≯ 6, 88-90% of apparent density
	WM2	Waterbound macadam	Max. size 75 mm, PI of fines ≯ 6, 86-88% of apparent density
	PM	Penetration macadam	Coarse stone + keystone + bitumen
	DR	Dumprock	Upgraded waste rock, max size $\frac{2}{3}$ layer thickness

UCS : Unconfined Compressive Strength.

ITS : Indirect Tensile Strength.

The SAMDM recommends various elastic moduli for the materials used in the pavement. It includes specifications for HMA, UGM and CTB, which are represented in Table 2.8 - Table 2.10.

Table 2.8: Suggested Elastic modulus for HMA

Material grading	Depth from surface (mm)	Stiffness values (MPa) based on temperature and material condition					
		Good condition or new material		Stiff, dry mixture		Very cracked condition	
		20° C	40° C	20° C	40° C	20° C	40° C
Values suggested by Freeme (11) in 1983							
Gap-graded	0 - 50	4000	1500	5000	1800	1000	500
	50 - 150	6000	3500	7000	4000	1000	500
	150 - 250	7000	5500	8000	6000	1000	500
Continuously graded	0 - 50	6000	2200	7000	4000	750	500
	50 - 150	8000	5500	9000	6000	1000	750
	150 - 250	9000	7500	10000	8000	1000	750
Values suggested by Jordaan (19) in 1993							
Gap-graded	0 - 50	1000	200	2000	300	600	200
	50 - 150	2000	300	3000	400	750	300
	150 - 250	3000	400	4000	500	800	400
Continuously graded	0 - 50	2000	300	3000	300	750	300
	50 - 150	4000	400	5000	600	800	400
	150 - 250	6000	1000	7000	1500	1000	750

Table 2.9: Suggested Elastic modulus for CTB

Original Code	UCS (MPa) for pre-cracked condition	Parent Material Code	Pre-cracked condition		Post-cracked condition			
			Phase 1		Phase 2	Phase 3		
			Stage 1: Intact (GPa)	Stage 2: Shrinkage cracking (MPa)	Stage 3: Traffic associated cracking, transitional phase with micro cracking (MPa)	Stage 4: Broken up in equivalent granular state (Mpa)		
						Dry condition	Wet condition	Equivalent code
C1	6 - 12	Crushed stone G1 Crushed stone G3	6 - 30	2500 - 3000	800 - 1000	400 - 600	50 - 400	EG1 EG2
C2	3 - 6	Crushed stone G2 Crushed stone G3 Gravel G4	3 - 14	2000 - 2500	500 - 800	300 - 500	50 - 300	EG2 EG3 EG4
C3	1.5 - 3	Gravel G4 Gravel G5 Gravel G6 Gravel G7 Gravel G8	2 - 10	1000 - 2000	500 - 800	200 - 400	20 - 200	EG4 EG5 EG6 EG7 EG8
C4	0.75 - 1.5	Gravel G4 Gravel G5 Gravel G6 Gravel G7 Gravel G8 Gravel G7 Gravel G8	0.5 - 7	500 - 2000	400 - 600	100 - 300	20 - 200	EG4 EG5 EG6 EG7 EG8 EG9 EG10

Table 2.10: Suggested Elastic modulus for UGM

Material Code	Material Description	Dry condition		Wet condition	
		Over cemented layer in slab state	Over granular layer or equivalent	Over cemented layer in slab state	Over granular layer or equivalent
G1	High quality crushed stone	250 - 1000 (450)	150 - 600 (300)	50 - 250 (250)	40 - 200 (200)
G2	Crushed stone	200 - 800 (400)	100 - 400 (250)	50 - 250 (250)	40 - 200 (200)
G3	Crushed stone	200 - 800 (350)	100 - 350 (230)	50 - 200 (200)	40 - 150 (150)
G4	Natural gravel (base quality)	100 - 600 (300)	75 - 350 (225)	50 - 200 (200)	30 - 150 (150)
G5	Natural gravel	50 - 400 (250)	40 - 300 (200)	30 - 150 (150)	20 - 120 (120)
G6	Natural gravel (sub-base quality)	50 - 200 (200)	30 - 200 (150)	20 - 150 (150)	20 - 120 (120)
G7	Gravel - Soil	30 - 200		20 - 120	
G8	Gravel - Soil	30 - 180		20 - 90	
G9	Soil	30 - 140		20 - 70	
G10	Soil	20 - 90		10 - 45	

2.6.3.2 Structural Analysis

Structural analysis is normally done with a static, linear elastic multilayer analysis program. The standard design load for South Africa is a 40-kN dual wheel load at 350-mm spacing between centres and a uniform contact pressure of 520 kPa.

The maximum horizontal tensile strains at the bottom of the asphalt and cemented layers are used as the critical parameters determining the fatigue life of these two material types. Note that the maximum tensile strain in a particular layer will not necessarily occur at the bottom of the layer (Shell manual 1978, Jordaan 1992), the position of maximum tensile strain is determined by the modular ratios of the pavement layers. The transfer functions for these materials were, however, developed as a function of tensile strain at the bottom of the layer and are used as such.

2.6.3.3 Pavement Life Prediction

Two concepts are involved in pavement life prediction. The first is to predict the individual layer life for each of the pavement layers and, second, the ultimate pavement life is predicted for the layered system. The basic material types considered are asphalt, cemented, granular, and subgrade materials. Each material type exhibits a unique mode of failure linked to critical parameters calculated at specific positions in the pavement structure under loading. Transfer functions provide the relationship between the value of the critical parameter and the number of load applications that can be sustained at that value of the critical parameter, before the particular material type will fail in a specific mode of failure.

Asphalt material fails because of fatigue cracking under repeated loading as a result of tensile strain (ε_t) at the bottom or in the layer. A distinction is made between thin asphalt surfacing layers (<50 mm) and thick asphalt bases (>75 mm). Transfer functions are provided for continuously and gap graded surfacing layers and asphalt base layers with stiffnesses from 1000 to 8000 MPa. The fatigue crack initiation transfer functions for asphalt surfacing layers are illustrated in Figure 2.27 - Figure 2.28.

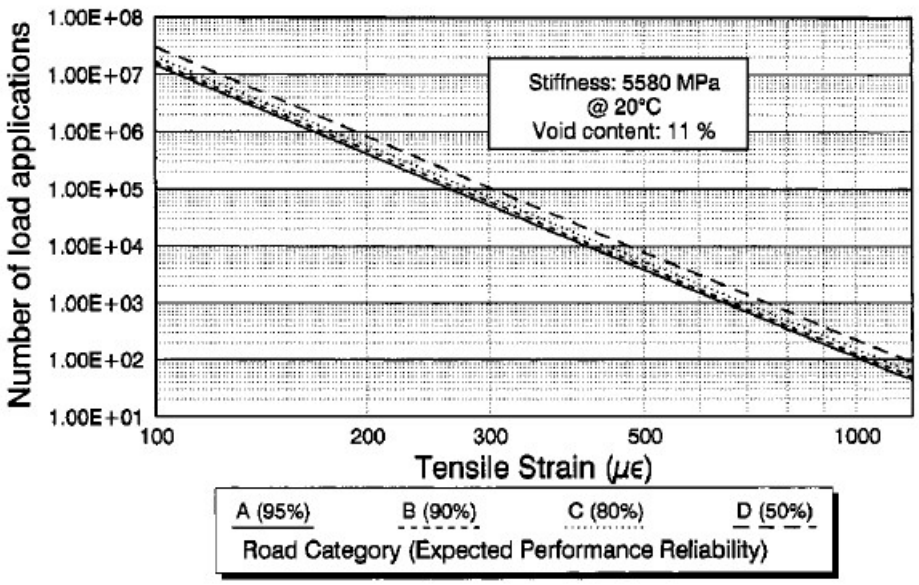


Figure 2.27: Fatigue crack initiation transfer functions for thin asphalt surfacing layers (continuous graded)

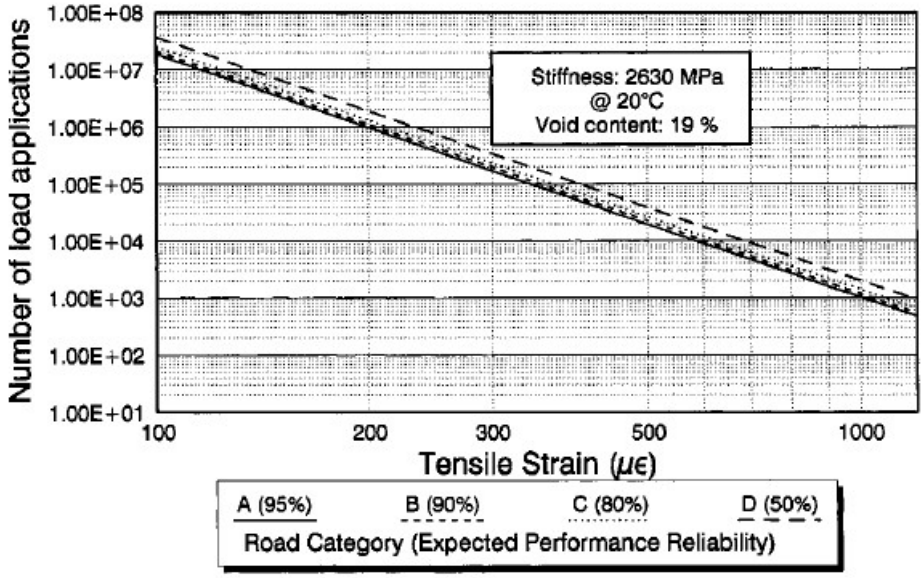


Figure 2.28: Fatigue crack initiation transfer functions for thin asphalt surfacing layers (gap graded)

Cemented material may exhibit two failure modes, namely effective fatigue and crushing (De Beer). The critical parameters for cemented material are (a) maximum tensile strain (ε) at the bottom of the layer controlling the effective fatigue life and (b) vertical compressive stress (σ_v) on top of the cemented layer controlling crushing life.

Granular material exhibits deformation caused by densification and gradual shear under repeated loading. The safety factor against shear failure for granular materials used in the SAMDM was developed from Mohr-Coulomb theory for static loading and represents the ratio of the material shear strength divided by the applied stress causing shear (Maree, 1978).

$$F = \frac{\sigma_3\left[K\left(\tan^2\left(45+\frac{\phi}{2}\right)-1\right)\right]+2KC\tan\left(45+\frac{\phi}{2}\right)}{(\sigma_1-\sigma_3)}$$

Or

$$F = \frac{\sigma_3\phi_{term} + c_{term}}{(\sigma_1 - \sigma_3)}$$

where

- σ_1 and σ_3 = major and minor principal stresses acting at a point in granular layer (compressive stress positive and tensile stress negative),
- C = cohesion,
- ϕ = angle of internal friction, and
- K = constant = 0.65 for saturated conditions, 0.8 for moderate moisture conditions, and 0.95 for normal moisture conditions.

Maree (1978) found that at values of the safety factor below a certain critical value the permanent deformation of granular material will increase rapidly under a few load applications because of shear failure; and at values above the critical value the permanent deformation increases gradually with increasing load applications. In both instances, however, the mode of failure will be the deformation of the granular layer, and the rate of deformation is controlled by the magnitude of the safety factor against shear failure.

The major and minor principal stresses, and hence the safety factor, are usually calculated at the midpoint of granular layers. Suggested values of the C and ϕ terms for granular materials are given in Table 2.11. The C-term in the table is in kPa.

Table 2.11: The granular material parametric values suggested by South African specification

Material Code	Moisture Condition					
	Dry		Moderate		Wet	
	ϕ-term	C-term	ϕ-term	C-term	ϕ-term	C-term
G1	8.61	392	7.03	282	5.44	171
G2	7.06	303	5.76	221	4.46	139
G3	6.22	261	5.08	188	3.93	115
G4	5.50	223	4.40	160	3.47	109
G5	3.60	143	3.30	115	3.17	83
G6	2.88	103	2.32	84	1.76	64
EG4	4.02	140	3.50	120	3.12	100
EG5	3.37	120	2.80	100	2.06	80
EG6	1.63	100	1.50	80	1.40	60

The mode of failure for the subgrade material is the permanent deformation of these layers, resulting in the deformation of the road surface. The critical parameter for these materials is the vertical strain (ε_v) on top of the layer.

After the layer life for each individual pavement layer is predicted from the transfer functions in the previous section, they should be combined to predict the ultimate life for the layered system. If there are no cemented layers in the pavement structure, the ultimate pavement life is determined by the shortest individual layer life predicted. If cemented layers are incorporated in the pavement, distinct phases in the pavement life cycle may be identified and should be included in the ultimate pavement life prediction.

2.6.4 Comparison of Inverted and Conventional

There have been many reports on performance comparison of inverted pavements and conventional flexible pavements. More deformation was reported by Johnson (Johnson 1961) in an inverted pavement section as compared to a flexible section one year after completion of the I-010-1 Road Folks-East project. Observations at the F-051-1 project in Santa Fe showed that the deformations in inverted pavements were approximately two-thirds of those in conventional flexible pavements. The findings are summarised in Table 2.12.

Table 2.12: Permanent deformation form Benkelman Beam (After Papadopoulos, data extracted from Johnson, 1961)

Test Section	Inverted Pavements		Conventional Pavements	
	Layer Thickness (mm)	Deflection (mm)	Layer Thickness (mm)	Deflection (mm)
I-010-1	AC (76)	0.43	AC (76)	0.28
			CTB 1.5% (152)	
			Untreated Base (152)	
	UAB 3-6 PI (152)		AC (76)	0.38
			CTB 1.5% (152)	
	CTB (152)		Untreated Base (356)	
			AC (76)	0.46
	Untreated subbase (89)		UAB non-plastic (152)	
			Untreated subbase (356)	
	AC (76)	0.41	AC (76)	0.25
			CTB 3% (152)	
			Untreated subbase (356)	
	UAB non-plastic (152)		AC (76)	0.28
			CTB 3% (152)	
	CTB (152)		Untreated subbase (178)	
			AC (76)	0.48
	Untreated subbase (229)		CTB 3% (152)	
			UAB non-plastic (152)	
F-51-8	AC (76)	0.36	AC (76)	0.61
	UAB non-plastic (152)		UAB non-plastic (152)	
			Subbase (254)	
	CTB 4% (152)		AC (76)	0.61
	AC (76)	0.48	UAB 3-6 PI (152)	
	UAB 3-6 PI (152)		Untreated subbase (254)	
	CTB 4% (152)		AC (76)	0.43
	AC (76)	0.43	Asphalt Treated Base (152)	
	UAB non-plastic (152)		Untreated subbase (254)	
			AC (76)	0.38
	Asphalt Treated Base (152)		CTB 4% (152)	
			Subbase (254)	
	AC (76)	0.46	AC (76)	0.43
	UAB 3-6 PI (152)		CTB 2% (152)	
	Asphalt Treated Base (152)		Subbase (254)	

Another study, Table 2.13, in Vicksburg, Mississippi by the US Army Corps of Engineers showed similar results for inverted and flexible pavements (Barker et al. 1973).

Table 2.13: Pavement Performance data from Mississippi (Barker et al 1973)

Layer Thicknesses [mm]	Load Assembly			
	1600 kN 12 Wheel Assembly			135 kN single wheel
	Surface Deflection (mm)	Subgrade Vertical Stress (kPa)	Load Applications to Failure	UAB Vertical Strains (microns)
Asphalt Concrete [72] Crushed stone base [152] Cement treated clay [381]	0.53	131	198	1800
Asphalt Concrete [72] Crushed stone base [152] Lime treated clay [381]	0.61	124	1871	800
Asphalt Concrete [72] Crushed stone base [533]	0.58	172	5037	900
Asphalt Concrete [72] Cement treated clayey gravely sand [533]	0.56	55	10406	-

In another laboratory study, Table 2.14, conducted at Georgia Tech, inverted pavements exhibited relatively low rutting (Barksdale and Todres 1983).

Table 2.14: Performance data on Georgia Tech laboratory study (Barksdale and Todres 1984; Tutumluer and Barksdale 1995)

Layer Thickness [mm]	Fail Mode	Reps to failure (thousands)	Rutting (mm)	AC Strain (microns)	Subgrade Strain (microns)	Base Strain (microns)
AC [89] UAB [305]	F/R	3000	12.7	465	170	-
AC [89] UAB [203]	R	1000	25	674	1310	2130
AC [229]	R	130	25	319	1380	-
AC [165]	R	440	25	460	1500	-
AC [178]	R	150	29.5	410	2200	-
AC [89] UAB [203]	R	550	15	300	1850	110
AC [89] UAB [203]	F	2400	7.1	280	1750	340
AC [89] UAB [203]	F	2900	8.6	390	2500	400
AC [89] UAB [203] Soil-cement [152]	F/R	3600	12.7	340	390	370
AC [89] UAB [203] CTB [152]	F/R	4400	11.2	260	340	420

Note: F: fatigue cracking, R; rutting failure

Titi et al. (2003) presented data, Table 2.15, from a Louisiana field study which showed similar rutting for inverted pavements and full depth soil-cement sections.

Table 2.15: Performance data on Louisiana field test study (Titi et al. 2003)

Layer Thickness [mm]	Inverted Pavement		Full-depth soil-cement pavement	
	Asphalt concrete [89] Crushed limestone [102] Soil-cement [152]		Asphalt concrete [89] Soil-cement [165]	
Average Rut (mm)	3.8		3.3	
Cracking Length (m)	Total: Low severity: Medium severity: High severity:	118 95 24 0	Total: Low severity: Medium severity: High severity:	233 152 64 17
Average SN	5.57		4.69	
Serviceability Index	4.2		4.0	
International Roughness Index	1.03 mm/m		1.25 mm/m	
Final subgrade resilient modulus	103.4 MPa		103.4 MPa	

Note: Structural number and Resilient Modulus were estimated through Dynaflect measurements (Kinchen & Temple 1980). Reported figures are at the end of 10.2 year monitoring period.

A Morgan county, Indiana, test section experienced negligible rutting after five years of construction as compared to approximately 25mm in a conventional flexible pavement section. Falling Weight Deflectometer (FWD) tests were conducted after 8 years on the same section in Morgan County for evaluation of the pavement life. It was observed that the inverted base

pavement section clearly showed better performance. The data is presented in Table 2.16

Table 2.16: Pavement performance data in Morgan County quarry (Terrell et al. 2002; Lewis 2012)

Layer Thickness [mm]	Max rut (mm)	Cracking	Max FWD Deflections (mm)	Remaining Life	E_{hor} (MPa)
AC [76] GAB [152] (slushing) CTB [203]	9.525	No cracking	0.28	94.61%	250
AC [76] GAB [152] CTB [203]	Minimal	No cracking	0.25	99.34%	550
AC [76] 203 GAB Surge Stone [152]	>25	Extensive	2.03	67.92%	650

Note: Remaining life was calculated by using FWD measurements. Horizontal Young's Modulus E_{hor} was measured for horizontal stress of 100 kPa.

2.6.4.1 Cracking

The first reported section of inverted pavements in New Mexico showed no sign of cracking after one year of construction as compared to significant cracking in a conventional flexible pavement section (Johnson 1961). The tensile strain in the asphalt surface in the laboratory study at Georgia Tech was greatly reduced by using cement instead of asphalt for inverted pavements (Table 2.14). Similarly, the inverted pavement section at the Louisiana state project showed much less cracking as compared to a full depth soil-cement section (Titi et al. 2003). The inverted pavement in the

Morgan County quarry road performed much better and showed no cracks on visual inspection while cracks could easily be seen on a conventional section especially near the quarry gate where trucks decelerated (Lewis et al. 2012). The Cement Treated Base (CTB) in the LaGrange County project was able to withstand the compaction process without cracking when it was properly monitored (Cortes and Santamarina 2013).

2.6.4.2 Aggregate Base Stiffness

Researchers have reported back-calculated resilient modulus data obtained from Heavy Vehicle Simulator (HVS) tests (Maree et al. 1981; Theyse 2002). It is obvious from the figure that the crushed stone base termed G1/G2 developed higher stiffness for the same stresses than the natural gravel base (G5). A Lightweight Deflectometer (LWD) device, the Dynaflect, was used in the Louisiana project for finding the resilient modulus of the subgrade by back-calculation (Titi et al. 2003). A Wave Propagation technique was used to calculate the stiffness in the granular base during the Morgan County project (Terrell net al. 2003). The results showed higher stiffness in the traditional section as compared to both inverted sections. Another observation was that the vertical stiffness in all the sections was higher than the horizontal stiffness for loaded as well as unloaded cases (Terrell et al. 2003).

There have been many studies in South Africa in the 1980s which declared inverted pavements as the most economical solution for all traffic levels and types in the country (Freeme et al. 1980; Mithcall and Walker 1985). Some of the recent studies have also shown that the inverted pavements can be more economical in terms of initial and life cycle cost (Cortes 2010; Jooste and Sampson 2005; Weingart 2009). It has also been reported by Titi that the inverted pavement section cost 20% more than the full depth soil-cement section by (Titi et al. 2003). The increased cost was justified by the increase in expected life of 4 times according to accelerated pavement testing (APT) and 2 times according to in-situ performance data (Metacalf et al. 1999).

Research studies conducted on a variety of different aggregate base materials having different properties concluded that horizontal stiffnesses

are only a small fraction of the vertical stiffness throughout the base layer. The horizontal stiffness for the aggregate base was also shown to be increased for crushed stone compared to the gravel base. This increase in the horizontal stiffness decreased nearly all the critical pavement responses i.e. asphalt concrete (AC) strains, surface and subgrade deflections, vertical subgrade strain and deviatoric stresses (Seyhan and Tutumluer 2002). These researchers found it to be in agreement with the general concept that lower pavement responses are associated with better performance which can be achieved by the use of the higher quality granular materials.

2.6.4.3 Economic Benefits of inverted pavements

Generally, it is very difficult to evaluate the financial comparison between inverted pavements and conventional flexible pavements due to the changes in constitutive material prices. The initial project construction cost also varies a great deal due to this fluctuation. Therefore, in order to compare the life cycle costs of the inverted pavements and conventional flexible pavements, the cost of the bitumen proves to be the determining factor. Similarly, the price of cement could be the determining force when inverted pavements are compared with concrete pavements. Determining an accurate construction cost is further complicated by the possible skewed costs associated with evaluating new technology and the relatively small size of test sections. The following are some limited cost comparisons (initial construction and/or life cycle) of inverted pavements relative to other pavements.

South Africa

- South Africa has determined that inverted pavements offer a 20 to 25% life cycle savings compared to asphalt base pavements (SANRA 1998).

Virginia DOT/Luck Stone Bull Run Bypass (Highway 659), project planned for 2010:

- Conventional Flexible Section: (11 inches=280mm HMA / 3inches=75mm Open Graded HMA Drainage Layer / 8 inches=200mm CTB)

- Inverted Section: (5 inches=125mm HMA / 6inches=150mm UGM / 10inches=250mm CTB)

An initial construction cost savings of 22 percent has been calculated for the inverted section (Weingart 2010).

Georgia DOT LaGrange Bypass

- Conventional Rigid Section: (9.5 inches=240mm PCC / 10inches=250mm UAB)
- Inverted Section: (5 inches=125mm HMA / 6inches=150mm UGM / 10inches=250mm CTB)

A life cycle cost analysis conducted by the Georgia DOT found a project savings of

$139,000 per lane mile for the inverted section (Cardosa 2008). Another advantage of the inverted pavement is its ability to force the distress to occur in the HMA layer due to its stiffer foundation layers. The distress in the thin HMA layers could be repaired economically and easily as compared to deeper rehabilitation. This is very similar to the perpetual pavement design concept in which the HMA layer serves as a sacrificial layer that is maintained or rehabilitated at intervals throughout the pavement life.

Apart from these advantages, inverted pavements present many other benefits including the potential for reduced energy demand as compared to conventional pavements (flexible or rigid). The Canadian Construction Association (CCA) reported a reduction of approximately 80% in total end use energy demand of UGM as compared to HMA or concrete (CCA 2005). When compared to a conventional flexible system, the overall energy demand of an inverted pavement may be lower as a result of 1) reducing the HMA thickness and 2) utilizing base and CTB (at a low cement loading). When compared to a concrete pavement, the potential energy savings would be gained through the elimination of the concrete pavement layer and replacement with an inverted structure.

2.6.5 Simulations of Inverted Pavements

It has been attempted in the USA to simulate the performance of inverted base pavements by Finite Element Methods. Various finite element programs like ABAQUS have been used for simulating the mechanical performances of such types of pavements. Cortes et al. (2012) and Papadopoulos et al. (2014, 2016) have simulated the performance of inverted base pavements by incorporating anisotropic stress-dependent material models into Abaqus. They highlighted the stress distribution difference between the conventional and inverted base pavements which was attributed to the variation of the stiffness between the pavements. Papadopoulos et al. (2016) concluded that there is no universally accepted thickness for any layer in an inverted pavement. It was also found that the stiffer asphalt concrete and cement treated base layers deform as beams, and tension is developed in those layers whereas the unbound granular base layer acts as a cushioning layer developing compression throughout the layer. The simulations for the inverted pavement with thin asphalt layers showed a decrement in the tensile strain at the bottom of the asphalt layer and an increment under the wheel load. The authors stated that, to benefit from this behaviour, the limiting value of asphalt concrete thickness should be in the range of 25-50mm depending upon the loading and environmental conditions. Due to lower tensile strains in a thin asphaltic layer, this contributes towards the longer fatigue life of the pavements. Another advantage of thin asphalt inverted pavements is economic benefits associated with it. As the granular material is stress-dependent, it shows a diversity of stiffness at various locations and instants which is even more noticeable in a thin surfaced asphaltic concrete layer. So, Papadopoulos et al. (2016) stressed the need for laboratory protocols to study the anisotropic stiffness of granular materials under traffic loading.

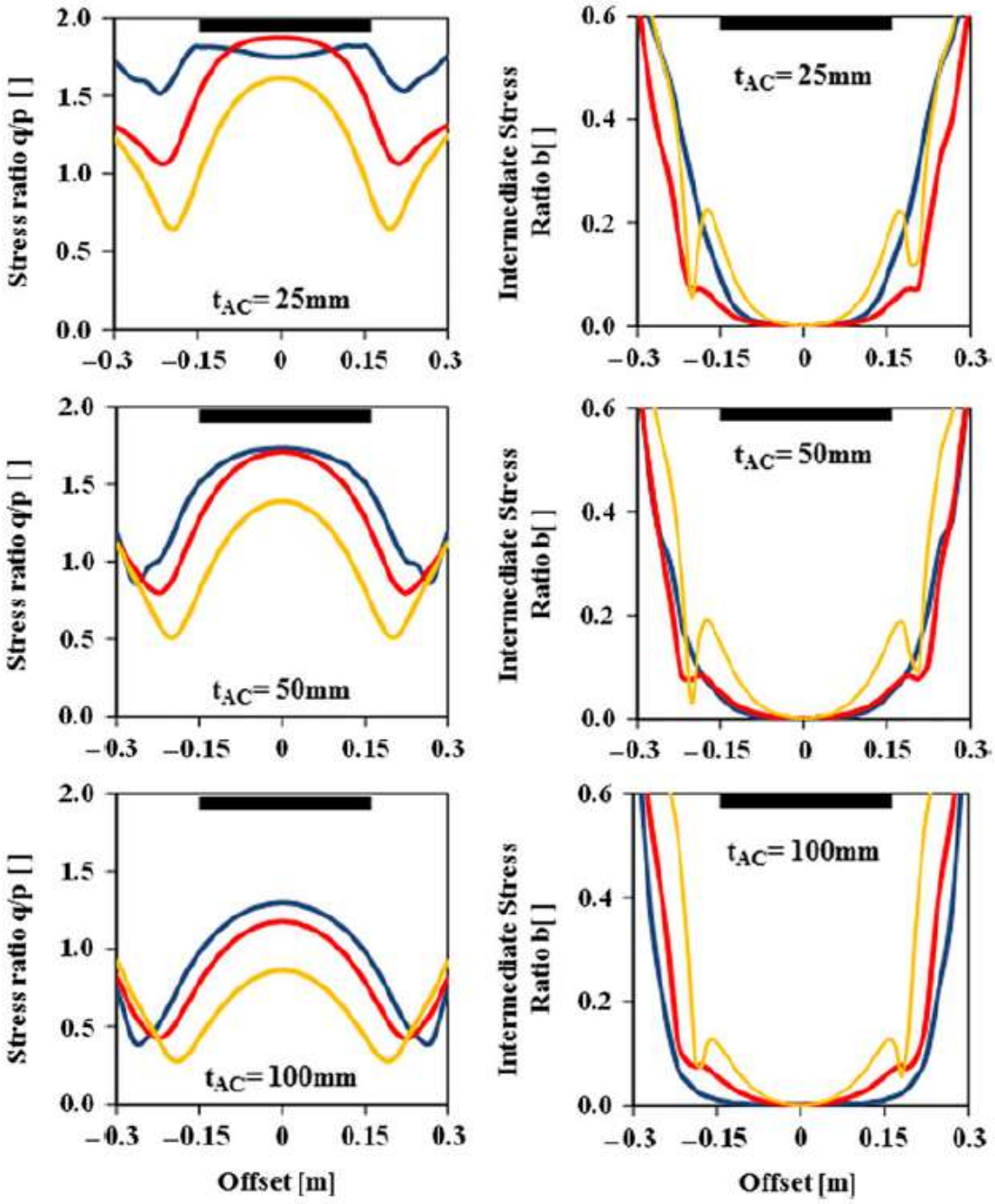


Figure 2.29: Stress evolution in the granular base along the wheel path. Stress ratio q/p (left column), and intermediate stress ratio b= (σ2 -σ3) / (σ1 - σ3) (right column) along the centreline for different asphalt thicknesses. In all cases, tGAB = 150mm and tCTB=300mm. The blue, red and yellow lines correspond to the top, half-depth and bottom of the GAB, respectively

Figure 2.29 show the different results obtained by numerical simulations of inverted pavements in the finite element environment Abaqus. Stress evolution in the granular layer of an inverted pavement is shown by the

figure at top, mid and bottom of the layer for different thicknesses of the top asphalt layer.

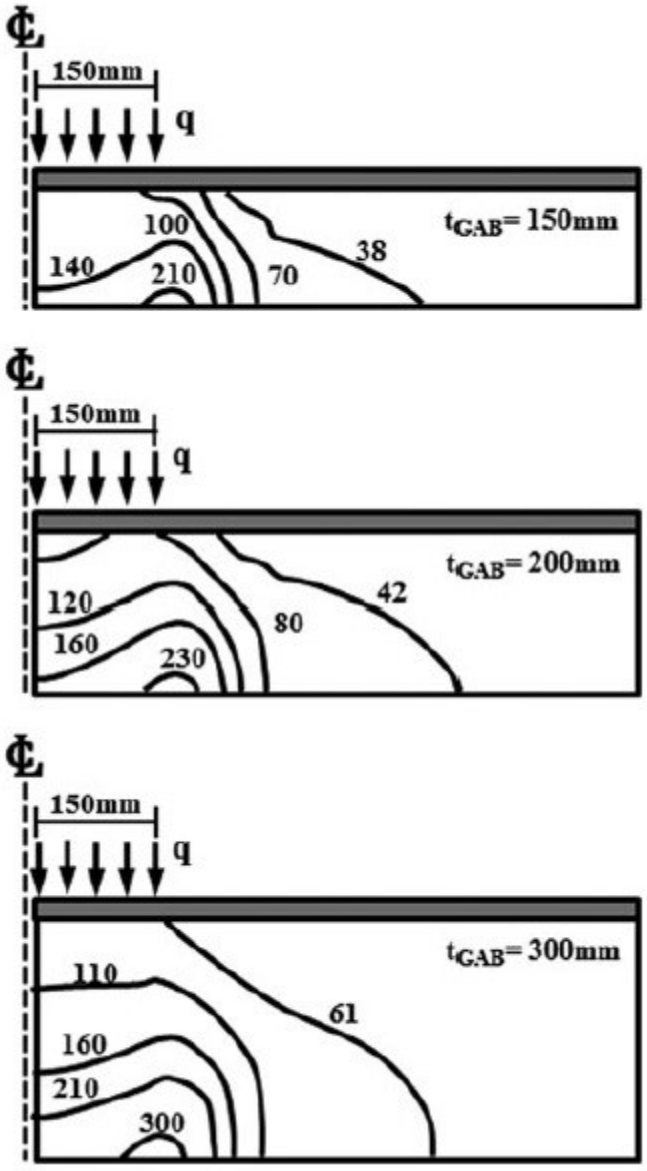


Figure 2.30: Stiffness contours (MPa) within the granular base under the applied wheel load q=650 kPa for different thicknesses of the granular base. In all cases, tAC = 50mm and tCTB = 300mm

The Figure 2.30 shows the stiffness contours in granular layers of varying thicknesses for a fixed top and bottom layer thickness under an applied wheel load. Higher vertical modulus is observed under the wheel load than away from it. The proximity of the granular material to the load improves the confinement and consequently its stiffness. It is also aided from the stiff reaction by the cement-treated base layer underneath.

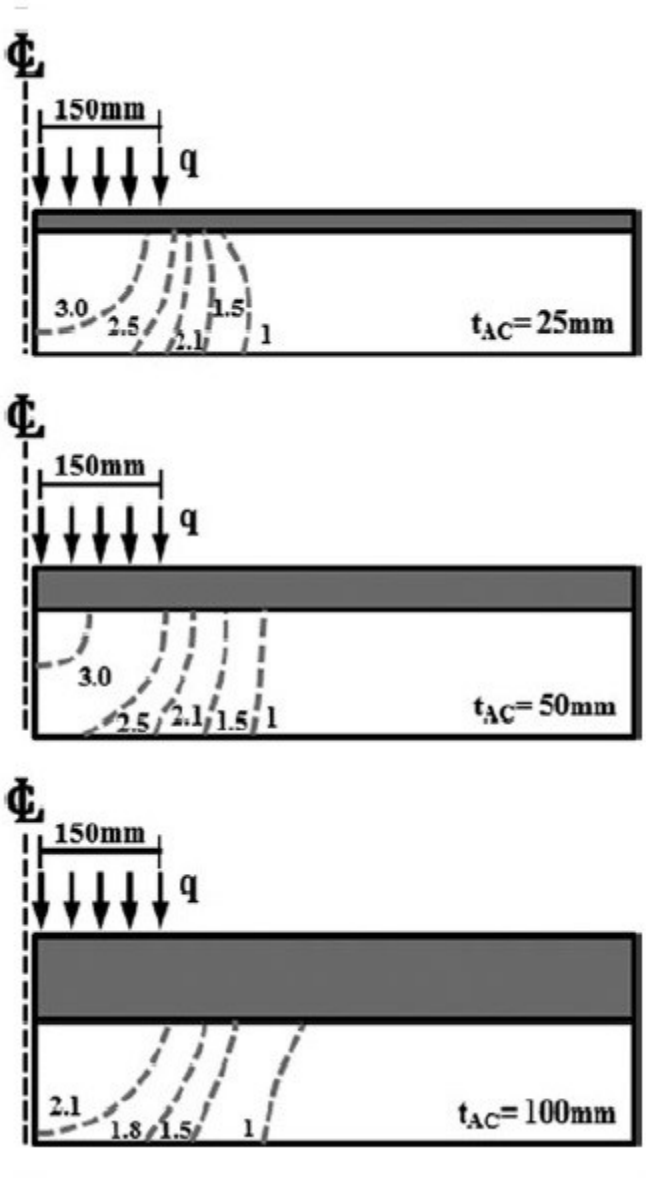


Figure 2.31: GAB stiffness anisotropy contours within the granular base for tGAB = 150mm and tCTB = 300 mm

The Figure 2.31 shows the stiffness anisotropy observed in the granular layer for different thicknesses of the asphaltic concrete layer. A thin asphalt layer introduces higher stresses in the granular layer resulting in greater stiffness anisotropy (vertical modulus/horizontal modulus) in the layer whereas the opposite happens for a relatively thicker asphalt layer.

2.7 Conclusions

As inverted pavements have performed significantly comparative to conventional pavements over the years in South Africa and the USA, the

performance of such a pavement design in the UK was essential. Therefore, this project was carried out considering environmental conditions prevailing in the UK. The project also takes its importance from the fact that there are currently no methodologies to predict the permanent deformation and reflective cracks (fatigue life) in an inverted pavement. A comprehensive performance data on unbound granular materials under varying stress and environmental conditions was also the need of the hour. This project, therefore, tries to fill those gaps in knowledge thereby presenting a better understanding of inverted pavements and hence utilising this improved design for more durable pavements.

2.8 Summary

This chapter has summarized the literature from past research related to the performance of UGMs in pavements, and factors affecting the permanent deformation performance of UGMs in pavements. It also encompassed the permanent deformation of HMA pavements under loading. A brief history of analytical models to predict the PD of HMA and UGMs was also tabulated. The chapter ended with a history of inverted pavement studies conducted in South Africa and the USA. A brief comparison of inverted pavement performance with conventional pavements was also tabulated.

3 Materials and Methods

3.1 Introduction

The research project focuses on the design of heavy-duty pavements by following new construction technology in which the unbound granular base layer is constructed between the thin asphalt concrete surfacing and cement treated base layers. The proximity of the unbound granular material layer to the wheel load speaks of its importance with regard to overall pavement performance. An inverted pavement relies on the performance of the unbound aggregate base layer for the overall mechanical response of the pavement unlike conventional pavements in which the stiffer top layers distribute the load to the less stiff bottom layers over a broader area. The performance of this pavement type in South Africa over the years and recent studies on test sections in USA prove its worth as an efficient and better performing alternative to conventional pavements under certain circumstances. This chapter documents all the materials and methods adopted to complete the project successfully.

3.2 Materials

The research was carried out using the conventional materials used in the pavement industry with the focus being on enhancing the performance of unbound aggregates and ultimately resulting in long-lasting and durable pavements. The following are the materials used to carry out this research project.

- Bitumen
- Aggregates
- Cement

3.2.1 Bitumen

A commonly used 40/60 pen bitumen has been used for the asphalt mix testing. Table 3.1 gives the properties of the bitumen used;

Table 3.1: Properties of Bitumen used in the study

Sr. No.	Parameter	Value	Test Method
1	Penetration @ 25^{0}C	43	BS EN 1426 (2015)
2	Softening Point (^{0}C)	51	BS EN 1427 (2015)
3	Specific Gravity	1.03	BS EN 15326 (2007)

3.2.2 Aggregates

Granite crushed stone has been selected for this research project due to its easy availability and wide usage in pavement industry in the United Kingdom. The source is the remains of an extinct volcano. It sits directly upon an old fault-line known as the Thringstone Fault, which originates in Derbyshire, UK and stretches to Germany, and which outcrops in several places in Leicestershire, UK. The particle densities of the aggregates used are presented in Table 3.2. Aggregate particle densities and gradation curves for each aggregate gradation have been used to calculate the aggregate gradation densities during the testing phase of this research project.

Table 3.2: Aggregate particle densities

Sr. No.	Aggregate Type	Source	Size (mm)	Particle Density (Mg/m^3)
1	Granite	Bardon Hill Quarry	28	2.78
2			20	2.78
3			24	2.81
4			10	2.83
5			6.3	2.84
6			Dust	2.80
7			Filler	2.68

To get an idea about the mineralogy of the different aggregates used in this study results from a mineral liberation analyser (MLA) are presented in Figure 3.1 for the granite. It is composed of more than ten different minerals with a major portion of Albite, Epidote, Quartz and Chlorite.

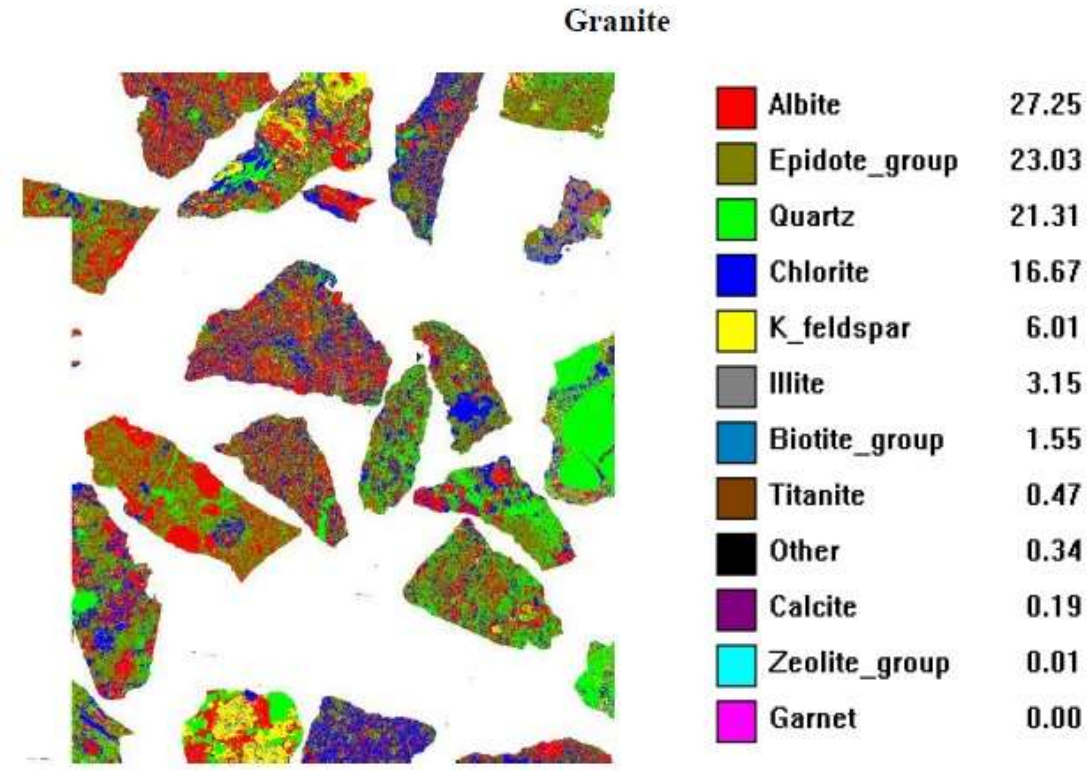


Figure 3.1: Mineral composition of granite using MLA analysis (Zhang et al. 2015)

3.2.3 Cement

Ordinary Portland cement supplied by Hanson was used in preparation of cement treated base layers. The general-purpose cement complying with the requirements of BS EN 197-1 CEM-II with strength grade 32.5N was used for preparation of cement concrete.

3.3 Experimental Programme

The experimental programme was divided into two major parts i.e. component and structural level testing. These two broad categories were then further divided into various types according to the need of the research project. All the component materials were tested for the properties required for the analysis and then selected materials were used in structure level testing to study the simulative laboratory performance of the inverted pavements. Figure 3.2 explains the testing programme in detail;

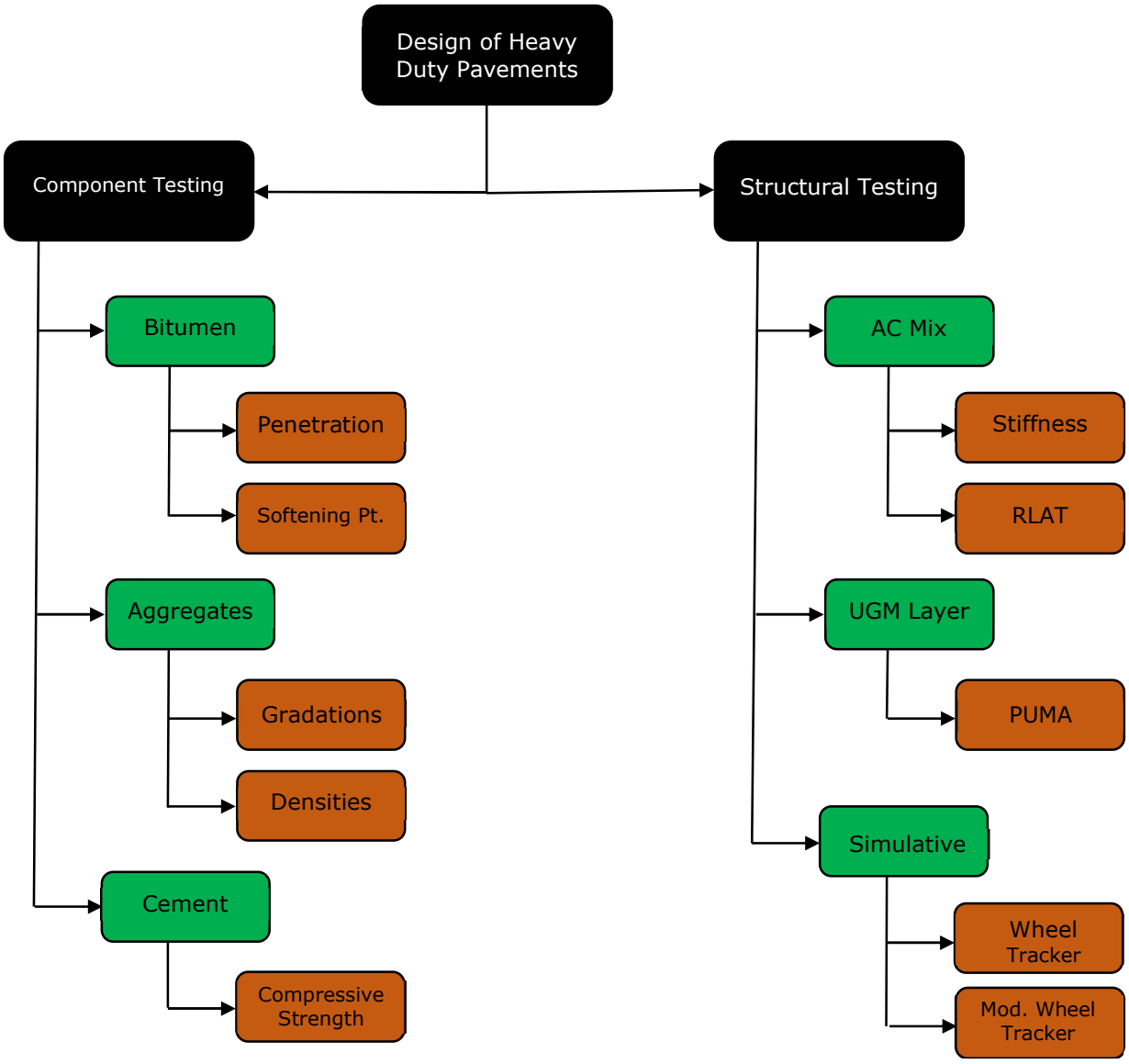


Figure 3.2: Laboratory testing matrix/plan

3.3.1 Component Level Testing

The project was initiated by selecting and acquiring the materials required for the study. The materials, then, were tested under various laboratory protocols according to the research requirements. The materials were tested separately, and basic properties were determined which were further utilized in constructing the simulative inverted pavements in the laboratory. The following sections details the testing methods adopted to find the properties of the different constitutive materials.

3.3.1.1 Aggregate Testing

The selected aggregates were graded with reference to the South African G1 base specifications limits with different fines contents in order to characterize their behaviour under different moisture, fines and stress levels. However, due to the mould size constraints, the maximum particle size could not be followed as per G1 specifications. The fines content, however, was determined according to the specifications due to unbound material behaviour's dependency on fines content. Different fines content gradations were selected close to the lower and upper limits of G1 specifications. Figure 3.3 shows the aggregate gradations selected for the study.

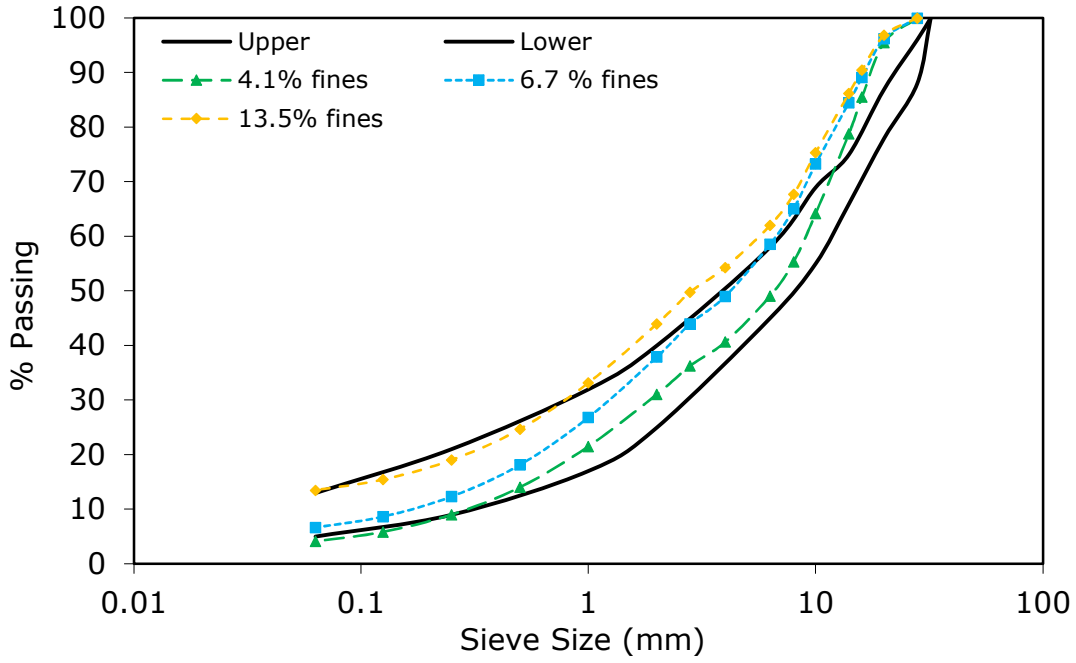


Figure 3.3: Aggregate gradations selected for the study + South African G1 limits

The following laboratory tests were performed on the selected gradations.

- Density/Moisture by Vibratory Compactor
- PUMA Test

The test descriptions are as follows;

3.3.1.1.1 Density/Moisture by Vibratory Compactor

After finalizing the gradations to be used in the research project, vibratory compaction tests were conducted in the laboratory for each gradation to

determine the dry density and optimum moisture content. Vibratory compaction was preferred over the proctor/modified proctor hammer since PUMA specimens were also prepared by vibratory compaction.

As per BS EN 13286-4:2003, the specimens of the selected gradation were compacted in three layers in a 150mm diameter mould by vibrating it for a total compaction time of 2 min ±5 sec. The specimens were compacted by holding the hammer vertically and moving the tamping foot from one position to the other in following order; N, S, W, E, NW, SE, SW and NE. The total compaction time of 2 minutes was equally divided between the above eight positions. The empty and compacted weight of the mould were determined in order to find the dry density at any moisture content. The test was repeated for several moisture content values (usually five) in order to determine the maximum dry density and optimum moisture content for the tested material. The value of the moisture content at maximum effective suction was determined by plotting the dry density versus moisture content as shown in the Figure 3.4. It is referred as the desired point because of the material's ability at this moisture content to take further water without sacrificing its load bearing capacity while maintaining the maximum dry density. The compaction test results are presented in Figure 3.5.

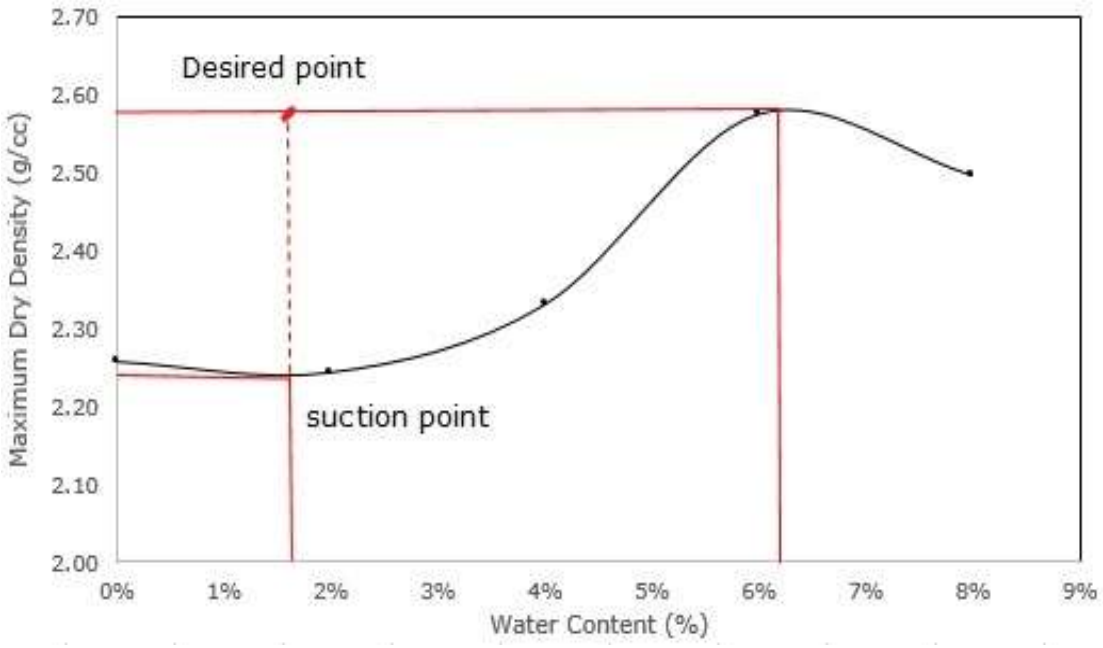


Figure 3.4: Suction temperature

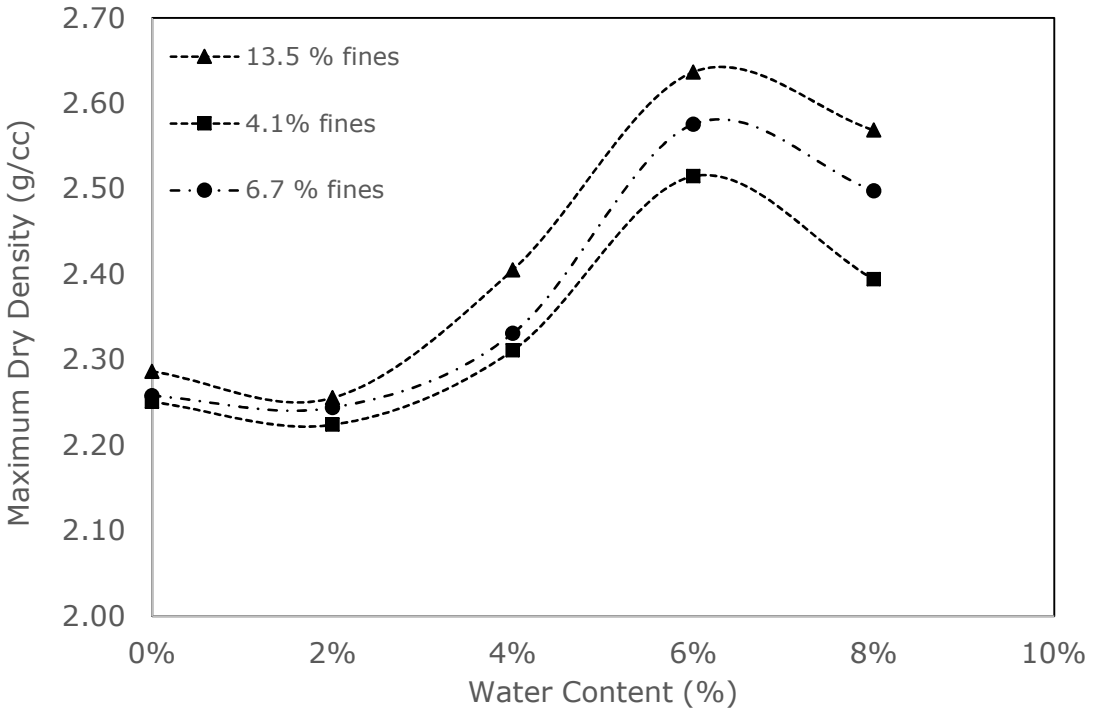


Figure 3.5: Proctor Test results

From the vibratory compaction test, the optimum moisture content and maximum dry density were found for each gradation; the results of which are presented in Table 3.3;

Table 3.3: Compaction test summary

Sr. No.	Fines Content (%)	OMC (%)	MDD (Mg/m^3)	Suction Water %age
1	4.1	6.08	2.52	1.8
2	6.7	6.20	2.58	1.8
3	13.5	6.27	2.64	1.9
4	7.4 (simulative test)	5.75	2.63	1.76

After calculating the optimum moisture and maximum dry density for the selected gradations, PUMA testing was carried out in the laboratory in order to characterize the Unbound Granular Layer in the Inverted Pavement under different stresses, moisture contents and fines contents. As the unbound granular layer is the key structural component of an inverted pavement, so a special testing and characterizing methodology was devised for it which will be discussed in the relevant chapter.

3.3.1.1.2 PUMA Testing

Many test methods have been devised over the years to study the behaviour of Unbound Granular Materials in the laboratory which range from the very simple CBR and Impact Hammer tests to rather complicated and time consuming Triaxial tests. Every test method has its pros and cons with Triaxial being the most sophisticated and instrumented method to get close to the actual stress conditions a material undergoes under traffic loading. Many researchers have tried to correlate the results from the simpler methods to that of Triaxial to reduce the cost and complications to get the material properties under loading. This has always been a very tricky subject to correlate the impact loading with the dynamic loading. So, an equipment named Precision Unbound Material Analyzer (PUMA) was developed by COOPER technology, UK with the aim to produce scientific results (stiffness modulus and resistance to permanent deformation) for unbound, hydraulically bound and asphaltic materials with the advantages of being low cost, easy to understand and practical. This method is an advanced testing technology which aims to fill the gap between the expensive and complex triaxial and rather empirical California Bearing Ratio tests and is designed to capture more realistic values of modulus and permanent deformation. The equipment has following advantages;

- It can be used with any Universal Testing Machine (UTM) for applying the load.
- It is compatible with the asphalt loading systems which are used for asphaltic testing.
- There is no need for separate compaction equipment; vibratory compactor is used.
- Stress conditions (axial and lateral) can be controlled.
- For unbound materials, particles up to 31.5 mm can be tested.
- It determines stiffness modulus under a variety of stress sequences allowing for a more scientific and representative material stiffness thus leading to appropriate pavement design.
- Rate of increase of permanent deformation with applied load can be easily studied.
- Cold mix asphalt can also be tested.

3.3.1.1.2.1 PUMA specimen: description, preparation and testing

There are different elements of a PUMA test mould for preparation of the specimen. These include

- the mould base,
- two compaction jackets; one upper and one lower,
- eight wall sections and
- H sections for connecting together the wall sections.

The mould is prepared by placing the lower compaction jacket on the mould base. The eight wall sections are then placed one after another by adjusting the H sections in between to obtain the circular shaped mould. The upper compaction jacket is fitted to maintain the mould shape. It is filled with the material and compacted to the desired density by vibratory compactor. The upper surface of the compacted material is kept as uniformly flat as possible and the top platen is placed. The load is applied with the help of a semi-circular steel ball for uniform application throughout. After the compaction of the specimen, the upper compaction jacket is removed with great care and a strain gauged band is positioned around the mould without disturbing its shape. The lower compaction jacket is also removed afterwards, and mould is placed in a universal loading frame. After installing the LVDTs and connecting the strain gauge to the computer, the specimen is ready for test. Figure 3.6 shows the PUMA mould and its components.

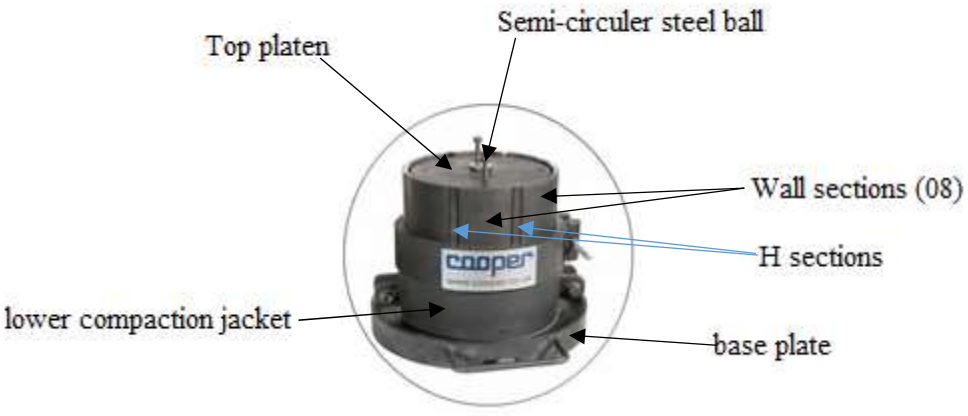


Figure 3.6: PUMA mould and its components

In the current project, the specimens were tested in a universal loading frame available at NTEC, University of Nottingham, following the description

above. Different stress levels were selected for the testing to investigate the unbound material behaviour under different loading conditions. The specimens were compacted and tested at different moisture contents, as described previously, to simulate varying environmental conditions, with the exception being the specimen tested at suction as it was compacted at OMC and dried out to reach moisture content at effective suction point. The PUMA software uses EN13286-7 protocol for stress, strain, Poisson's ratio and modulus calculations.

An ongoing PUMA test is shown in Figure 3.7 which clearly shows a specimen under load applied from a universal loading machine. LVDTs and strain gauges are also clearly seen. The testing was performed at 30^0C to correlate with the later stages of the research project.



Figure 3.7: PUMA test in progress

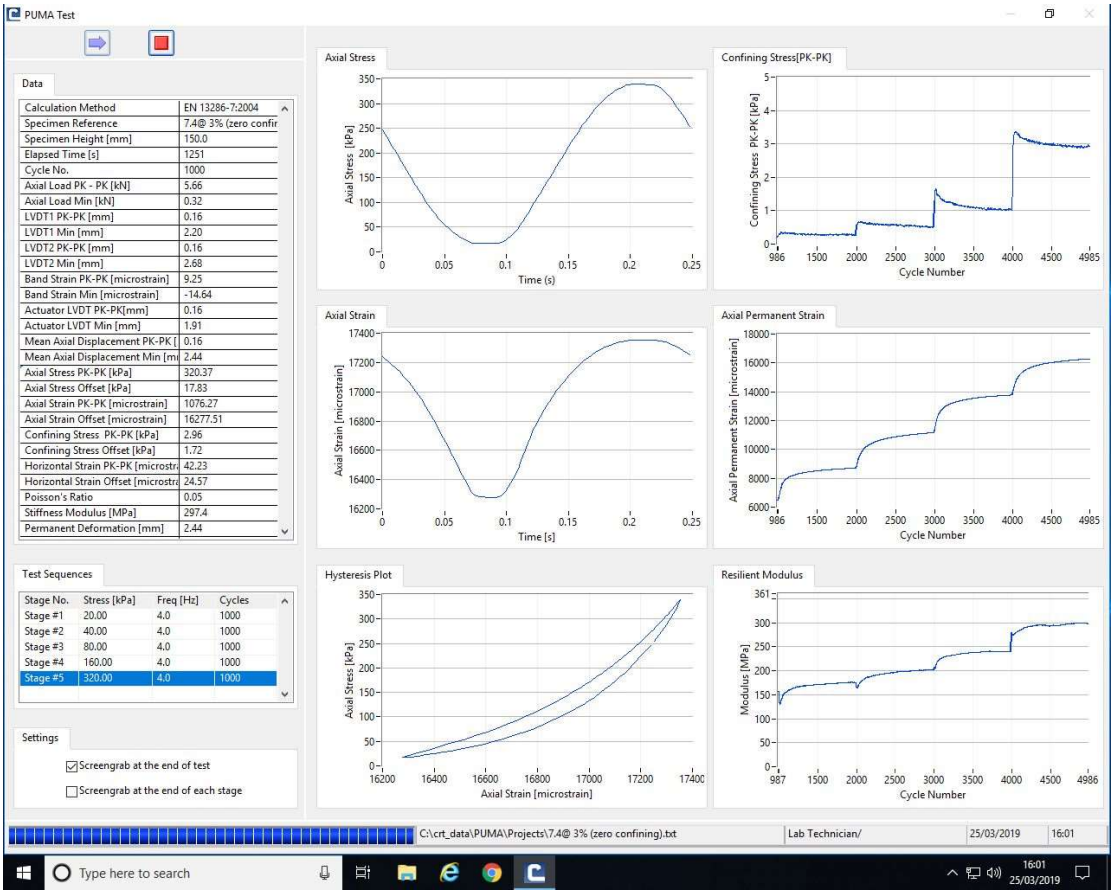


Figure 3.8: Screen shot of an on-going PUMA test at 5th loading stage

Figure 3.8 shows screenshots captured during a PUMA test with 7.4% fines content compacted and tested at 3% moisture. It can be seen that Strains (axial and horizontal), Stresses (axial and confining), LVDTs readings, Cycle Nos, Band Strains, Poisson's Ratio, Stiffness Modulus and Permanent Deformation are captured. The software plots different graphs during the test including stresses, strains and stress vs strain. The graphs can be easily related to the progression of the test. The software also shows the progress during different stress stages which can be seen at the lower left side of the screenshot.



Figure 3.9: PUMA samples after testing

Figure 3.9 shows different PUMA samples tested during the study. These samples contain different fines and moisture contents. The difference in compaction and adjustment of fines during compaction can also be seen very clearly from the figure 3.9, this also plays a role in permanent deformation and stiffness behaviour of the unbound granular materials which is presented in later chapter.

3.3.1.2 Bitumen Mixes

The properties of the 40/60 bitumen were already presented in Table 3.1. The bitumen mixes were prepared to construct the wearing course/ top layer of the inverted pavement simulative testing slabs by adding it to the aggregate layer.

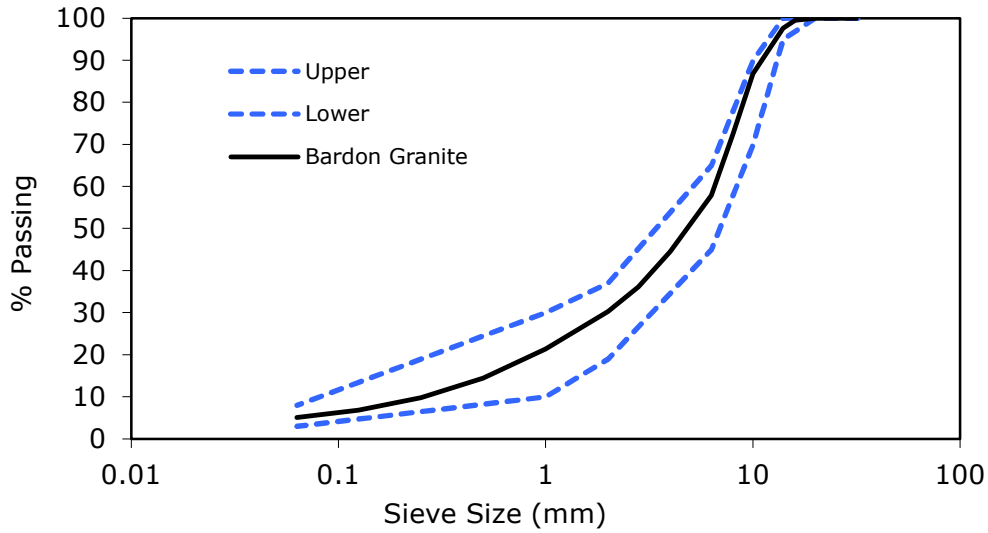


Figure 3.10: Granite gradation for 0-14mm dense graded mix

The mixes of dense grade 0-14mm particle size were prepared in the laboratory. Figure 3.10 shows the granite gradation adopted according to the BS 4987-1-2005. The bitumen was added at 5% as per British Standard and the mixtures were mixed at 160^0C by using an asphalt mixer in the laboratory. The mixes were, then, compacted into the desired samples as per the testing requirements. The mixtures were tested for stiffness and permanent deformation in the Indirect Tensile Test and Repeated Load Axial Test (RLAT) respectively.

3.3.1.2.1 Stiffness Test for HMA

The Indirect Tensile Stiffness Modulus Test (ITSM) has been performed in the laboratory to determine the stiffness values of the Hot Mix Asphalt (HMA) used in this project. British standard EN 12697-26:2004 (E) Annex C was followed to determine the stiffness of the HMA mixes in the laboratory. A test in progress is shown in Figure 3.11.

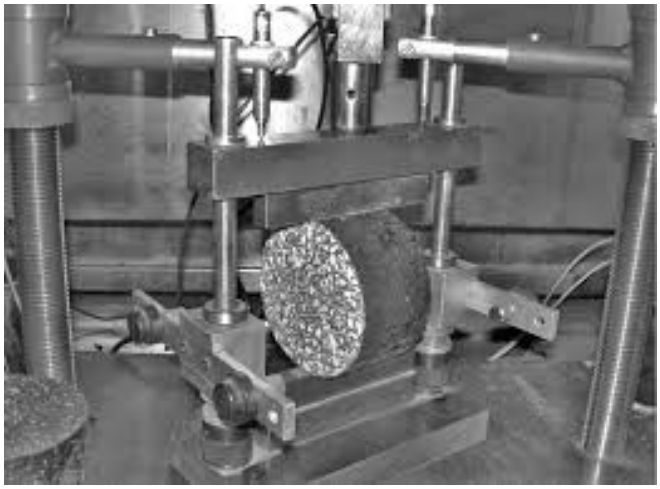


Figure 3.11: An ongoing ITSM test

3.3.1.2.2 Repeated Load Axial Test (RLAT)

Repeated load axial tests were also performed on the same density HMA specimens, as used in ITSM test, in order to get the permanent deformation of HMA under varying stresses, frequencies and temperature levels. The RLAT, Figure 3.12 determines the permanent deformation of HMA under different stresses and frequencies. The permanent deformation values obtained from the RLAT were used to develop a rutting prediction mechanism for an inverted pavement which is explained in detail in the

relevant chapter. RLAT test was conducted in the laboratory according to BS EN 12697-25:2016. The thicknesses of the RLAT specimens in the Figure 3.13 are also explained in the appropriate chapter.



Figure 3.12: Repeated load axial test for AC permanent deformation



Figure 3.13: RLAT tested samples

3.3.1.3 Compressive Strength of Concrete used for Cement Treated Base

Ordinary Portland cement was used in constructing the cement treated base in the inverted pavement simulative testing. G1 base gradation as shown in Figure 3.15 was used to construct cement treated base. The compressive strength test according to BS EN 13290-3:2019 was performed on the cubes, prepared with the same cement aggregate mix as used in the cement treated base layer. The peak Compressive strength found from the laboratory tests conducted on three concrete cubes was averaged and found to be 30.81 kN/mm^2 as shown in Figure 3.14.

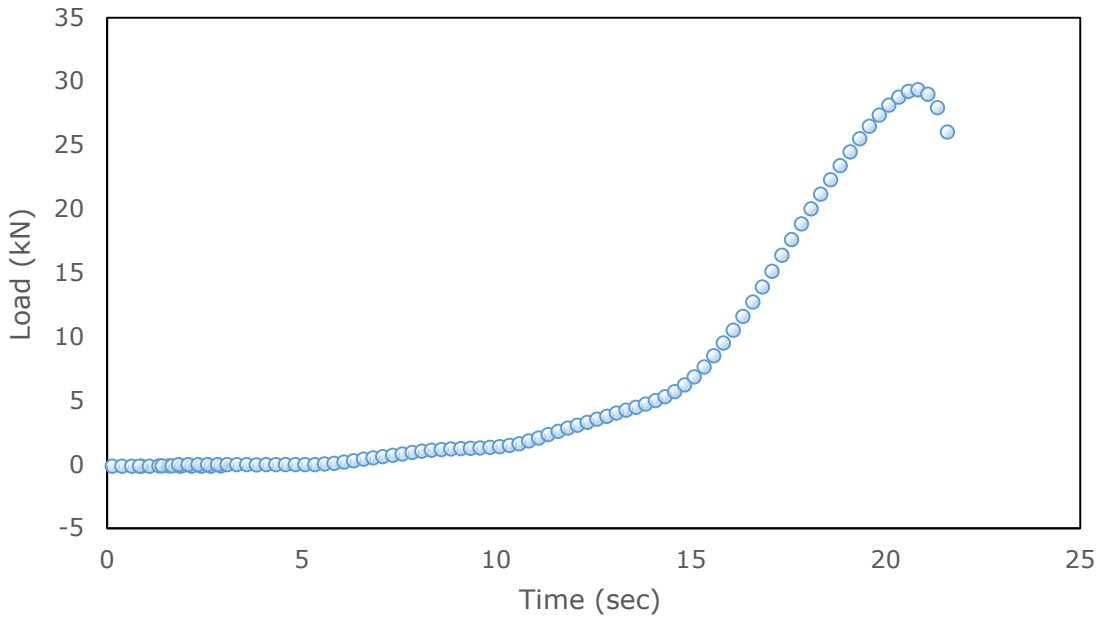


Figure 3.14: Compressive strength of CTB

3.3.2 Structure Level Testing

The second phase of the research comprised of testing at structure level. The commonly available equipment in the laboratory for such testing is the wheel tracker. Due to the constraints of size, space, equipment and budget, a simulative testing matrix was developed with the ability to test different combinations of pavement layers within the range of available laboratory equipment and testing environment. The testing program was developed with the aim to get positive results which could then be used to predict the pavement performance and hence provide data for designing the pavement.

The major structure level testing comprised of wheel tracking tests for i) Rutting and ii) Cracking. This section is, therefore, divided into categories;

1. Wheel Tracking for Permanent Deformation
2. Wheel Tracking for Cracking

3.3.2.1 Wheel Tracking for Permanent Deformation

Wheel tracker devices are used in the laboratory to perform simulative testing to measure the permanent deformation in HMA mixtures or in a pavement structure under a small wheel capable of applying different loads to the pavement slab. The laboratory test data is then, very carefully, correlated to the in-situ pavement performance. Therefore, careful consideration should be given to establishing the conditions in the laboratory such as loading condition, number of wheel passes, test temperature etc. to get efficient correlations with the pavement in-situ performance. Wheel tracking devices are used in the laboratory to predict the rutting, fatigue, moisture susceptibility, cracking and stripping in the pavement by carefully deciding the testing parameters. Many different types of wheel tracking devices are commercially available having the ability to test different samples under different testing conditions. These include Hamburg Wheel Tracker, Asphalt Pavement Analyser (APA) and French Rutting Tester. These devices are capable of testing different test samples including beam, cylinder and slab of different sizes and thicknesses. A specially commissioned wheel tracker was used during the project which was developed by the technicians at NTEC and referred to here as the University Wheel Tracker (UWT). The UWT has the ability to test a specimen with more than 100mm thickness which was a necessity of the project, but it has the disadvantage of not being able to collect data electronically.

To calculate the permanent deformation in an inverted pavement under a moving load, the thicknesses of all pavement layers were reduced to approximately $1/4^{th}$-$1/5^{th}$ of their actual dimension. This was forced due to the size of the commonly available wheel tracking mould. For simulative testing, based on the limitations of the layer thicknesses, the nominal aggregate size was reduced to 14mm and an appropriate gradation was selected for simulative testing. The wearing course was designed according

to Highway England specifications with a nominal size of 14mm with 5% by weight of bitumen as was used for RLAT and ITSM tests previously mentioned. The selected gradation compacted at optimum moisture content was used in unbound layer and 4% by weight of cement was added to it to construct the cement treated base layer. The subgrade layer was simulated by a 12mm thick rubber sheet at the bottom of the wheel tracking mould. The adjusted gradation for nominal size of 14mm is shown in Figure 3.15.

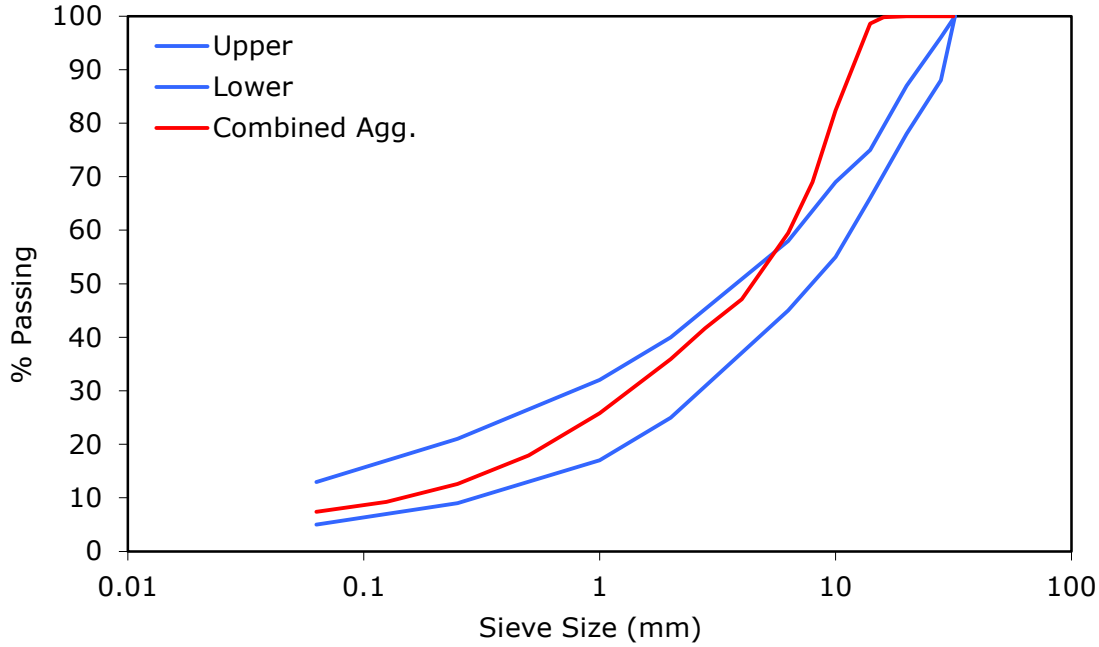


Figure 3.15: Aggregate gradation for simulative testing with the maximum particle size of 14mm

To study the performance of an inverted pavement under load, different thickness combinations of pavements layers were tested in the laboratory. Table 3.4 shows the testing matrix adopted for this purpose.

The test specimens were prepared by placing the 12mm rubber sheet into the mould; an already constructed and cured concrete slab was then placed on top of the rubber to simulate the CTB layer. The aggregates as per the 7.4% fines content gradation were weighed and mixed with optimum moisture content. The prepared unbound granular materials were then compacted in-situ with a Kango compactor in multiple layers. The density of the layer was monitored by measuring the thickness of the compacted layer and layers were compacted until the desired density. A similar

procedure was followed for constructing in-situ asphalt wearing course. A wooden collar was made in the laboratory to restrain the loose material in excess of the mould height during compaction.

Table 3.4: Testing matrix for Wheel Tracking test

Simulative Testing (Rutting & Cracking)					
Sr. No.	Layer Thickness (mm)				Total Thickness (mm)
	HMA Wearing Course	UGM	CTB/ Simulation	Subgrade	
1	15	20	30	12	77
2	15	35	30	12	92
3	15	50	30	12	107
4	15	60	30	12	117
5	20	20	30	12	82
6	20	35	30	12	97
7	20	50	30	12	112
8	20	60	30	12	122
9	25	20	30	12	87
10	25	35	30	12	102
11	25	50	30	12	117
12	25	60	30	12	127

All the compaction setup including wooden collar, Kango compactor, steel plates etc. were kept ready before mixing the material in order to compact the material at the specified temperature. The materials, aggregate and bitumen, were mixed in the mixer at 162^0C. An additional 2^0C was applied to compensate for the time taken to transport the mix from mixer to mould. After placing the material into the mould, in-situ compaction was performed using a Kango compactor. Hot steel plates were used to provide a smooth surface without sacrificing the compaction temperature. The density of the layer was, again, monitored by measuring the thickness during compaction. Since the compaction temperature was maintained, the asphalt wearing course was compacted in single layer. A prepared and tested wheel tracker specimen is shown in Figure 3.16.

Due to the thickness constraint, the thickest available mould was used with the ability to test specimens up to 130mm thick. In contrast to the thickness advantage, the equipment has a disadvantage in not having an automated system of collecting the data. The permanent deformation data was, therefore, collected manually from the test. A few steps have been taken to

minimize the errors associated with manual data collection. The permanent deformation values were taken at 3-4 points based on visual inspection of the slab and an average value was considered in most cases unless a significant difference occurred in which case the highest deformation value was reported. The data was collected following two procedures; a profilometer and depth gauge with holed straight metal plate longer than the rut profile thickness. The holed metal was placed across the rut line and the depth gauge was used through the holes to measure the rut depth. Special care was taken to avoid the depth gauge creating voids while taking measurements which could have given greater rutting values. As stated earlier, the procedure was followed at multiple points along the rut line to get the rutting.



Figure 3.16: Wheel Tracker tested specimen

The vertical stress on the specimen was applied and controlled by hanging weights attached with the moving wheel. The loads applied by the hanging weights on top of the surface was measured by a balance and used to calculate the contact stress under the wheel. The detailed description of manual rut measurements along with the results is mentioned in chapter 5. A wheel tracking test setup is shown in Figure 3.17.



Figure 3.17: Wheel tracking device

3.3.2.2 Wheel Tracking for Cracking

The wheel tracking test is a simulative laboratory test in which a small loaded wheel is repeatedly rolled on the laboratory prepared pavement layer (HMA usually) as explained already in the previous section. As the research project focusses on performance of inverted pavements, the rutting and cracking resistance were studied. The reflective cracking also needs to be studied due to presence of a cement treated base in an inverted pavement. The brittleness of the concrete makes it vulnerable to cracks which can then be reflected to the surface.

The wheel tracking test to study reflective cracking was performed on the same materials and thickness combinations as with the rutting testing setup. The only difference between the test setups was the testing moulds.

With the maximum tensile strain being at the bottom of the top layer in a pavement, it is impossible to study crack development closely by using a standard wheel tracker mould due to its closed wall setup. So, a mould was designed for the tests to study the crack development under loading in an inverted pavement. The mould was designed with removable side walls so

that crack propagation may be seen and recorded along with the loading cycles.

3.3.2.2.1 Wheel Tracker mould for Cracking test setup

Due to the constraints of the cracking test setup and in-situ compaction of inverted pavement layers, a mould was designed to compensate all of these. The mould was designed to study the behaviour of crack initiation and propagation in an inverted pavement simulative test conducted in the laboratory. The following are the parts of the moulds, followed by a brief description:

A base plate, long side walls, short side walls, varying sized angles for support, metal plate for holding the specimen in place, welds and bolt joints.

The mould was manufactured by welding the side walls of different heights to the steel base plate. A steel angle was welded on the top side of the short side walls to provide adequate lateral support and keep the mould in shape during compaction as well as testing. Another advantage of this setup was to use it as a handle to pick up the mould. The longer side walls were welded to the base plate up to a height of 105mm out of 130mm of total mould height. This provided enough height to accommodate any thickness combination up to the top of unbound layer, so that the HMA layer was always visible during the test to observe/study the cracking behaviour. The remaining height on the long side walls was adjusted by making removable side walls which were placed during the compaction and removed during testing. The removable side walls were manufactured with more height than 25mm to accommodate the loose materials before compaction as all the compaction was done in-situ. The long side walls were also supported by the steel angles along the length at 105mm height to provide lateral support while maintaining the shape of the mould during compaction and testing. All the walls were placed during preparation of the specimen while the removable wall portions were removed after the specimen was prepared and ready for testing. As the prepared samples didn't have any lateral support on the top HMA layer, so steel angles of approximately $1/8^{th}$ of the specimen length on each end were designed to provide the lateral support and keep the specimen in place during loading. To avoid upward movement

of the specimen during wheel loading, a steel plate was designed to cover the specimen top surface up to a length of 7-8mm. The plate was designed to prevent the specimen surface's upward movement due to a tyre load on the opposite end. The wheel loading is controlled by hanging weights on a lever arm and calculating the corresponding load in kilo Newtons. The cracking test results were captured by GoPro camera. The camera was used to capture the images of the on-going test at an interval of 30 sec. The images captured and continuous visual inspection of the specimen during testing were used to determine the number of cycles to initiate the crack at a given wheel loading and used in analysis. The number of cycles were counted by a counter attached to the wheel tracking setup. It was also counter-checked by calculating the number of images captured till the crack initiation on the basis of image capturing frequency of the camera and wheel tracking loading speed which was set at 26.5 rpm. It was found that the designed mould proved to be an effective way of studying the pavement cracking behaviour having the capacity to visually inspect the cracks at all times, the ability to provide enough space and strength for in-situ compaction as well as being suitable for the pre-compacted specimen.

Similar to the wheel tracking mould preparation for rutting, the specimen was prepared by placing the 12mm thick rubber sheet as a subgrade layer. The cement treated base was pre-compacted and cured as a slab and then cut into beams to be able to fit into the new mould. The beams were then also cut in the middle to provide a crack in the CTB layer. The crack was provided intentionally to speed up the reflective cracking process. After placing the CTB as two beam segments showing a crack in the middle, the UGM was compacted in-situ, mixing the aggregates at optimum moisture content. The compaction was done using a Kango compactor and density was monitored by measuring the layer thickness. The same in-situ compaction was adopted to compact the HMA wearing course on top of the UGM layer. The mould, compactor and all other relevant parts were kept ready before the materials were mixed in the mixer. It enabled compacting of the HMA mix as wearing course without dropping the temperature of the mix after mixing. After preparation of the mould and letting it cool down for a specific time, the removable walls were removed, and steel angles and

top plates were placed for lateral and downward support of the specimen under loading. The sides of the wearing course were then painted white. The paint provided a smooth side of the specimen. It was done for easy visual recognition of crack initiation. The loading on the specimen was applied and controlled by hanging weights to the lever arm.

3.3.3 Predictive Analysis

The third phase of the project didn't involve any laboratory testing but the predictive analysis of all the results. The analysis was performed on the measured data to predict the permanent deformation and cracking in the pavements. The predictive analysis was also divided into two phases;

- Predictive Analysis for Permanent Deformation
- Predictive Analysis for Cracking

3.3.3.1 Predictive Analysis for Permanent Deformation

A comprehensive predictive analysis was performed using Microsoft Excel to predict the rutting in inverted pavements both at layer as well as structure level. The predictive analysis for permanent deformation can be divided into two categories;

- Prediction in HMA
- Prediction in UGM

3.3.3.1.1 Prediction in AC

A pseudo-viscosity concept has been utilized in this research to predict the permanent deformation in the HMA mixture top layer of the inverted pavements under study. The following is the brief description of the method;

A laboratory wheel tracking test is performed on the specimen to find the permanent deformation. The test data is to be used to make a laboratory determined rut depth curve.

Another slab with the same density is prepared in the laboratory and cores are taken out of it. The cores are then trimmed to the thicknesses used in the wheel tracking test. All the cores are then tested in the RLAT under different stress levels corresponding to those applied during the laboratory wheel tracking test.

The strain rate for each loading cycle applied in the RLAT is calculated by the following equation;

$$\varepsilon' = \frac{\varepsilon 2 - \varepsilon 1}{t2 - t1} \qquad (1)$$

where t_2 and t_1 are the time (in seconds = number of cycles) corresponding to strains

In the next step, the viscosity of the mixture is determined as a function of strain which can be calculated by dividing the axial stress in MPa by the strain rate already computed. (Nunn, 1986).

$$\eta = \frac{\sigma}{\varepsilon'} \qquad (2)$$

The mixture viscosity is then plotted against the strain. The plot is then used to establish the material's viscous properties for permanent deformation prediction. A typical plot representing a mixture showing all three stages of creep (primary, secondary, and tertiary) is shown in Figure 3.18.

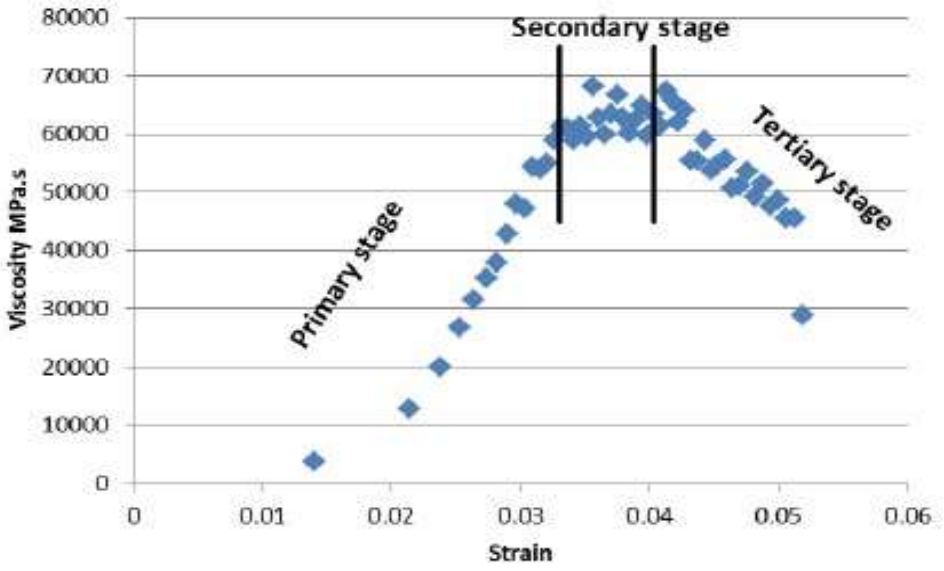


Figure 3.18: Viscosity vs Strain (Stages)

After that, an initial material viscosity is determined from the viscosity-strain curve by extrapolating to zero strain. This initial value is then used in the 1st deformation analysis increment.

The asphalt slabs are then modelled in KENLAYER (multi-layer elastic analysis) with varying thicknesses depending on which wheel tracking slabs. The following are the data to be input in the software for slab modelling;

Vertical Stress: 850 kPa corresponding to the stress in wheel tracking test

Radius: 0.0236m.

The number of layers (different for different HMA thicknesses) are then assigned viscosity values, all having the same viscosity for the first interval. A very stiff subgrade layer is added having effectively infinite viscosity. All the layers are assumed to be incompressible (Poisson's ratio of 0.5) to ensure that the deformation is due to viscous flow not densification, and full friction between layers is adopted.

The analysis is then performed and the strain rate (strain/second = strain/-cycle) in the middle of each layer under the centre of the load is used in further calculations.

A surface deformation increment of 0.1 mm is applied and the layer strains and the number of cycles to cause this increment are determined.

The new layer strains require new corresponding viscosities from the strain viscosity curve, Figure 3.18, established earlier in the process giving new viscosities for each layer; these are used in KENLAYER for the following deformation increment.

This loop is continued until a specified deformation is reached. No adjustment was made to the loading time because it was similar in both cases (RLAT and wheel track). In the RLAT the stress was applied for 1 second and in the wheel tracking test the rate of loading was 26.5 cycles/minute and each cycle consisted of two passes. To clarify the above methodology, see the flow chart in Figure 3.19.

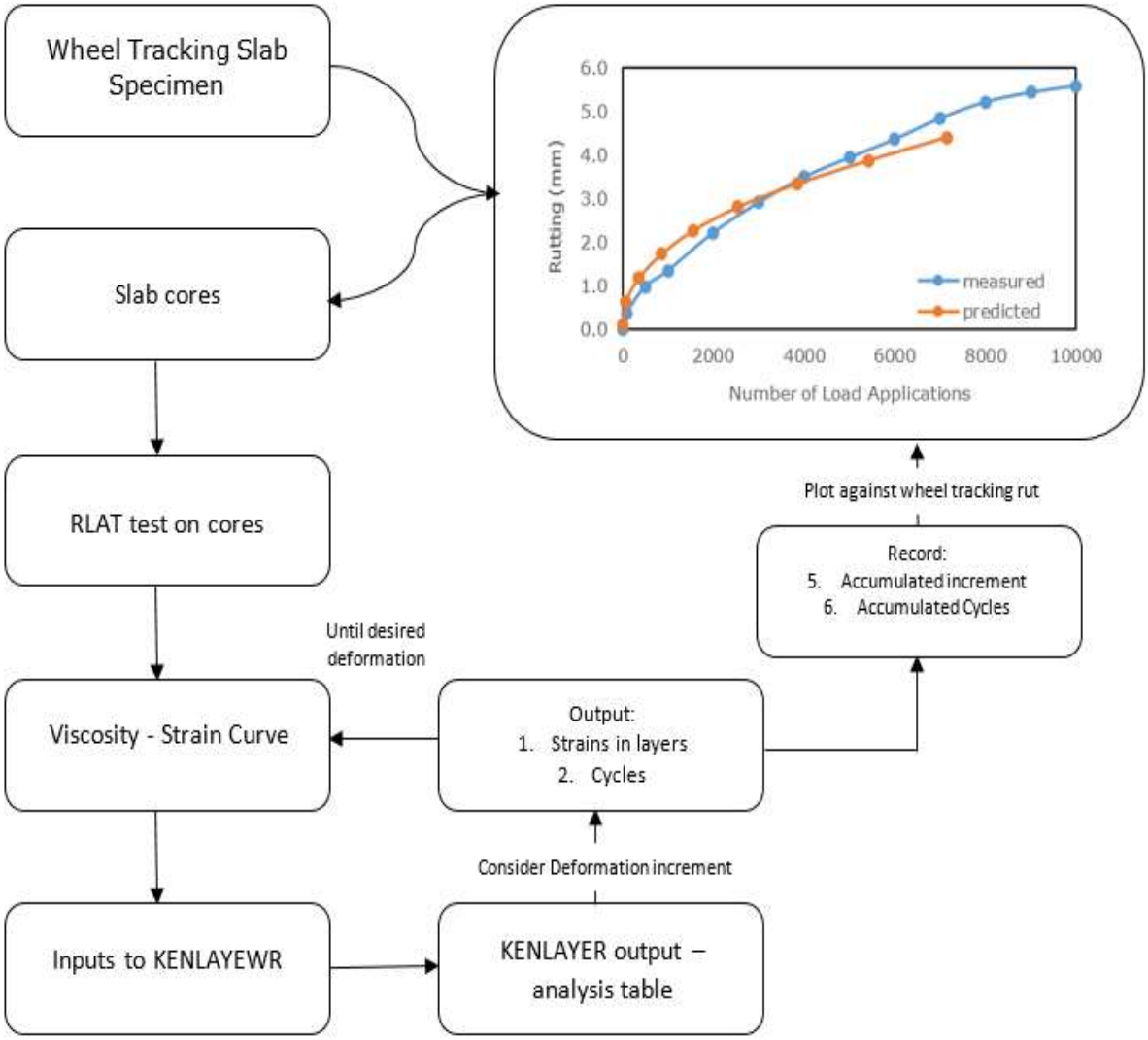


Figure 3.19: Methodology for AC rutting prediction

3.3.3.1.2 Prediction in UGM

The predictive analysis in UGM was more complicated due to stress-dependent nature of the material. The dependency of permanent deformation behaviour of unbound materials on various factors has led many researchers to develop different strain predictive models dependent on stresses, number of load applications and other factors by testing different UGMs in the triaxial test. Most of the models developed by the researchers considered the single stage stress application which is in contrast of the in-situ stress conditions within a pavement at any given moment. Rahman and Erlingsson (2015) applied a strain hardening approach to various previous single stage stress models to develop

multistage stress dependent models. Along with modifying the previous models, they also developed a new model for strain prediction based on number of load applications and stress.

For the purpose of strain prediction based on multistage stress application in the PUMA test, a strain predictive model developed by Rahman and Erlingsson (2015) was selected which considers the multistage stress profile. PUMA data related to stress applied in multiple stages and the model was, therefore, an excellent choice. It considers the time hardening approach and accounts for the number of cycles at any stress levels to calculate the strains at that level without applying the previous stress conditions.

The following equation shows the Rahman-Erlingsson model for strain prediction;

$$\hat{\varepsilon}_p\,(N) = a\,N^{bS_f}\,S_f$$

Equation (3) defines the Rahman-Erlingsson (R-E) model to predict permanent strain on the basis of stress ratio and number of load applications, where $\hat{\varepsilon}_p(N)$ is the accumulated permanent strain after N load cycles and a and b are regression parameters related to the material. The term S_f describes the effect of stress condition on the development of permanent strain and is expressed as

$$S_f = \frac{(q/p_a)}{(p/p_a)^{\alpha}}$$

where q is the deviator stress, p is the hydrostatic stress (one-third of the sum of the principal stresses) and α is a parameter determined using regression analysis. The term p_a = 100 kPa (reference stress taken equal to atmospheric pressure) is used to make the expression non-dimensional.

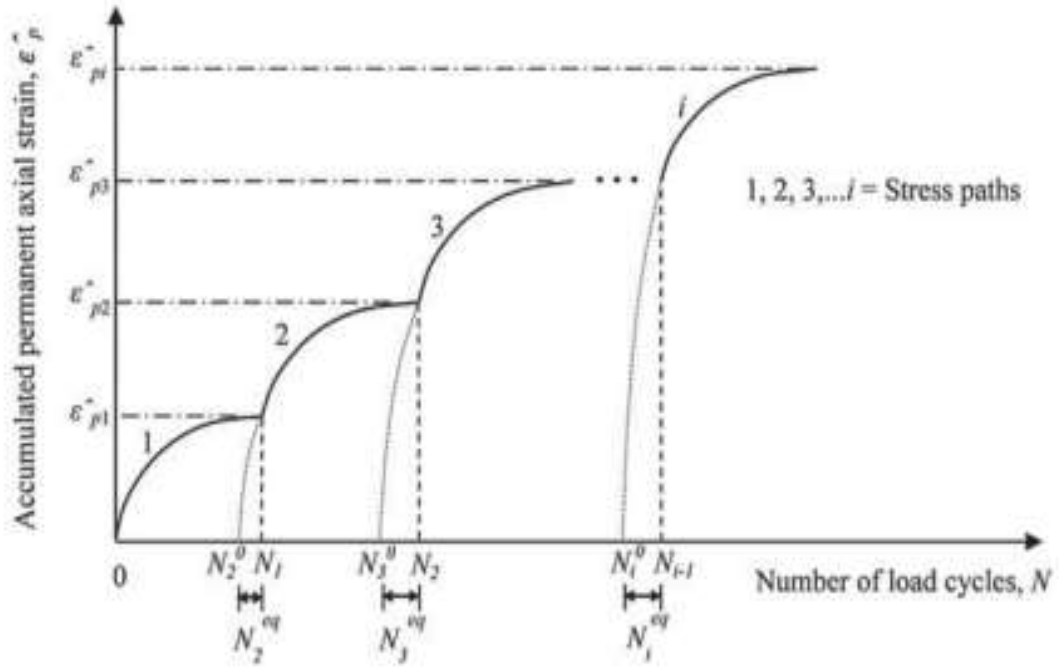


Figure 3.20: Time Hardening approach (After Rahman and Erlingsson 2015)

Applying the time hardening concept, shown in Figure 3.20, at the beginning of any level (*i*) of the multistage repeated load triaxial (MS RLT) test, the accumulated permanent strain from the previous loading stages is used to calculate the equivalent number of load cycles (N_i^{eq}) required to attain the same amount of strain for the current stress level alone. This N_i^{eq} is then used to modify the total number of load cycles, *N* from the beginning of the test to get the effective number of load cycles as $(N - N_{i-1} + N_i^{eq})$, where N_{i-1} is the total number of load cycles at the end of (*i*-1)th stress path. Thus, this effective number of load cycles is used to calculate any further accumulation of permanent strain during the current loading stage. If the stress level during the current loading stage is significantly lower than the previously occurring stress levels, the calculated N_i^{eq} approaches infinity and it is assumed that no further permanent strain will occur during this stage. Hence, using this procedure, it is possible to model the entire range of the MS RLT test continuously.

Equation (3) can be modified as shown in equation (5) to consider the time/strain hardening approach.

$$\hat{\varepsilon}_p\,(N) = a\,(N - N_{i-1} + N_i^{eq})^{b(S_f)_i}\,(S_f)_i$$

where

$$N_i^{eq} = \left[\frac{\hat{\varepsilon}_{p_{i-1}}}{a\left(S_f\right)_i}\right]^{b^{-1}\,(S_f)_i^{-1}}$$

As the model was developed using triaxial data, and it was to be fitted to the PUMA data, this proved to be a difficult element of the prediction. The model fitting was composed of the following steps;

- Select the Rahman and Erlingsson model based on the similar stress conditions.
- Calculate the total axial and confining stress by adding the Max and Min stresses from the PUMA data.
- Based on step 2 calculations, find the 'q' and 'p' stress values and hence calculate the S_f values at different alpha values.
- Take the data points at each stress stage (total of five) at cycles 1 and multiples of 100 up to 1000 to get 11 data points containing S_f and measured strains. The strains for these 11 data points were then predicted from the above equation using the sum of difference of squares method. It gives us the corresponding 'a' and 'b' values.
- Use the values of data points at each stress stage to find the best fitting 'a' and 'b' values by summing the square of the difference between measured and predicted strains.
- This exercise resulted in 5 different 'a' and 'b' values at five different stress stages.
- The average values of five 'a' and 'b' values was also calculated and later used to predict the strain in a full PUMA test.
- The first stress stage was predicted by using the number of load applications. For the rest of the stress stages, N^{eq}, equivalent number of load applications, was also calculated and used in predicting strains at respective stress stage.
- Thus, the strains were predicted at five different stress stages by using five different values of the parameters 'a' and 'b'.
- Another strain prediction line was developed by using the average values as calculated in the previous step.

- One more strain prediction line was developed by using the same 'average' values of the parameters in another MS Excel column. The values in this column were, then, adjusted manually while carefully inspecting the visual results between measured and predicted strain against Number of load applications. The values of 'a' and 'b' were termed as 'adjusted'. The equivalent number of load applications for these 'adjusted' values were also calculated and used in permanent deformation prediction.
- The whole process was repeated for the data at a different alpha value as well to find the best fitting alpha to the PUMA data. The visual inspections and R^2 calculations between the measured and predicted values at 'average a and b' and 'adjusted a and b' were used to find the values of constants to best fit the PUMA data.
- The same procedure with different alpha values was applied for all the PUMA tests performed with varying fines and moisture contents. From the predicted result comparison, it was found that the alpha value of 0.75 results in better predictions.
- All the regression parameters were then summarised and used to find the best fit alpha values to PUMA test data for predicting strains against number of load applications at a given stress ratio.

3.3.3.2 Predictive Analysis for Cracking

A methodology was developed for predicting the fatigue characteristic of inverted pavements by using the laws of mechanics. The forces and moments within a pavement under the wheel load application were calculated and resulting deformed shape of the asphalt concrete layer was considered for calculating the tensile strains at the bottom of the HMA layer. The strains calculated were used to develop a fatigue characteristic which was further used to evaluate the number of cycles to failure for pavements without the unbound granular layer. The results for pavements with and without the unbound granular layer were compared to find the significance of the unbound granular layer to reduce the possibility of reflective cracking which results in improved fatigue life. The methodology developed was also applied to the real pavements.

3.3.4 Summary

The chapter summarizes all the materials and methods used throughout the research project. The materials, their properties, testing techniques and predictive analysis techniques are mentioned in this chapter.

4 Unbound Granular Materials Characterization in an Inverted Pavement

4.1 Introduction

Unbound Granular Base Layer (UGBL) is constructed between asphalt mix wearing course and the subgrade (foundation) layer in a typical flexible pavement. Its main function is to provide support to the wearing course as well as spreading the load over a larger area of the subgrade to protect it from permanent deformation. The pavement can come under severe deformation if the UGBL cannot withstand the stresses induced by the moving vehicular traffic. Therefore, understanding the deformation behaviour of the UGBL under load plays a significant role in evaluating and predicting pavement performance. It is believed to be a very important layer for structural integrity of a conventional flexible pavement by supporting the asphalt and protecting the subgrade layers. The stiffness behaviour of UGMs is inherently anisotropic and stress-dependent due to their nature. There have been various instances of researches studying stress-dependent stiffness of UGMs (Roesler 1979; Kopperman et al. 1982; Santamarina and Cascante 1996; Yimsiri and Soga 2002; Terrell et al. 2003). But the stiffness of UGMs is a very important and critical parameter for the analysis and design of pavements especially for inverted pavement structures where the proximity of the load to the UGMs is experienced (Tutumluer 2013; Cortes and Santamarina 2013; Papadopoulos and Santamarina 2014; Papadopoulos et al. 2015).

The unbound aggregates in a pavement display stress dependent non-linear elastic behaviour under cyclic loading (Morgan 1966; Monismith et al. 1967; Hicks and Monismith 1971; Allen and Thompson 1974; Barksdale 1984; Adu-Osei 2000; Lekarp et al. 2000). The presence of a very thin asphalt layer accompanied by the stiff cement treated foundation in an inverted pavement develops extensive stresses in unbound aggregate base under traffic loading. Larger fluctuations in the state of stress intensify the non-linear response of the unbound aggregate base in an inverted structure

(Cortes 2010). The mechanical response of an unbound aggregate layer in a pavement under compaction and during service loading is, therefore, the most important parameter to be thoroughly considered and evidently understood before the design methods for this type of pavements can develop.

The research project, therefore, starts with a comprehensive laboratory study of the mechanical response of the unbound granular material under loading. A commonly used unbound granular material was selected for the research study i.e. granite. The unbound granular materials were tested under laboratory procedures for base characterization in laboratory equipment called the Precision Unbound Material Analyser (PUMA) under different loading and environmental conditions as documented in detail in chapter 3.

4.2 Materials and testing program

The mechanical response of unbound granular materials was studied in the PUMA. The gradations adopted for the study are presented in *Figure 4.1* as explained already in the previous chapter.

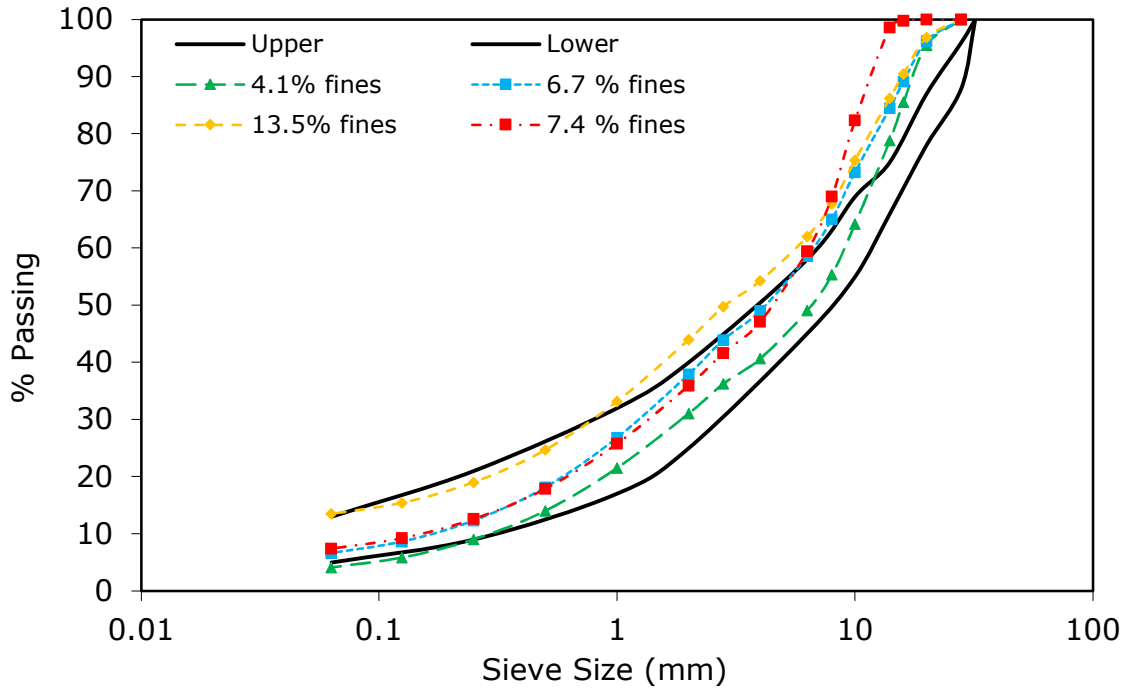


Figure 4.1: UGM (Granite) gradations for PUMA and Triaxial (South African specification)

The gradations were selected to study the effect of fines content on unbound materials behaviour under loading in an inverted pavement. The unbound base materials according to South African G1 specification consider a particle size of up to 50mm which could not be accommodated in the PUMA testing mould due to the size constraints. The PUMA mould has a diameter of 150mm which was not suitable to accommodate a particle size of 50mm and the results would not be trustworthy. To accommodate the size restraints, three aggregate gradations were selected with a maximum particle size of 28mm and having different fines content of 4.1, 6.7 and 13.5 corresponding to both envelopes and the middle of the gradation curve limits. The project requires wheel tracking testing at later stages which involved the usage of an aggregate gradation with a maximum particle size of 14mm due to the reasons explained in the relevant chapter. All the four gradations were tested in the laboratory for physical and mechanical properties.

The selected UGMs were tested in the PUMA under various stress conditions to account for material behaviour subjected to a wide range of loading. The stress conditions are presented in Table 4.1.

Table 4.1: Stress sequence for preliminary PUMA testing

Stage No.	Stress (kPa)	Frequency (Hz)	Load Cycles
1	20	4-5	1000
2	40	4-5	1000
3	80	4-5	1000
4	160	4-5	1000
5	320	4-5	1000

The selected materials were compacted using a vibratory Kango compactor in the laboratory to achieve the maximum dry density at the respective moisture content levels. Different fines and moisture levels were selected to study the behaviour of a wide variety of the materials under varying stress conditions. Table 4.2 shows the testing matrix adopted for the PUMA test in the laboratory.

Table 4.2: Testing matrix

Sr. No.	Material	Fines Content (%)	Moisture Content (%)			
1	Granite	4.1	Suction	3	5	OMC
2		6.7	Suction	3	5	OMC
3		13.5	Suction	3	5	OMC
4		7.4	Suction	3	5	OMC

The column "suction" in Table 4.2 refers to the moisture content (%) at effective suction point. Two samples of each combination were made and tested to avoid any personal errors during testing. The materials tested at suction moisture content were prepared at optimum moisture content and dried in the oven to reduce the moisture levels up to suction level while keeping the density at maximum values. This mechanism was adopted with the idea to get the maximum dry density for the given material having the ability to take more moisture without sacrificing the structural response to the load.

4.3 UGM stiffness by PUMA

One of the important parameters to characterize unbound granular materials (UGMs) within a pavement is the resilient modulus. The Resilient Modulus (M_R) is a measure of subgrade material stiffness. A material's resilient modulus is actually an estimate of its modulus of elasticity (E). While the modulus of elasticity is stress divided by strain for a slowly applied load, resilient modulus is stress divided by strain for rapidly applied loads – like those experienced by pavements (pavement interactive). It is denoted by Figure 4.2;

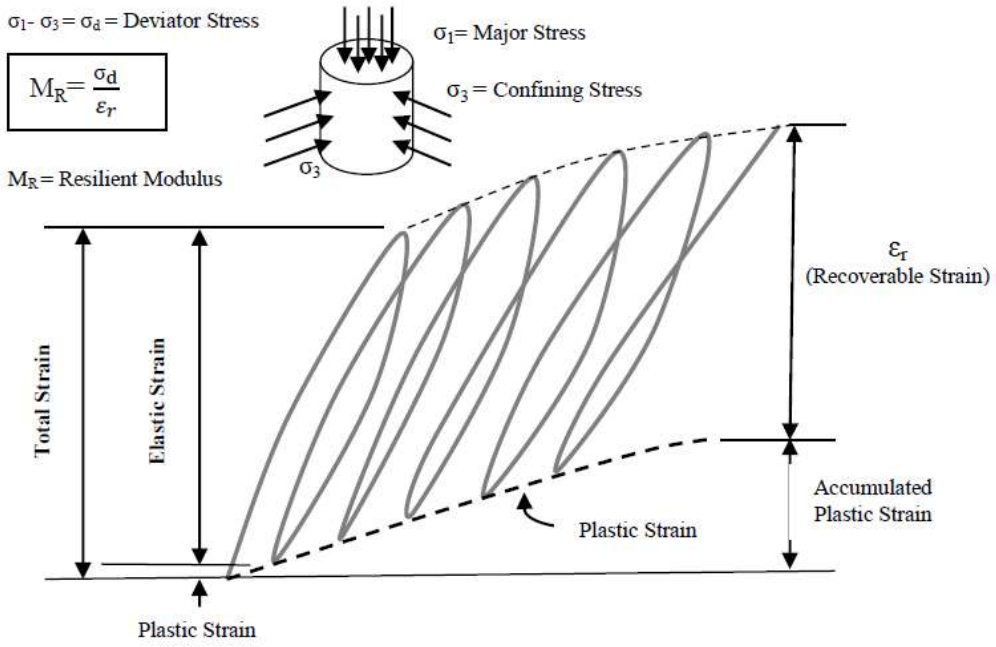


Figure 4.2: Resilient modulus definition (after Sadrossadat et al. 2018)

Resilient Modulus (M_R) is a fundamental material property used to characterize unbound pavement materials. It is a measure of material stiffness and provides a means to analyse stiffness of materials under different conditions, such as moisture, density and stress level. The resilient modulus results of the granular materials in a PUMA test are presented and discussed in detail as follows:

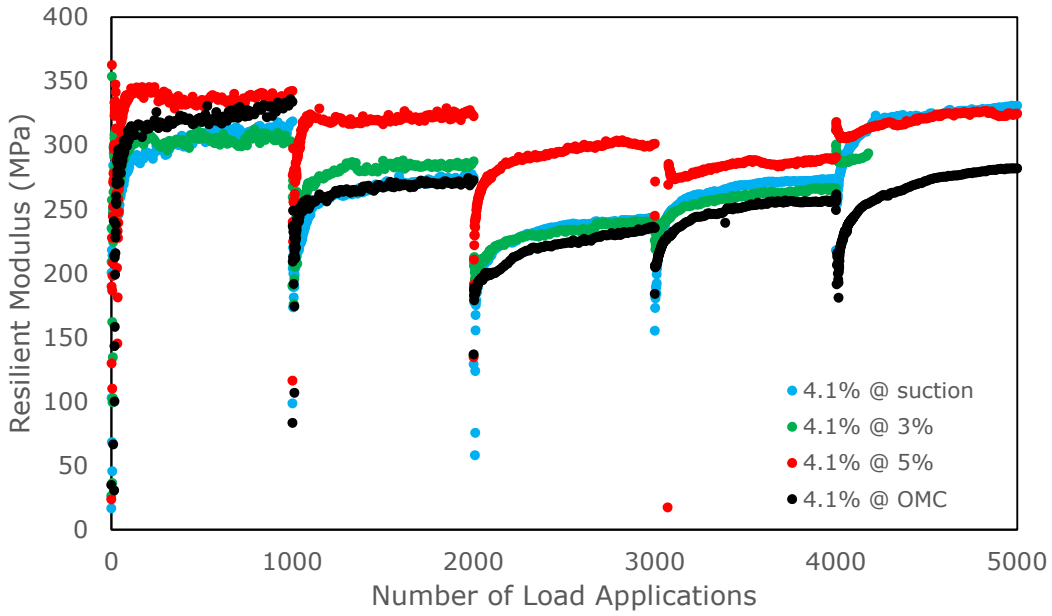


Figure 4.3: Stiffness at different moisture contents for 4.1% fines unbound granular base material

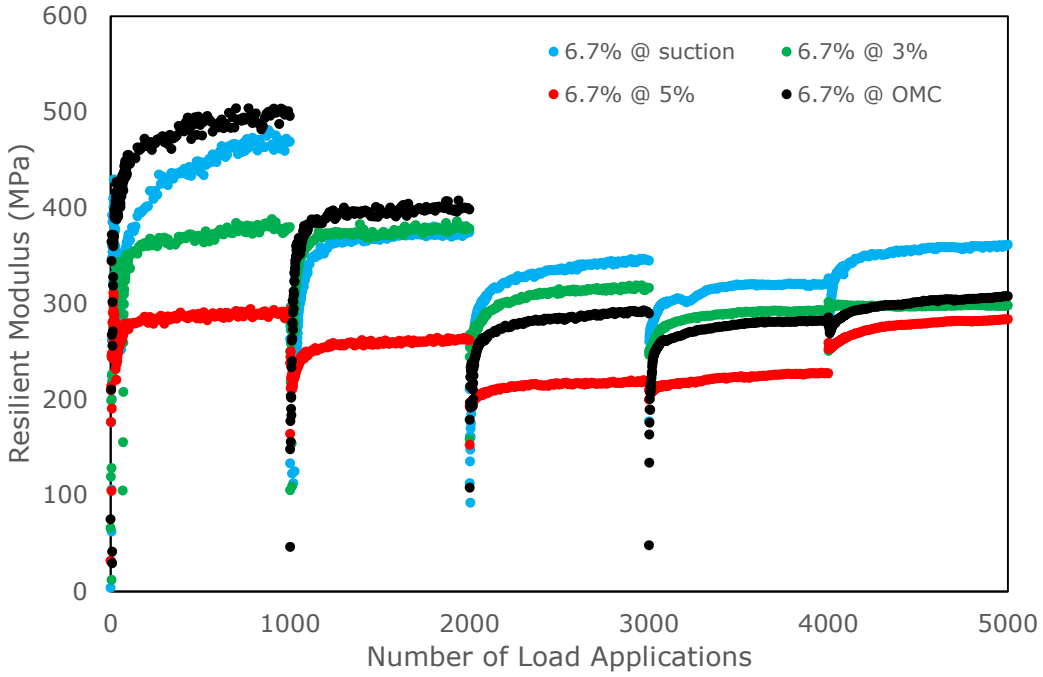


Figure 4.4: Stiffness at different moisture contents for 6.7% fines unbound granular base material

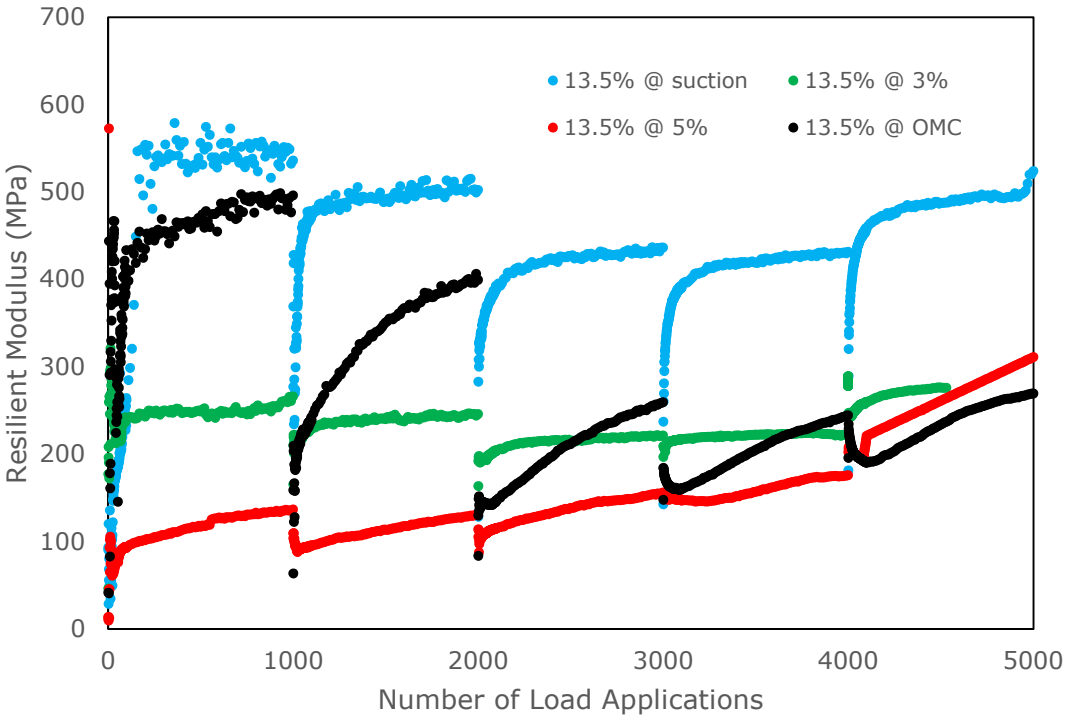


Figure 4.5: Stiffness at different moisture contents for 13.5% fines unbound granular base material

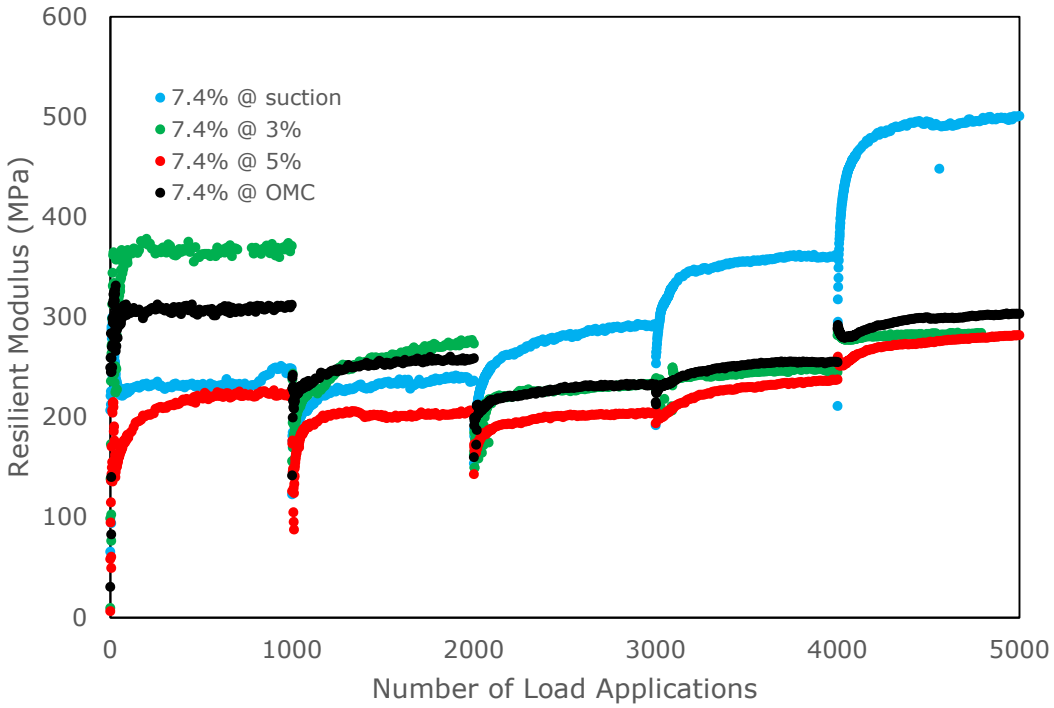


Figure 4.6: Stiffness at different moisture contents for 7.4% fines unbound granular base material

The Figure 4.3 -Figure 4.6 show the resilient modulus against the number of load applications for UGM gradations containing 4.1, 6.7, 13.5 and 7.4% fines content respectively. The effect of different moisture contents on stiffness of UGMs under loading is also shown in these plots. The figures represent the total number of load cycles applied to a test specimen under different stress levels mentioned. Each thousand cycles in the Figure 4.3-Figure 4.6 responds to one stress level. The specimens were confined initially by tightening the strain band which accumulated the stresses in the specimen pre-testing. The resilient modulus behaviour for unbound granular materials was characterized by its stress ratio between axial and confining stresses. The resilient modulus at all moisture and fines content levels was highest at the start of the test when the applied vertical stress was 20kPa and the 10kPa confining stress was applied by tightening the strain band. The stiffness decreased with increasing axial stress up to a certain value, 80kPa, whereas further increase in the stress, from 80kPa to 160 and 320kPa, led to stiffness increase. Another important point from the figures was that the difference between the resilient modulus at different moisture contents for any given gradation was higher at lower stress levels.

With an increase in stress, the window of difference between the resilient modulus values at different moisture contents got smaller. At the highest applied axial stress, the resilient modulus at different moisture values was nearly the same as in first stress phase of the test. The stiffness values at 5% and OMC were highest at 20kPa applied axial stress with the strain band applying confining stress. A few exceptions observed from the results are summarised below for readers: the UGM gradation containing 4.1% fines content exhibited highest stiffness modulus values at 5% moisture at which all the materials showed lowest stiffness except the last stress stage stiffness value for the material having 13.5% fines contents. The greater fluctuation between the stiffness modulus at different moisture contents at any given axial stress was observed for the materials with 13.5% fines content. The reason for this behaviour was combined dependency of the UGM on moisture and fines content so a detailed discussion on the effect of moisture and fines contents on resilient behaviour of UGMs is included in the following sections.

4.3.1 PUMA test summary

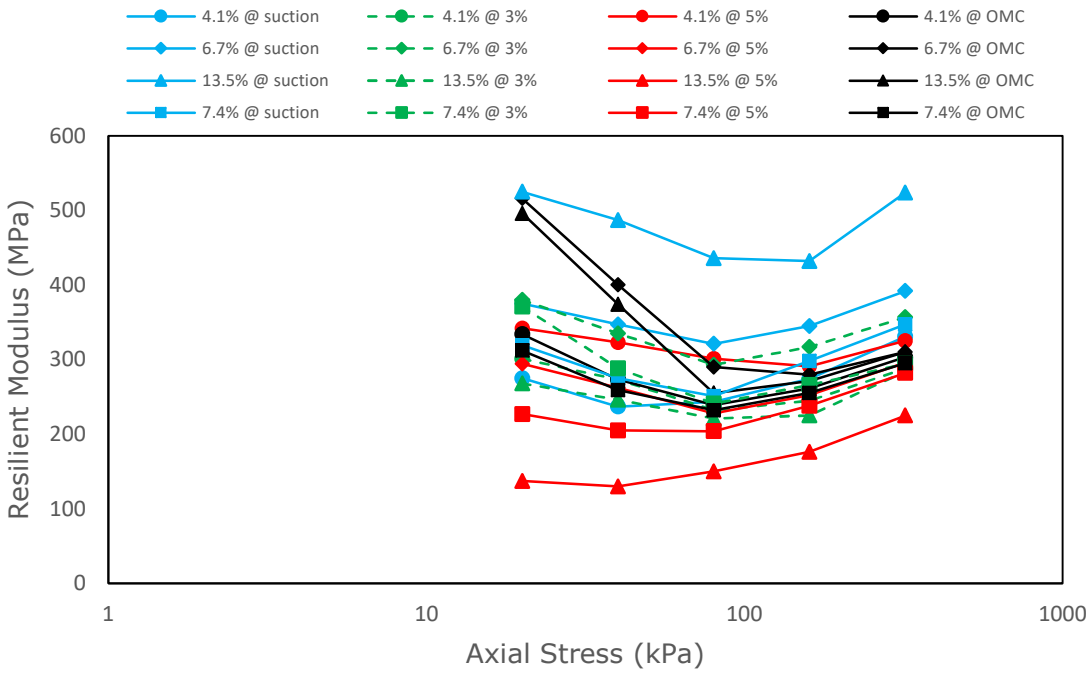


Figure 4.7: Stiffness summary at different moisture contents

The Figure 4.7 shows the resilient modulus values of different granular materials compacted at various moisture contents and axial stresses

(kPa). Different colours are used for different moisture contents for better understanding and comparison. It is very clear from the figure that for a range of unbound material gradations, the specimen compacted at optimum moisture content and tested at suction point (after drying out) showed the highest stiffness modulus values. This behaviour corresponds to the conceptually ideal density-moisture relationship of an unbound material under load. Pavement engineers and researchers idealize an unbound base layer having maximum dry density, which is generally achieved at optimum moisture content, with the ability to take further moisture without saturating and developing excessive pore water pressure, as higher pore water pressure results in low effective stress and hence low stiffness and deformation resistance of the material.

4.3.2 Effect of Moisture content on Unbound Base Performance

It has already been mentioned that different axial stresses are applied during a PUMA test with the help of a universal testing machine (UTM). The strain gauge band wrapped around the specimen also applied different levels of horizontal stresses as well. The Figure 4.8 shows a representative stress ratio calculated during PUMA test on a sample with 4.1% fines content and tested at different moisture contents.

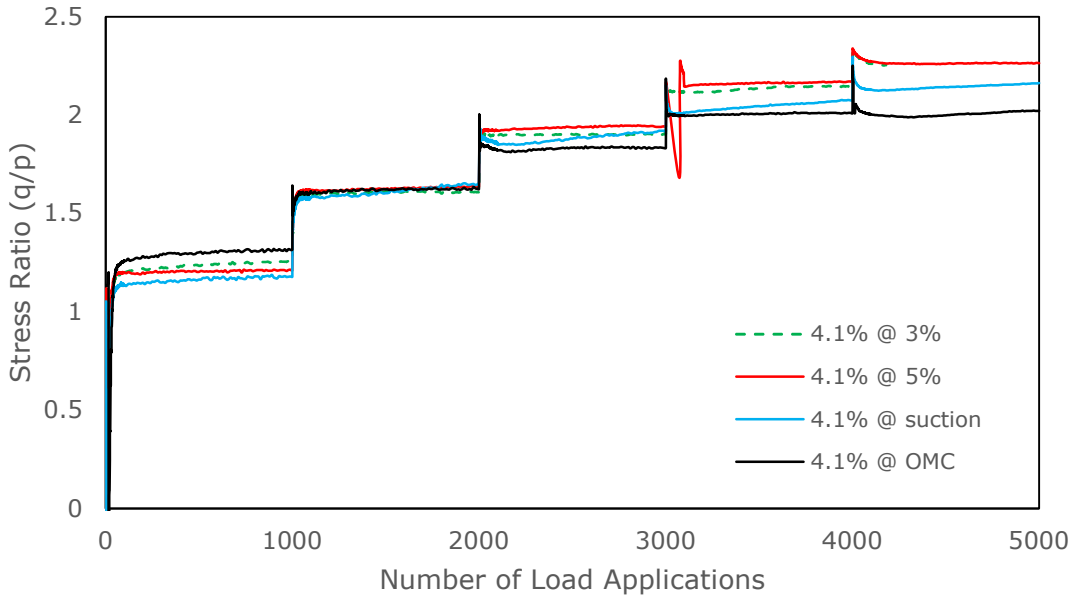


Figure 4.8: Stress ratio applied during PUMA test

The Figure 4.9 -Figure 4.12 represent the effect of moisture content on performance of unbound granular materials with different fines content at different stress stages for UGM gradations of 4.1, 6.7, 13.5 and 7.4% respectively. Starting from gradation having 4.1% fines content, the specimen compacted at higher moisture content values i.e. 5% and OMC showed greater stiffness at the start of the test which gradually decreased with axial stress increment. The opposite was observed with lower moisture values i.e. suction and 3% moisture; the specimens showed approximately 15% and 20% less modulus values at 3% and suction point respectively during the initial axial stress of 20kPa. The specimens at suction, OMC and 3% resulted at almost same stiffness at mid-way during the test whereas the specimen tested at suction and OMC started to get stiffer with further increase in axial stress although the highest stiffness was resulted at suction point at the end of the test. The specimen at 5% moisture behaved differently in showing the highest stiffness modulus throughout the test with almost the same stiffness at the end of the test as the one at suction moisture content. The same behaviour was not observed with specimens at other fines and moisture contents as well as the literature thereby hinting at the possibility of an over compaction of the specimen.

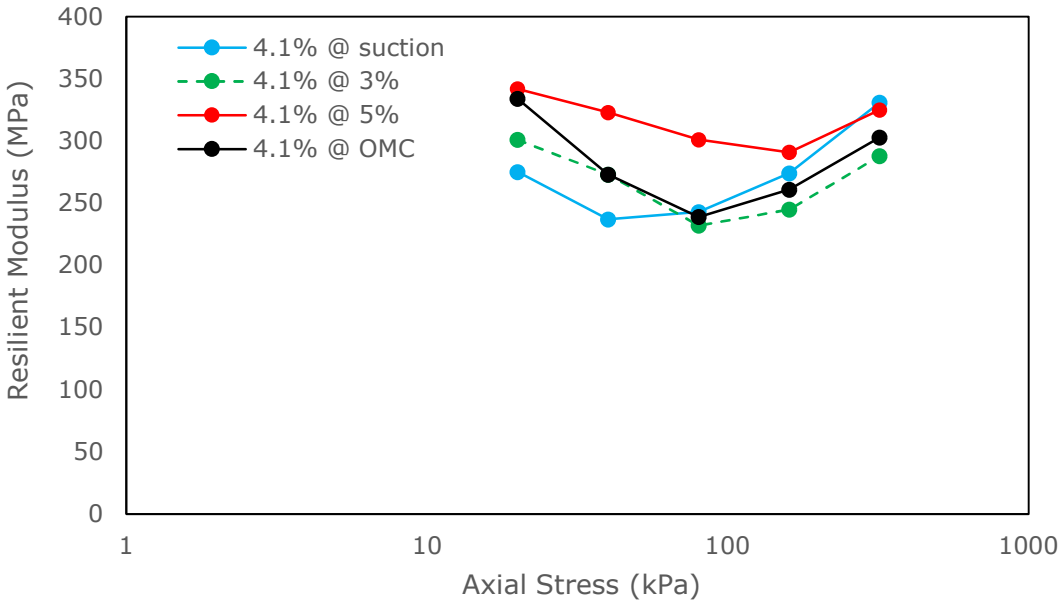


Figure 4.9: Stiffness summary for 4.1% fines content at different moisture contents at end of 1000 cycle each

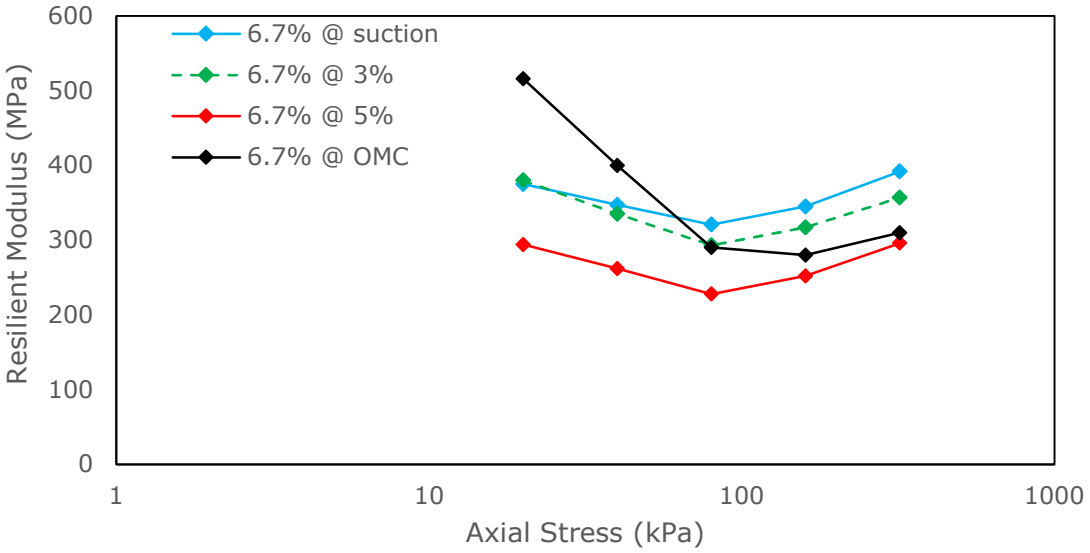


Figure 4.10: Stiffness summary for 6.7% fines content at different moisture contents at end of 1000 cycle each

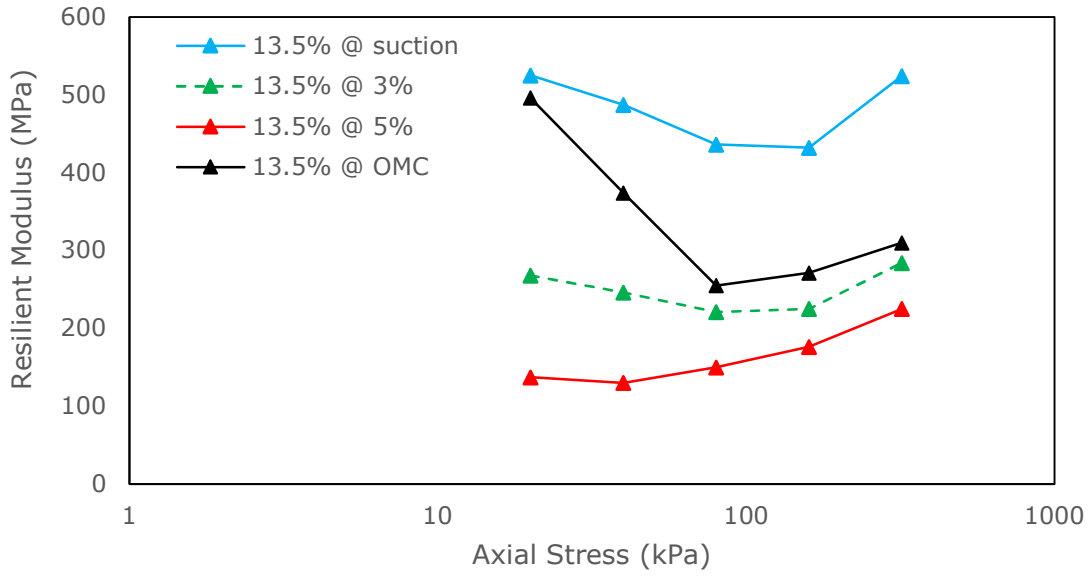


Figure 4.11: Stiffness summary for 13.5% fines content at different moisture contents at end of 1000 cycle each

For the specimens with gradation having 6.7% fines content, Figure 4.10, the greatest modulus values were found at optimum moisture content at the start of the test while least modulus was reported at 5% moisture. The decrease in stiffness with increasing axial stress was lesser for suction and 3% moisture contents. At the end of the test, the specimen tested at suction moisture content showed the highest modulus values which corresponded to the theoretical suction behaviour. The material with highest fines

contents (13.5%), Figure 4.11, behaved differently than the others. The specimen compacted at suction point performed better than the others at all stress levels demonstrating higher modulus values at each stage. The difference between stiffness of the specimens tested at different moisture contents during all the stress stages was the highest with this gradation. It was probably due to the presence of the highest fines contents which enhanced the moisture dependency even more. At the lowest stress levels, the material's performance at suction and OMC was very comparable which deviated to a great deal at the end of the test resulting in around 40% less stiffness modulus at OMC with respect to the one at suction.

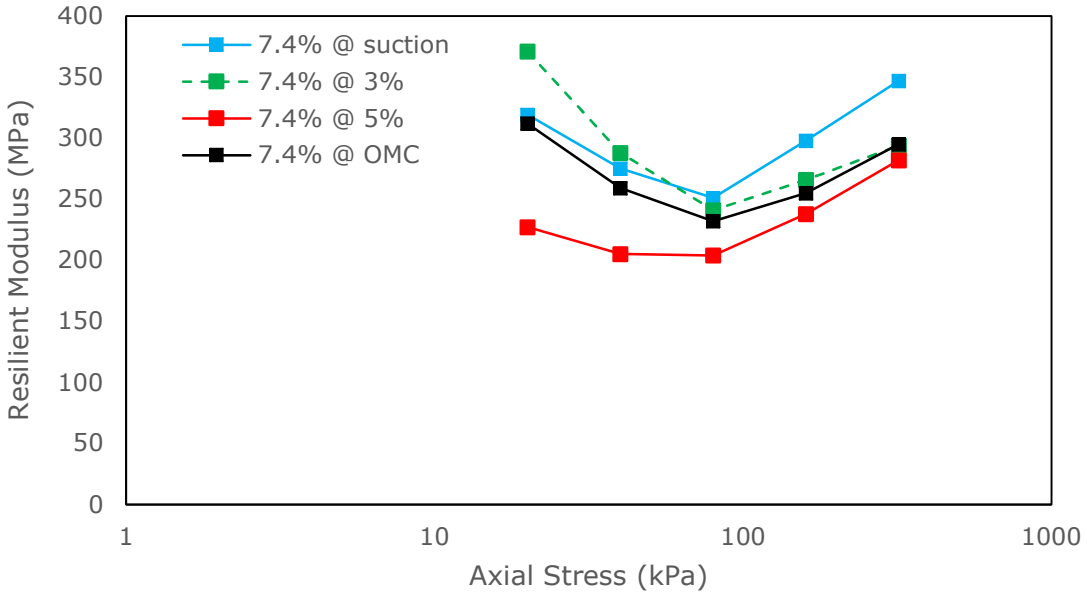


Figure 4.12: Stiffness summary for 7.4% fines content at different moisture contents at end of 1000 cycle each

The results obtained from the PUMA tests performed on a gradation having 7.4% fines content and maximum particle size of 14mm are shown in Figure 4.12. The results showed higher modulus values at lower moisture content values i.e. 3% and suction point at all the stress stages although the end of the test stiffness of the specimen tested at OMC is more than the one tested at 3%.

4.3.3 Effect of Fines content on Unbound Base Performance

The effect of fines content on UGM resilient performance is presented and discussed in this section.

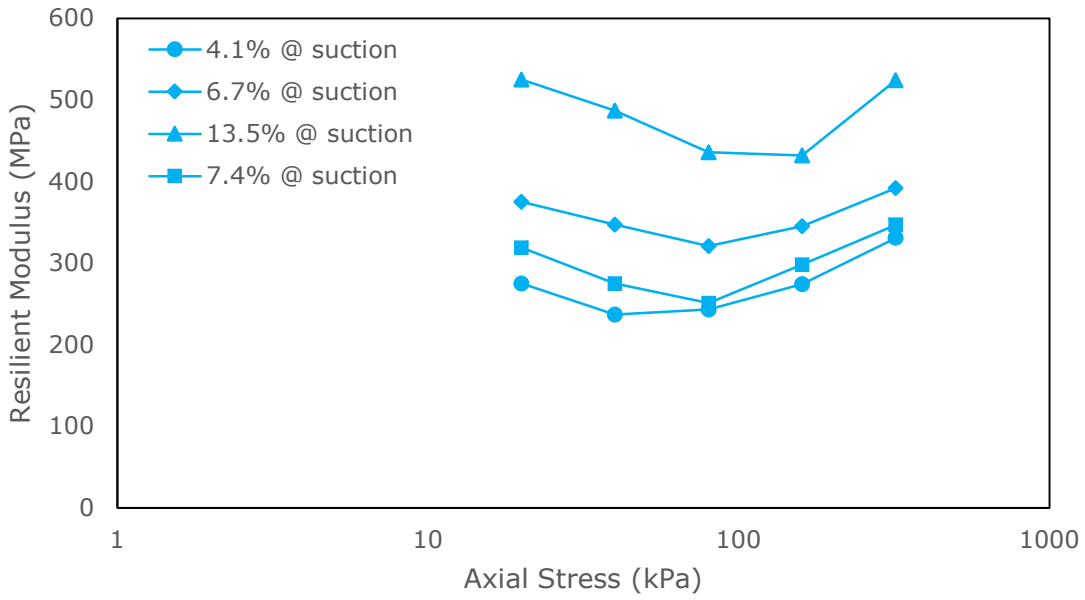


Figure 4.13: Stiffness summary for specimen with different fines contents tested at suction

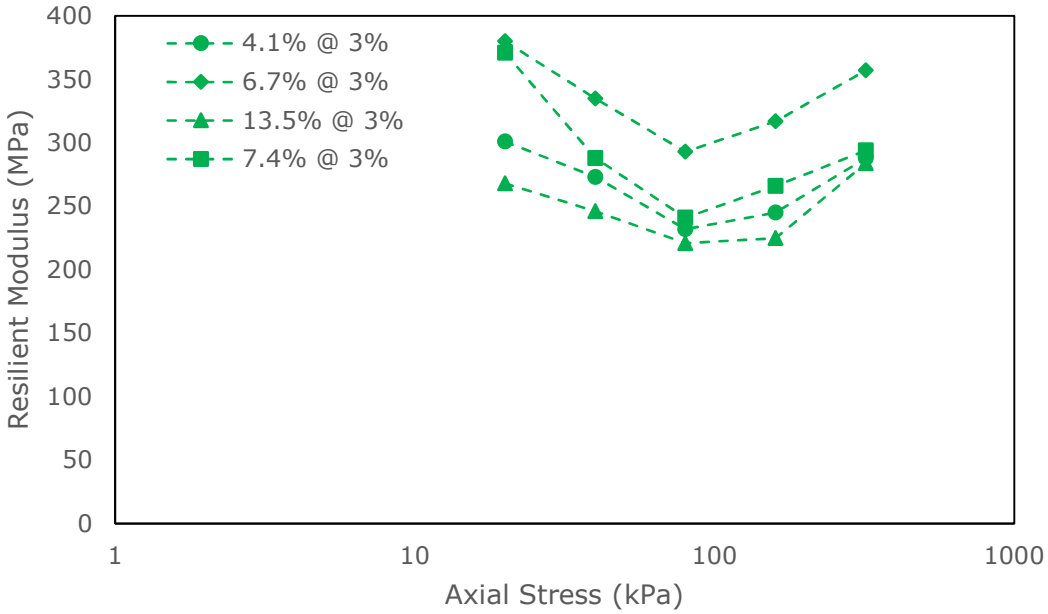


Figure 4.14: Stiffness summary for specimen with different fines contents tested at 3% moisture

Figure 4.13 -Figure 4.16 show the effect of fines content on unbound material resilient performance at suction, 3%, 5% and optimum moisture contents respectively. It is very clear that materials behaved differently at different moisture contents.

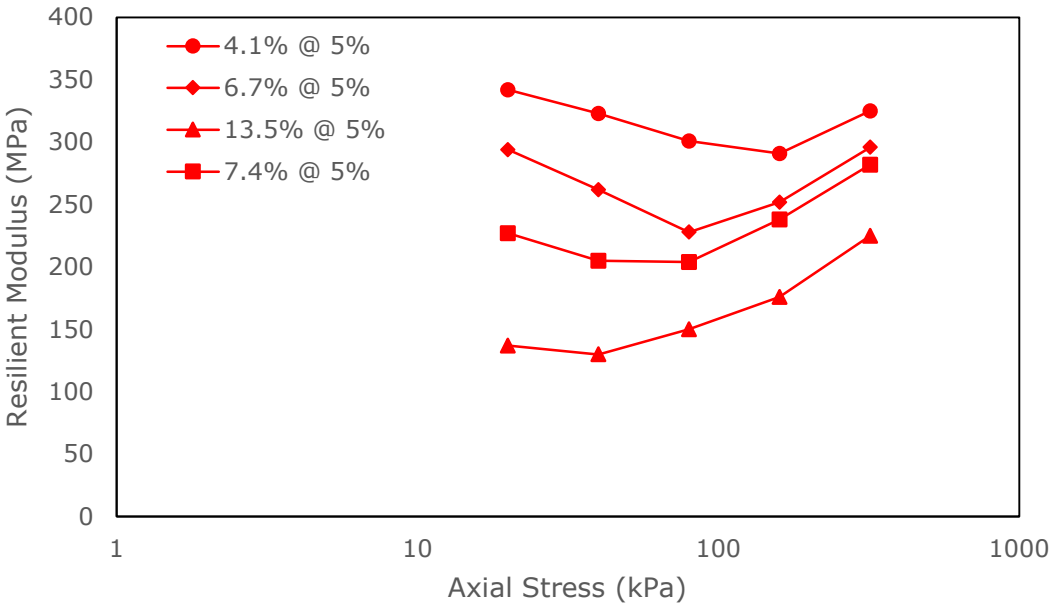


Figure 4.15: Stiffness summary for specimen with different fines contents tested at 5% moisture

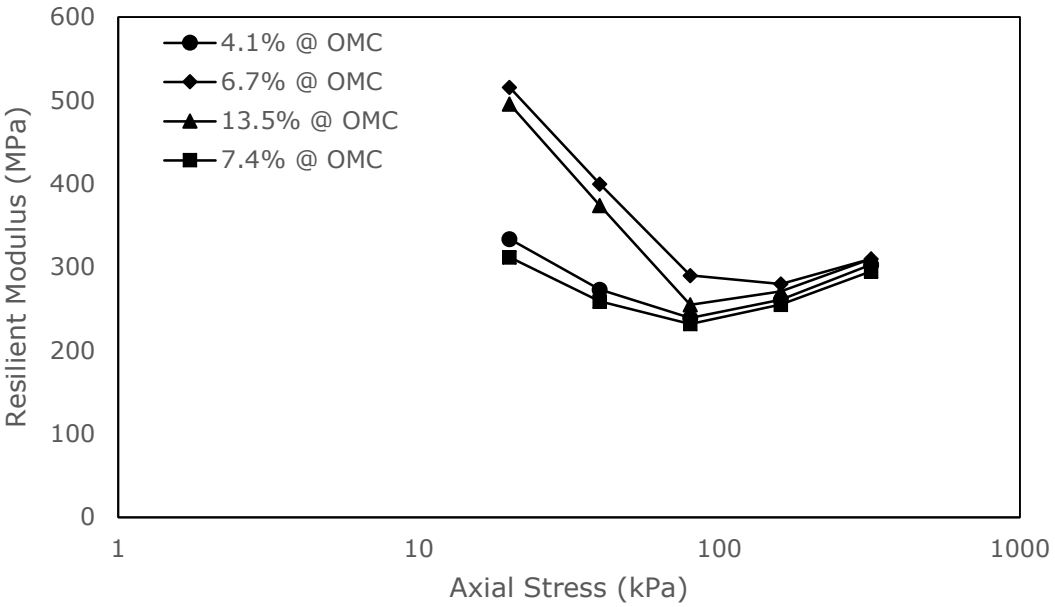


Figure 4.16: Stiffness summary for specimen with different fines contents tested at optimum moisture

At suction, Figure 4.13, the material with highest fines content i.e. 13.5% showed higher stiffness from the start till the end. This was probably due to the presence of more fines which went through more particles settlement under loading thus achieving the dense mix and hence higher stiffness values. The material with lowest fines content demonstrated lowest

modulus values at suction which was probably due to lack of moisture and fines which could not contribute to a dense aggregate skeleton either by filling the voids or lubricating effect. The materials having 6.7 and 7.4% fines content showed similar results with 6.7% fines material exhibiting relatively higher modulus values. It could be contributed to greater resistance to deformation due to the greater particle size in 6.7% material than 7.4% materials. Figure 4.14 shows the effect of fines content on unbound granular materials compacted at 3% moisture. The materials behaved differently than at suction. With an increase in moisture from suction, the materials with 6.7% fines content showed higher stiffness. The reason was probably due to post compaction and particle settlement under loading. The rest of the materials showed lesser stiffness at all stress stages. The highest modulus values observed at 3% moisture were also found to be approximately 25% less than the modulus values observed at suction which also makes the suction point an ideal scenario for the pavement engineers to achieve in a pavement while construction. The effect of fines content on performance of unbound granular materials compacted at 5% moisture is shown in Figure 4.15. The modulus values were comparable to that obtained for specimens compacted at 3% moisture. But the effect of fines content is considerably different for 4.1% fines. The lowest fines content material behaved stiffer as compared to the rest of the materials at 5% moisture. The rest of the materials behaved similar to the ones at 3% showing relatively smaller modulus values which was probably being away from suction as well as getting near to optimum moisture content. The optimum moisture content has its significance as being the moisture content at which the unbound granular materials achieve highest dry density thus performing as a load carrying layer to an optimum level. The significant finding from the tests performed at optimum moisture content, Figure 4.16, was the almost same modulus values observed at the end of the test after application of five different axial stress stages. 6.7 And 13.5% fines content materials showed similar stiffness at the end of each stress stage whereas material with 4.1 and 7.4% fines were of similar stiffness. It was because of lesser fines content for 4.1% material thereby not achieving the optimum dense mix within the specimen whereas the same in 7.4% material was observed because of lower particle sizes within the gradation.

4.4 Permanent Deformation from the PUMA

The permanent deformation in any material under load is one of the main indicative parameters of its performance. It was measured in PUMA test for all the different materials under loading. This section presents and discusses the findings from the permanent deformation of UGMs in detail.

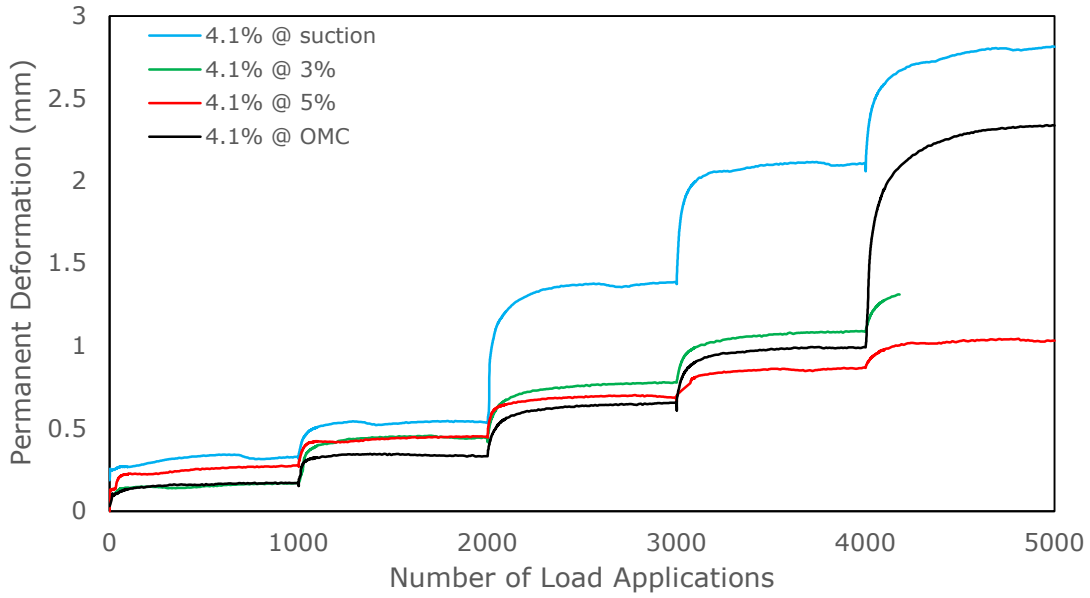


Figure 4.17: Permanent Deformation at different moisture contents for 4.1% fines unbound granular base material

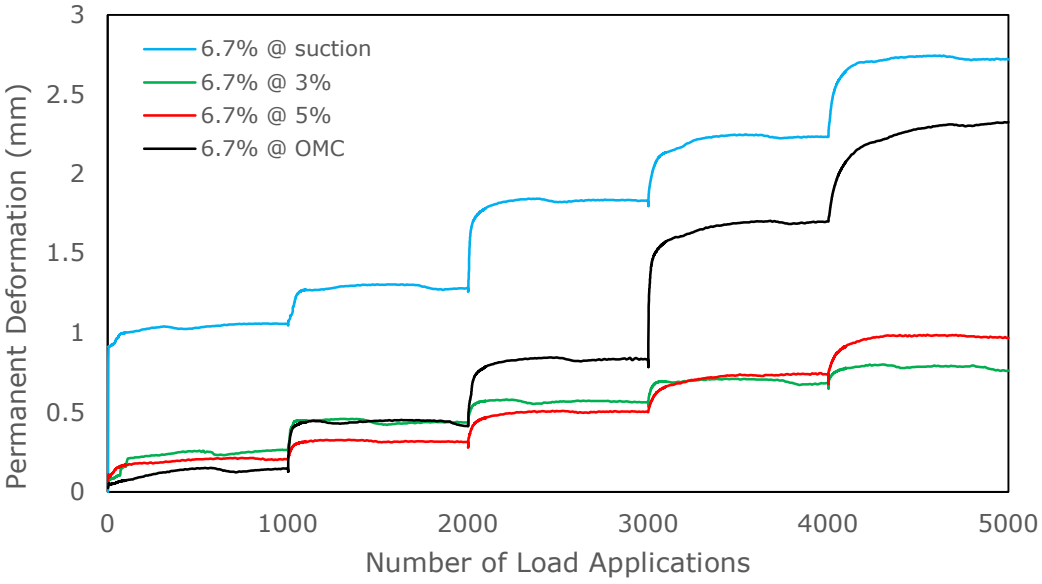


Figure 4.18: Permanent Deformation at different moisture contents for 6.7% fines unbound granular base material

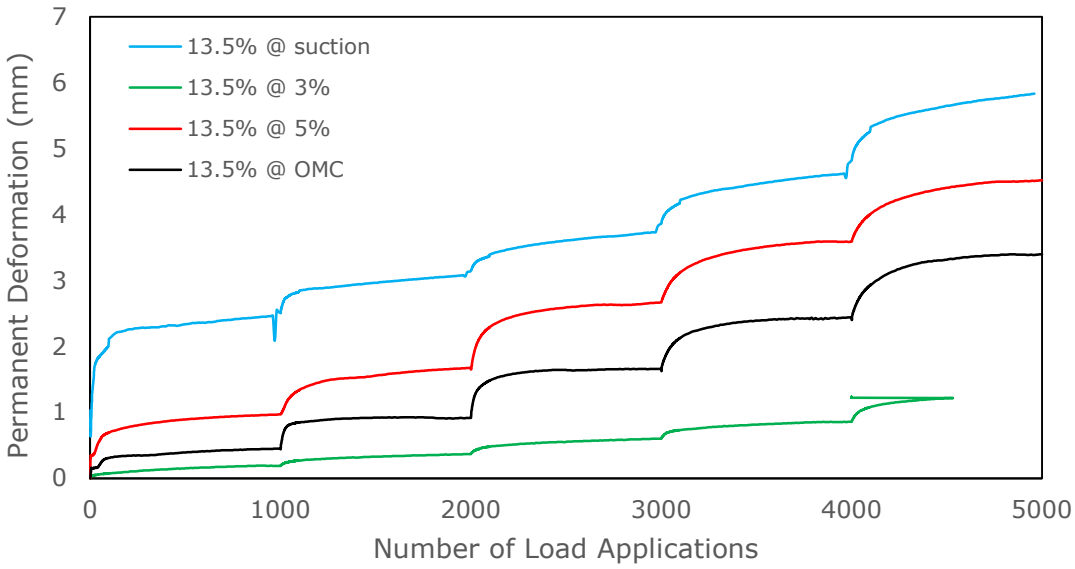


Figure 4.19: Permanent Deformation at different moisture contents for 13.5% fines unbound granular base material

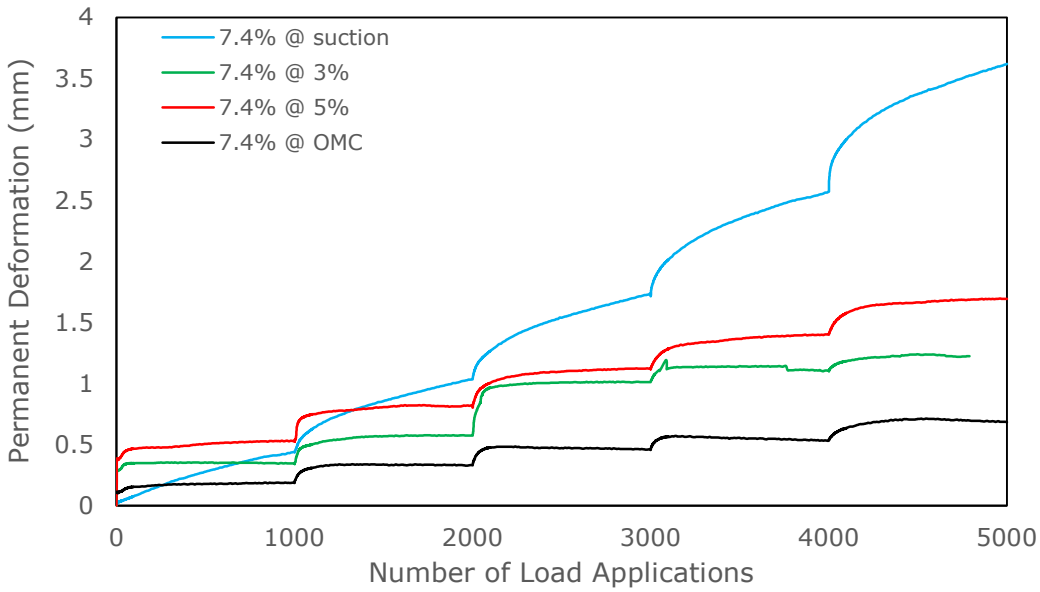


Figure 4.20: Permanent Deformation at different moisture contents for 7.4% fines unbound granular base material

As the results focus on the permanent deformation behaviour during the axial stress stages, it can be observed that at each stress stage, the permanent deformation increased abruptly at the start of the test which settled with the number of further load applications. With the increase in axial stress, the permanent deformation increased from the previous stress levels. The effect of the moisture content on permanent deformation performance of unbound granular materials (UGMs) containing 4.1, 6.7,

13.5 and 7.4% fines content is depicted in Figure 4.17 -Figure 4.20 respectively.

From the figures, it is very clear that the maximum permanent deformation is resulted in the specimens tested at suction moisture (compacted at optimum moisture content and dried out). The uneven distribution of the moisture in the specimens due to the accelerated drying induced in the oven resulting in almost dried up top half probably resulted in the higher permanent deformation. It can also be verified from the fact that in almost half the specimens tested at suction moisture, up to 30-40% of total permanent deformation after 5000 load applications was observed in the first few cycles alone. The concept can further be verified by comparing the suction moisture results with the ones obtained at 3% moisture. A very wide range difference between permanent deformations at these two moisture contents could be attributed to the moisture distribution within the specimen where the moisture was uniformly distributed at 3% opposed to uneven distribution at suction point. It is, therefore, believed that achieving maximum density along with uniform distribution of moisture equal or near to suction point can result in very small permanent deformation values in unbound granular materials. The specimens behaved differently at optimum moisture content showing their dependence on fines content relatively more at this moisture content. The specimens with low fines content, 4.1 and 6.7%, deformed more at optimum moisture content than all other values except suction point whereas an increase in fines content to 13.5% resulted a better material response at this moisture although the least permanent deformation was observed at 3% moisture. The better behaviour at 3% is already explained. The reason was this behaviour could be attributed to the lubricating effect induced by the water to the aggregate particles which is more significant in case of higher particles sizes and results in more permanent deformation in gradations having 4.1 and 6.7% fines contents. Whereas the better material performance at optimum moisture content for gradation having higher fines content could be due to the dense aggregate skeleton by the presence of fines occupying the voids more efficiently. This could be further verified by the analysis of the results of the gradations having 7.4% fines content with a maximum particles size of 14mm. The

specimens deformed most at suction like all other materials with the difference being the ever-increasing deformation at the end of each axial stress stage indicating the materials had not settled. The least permanent deformation was observed at optimum moisture content attributing to the better material performance at this moisture content. It also established the dependence of the material behaviour on a combined effect of fines and moisture contents along with maximum particles size. The detailed effect of the moisture and fines contents to the permanent deformation of the materials is described in the subsequent sections.

4.4.1 PUMA test summary at each Stress Stage

Figure 4.21 presents the summary of permanent axial strains resulted in PUMA tests at the end of 1000 cycles at each stress stage. From the colour codes, it can generally be established that the specimens tested at suction point deformed more than the others with only a couple of exceptions. As the figure encompasses all the test results so it is difficult to conclude. Therefore, for a better explanation, few more graphs are plotted with different combinations of fines and moisture content for better understanding.

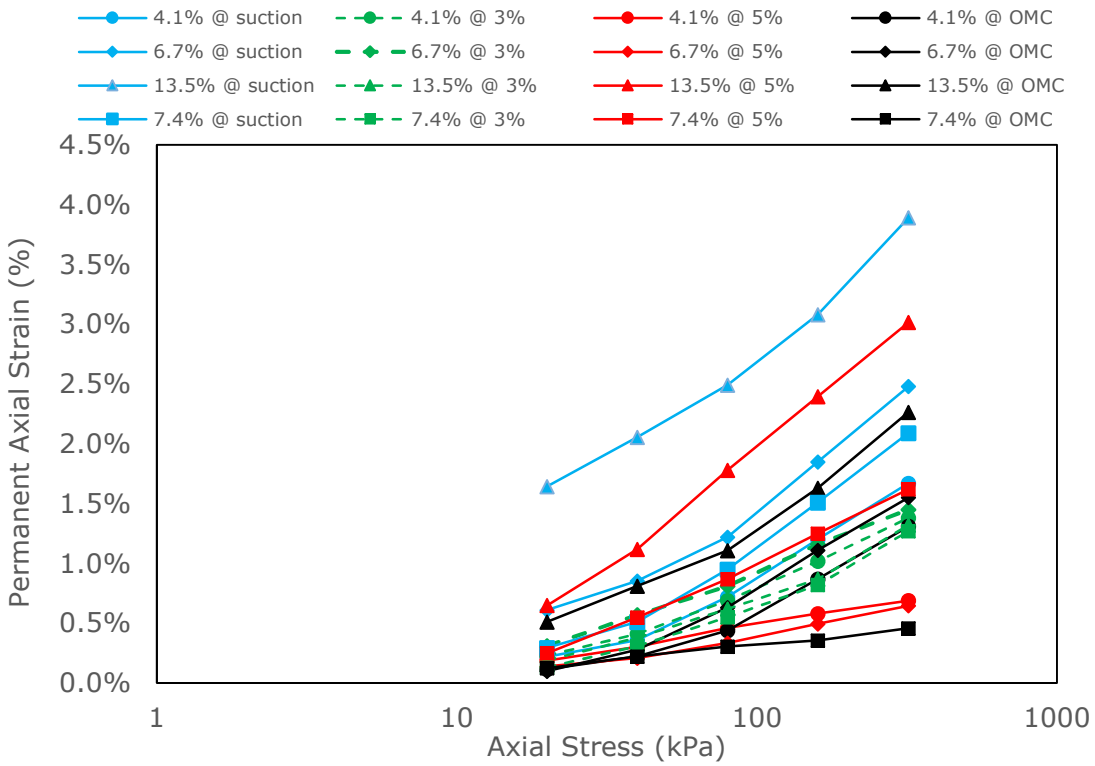


Figure 4.21: Permanent Deformation summary

4.4.2 Effect of moisture on UGM permanent deformation

The effect of different moisture contents on permanent deformation performance of UGMs containing 4.1, 6.7, 13.5 and 7.4% fines contents against applied axial stresses is shown in Figure 4.22 -Figure 4.25 respectively.

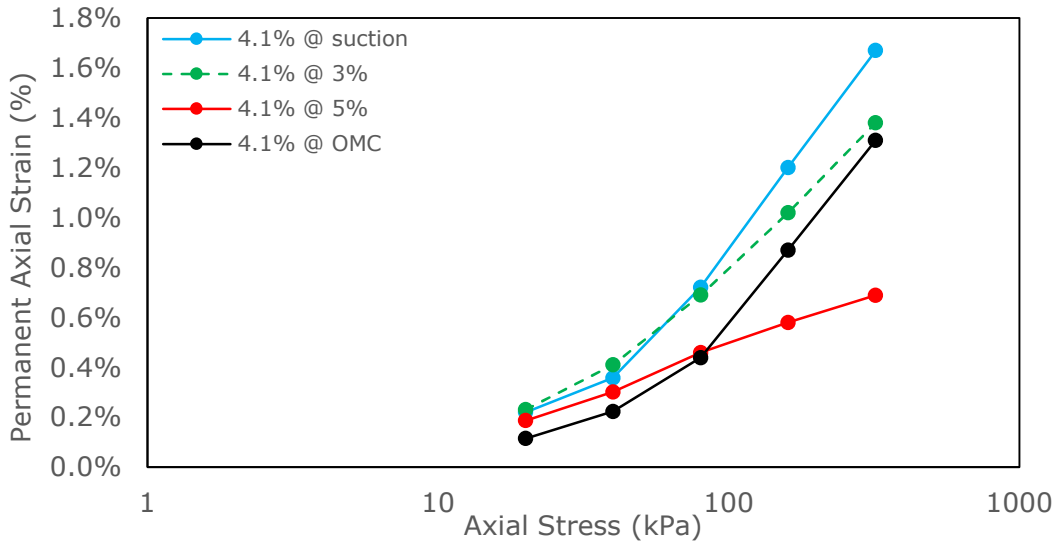


Figure 4.22: Permanent Deformation at different moisture contents for 4.1% fines material at the end of each stress stage

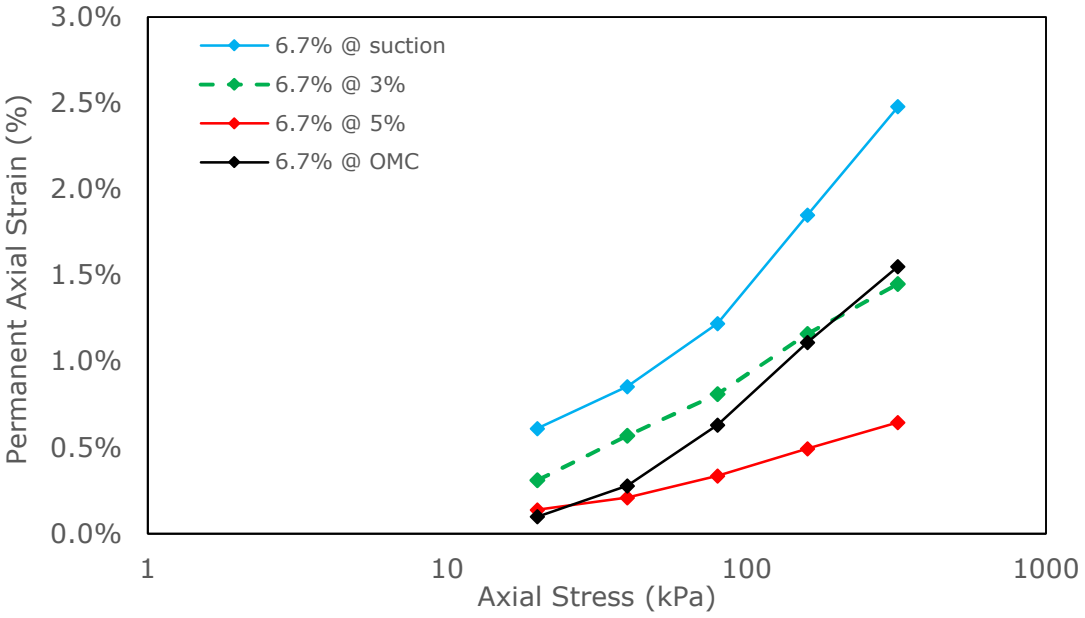


Figure 4.23: Permanent Deformation at different moisture contents for 6.7% fines material at the end of each stress stage

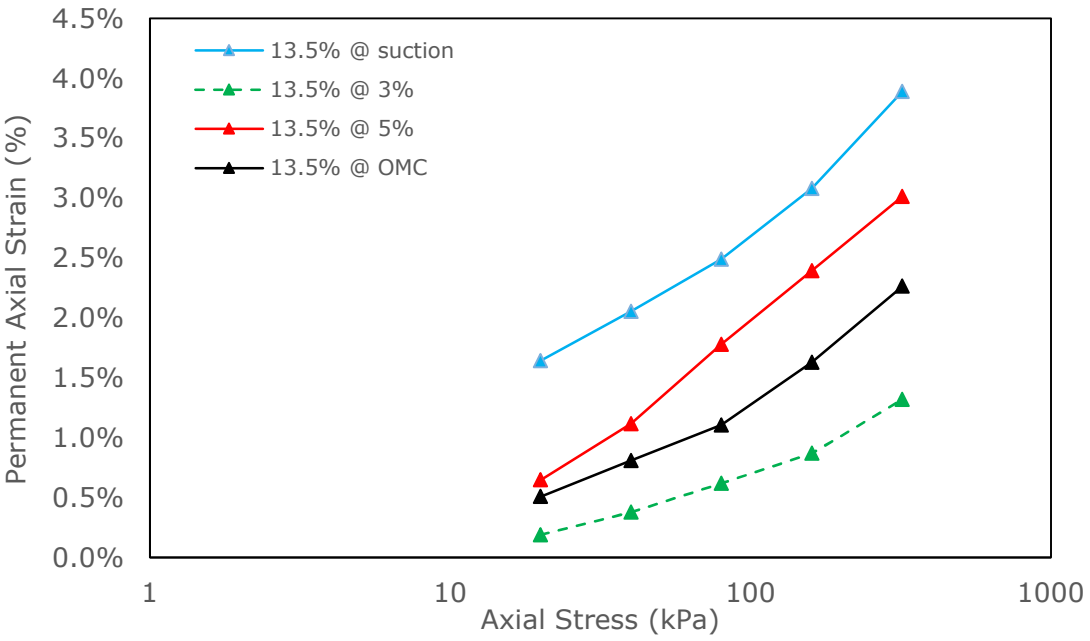


Figure 4.24: Permanent Deformation at different moisture contents for 13.5% fines material at the end of each stress stage

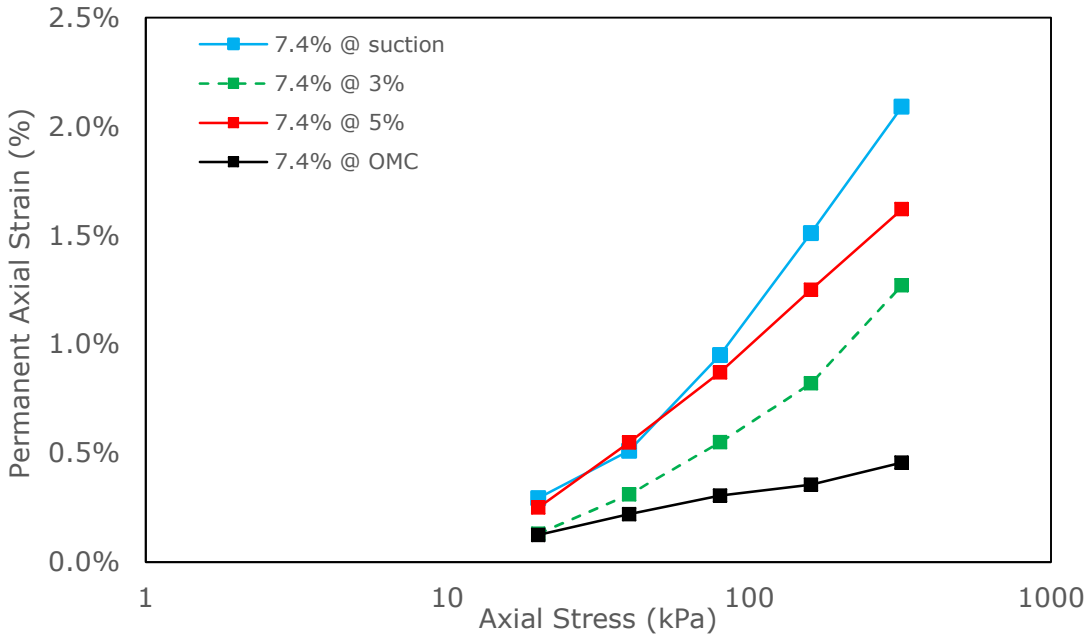


Figure 4.25: Permanent Deformation at different moisture contents for 7.4% fines material at the end of each stress stage

In the previous section, the permanent deformation values were plotted against the number of load applications showing all the data points collected during the test. The current figures show the same permanent deformation values in terms of percentage strain against the axial stresses. The five data points correspond to the permanent deformation values at the end of each

axial stress. The explanations of all the results, as mentioned in the previous section, can easily be verified by the current figures. As expected, with an increase in axial stress and number of load applications, the specimens deformed more, although the slight convex curves for most of the specimens show an increased permanent deformation with stress moving to the higher values. As another general observation, it can be stated the UGM gradation containing 4.1% fines content showed the overlapping behaviour more than the other materials illustrating its dependency on the stresses for resisting the permanent deformation.

4.4.3 Effect of Fines Content on UGM permanent deformation

Figure 4.26 -Figure 4.29 represent the effect of fines content on permanent deformation behaviour of the UGMs having 4.1, 6.7, 13.5 and 7.4% fines contents respectively. At suction moisture content, the permanent axial strain (%) increased with increasing fines content, without considering the gradation having 7.4% fines content, with the highest permanent strain observed at suction moisture for gradation having 13.5% fines content. It is also worth stating that the permanent deformation at suction point was higher than the respective other moisture content levels. The higher permanent deformation for all the gradations at suction point was probably more affected by the uneven moisture than the fines content with 0.5-1.5% permanent strain induced by only few number of load cycles at the minimum stress. The specimens tested at 3% moisture showed greater and complex dependency on fines content with the maximum strains observed for the gradation having 6.7% fines content. Although the material behaviour was very complex, a few findings from the tests include the existence of least overall average permanent axial strains. Another finding was relatively narrow gap between the permanent axial strains observed for gradations having different fines contents as compared to the gaps observed at other moisture levels. From the analysis of the results obtained at 5% and optimum moisture contents, it is very clear that like suction point, the permanent axial strains increased with increasing fines content except 7.4% fines content. The small exception was almost same permanent strains observed at 5% moisture for gradations having 4.1 and 6.7% fines content with the latter showing the slightly better performance. For

establishing a general trend, this could be attributed to the personal error. The gradation with maximum particle size of 14mm having 7.4% fines content behaved very comparable to the other gradations at all moisture levels exhibiting permanent axial strains in between the other materials except at optimum moisture content where it outperformed the other gradations. The reason could be the associated with achieving the maximum possible density due to the a dense particle arrangement.

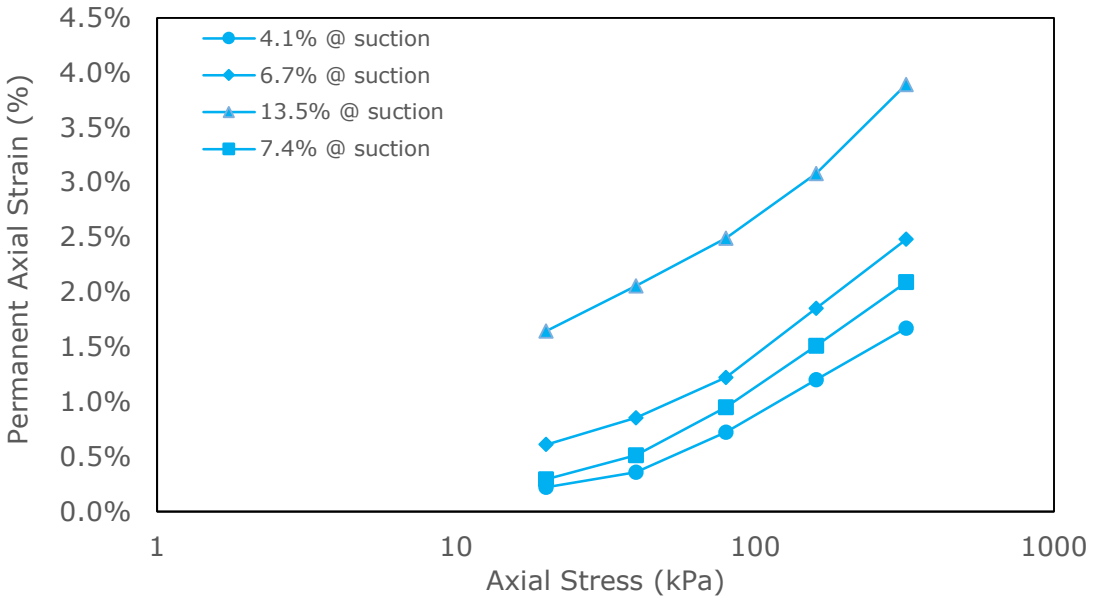


Figure 4.26: Permanent Deformation for different materials at suction

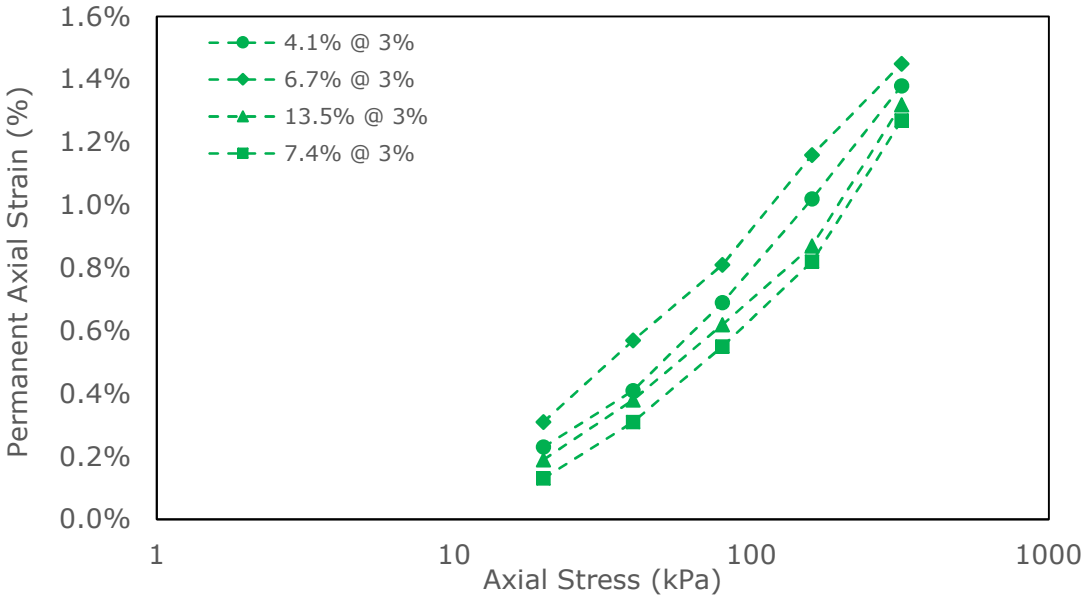


Figure 4.27: Permanent Deformation for different materials at 3% moisture

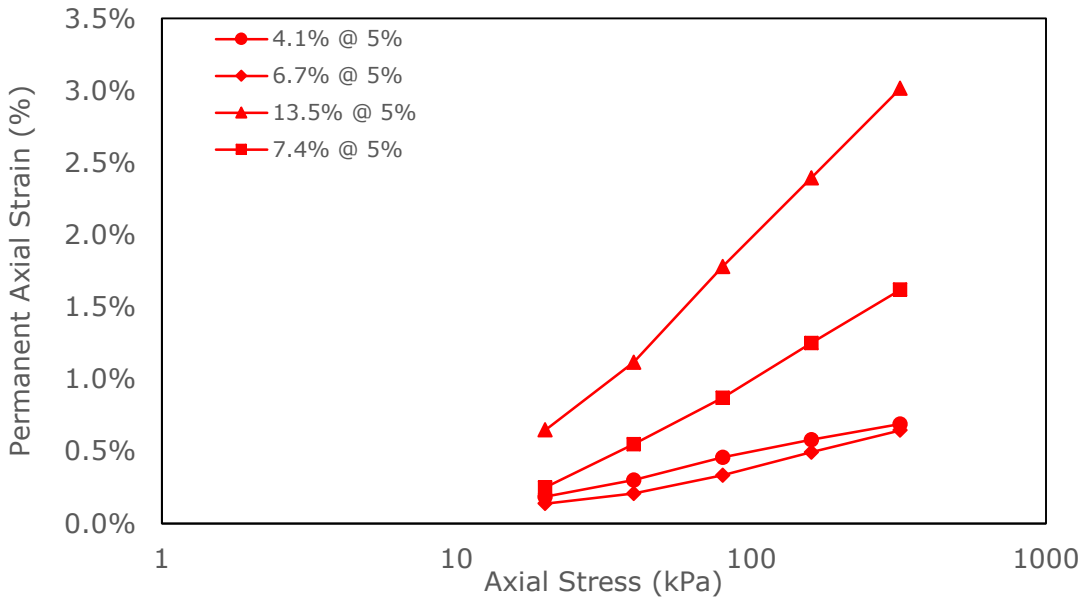


Figure 4.28: Permanent Deformation for different materials at 5% moisture

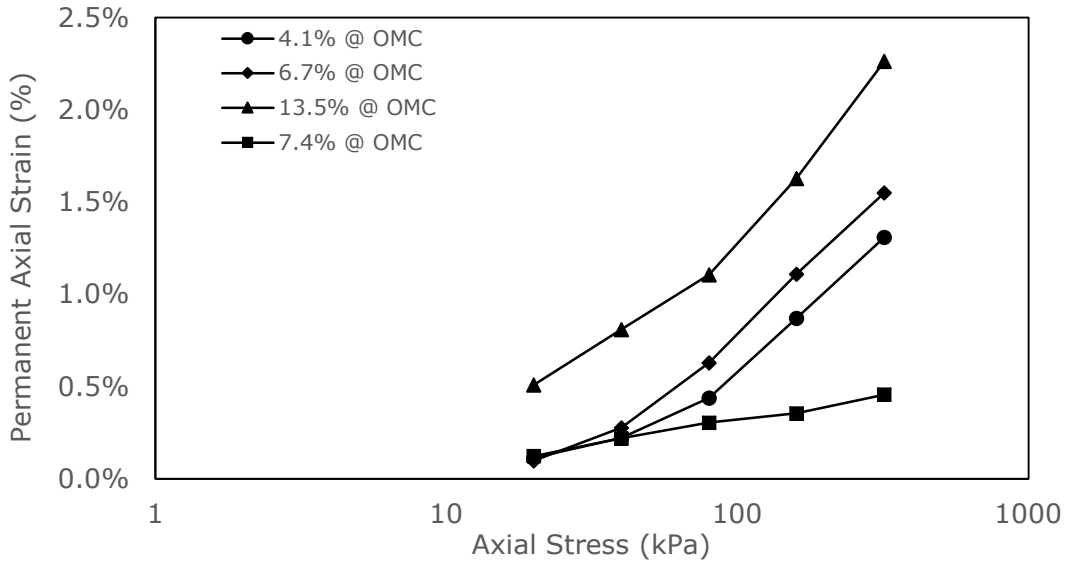


Figure 4.29: Permanent Deformation for different materials at optimum moisture

The effect of fines and moisture contents on UGM performance, explained in previous sections, can be summarized in Figure 4.30 -Figure 4.33. The figures represent the permanent axial strains and resilient modulus values at the end of 5000 cycles applied on the specimens. The effect of moisture content on permanent axial strain and resilient modulus at the end of the test for the gradations containing 4.1, 6.7 and 13.5% fines content is shown in Figure 4.30 and Figure 4.31 respectively whereas the reverse is shown in Figure 4.32 and Figure 4.33 respectively.

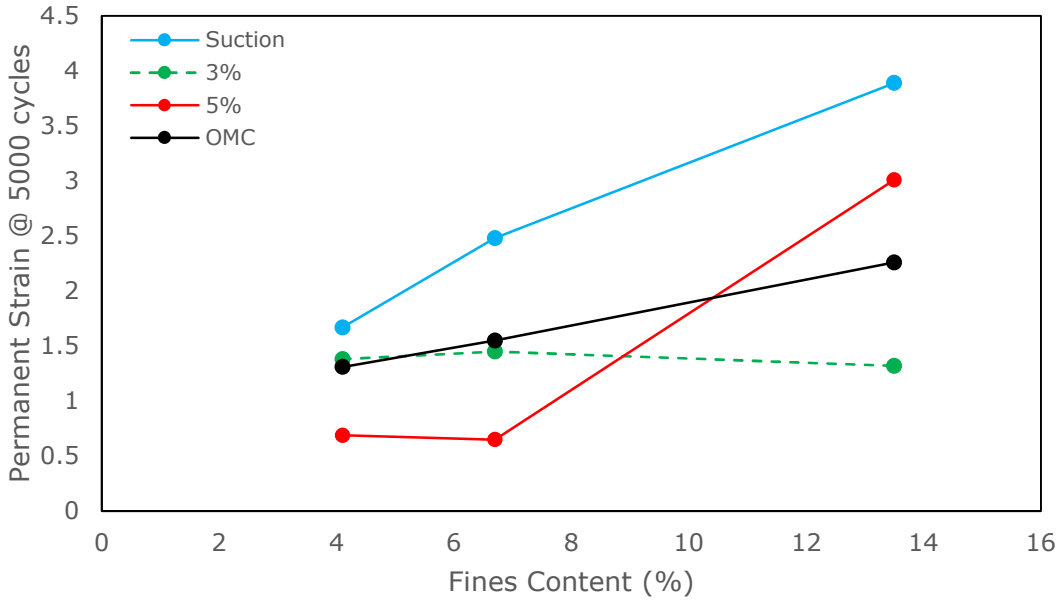


Figure 4.30: Effect of moisture contents on permanent strain of UGMs with different fines contents

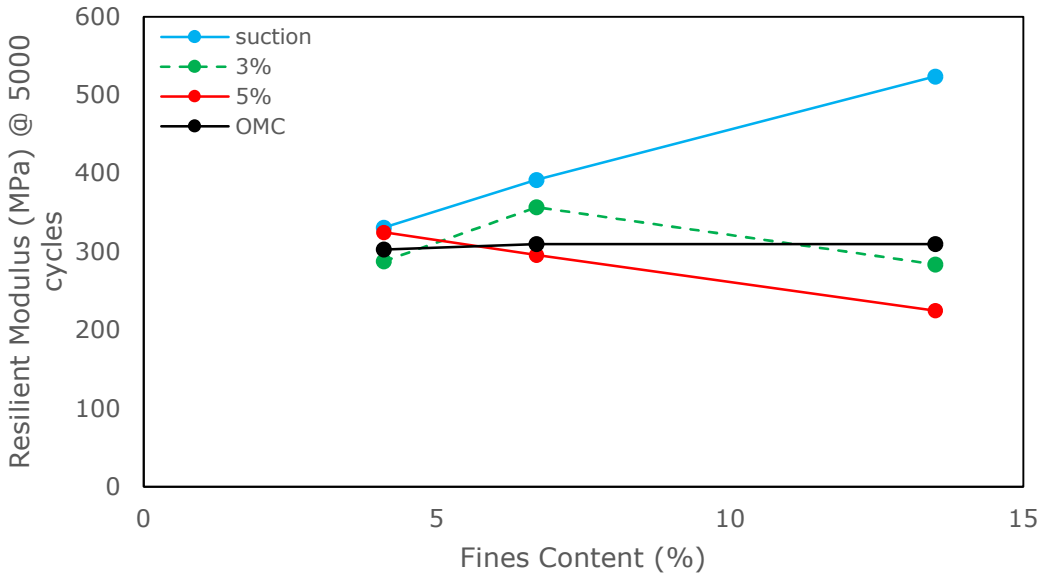


Figure 4.31: Effect of moisture contents on resilient modulus of UGMs with different fines contents

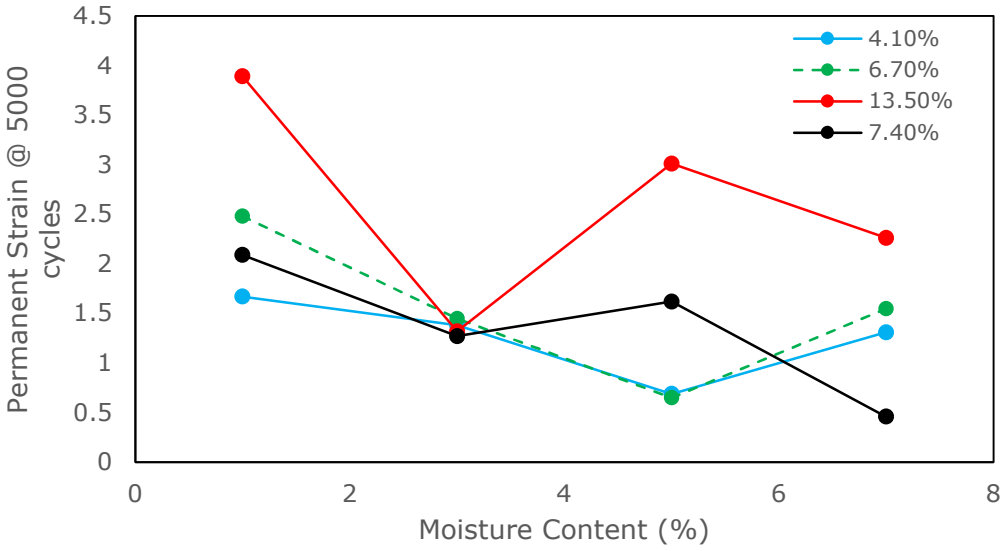


Figure 4.32: Effect of fines contents on permanent strain of UGMs tested at different moisture contents

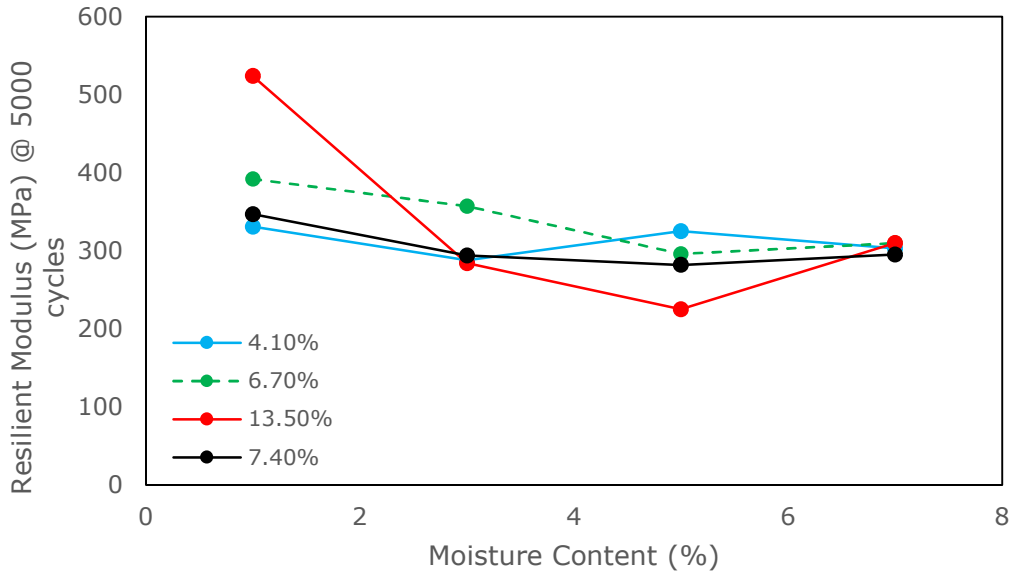


Figure 4.33: Effect of fines contents on resilient modulus of UGMs tested at different moisture contents

A different method of representing the permanent deformation results obtained from the laboratory testing, mostly triaxial test, was devised by Dawson and Wellner (1999). They recommended plotting permanent strain on x-axis versus permanent strain rate on y-axis. The following figures show the similar plots on logarithmic scale for the PUMA test performed in the current project. Based on the literature review, it can be seen that most of the results are in Range A to B of the shakedown limits corresponding to the Plastic Shakedown and Intermediate response.

A few examples of these plots are shown in Figure 4.34 -Figure 4.36.

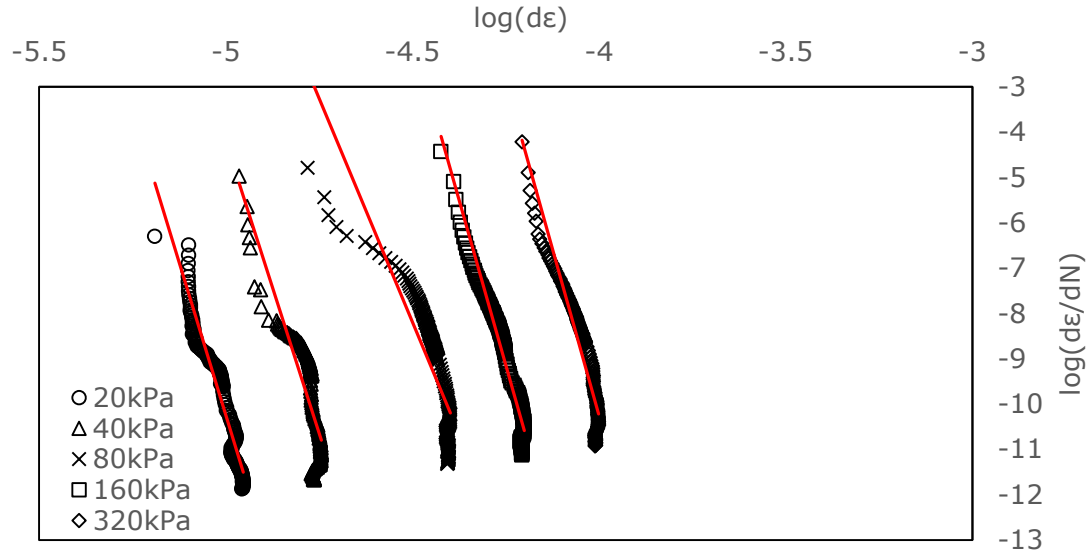


Figure 4.34: Permanent strain vs rate of permanent strain at various axial stresses for UGM having 6.7% tested at suction

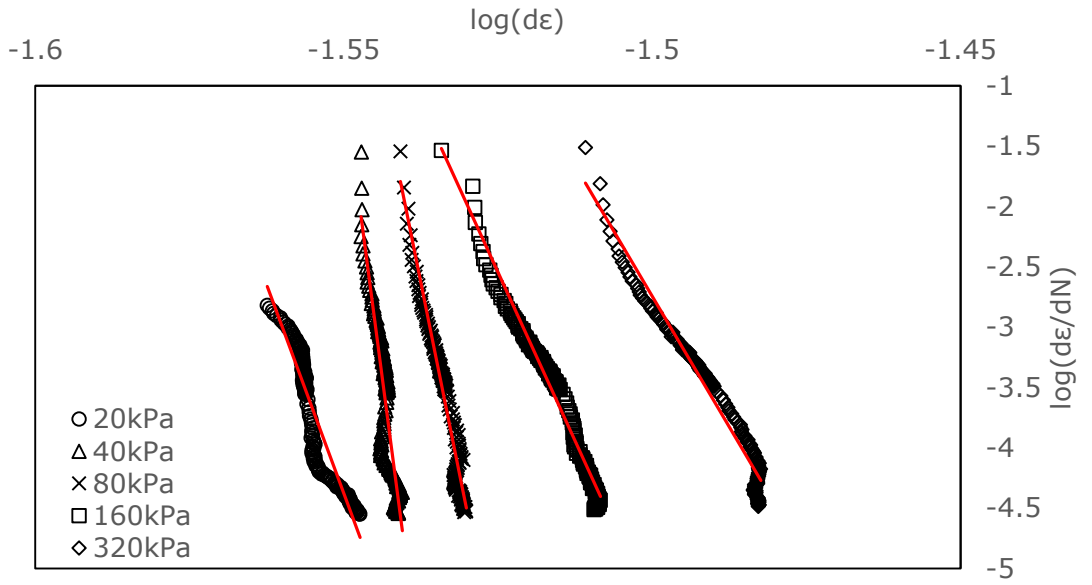


Figure 4.35: Permanent strain vs rate of permanent strain at various axial stresses for UGM having 13.5% tested at 3% moisture

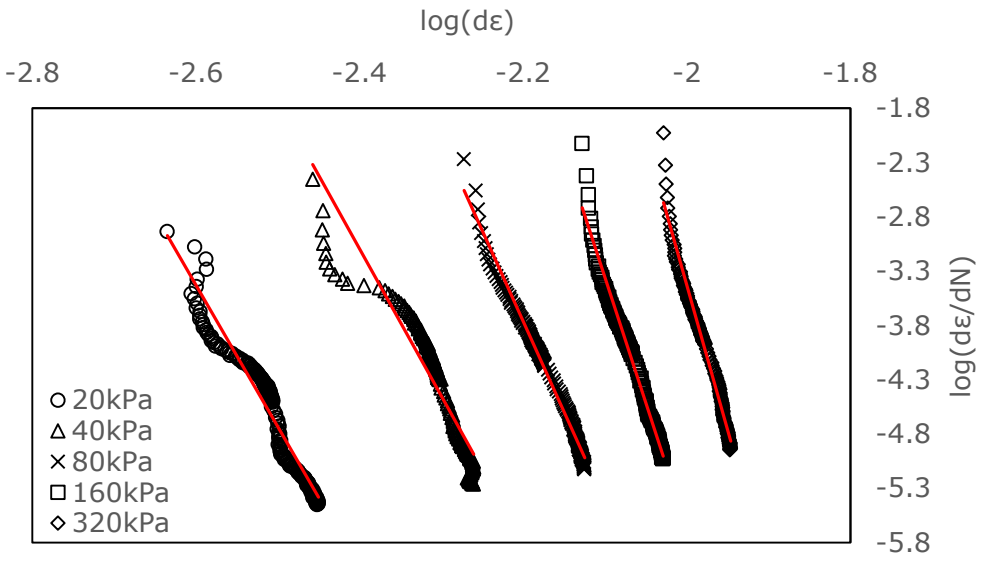


Figure 4.36: Permanent strain vs rate of permanent strain at various axial stresses for UGM having 7.4% tested at OMC

4.5 Correlating PUMA data to Triaxial developed stress strain model

A relatively new device called the PUMA, as previously explained, has been used in this research study to characterize the unbound granular materials. It is a well-established fact that historically triaxial equipment, along with various others with a range of pros and cons, have been used to characterize the unbound materials in a pavement. Laboratory test data from the triaxial equipment have been used to develop various models to predict unbound material behaviour in a pavement under different stress conditions. These models have considered different variables affecting the material's behaviour in different conditions. One of the most important variables affecting the unbound materials is stress. The predictive models have, along with the advantage of predicting material response under loading, a few limitations as well; one of the limitations in stress dependent models being the application of single stage stress, as mentioned in literature review, unlike the multi stress stages in a real pavement under loading. Rahman and Erlingsson performed a study to predict the unbound material deformation response under traffic loading by using the stress hardening approach to consider multi stress stages. They also extended their strain hardening concept to the previously developed single stress

stage models and compared the performance with their own developed multi stress stage model. The stress hardening approach seems to work well in predicting the permanent deformation performance of unbound granular materials in a multi stress stage environment. Therefore, the Rahman and Erlingsson model was selected to correlate the PUMA performance with much developed and universally agreed triaxial equipment performance in a multi stress stage application. The model considers the stress hardening approach to study the effect of different stress levels on deformation performance of unbound materials as encountered in a typical real pavement under traffic loading. The model considers the effect of N (No. of load applications), stress ratio and material parameters. As the model was developed based on triaxial data, it required a rather different methodology to fit the PUMA data. The model fitting was composed of the following steps;

- Selecting the Rahman and Erlingsson model based on the similar stress conditions.
- Calculating the total axial and confining stress from the PUMA data.
- Based on step 2 calculations, finding the 'q' and 'p' stress values and hence calculating the S_f values at different alpha values as mentioned in Chapter 3 and shown below.

$$\hat{\varepsilon}_p\,(N) = a\,(N - N_{i-1} + N_i^{eq})^{b(S_f)_i}\,(S_f)_i$$

$$S_f = \frac{(q/p_a)}{(p/p_a)^{\alpha}}$$

- The data points at each stress stage were then taken at cycles 1 and multiples of 100 up to 1000 to find corresponding 'a' and 'b' values. The data points contained S_f and measured strains values.
- The values for data points at each stress stage were used to find the best fitting 'a' and 'b' values by the 'sum of square of difference' between measured and predicted strains method.
- This exercise resulted in 5 different 'a' and 'b' values at five different stress stages.
- The average values of the five 'a' and 'b' values was then used to predict the strain in a full PUMA test.

- The first stress stage was predicted by using the real number of load applications. For the rest of the stress stages, N_{eq}, an equivalent number of load applications, as mentioned in the equation, was also calculated.
- Another column was added in MS Excel with the average 'a' and 'b' being used for prediction and adjusted manually while carefully inspecting the visual results between measured and predicted strain against Number of load applications. The values of 'a' and 'b' were termed as 'adjusted'. The equivalent number of load applications for these 'adjusted' values was also calculated and used in permanent deformation prediction.
- The whole process was repeated for the data at a different alpha value as well to find the best fitting alpha to PUMA data. The visual inspections and R^2 calculations between the measured and predicted at 'average a and b' and 'adjusted a and b' were used to find the values of constants to best fit the PUMA data.
- The same procedure with different alpha values was applied for all the PUMA tests performed with varying fines and moisture contents. From the predicted result comparison, it was suggested to use an alpha value of 0.75 for predicting permanent strains from PUMA tests.
- All the regression parameters were then summarised and used to find the best fit alpha values to PUMA test data for predicting strains against number of load applications and stress ratio.

Here are the results from model fitting.

Figure 4.37 shows the permanent axial strains for 4.1% fines content at the suction point measured during PUMA tests and predicted by using the methodology explained earlier. From the statistical analysis, it was found to perform reasonably well for predicting the permanent strains. Figure 4.38 shows the comparison of measured and predicted permanent axial strains for 4.1% fines content at the suction point. The statistical parameter (R^2) value, 0.9872, shows a reasonable relationship between the two values.

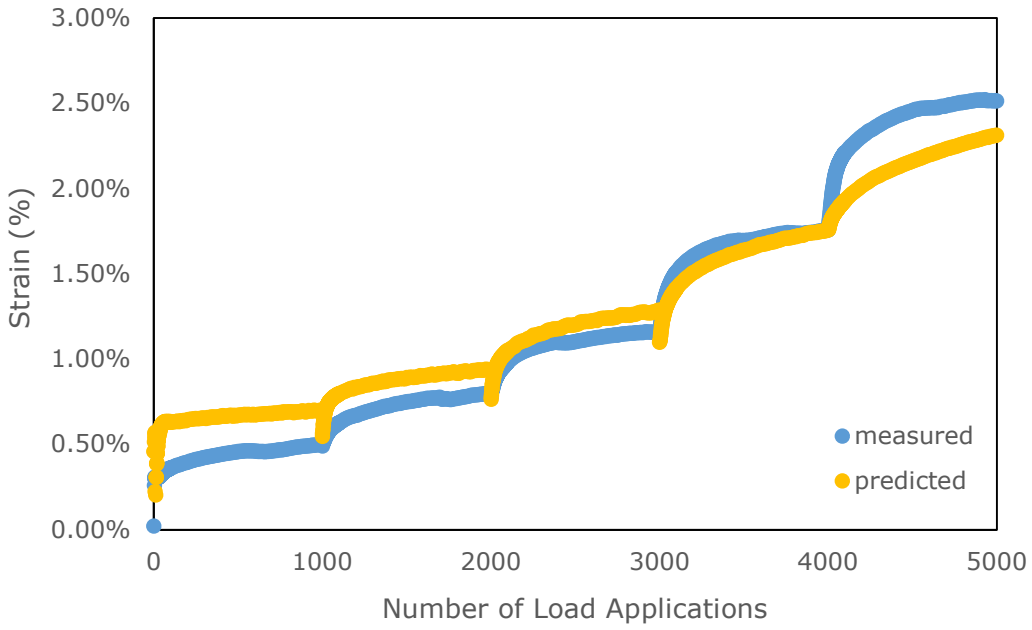


Figure 4.37: Permanent deformation measured and predicted for 4.1% fines at suction moisture content

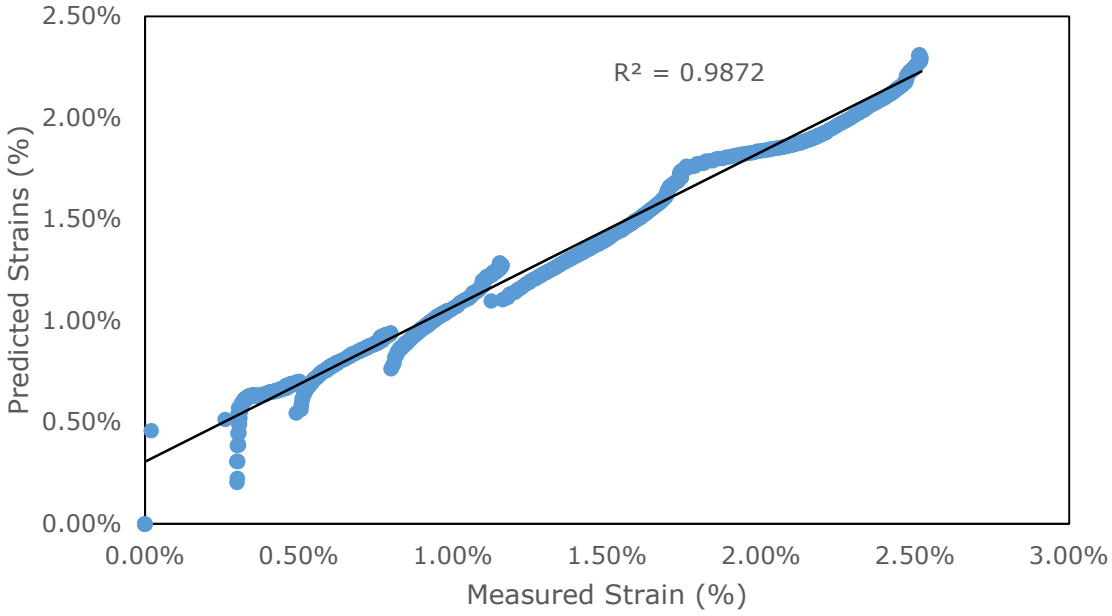


Figure 4.38: Measured vs predicted strains (%)

Table 4.3 shows the predictive analysis parameters calculated during the permanent axial strain prediction for different unbound granular materials at varying moisture content values. The regression parameters (a and b), statistical parameter (R^2), and equivalent number of load applications at each stress stage (N_{eq}) for all the materials are summarised at alpha value

of 0.75. From careful observation of R^2 values, it can be established that the methodology adopted for predicting the permanent strain from PUMA data using equations from Triaxial test data is reasonable. All the predictive analyses have suggested R^2 values of more than 0.87 which is quite a good fit statistically. The visual inspection of the relationship between measured and predictive permanent axial strains for all the materials at varying moisture contents are shown in Figure 4.39 -Figure 4.41. A good relationship between measured and predictive strains can be seen.

Table 4.3: Predictive analysis parameters

Fines Content (%)	Moisture Content (%)	alpha value						
		0.75						
		a	b	R^2	Neq_2	Neq_3	Neq_4	Neq_5
4.1	Suction	0.0036	0.053	0.9509	2.6E-05	4.3E-03	1.5E+01	5.5E+01
	3%	0.002	0.05	0.9753	4.0E-06	6.4E-01	1.4E+01	2.5E+01
	5%	0.0023	0.015	0.9813	6.8E-10	4.9E-04	7.2E-01	1.9E+00
	OMC	0.0017	0.06	0.9055	4.0E-04	2.3E-01	1.6E+01	6.4E+01
6.7	Suction	0.0065	0.006	0.9663	7.8E-14	3.2E-13	8.3E-06	2.1E-04
	3%	0.0021	0.0046	0.9239	1.9E-29	1.1E-10	5.4E-08	3.2E-06
	5%	0.0021	0.02	0.9922	1.1E-10	1.6E-06	1.0E-02	6.7E-01
	OMC	0.003	0.04	0.9608	2.2E-12	1.5E-04	2.7E-01	5.5E+01
7.4	Suction	0.0047	0.032	0.9897	5.2E-08	9.9E-02	5.8E+00	3.5E+01
	3%	0.0031	0.0052	0.9093	1.4E-35	1.9E-15	1.5E+01	1.1E-02
	5%	0.005	0.0045	0.966	1.3E-33	8.4E-15	7.1E-08	1.6E-06
	OMC	0.0021	0.001	0.9162	6.7E-219	6.1E-74	2.2E-48	2.5E-57
13.5	Suction	0.014	0.007	0.9744	5.4E+04	2.7E-03	1.5E-04	1.1E-03
	3%	0.0018	0.03	0.9901	7.2E-07	2.9E-02	3.0E+00	2.0E+01
	5%	0.01	0.04	0.8798	4.2E-06	5.0E-02	1.5E+01	3.2E+01
	OMC	0.007	0.04	0.9402	7.2E-10	9.3E-04	3.4E+00	2.8E+01

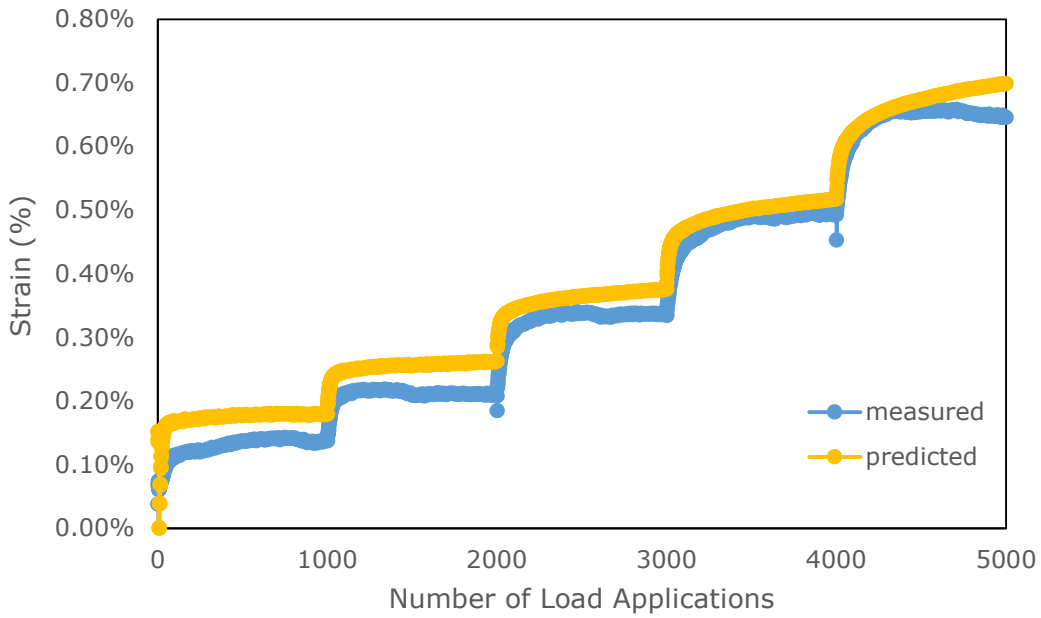


Figure 4.39: Permanent deformation measured and predicted for 6.7% fines at 5% moisture

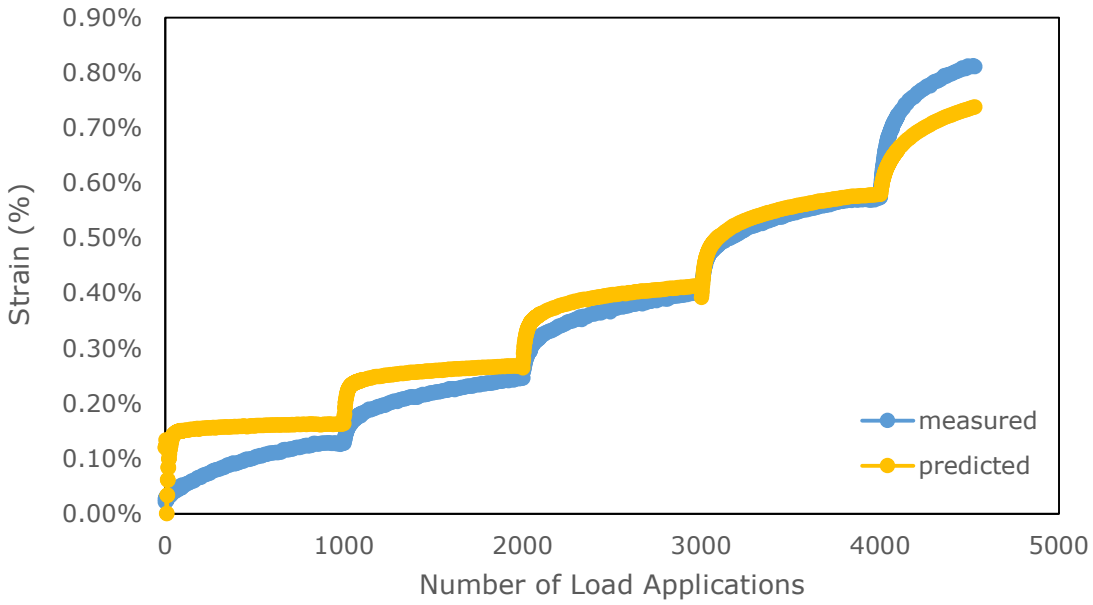


Figure 4.40: Permanent deformation measured and predicted for 13.5% fines at 3% moisture

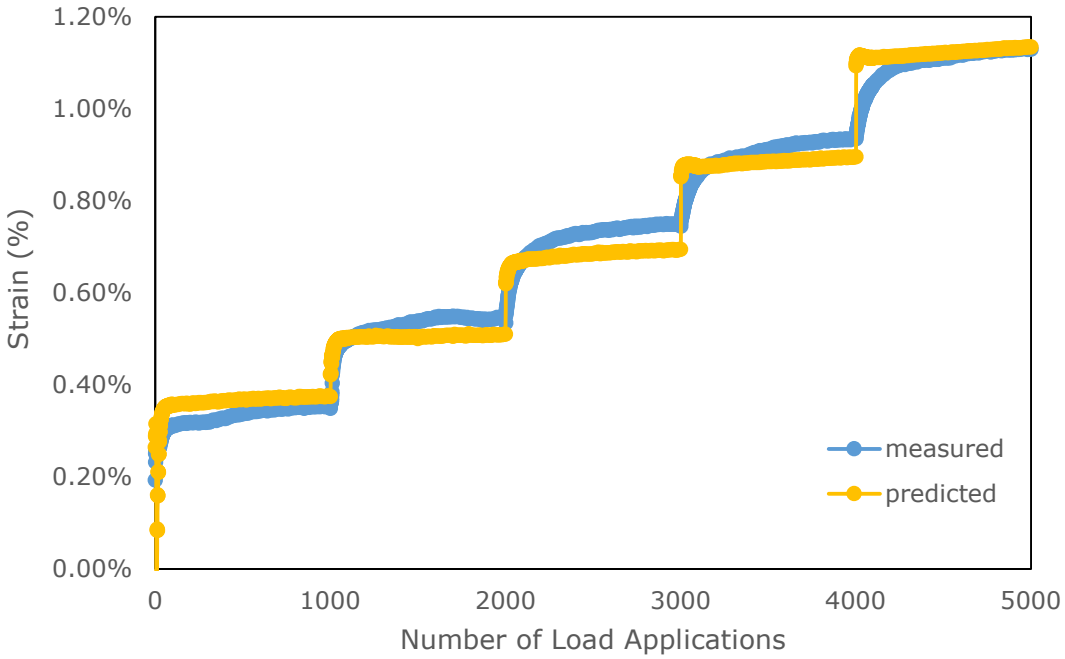


Figure 4.41: Permanent deformation measured and predicted for 7.4% fines at 5% moisture

4.6 Conclusions

The materials with highest fines content deformed most at all moisture levels.

- The resilient and permanent deformation of UGMs tested in the PUMA depended significantly on moisture and fines contents.
- For a given maximum particle size UGM gradation, the PD increased with increasing fines content although with a small particle size, the deformation decreased at optimum moisture content. A similar trend was observed for the resilience behaviour of UGMs.
- The effect of moisture content at any given fines content was relatively complicated. One of the findings was the higher resilient modulus and permanent deformation values at suction point as compared to all other moisture contents. An increase in moisture content from suction to OMC resulted in an increase in the permanent deformation of the UGMs.
- Applying shakedown theory to the permanent deformation of UGMs, all the materials behaved between Range A and B.

5 Simulative Testing of Inverted Pavements

5.1 Introduction

Pavements experience different types of damage under the loads imposed by moving traffic over their lifetime. Flexible pavement failures have been under scrutiny by pavement engineers due to those being the major type of the pavement throughout the world. Different types of laboratory and in-situ methods have been developed through extensive research in last few decades to study pavement distress modes and find possible solutions to overcome them. The present study also focusses on understanding the effect of different pavement layers within an inverted pavement on the performance under loading. For the performance analysis of the pavement, one of the most critical and often observed failure criteria, rutting, has been selected. In addition, due to the assembly of an inverted pavement explained in earlier chapters, reflective cracking has also been selected. The following sections explain the details of the research study involved to find the effect of the layer thicknesses on pavement performance with respect to rutting and reflective cracking under load.

5.2 Permanent Deformation (Rutting) in Inverted Pavement

Flexible pavements develop longitudinal grooves within the structural layers when subjected to vehicular load. The grooves are called ruts and the phenomenon is termed as rutting. It is one of the major failure modes observed on pavements especially under heavy slow-moving traffic and it is a major cause of worry for pavement engineers throughout the world. It is divided in to two major categories namely layer and structural rutting. The layer rutting involves deformation of the top asphaltic layer only where an overlay can be performed for restoration of the pavement, whereas structural rutting, often termed as critical rutting, is the rutting in the subgrade causing grooves in all the top layers where a major reconstruction of the pavement is usually the solution. Pavement engineers have been researching to minimize the rutting under loading by different ways

including improving construction materials, advancement in laboratory testing equipment, innovation in construction machinery and invention of new types of pavements.

Over the years, different methods have been developed and employed in the laboratory and in-situ for observing the pavement performance under loading. The methods have equally been used for different types of pavement structures. The current project is involved with designing inverted pavements in the laboratory. For this purpose, different laboratory procedures were considered and discarded due to the thickness and loading limitations. The project involves constructing and testing a full pavement containing four layers of different thicknesses in the laboratory. The study objectives emphasize the requirement for a testing mould and equipment capable to accommodate all the layers. Of all the equipment available in the laboratory, wheel tracking has all the qualities required for preparing and testing an inverted pavement including the required depth, simulative wheel load, proven testing history, ability to apply different loads and chamber for controlling the temperature. The wheel tracking equipment has, therefore, been used for the construction and testing of inverted pavements in the laboratory.

It is also worth mentioning that lack of resources and equipment prevented the construction and testing of a pavement test section for better understanding. To overcome the financial and equipment limitations, a simulative testing matrix was developed with the aim to study the inverted pavement behaviour under load in the laboratory while being within the available resources. The materials and testing matrix developed are represented in detail in the following sections.

5.2.1 Materials and Testing Program

The research project involved constructing and testing inverted pavements in the laboratory with varying thickness combinations. The materials for constructing the pavements were selected on the basis of the properties and limitations mentioned in chapter 3. This chapter focusses on a brief reminder of the materials, the testing matrix involved, a detailed description

of the construction of the pavements and testing in the wheel tracker. The results obtained from the test are also documented.

5.2.1.1 Materials

The different materials used to construct an inverted pavement for the permanent deformation (rutting) testing in a wheel tracking equipment included granite aggregate and bitumen for wearing course, granite aggregate for unbound granular layer, granite aggregate and cement for cement treated base layer and 12mm thick rubber to simulate the subgrade layer. The basic properties of all the materials have been documented in detail in chapter 3. The gradation adopted for the testing are shown in Figure 5.1 and Figure 5.2. Out of the different UGM gradations presented in chapter 3 and 4, 7.4% fines content gradation was used in simulative testing of inverted pavements having maximum particles size of 14mm. It was used in simulative testing to correspond to the lowest layer thicknesses.

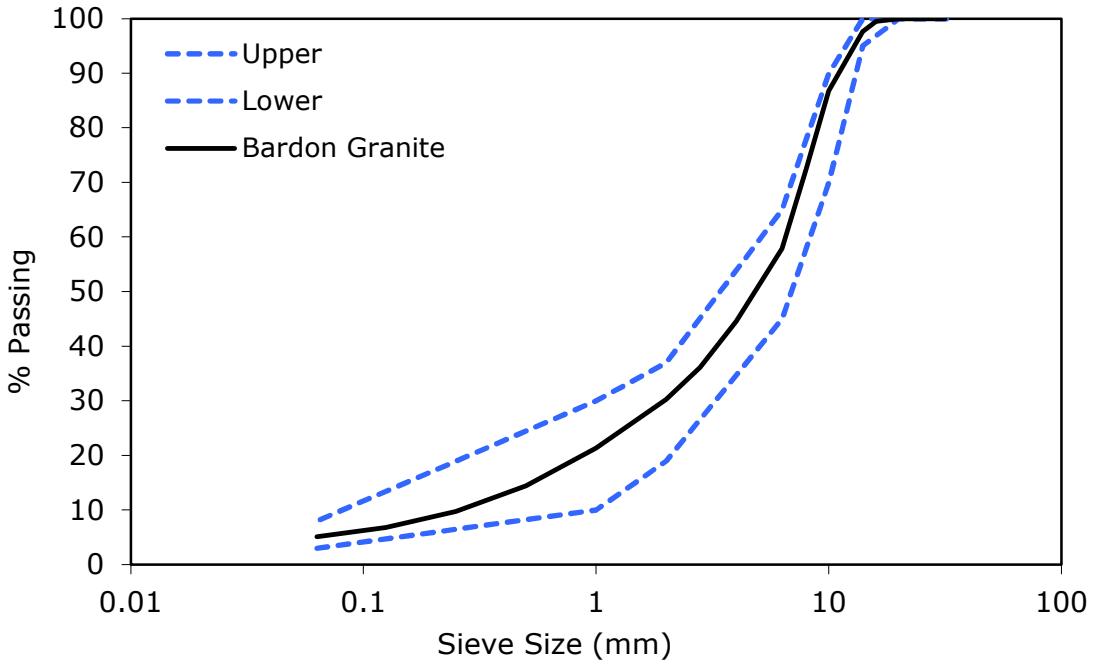


Figure 5.1: Granite gradation for 0-14mm dense graded asphalt mix

5.2.1.2 Testing Program

A detailed testing programme was devised to study the permanent deformation behaviour of an inverted pavement. Different thickness combinations were made to document the effect of layer thickness on overall deformation performance of an inverted pavement under loading.

The utmost effort has been made throughout the research to keep all the parameters including particle gradation size, moisture, density, testing load and testing temperature the same for all the specimens tested in order to get representative results from the tests.

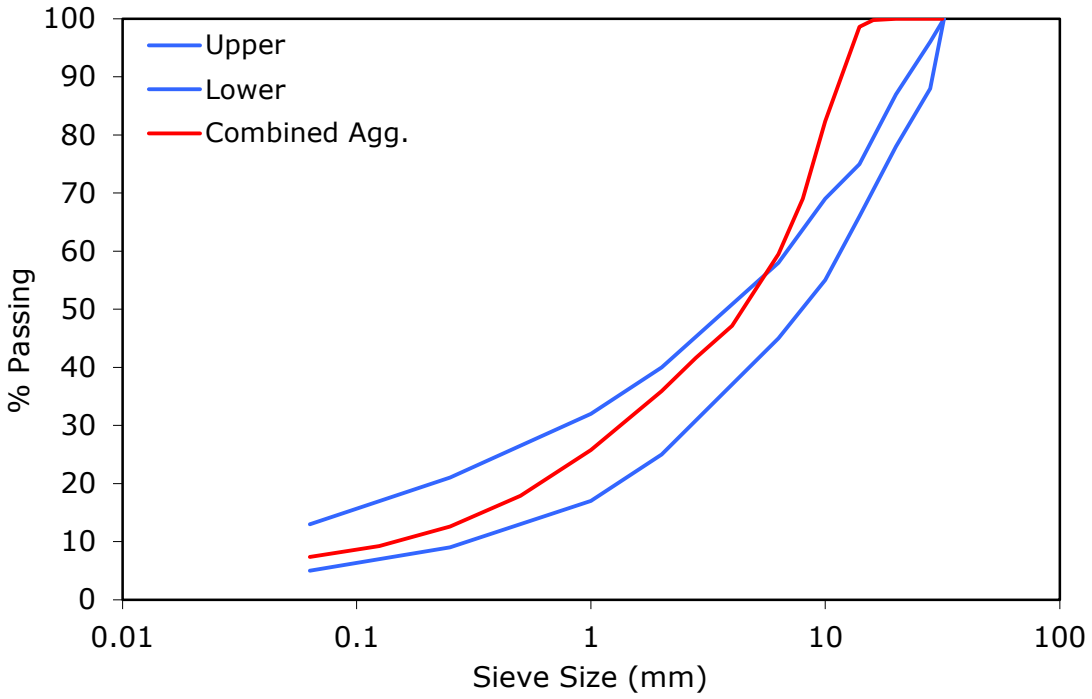


Figure 5.2: Unbound layer gradation for simulative testing

Table 5.1 shows the testing matrix adopted for the study. It explains the layer thicknesses used for the study. The thicknesses of all the structural layers of the pavement i.e. asphalt concrete, unbound layer, cement treated base and subgrade are tabulated. The 'wooden filler' column corresponds to the thickness taken up by wooden blocks to fill the additional space from the combined layer thickness to arrive at the total thickness of the mould (130mm). The wooden blocks thickness was determined by total thickness of the mould (130) minus combined thickness of the four structural layers (AC+UGM+CTB+SG), although the subgrade was not an actual structural layer in the pavement, being simulated by rubber. The wooden filler was needed as the specimen compaction and testing was performed in-situ i.e. within the mould. This assembly made it necessary to fill the remaining thickness of the mould by wooden filler blocks to let the wheel pass on the pavement without direct contact with the mould corners. This, if it happened, could have affected the results as well as a being safety hazard.

Table 5.1: Simulative testing matrix

Simulative Testing						
Sample No.	Layer Thickness (mm)					Total Thickness (mm)
	Asphalt concrete	UGM	CTB/ Simulation	Subgrade	Wooden Filler	
WT-2	15	20	30	12	53	130
WT-4	15	35	30	12	38	
WT-6	15	50	30	12	23	
WT-8	15	60	30	12	13	
WT-10	20	20	30	12	48	
WT-12	20	35	30	12	33	
WT-14	20	50	30	12	18	
WT-16	20	60	30	12	8	
WT-18	25	20	30	12	43	
WT-20	25	35	30	12	28	
WT-22	25	50	30	12	13	
WT-24	25	60	30	12	03	

5.2.1.3 Wheel Tracking Mould and Specimen preparation

Wheel tracking devices are some of the most reliable pieces of laboratory equipment to simulate wheel load, either on one layer or a full pavement. Out of the various wheel tracking devices available at NTEC, a university-built wheel tracking device was selected for the project due to its ability to test a thick specimen. The mould used for preparation of the specimen has dimensions of 305 x 305 x 130 mm. The mould chosen for the study is the deepest available at NTEC, which was the reason for its selection as a full depth inverted pavement comprising of four layers was to be simulated in it. The following is a brief description of the laboratory specimen preparation.

The laboratory work started, after finalizing the gradations, with batching the materials for different pavement layers according to the calculations based on moisture-density values from the vibratory compaction test. As a pre-compacted cemented base layer was used for constructing the full pavement, so the first step in the laboratory was preparing the cement treated base layer. Its preparation was started by adding 4% cement, by weight, and optimum moisture content to the already batched aggregates. The prepared mixture was placed in an already greased wheel tracking

mould homogeneously and compacted to the desired density in a roller compactor machine. The wheel tracking mould was greased evenly prior to compaction in order to be able to remove the prepared specimen undamaged. The prepared cement treated base layer specimen was taken out of the mould after 24 hours minimum and used for constructing an inverted pavement as shown in Figure 5.3.



Figure 5.3: A) Aggregate mixed with water and (B) Prepared cemented slab

After the cemented base layer had been constructed in a separate wheel tracking mould, the full depth inverted pavement construction followed. For the full pavement construction, the wheel tracking mould was assembled by loosely bolting all the parts and keeping one side open. This was to provide space for smooth transfer of the already compacted cemented layer within the mould without damaging it. To start the pavement construction, the bottom of the mould was filled with wooden filler of the required thickness.

A 12mm thick rubber sheet was then placed on top of the wooden filler to simulate the subgrade layer in the pavement. The same thickness rubber was used for all the specimens tested in order to have the comparable results. The already roller compacted cemented slab was then placed on top of the rubber subgrade. A very gentle compaction effort by Kango Compactor was applied to ensure filling of any voids between the slab and rubber. It was carried out with a wooden plate of the same size as the top of cemented slab in order to protect the slab from the compaction force. After completing the bottom three layers, the in-situ compaction of unbound

and asphaltic layers followed. The batched material for the unbound granular layer was given a thorough mix to equally distribute the fines. The mixed material was then poured with the water at optimum moisture content and given a consistent mix as shown in Figure 5.4. The mixing was done manually until the moisture was distributed equally throughout the mixture based on visual inspection. In order to avoid any inconsistencies in the results, the mixing for all the specimens during the research was performed by the same person with the same effort.



Figure 5.4: Mixing water at OMC into unbound granular materials

The mixed materials were then poured on top of the prepared cemented slab in layers. The number of layers depended on the thickness of the compacting layer. For example, a 60mm thick unbound layer was compacted in 3 layers as compared to 2-layer compaction for 20mm thick UGM. The Kango compactor was used for compacting the unbound layer in-situ in layers. A wooden plate was placed on top of the loose material and compacted by applying the compaction force. The compacted densities were controlled for different specimens by measuring the thicknesses. As the materials were batched by working out the density-volume relationship, the compaction up to required depth corresponded to the desired density. The materials were scarified on top of each layer with the help of a trowel before pouring the materials for later layers in order to get a homogeneous material. After compacting all the layers of unbound material, the mould was left in the laboratory for some time in order to dry the top of the specimen. The nearly dry top of the unbound layer was then covered with bitumen emulsion in order to provide a bond between the layers. The bitumen emulsion content was judged by visual inspection and its values

calculated by weighing the specimen before and after applying it ranged from 0.34-0.63 kg/m^2. Due to the need for bond between wearing and unbound layers, the wearing course was also compacted in-situ in the laboratory. The batched aggregates for the wearing course and bitumen were placed in the oven at 160±2^{0}C for 7-8 and 3 hours respectively. The mixer was also kept at the same temperature before mixing. The already warmed aggregates were placed in the already heated mixer and given a manual mix to ensure equal distribution of fines. The bitumen was then added at 5% by weight to the aggregates in the mixer and mixing was performed for 3 minutes. The mixer was stopped after half the time and a manual mixing was given to ensure the fines remaining under the mixing paddles also got picked up. Before starting the mixing process, the mould containing prepared layers up to unbound level was prepared for wearing course compaction. All the setups were done before starting the mixing process in order to ensure 150-160^{0}C temperature during compaction. The mould, Kango compactor, compacting plate and brown paper to avoid direct contact of the compactor with the asphalt were kept to hand. A wooden collar was also placed on top of the mould in order to accommodate the loose material before compaction. The mixed material was then poured into the mould on top of the unbound layer with great care due to the temperature. The mould was then, as fast as possible, taken to the compaction place and compaction was started by placing a wooden plate on top of the loose material in order to distribute the compaction force uniformly. The thickness was monitored while compacting in order to reach the desired density. The wooden collar was then removed carefully, and the prepared specimen was kept in the laboratory in order to decrease the temperature. The compaction temperature was monitored by placing a thermometer on top of the layer after compaction. After the specimen temperature decreased to room temperature, it was transported to the laboratory for testing. As the rutting testing was performed at 30^{0}C, the specimen was conditioned at the test temperature for 10-24 hours for different specimens depending on difference in preparation and testing times. A prepared specimen is shown in Figure 5.5.

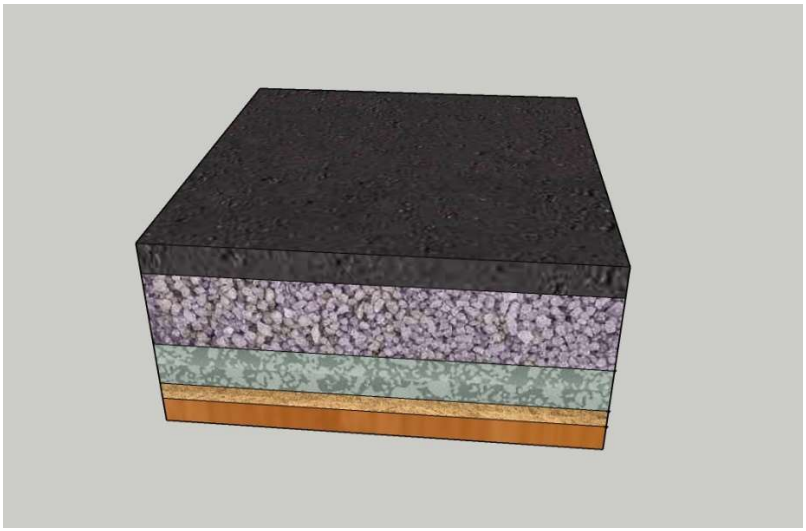


Figure 5.5: A depiction of a wheel tracking specimen with 20mm AC, 50mm UGM, 30mm CTB, 12mm rubber as SG and 18mm wooden filler

5.2.1.4 The Wheel Tracking Machine

Wheel tracking devices have been used throughout the world to study pavement permanent deformation behaviour under loading. Different wheel tracking devices are available commercially as mentioned in chapter 3. The University-built wheel tracker was used for this research project. It consists of various parts including a basic frame, to and fro moving base supporting the specimen, lever arm with hanging loads to control the applied load, cycle counter and electric motor to move the base under load. The basic frame of the equipment encompasses all the parts within or on top of it. The equipment has a base like a table top to rest the mould on. The base moves to-and-fro under load. The frame has top side walls and a top horizontal steel column on top of the side walls. The steel horizontal wall is used to support the wheel by a lever arm which is further extended out of the frame and this can be used to hang a weight in order to apply the desired load on the specimen. The moving base is connected with a small steel rod which, upon completion of one cycle, activates a counter attached to the other end thereby helping to count the number of cycles under load. Each load cycle comprises two passes of the wheel on the specimen. The base plate is attached to an electric motor which provides the to-and-fro movement of the base plate containing the specimen and hence applying the load under the wheel. Figure 5.6 shows a wheel tracking machine used for testing in the laboratory.

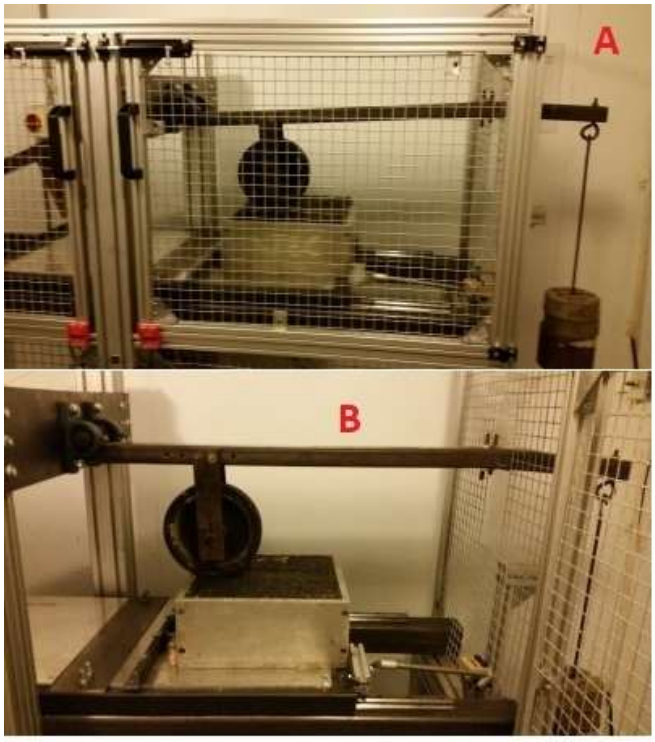


Figure 5.6: Wheel tracking equipment a) with hanging loads b) Zoomed to wheel

The test was carried out for 10,000 cycles and rutting was recorded manually. Due to the lack of an automated data collection system on the university wheel tracker, the rutting was collected at different intervals. The data collection intervals were increased with number of load applications i.e. as many as 10 data points for the first 100 cycles were reduced to 2 data points for every 1000 cycles later in the test. As the data was collected manually, great care was taken to achieve uniformity of data collecting. The rutting results were reported manually based on two methods; one being the profilometer while the other used the depth gauge. The depth gauge was used with the help of a holed steel plate. The steel plate, longer than wheel width and hence rut width, was placed across the rut developed in the specimen. The depth gauge was passed through the holes in the plate to reach the rut depth. As it is a manual method to measure the rutting, utmost care was taken not to put the gauge into surface voids. The data was collected at multiple points, up to four, along the rut length and an average value was reported. Both the methods to calculate rutting manually are illustrated in Figure 5.7. The data was collected by using both or one of the methods depending on the rut profile. For a uniform rut profile, either, but mostly the depth gauge, was used whereas for an uneven rut along the

length, both the methods were used, and average values were reported. The data was collected for all the specimens following the same procedure.

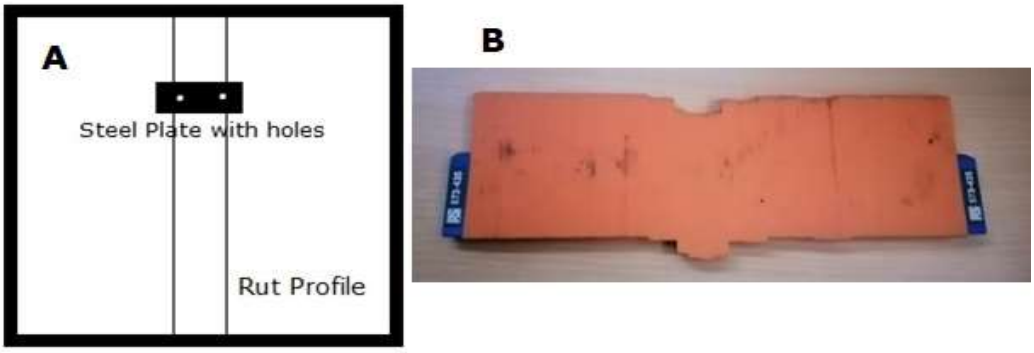


Figure 5.7: Methods for rutting manual calculation a) Depth Gauge with steel plate and b) Profilometer

5.2.1.5 Effect of layer thickness on the performance of an inverted pavement in a simulative testing environment

The inverted pavements were constructed and tested in the laboratory with different combinations of layer thickness. The thickness of wearing course and unbound layer were varied while that of cement treated base and subgrade was the same throughout the project. Different specimens at different phases of the test are shown in Figure 5.8. The figure shows a prepared untested specimen as well as random wheel tracking tested specimens showing different levels of rutting.

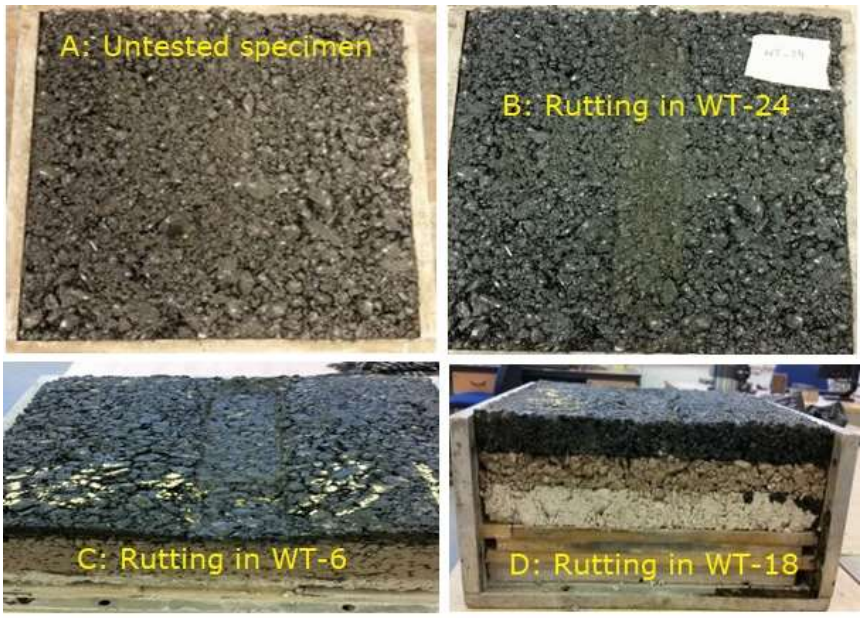


Figure 5.8: Wheel tracking specimen (untested vs tested)

The effect of layer thicknesses on permanent deformation performance of an inverted pavement under load is shown in Figure 5.9 and discussed in the following paragraphs. It is to be noted that the legends show the thickness of asphalt wearing course and unbound granular base respectively in mm. The testing was performed at 30^0C and the specimen were conditioned at the test temperature for up to 24 hours. The test conditions comprised a wheel load of 1.5kN, contact radius of 23.6mm and contact pressure of 850kPa.

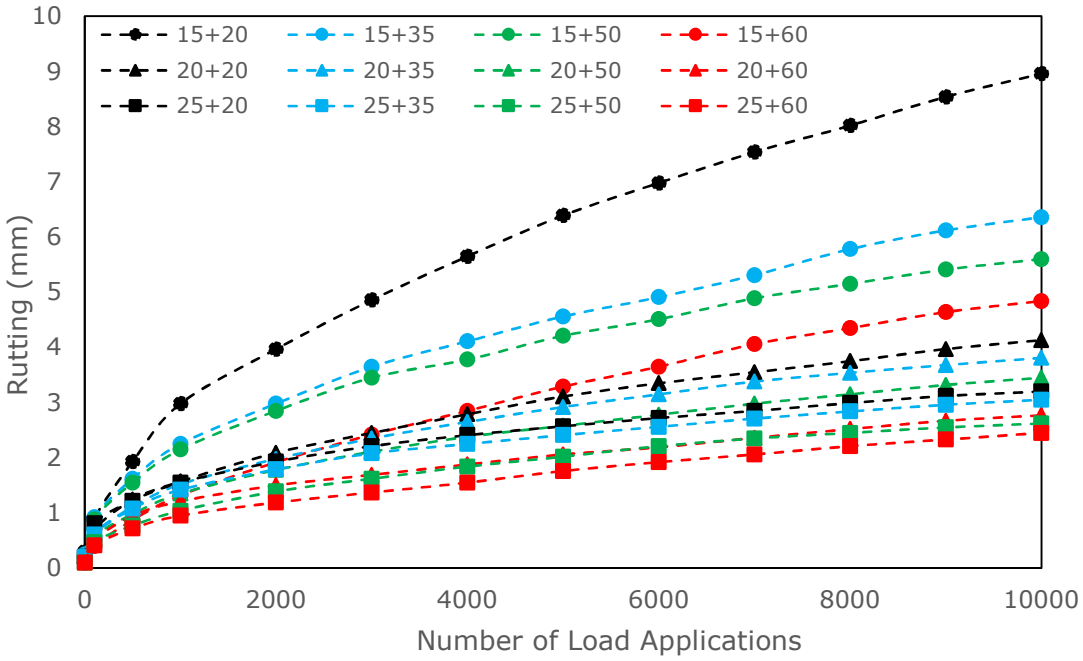


Figure 5.9: Summary of simulative wheel tracking test results

5.2.1.5.1 Base layer as an indicator of inverted pavement performance

The Figure 5.10 -Figure 5.12 show the effect of varying thickness of unbound granular materials on rutting performance under loading with asphalt concrete thicknesses of 15, 20 and 25mm respectively. It is very clear from the figures that the rutting resistance of the pavement increases with the increase of unbound granular layer thickness while keeping the asphalt thickness, loading, testing temperature and all other factors the same. It is worth noting that with a 15mm thick AC layer, the rutting resistance increases considerably by increasing the unbound thickness from 20 to 35mm. Further increases in unbound thickness to 50 and 60mm

respectively increase the rutting resistance steadily. The rutting resistance of the specimen with 35mm thick unbound granular material increased by 29% compared to that of the specimen with 20mm. Further increments of 15 and 10mm increased the rutting resistance by 11 and 10% respectively.

Similar results were observed with asphalt thicknesses of 20 and 25mm. The difference between the two was the different rutting resistance percentage increases when increasing the thickness of the unbound layer in the pavement. In the case of the specimen with 20mm thick wearing course, increases in unbound thickness from 20 to 35 and 35 to 50mm, increased the rutting resistance by 7 and 9% respectively, whereas a further increase in thickness from 50 to 60mm, increased it by 20%. The reason for improved pavement performance by increasing the unbound layer thickness is the better load spreading. The rutting resistance improved gradually with increase in unbound layer thickness with 25mm thick wearing course. A significant increase (~15%) in rutting resistance was observed when the unbound thickness was increased to 50mm from 35mm. As the wearing course thickness increased, the rutting resistance percentage increase decreased, although a significant reduction in permanent deformation still resulted from increasing the wearing course thickness from 15 to 20 and 20 to 25mm.

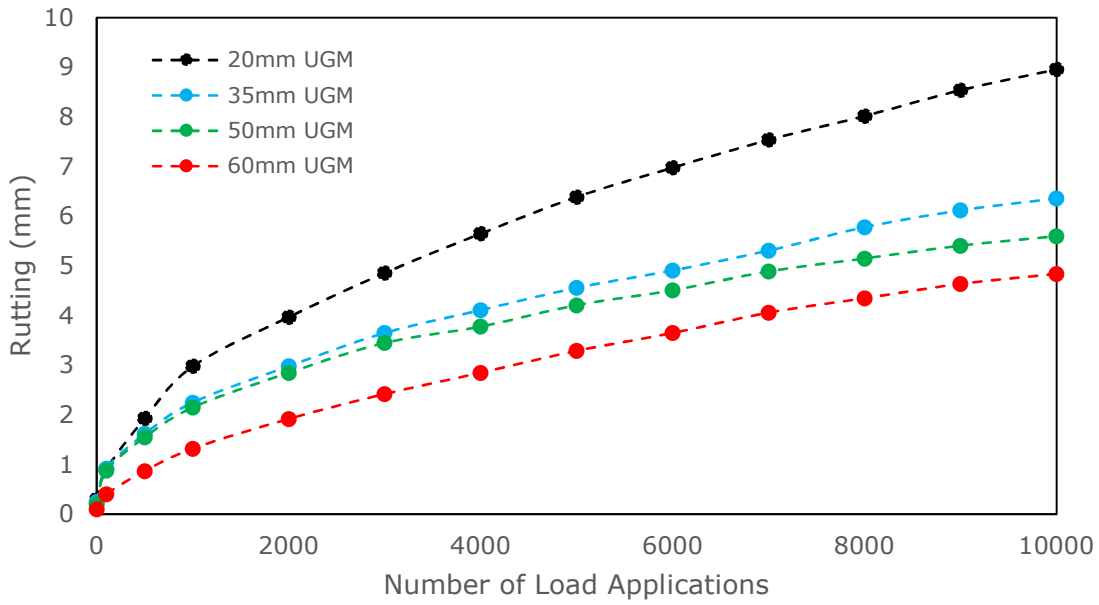


Figure 5.10: Permanent deformation of inverted pavements with 15mm thick AC

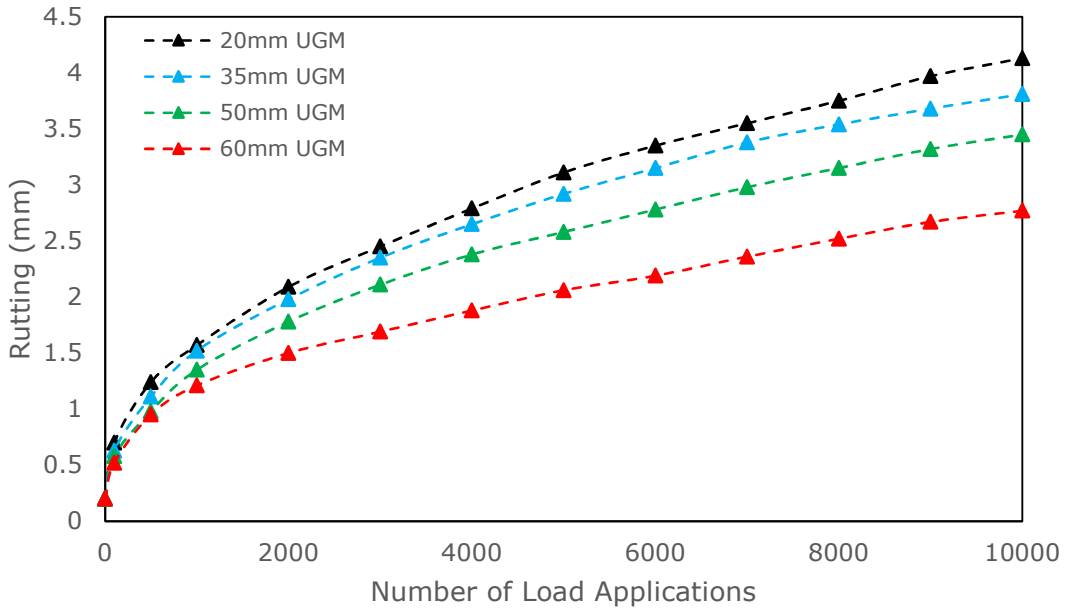


Figure 5.11: Permanent deformation of inverted pavements with 20mm thick AC

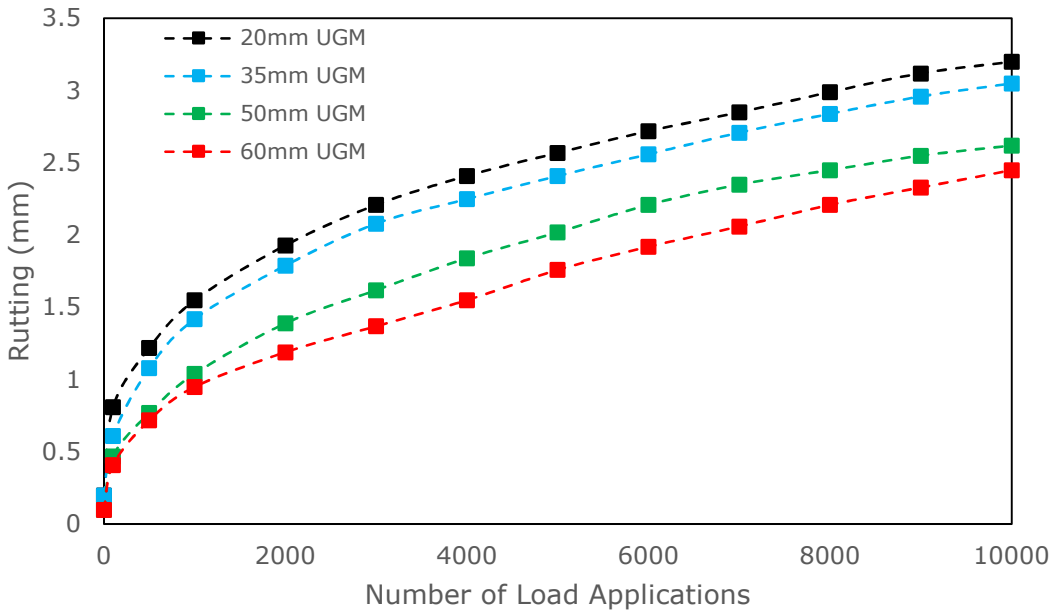


Figure 5.12: Permanent deformation of inverted pavements with 25mm thick AC

5.2.1.5.2 Effect of asphalt on pavement performance

The Figure 5.13 -Figure 5.16 show the effect of an increase in wearing course thickness on overall pavement performance while keeping the unbound layer thickness constant. It is evident from the figures that an increase in wearing course thickness at any given thickness of unbound granular layer resulted in an improved pavement resistance, although the increase in pavement resistance was not as significant for an increment in

AC thickness from 20 to 25mm as compared to one from 15 to 20mm. It is clear from these figures that the pavement resistance to permanent deformation increased by manifold at all unbound layer thicknesses by increasing the asphalt wearing course thickness from thinnest to the thickest. The analysis of the results shows that almost 80% of permanent deformation resistance was caused by increasing the wearing course thickness from 15 to 20mm alone. A further increase to 25mm contributed to approximately 20% of pavement resistance to permanent deformation. For an example calculation, the pavement response by increasing the wearing course thickness from 15 to 25mm in two increments while keeping unbound layer thickness to 20mm can be presented. For the said layer thickness combination, the permanent deformation decreased by 64% for both the increments of wearing course of which 54% was contributed by the first one alone. Similarly, for unbound layer thicknesses of 35, 50 and 60mm, an increase in asphalt layer thickness from 15 to 25mm decreased the permanent deformation by 52, 53 and 49% respectively. The detailed analysis of these results also shows that up to 80% of increase in pavement resistance to permanent deformation was cause by the first increment in wearing course thickness alone. The permanent deformation tests, thus, result in an increased pavement response by increasing the individual layer thickness as well as the overall pavement thickness. The increase in the pavement response, though, was different for different increments in the layer thickness combinations. The results indicate that both the layers are important structural layers within an inverted pavement and a thickness increase in either improves the pavement response. As the permanent strains are resulted form the transient strains in UGMs, an increase in AC thickness reduced these thereby decreasing the PD. Similarly, an increase in UGM thickness decreased the influence of the soft rubber sheet underneath which also resulted in reduced transient strains. So, an increase in either of the layer thicknesses resulted in reduced PD.

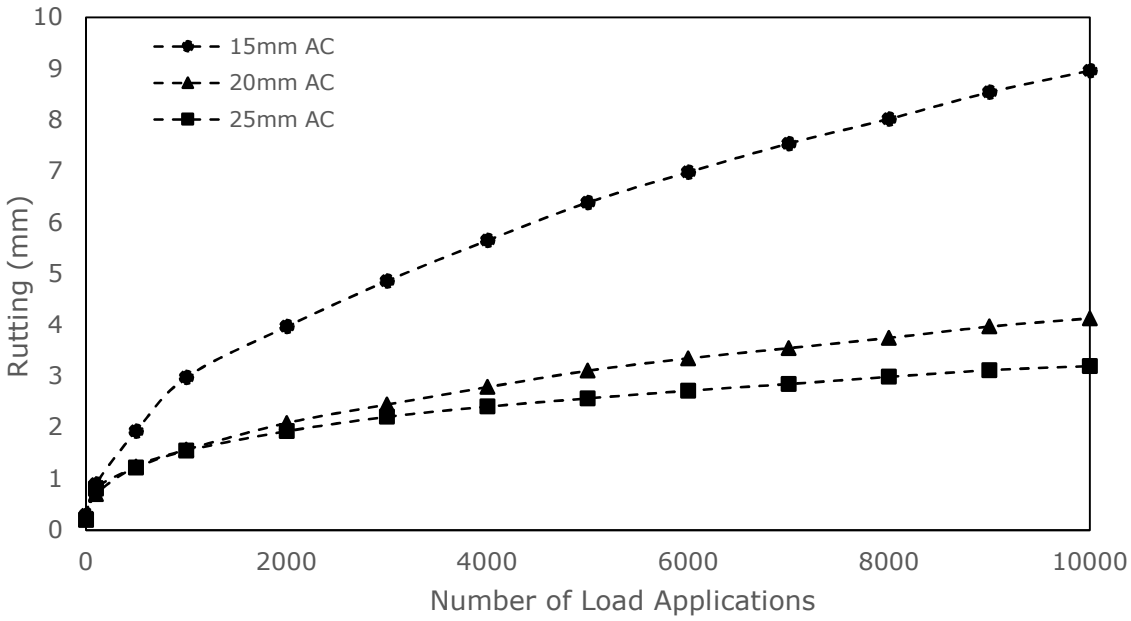


Figure 5.13: Permanent deformation of inverted pavements with 20mm thick UGM

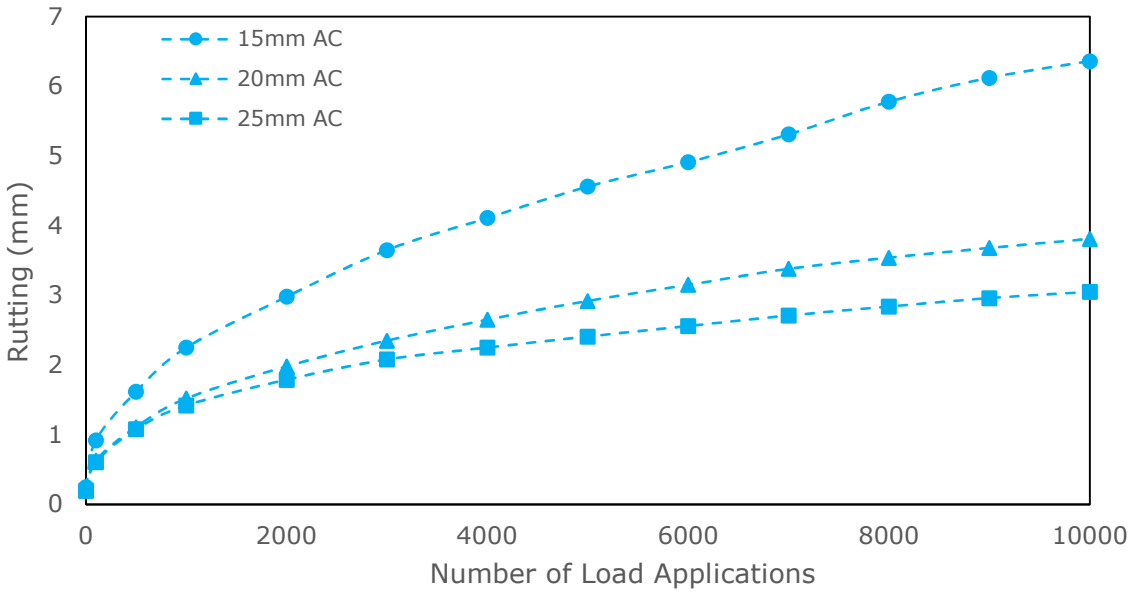


Figure 5.14: Permanent deformation of inverted pavements with 35mm thick UGM

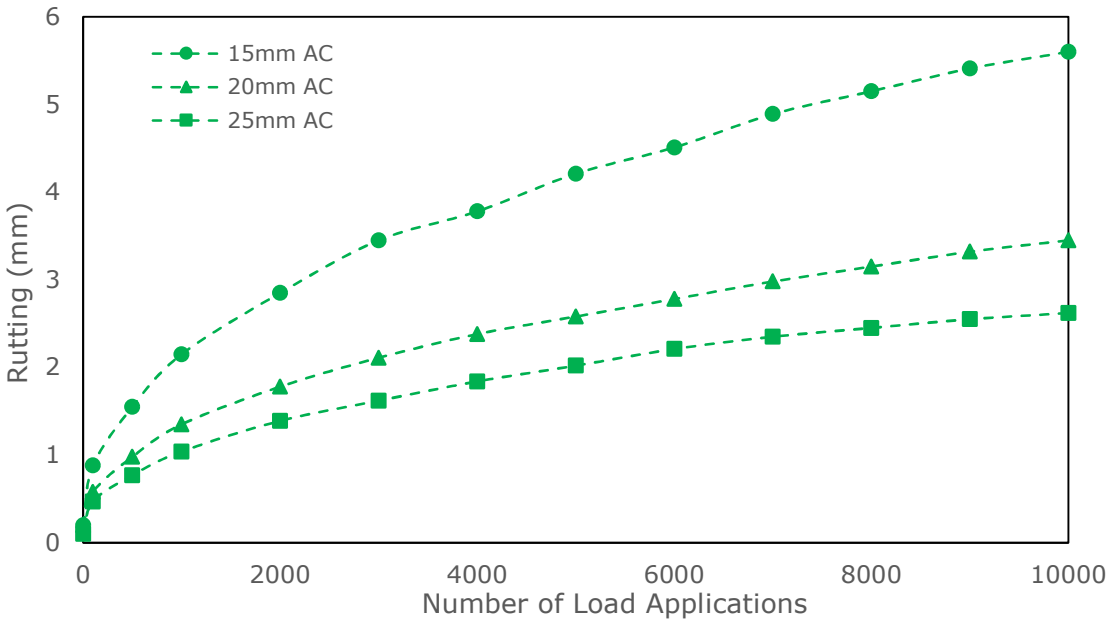


Figure 5.15: Permanent deformation of inverted pavements with 50mm thick UGM

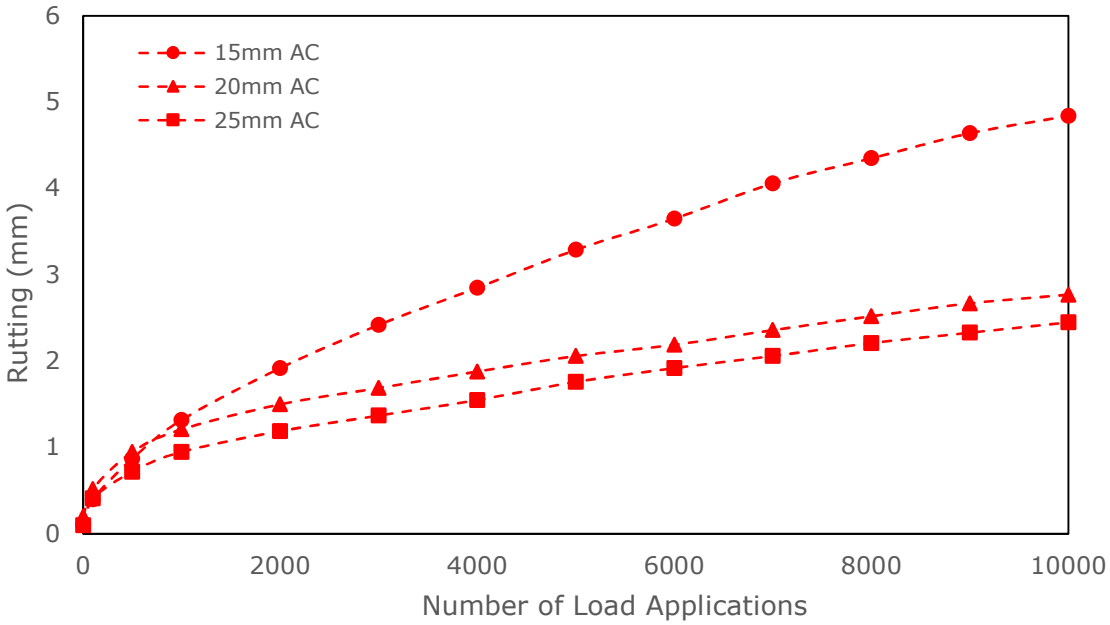


Figure 5.16: Permanent deformation of inverted pavements with 60mm thick UGM

The findings from the wheel tracking test correlating the permanent deformation to the number of load applications can also be explained with reference to shakedown theory. Shakedown theory has been developed to explain the permanent deformation behaviour of unbound granular materials but there has not been a single instance of using the shakedown

concept to understand full pavement behaviour under load. Therefore, the rutting calculated at the end of every test in each individual layer, AC and UGM, has been used to implement the shakedown concept. After the end of each wheel tracking test, the mould was opened and emptied very carefully, removing the AC layer from the specimen with the help of a hammer and chisel. The utmost care was taken not to disturb the rut line in the AC as it was used in further calculations of individual layer rutting. The rutting in the AC layer was calculated manually in the laboratory using the same methodology. The individual AC rutting and total rutting in the specimen were used to deduce the rutting in the UGM layer. Table 5.2 shows the individual rutting observed in the pavement layers at the end of each test.

Table 5.2: Rutting in individual layers

AC + UGM Thickness (mm)	Rutting (mm)			Rutting (%)	
	Total	AC Layer	UGM Layer	AC Layer	UGM Layer
15+20	8.96	7.1	1.86	79.24%	20.76%
15+35	6.36	5.36	1	84.28%	15.72%
15+50	5.6	4.7	0.9	83.93%	16.07%
15+60	4.84	4.3	0.54	88.84%	11.16%
20+20	4.13	3.21	0.92	77.72%	22.28%
20+35	3.81	3.15	0.66	82.68%	17.32%
20+50	3.45	3	0.45	86.96%	13.04%
20+60	2.77	2.35	0.42	84.84%	15.16%
25+20	3.2	2.68	0.52	83.75%	16.25%
25+35	3.05	2.7	0.35	88.52%	11.48%
25+50	2.62	2.5	0.12	95.42%	4.58%
25+60	2.45	2.41	0.04	98.37%	1.63%

As the rutting was calculated at multiple intervals during the test, so the rutting in the specimen at every 1000 cycles was known, the rutting values at 3000 and 5000 values were used for calculating the shakedown range in unbound granular materials. The difference between strains at 3000 and 5000 cycles was noted. The values were divided into AC and UGM based on percentage deformations from Table 5.2 and used to demonstrate the pavement suitability on the basis of shakedown criteria. Based on the methodology adopted, the findings are presented in Table 5.3.

Table 5.3: Shakedown Range in UGM

AC + UGM Thickness (mm)	Strain Difference 3000-5000 cycles			Shakedown Range
	Total	AC Layer	UGM Layer	
15+20	0.0102	0.0081	0.0021	C
15+35	0.0061	0.0051	0.001	C
15+50	0.0051	0.0043	0.0008	C
15+60	0.0058	0.0052	0.0006	C
20+20	0.0044	0.0034	0.001	C
20+35	0.0038	0.0031	0.0007	C
20+50	0.0031	0.0027	0.0004	B
20+60	0.0025	0.0021	0.0004	B
25+20	0.0024	0.002	0.0004	B
25+35	0.0022	0.0019	0.0003	B
25+50	0.0027	0.0025	0.0001	B
25+60	0.0026	0.0026	4E-05	A

It is very evident from Table 5.3 that the UGM behaviour in first six thickness combinations makes it unsuitable for good performance and long-lasting pavements with respect to permanent deformation. The next five thickness combinations for the said conditions lie in Range B as per shakedown criteria which means that the material undergoes significant deformation in the initial cycles which tends to settle to a nearly constant value accumulating at a very slow rate. The best behaviour observed was for the thickest pavement. The reason may lie in the same stress conditions for all the thickness combinations allowing the thick specimen to deform least thereby making it the best choice for the said load and environmental conditions. It is to be noted here that in previous studies, shakedown criteria have mostly been used to differentiate between different unbound materials for selecting the most suitable for optimum performance of a pavement unbound layer whereas in the current study, the criteria have been used to differentiate between unbound layers constructed in varying thicknesses of the same material under the same testing conditions

5.3 Reflective Cracking in Inverted Pavements

Alongside permanent deformation, cracking is one of the major failure criteria causing massive difficulties for pavement engineers to maintain smooth, durable and long-lasting pavements both financially and structurally. There are many different types of cracking observed in

pavement including longitudinal, transverse, thermal, reflective and many more. Reflective cracking is the phenomenon noticed in pavements having cement stabilized sublayers in which a crack that has developed under load due to its brittleness tends to move upwards causing failure in all the layers up-to wearing course. These cracks are developed in the wearing course above cracks in the cemented layer. As an inverted pavement is built by constructing an unbound granular layer between a cement treated base and asphalt concrete wearing course, the potential chances of reflective cracking are much more than in a conventional flexible pavement. This chapter, therefore, focusses on simulating an inverted pavement in the laboratory to study its reliability for minimizing reflective crack initiation and propagation. The materials, testing program, specimen preparation, testing mould parts and description, testing equipment and results obtained in the laboratory are documented respectively.

5.3.1 Materials and Testing Matrix

As the study was conducted to study layer thickness combinations by analysing the performance under load, so the same thickness combinations have been used for cracking tests as for rutting shown in Table 5.4.

The same materials and same gradations have been used for preparation of the specimens for cracking tests as for rutting tests. There were a few differences, though, depending on the requirements of the testing procedure. One of the differences was the testing temperature. The laboratory wheel tracking testing for crack propagation analysis has been carried at 10 ^{0}C as compared to 30 ^{0}C for rutting. Different temperatures for different testing procedures were adopted corresponding to the most severe conditions observed in a pavement i.e. the tendency of higher rutting and cracking at higher and lower temperatures respectively. The main difference between rutting and cracking testing was the sample preparation and testing mould. Due to the study requirements, a new mould was designed and manufactured in the workshop to carry out the cracking test in the laboratory. The details of the mould parts and assembly are described in the following section.

Table 5.4: Testing Matrix for cracking tests

Layer Thickness (mm)					Total Thickness (mm)
Asphalt concrete	UGM	CTB/ Simulation	Subgrade	Wooden Filler	
15	20	30	12	53	130
15	35	30	12	38	
15	50	30	12	23	
15	60	30	12	13	
20	20	30	12	48	
20	35	30	12	33	
20	50	30	12	18	
20	60	30	12	8	
25	20	30	12	43	
25	35	30	12	28	
25	50	30	12	13	
25	60	30	12	03	

5.3.2 Wheel Tracking Mould parts and description

The laboratory study to characterize a simulative inverted pavement could not be performed in a conventional wheel tracking mould due to its steel walls hindering the ability to monitor the crack initiation at the bottom of the asphalt layer. One of the solutions could be replacing the material of the mould walls from steel to transparent glass. The idea was dropped due to the financial constraints of the project; transparent glass able to take the compaction and testing load being expensive. Another reason to drop the idea was the mould size where more load applications would probably be required to develop and observe a crack distant from the wheel path near the transparent glass. To overcome these problems, a mould was designed and manufactured with the ability to monitor crack propagation without compromising compaction effort and testing load.

The following is a brief description of the parts of the mould assembled at NTEC. The parts of the mould included a base plate, long side walls, short side walls, long side angles, short side angles, angles to support the specimen and a steel plate to support the top of the prepared specimen. All the angle sections were 40 x 40mm with the length being equal to the wall

to which they were welded or bolted. All the parts were made of steel and are shown in the forthcoming figures.

The mould was designed since the highest tensile strains are present at the bottom of the asphalt layer causing crack initiation. Along with the higher tensile strains, the bottom cracked cemented layer would also initialize the cracks from the bottom of the wearing course under load. Based on these concepts, the mould was designed to allow viewing of the wearing course's full thickness at all times which could be vital for recording crack initiation and propagation.

The base plate is the foundation of the mould which encompasses all the other components providing the required strength during compaction and testing. The base plate is made of steel having a thickness of 3mm which was ample for providing the requisite strength to hold the mould together during compaction and keeping the specimen together under load in a wheel tracking test. The base plate was welded to the long and short walls to assemble the basic mould frame. The short walls corresponding to the width of the mould were assembled to the full depth of the mould which is 130mm. As the mould was developed for monitoring cracks which would not be observed at the ends of the specimen, so short side walls were made to the full depth of the mould. Along the length of the transverse side walls, angle sections were welded to provide the lateral support to the mould during compaction and testing. Another advantage of the angle sections was using them for connecting / bolting different mould parts at different stages of compaction and testing by providing the holes in them. The angle supported full depth transverse side walls also contributed to the overall mould strength. The longitudinal side walls were welded with the base plate and transverse side walls up to a height of 105mm. A wheel tracking mould assembled for cracking without the removable parts is shown in Figure 5.17.

The remaining height on the side walls was achieved by the removable steel walls which were positioned and removed during compaction and testing respectively. It was done to make the crack initiation monitoring on the bottom of asphalt concrete wearing course possible as the thickest wearing course was 25mm during the project. This kind of assembly made it possible to monitor cracks at the bottom of the wearing course for all the different

combinations of the layer thicknesses under consideration. Additional angles sections were also welded from top of 105mm longitudinal side walls going downwards up-to 40mm depth. These were assembled to provide the adequate lateral support along the length of the mould as well as base for connecting the removable walls. These removable longitudinal walls were made with angle sections welded providing the support as well as easier connection through bolted joints. The removable side walls were made of 50 and 40mm height to fill up the remaining 25mm height in different combinations. The additional height on the removable side walls were provided in order to accommodate the loose material as all the compaction of unbound and wearing course was done in-situ. (Figure 5.18)



Figure 5.17: New assembled mould for cracking tests



Figure 5.18: 40mm and 50mm high longitudinal side walls with welded angle sections

An additional removable longitudinal wall was manufactured with a height of 10mm to accommodate the thinnest asphalt layer in order to hold the in-situ compacted unbound granular layer in position during the testing.. Apart from the angle sections welded at various parts of the mould to provide the support, a set

of 4 angle sections of 40 x 40 mm were manufactured in the lab with holes to allow bolted connections with the welded longitudinal side wall's angle sections.

Figure 5.19 shows the 10mm high removable wall and four angle sections as parts of the mould. During compaction, the removable walls were bolted to the welded longitudinal walls whereas after the specimen was manufactured, these were removed. The 4 angle sections were bolted to four corners of the welded longitudinal walls to keep the in-situ compacted wearing course in place under load.



*Figure 5.19: Mould parts a) 10mm high longitudinal side walls and b) 40*40 angle sections for lateral support*

Two more steel plates of 56 x 47mm were manufactured in the workshop. These steel plates were manufactured to provide support to the specimen during testing. The plates were made long enough to have 7mm overlapping on top of the specimen to avoid the uplift during wheel load application on the opposite end. The use of top steel plate and angle sections is depicted in the Figure 5.20. It is to be noted that all bolts were fastened tightly to secure the specimen intact during compaction and testing.



Figure 5.20: Explaining the function of top steel plate and angle sections (unbolted)

5.3.3 Specimen Preparation

The specimens were prepared as for rutting test specimen in the laboratory. The difference between rutting and cracking specimen was the mould dimensions. The 305*305*130mm moulds for the rutting specimen were replaced by the 320*60*130mm for cracking specimens in which the width was almost equal to the wheel width in the wheel tracking machine. The width of the specimen was reduced in order to hasten the crack initiation in the specimen. The length of the specimen was also increased by 15mm in the new mould in order to accommodate the moving wheel up to the corners of the mould without sacrificing the results. It also benefits the entire testing process to be secure from any safety hazards due to the contact of the moving wheel with the mould corner. The wooden filler, as explained previously, was also made of the mould width and used for filling the space under all the structural layers. Similarly, a subgrade of 12mm thick rubber sheet was also cut to the mould width. The cement treated base layers were prepared in the same way as for rutting specimens and cut into beams corresponding to the new mould assembled for cracking tests. Another significant difference was that a crack was developed in the cement treated base intentionally to monitor the crack propagation from lower layer to the bottom of the wearing course. The crack was always developed in the middle of the cemented layer whereas upon opening the mould and inspecting the under layers after testing, it was observed that the cement treated base had almost always undergone three cracks at ¼, ½ and ¾ of the specimen length. The cracks at ¼ and ¾ were developed due to the compaction force employed for in-situ compaction of unbound granular and wearing course. Figure 5.21 shows prepared and marked cemented slabs for cutting into beams in its first part while the second part shows a prepared specimen up to cement treated base having a crack in the middle. Two more cracks are also visible at approximately ¼ and ¾ length as explained earlier.

The remaining procedure for preparing the sample was exactly as for rutting specimens explained earlier. After preparing the specimen and letting the

temperature drop to room temperature, the cracking specimens were also painted in order to be able to observe and monitor the cracks effectively. Like rutting specimens, all the specimens were conditioned at the test temperature up to 24 hours. A specimen with bitumen emulsion on top of the unbound granular layer before constructing the wearing course and few fully prepared and painted specimens are shown in Figure 5.22.



Figure 5.21: Cement treated slab for cracking test a) marked for cutting into beams and b) cracked in a prepared specimen



Figure 5.22: Wheel tracking specimen for cracking test a) bitumen emulsion on top of UGM and fully prepared multiple specimen

5.3.4 The Wheel Tracking Machine

The same wheel tracking machine has been used for cracking testing as was used for rutting testing. The testing equipment was only updated for cracking tests by placing a GoPro camera for capturing and saving pictures of the asphalt face at certain intervals. For this study, the interval was set

at 30sec i.e. a picture was taken and saved every 30 sec which helped monitor the crack initiation up to 30 sec accuracy. The space created in the base plate of the machine by reducing the mould size was used to adjust a platform for placing a camera. The camera installed provided two main benefits, one being the monitoring of the cracks and the other being calculation of the total number of cycles to initiate the crack by multiplying the revolutions/cycles per 30 sec in a wheel tracking machine by the total number of pictures taken before crack initiation. Figure 5.23 shows the wheel tracking equipment showing all parts including the base, prepared specimen, hanging loads and GoPro camera.



Figure 5.23: Wheel tracking setup to study the crack propagation in an inverted pavement

Different views of the wheel tracking equipment setup in a zoomed window for better understanding are also shown in Figure 5.24.

The cracking tests were not carried out to a certain number of load applications, rather to a visual inspection of crack propagation up to the top of the asphalt layer. The number of cycles to initiate a crack at the bottom

of asphaltic layer and till the end of test, where visual inspection suggested significant damage in asphaltic layer, were reported during the test. The test findings along with the images of cracked asphaltic layer side and top views for different specimens are reported. A cracked specimen is shown in Figure 5.25.



Figure 5.24: Side and end views of the wheel tracking equipment



Figure 5.25: Wheel tracking specimen after testing

Figure 5.25 represents the top view of the tested specimen after removing it from the wheel tracking machine. The side view is presented in Figure 5.26 and 5.27 which shows the GoPro captured picture during the test. Figure 5.26 represents the progression of cracks in one specimen during the wheel tracker test at equal intervals whereas various specimens are shown in Figure 5.27 as can be seen from the different visible asphalt thicknesses.



Figure 5.26: Progression of a crack in wheel tracker specimen

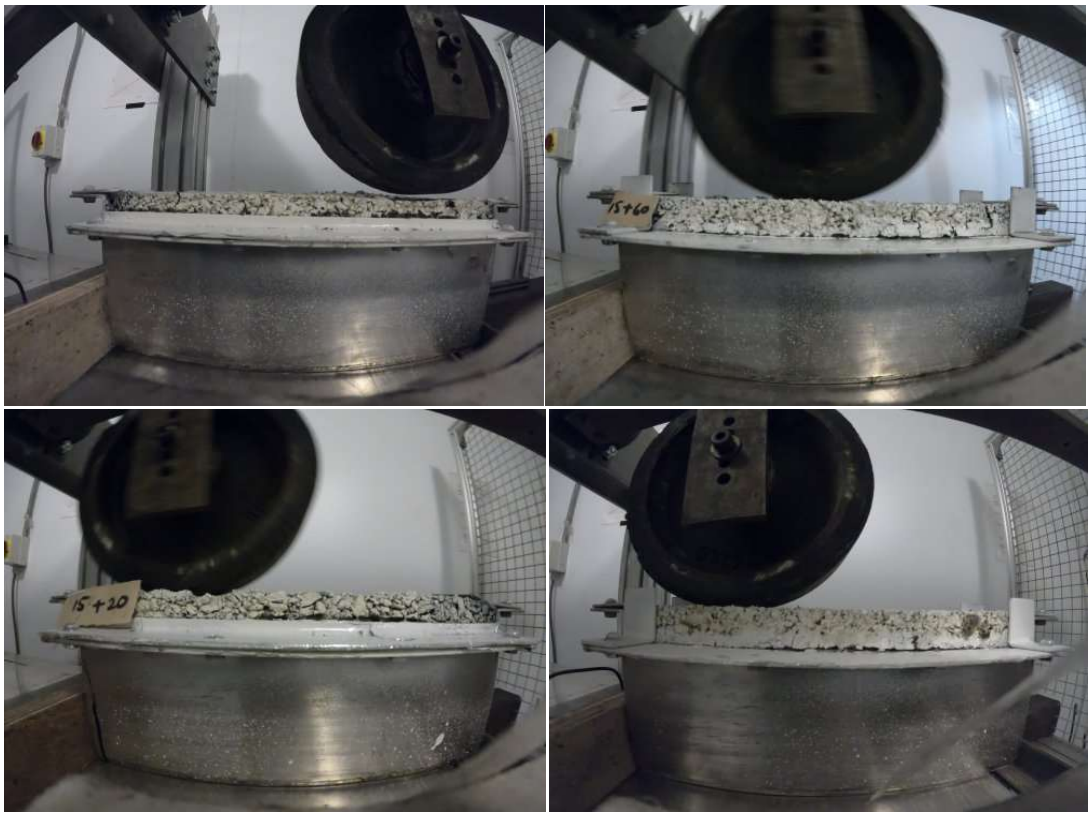


Figure 5.27: Random specimens during test

5.3.5 Cracking test results and discussion

The layer arrangement in an inverted pavement theoretically represents an opportunity for minimizing the reflective crack propagation from a brittle cement treated base layer to the asphaltic wearing course due to the presence of an unbound granular layer in between the two. For the same purpose, different combinations of layer thicknesses have been constructed in various specimens to study the response of the unbound granular layer in initiation and propagation of the reflective cracks. As stated earlier, the testing was performed at 10^0C to expedite the cracking process. All the tested specimens were conditioned at the test temperature for up to 24 hours. The test conditions comprised of a wheel load of 1.5kN, contact radius of 23.6mm and contact pressure of 850kPa. The results obtained from the cracking tests performed in the laboratory are presented in Figure 5.28 -Figure 5.30.

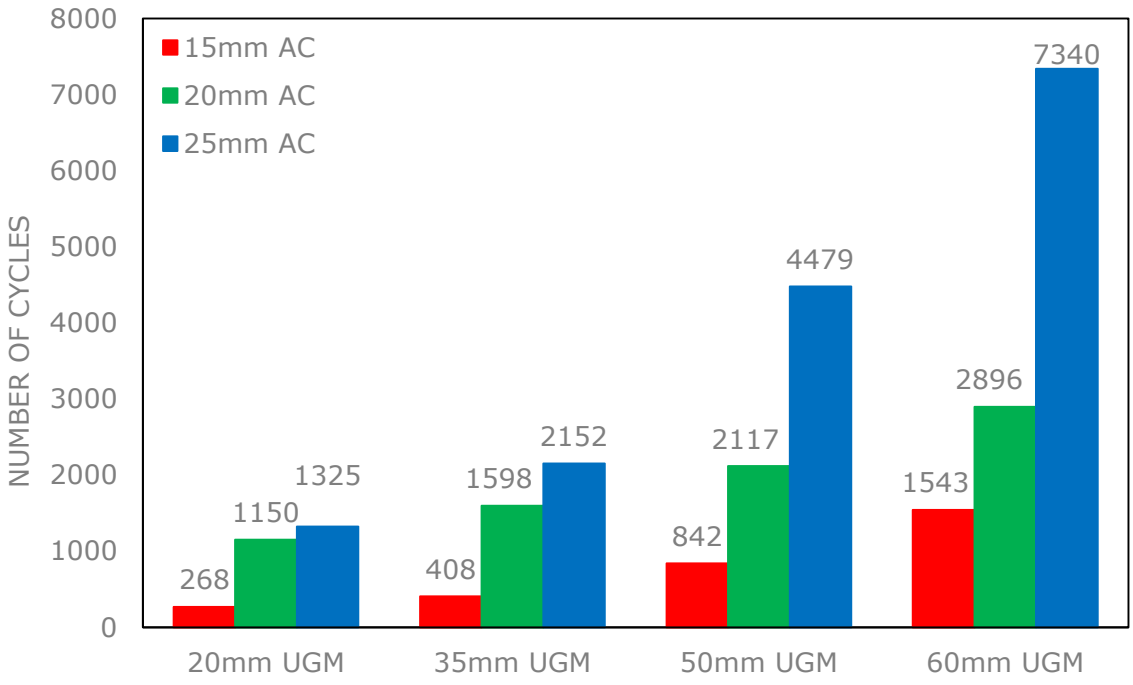


Figure 5.28: Cycle to initiate cracking in wheel tracking specimen

Figure 5.28 represents the number of cycles to initiate a reflective crack in an inverted pavement specimen having different thickness combinations of AC wearing course and UGM base. Different colours represent the different AC thicknesses and set of columns represent the UGM thicknesses. The results obtained clearly show better pavement performance, as expected,

under loading with increased thickness combinations. With the increase in the unbound layer thickness for any asphaltic thickness, the pavement resistance to cracking increased. Taking the first thickness combination, 15mm AC and 20mm UGM, as a baseline, the number of cycles required to initiate the cracks in the pavement increased by 52, 214 and 475% in specimens with 35, 50 and 60mm UGM respectively having same AC thickness under the same test conditions. So, it can be concluded from the results, that for 15mm thick asphaltic wearing course, an increase in unbound granular layer from 20 to 60mm has increased the pavement response by 475% with reference to the baseline. Similar results can be seen for asphaltic layer of 25mm where an increase in pavement life up to 454% was observed with an increase of unbound thickness from 20 to 60mm. The percentage increase in pavement life with an AC thickness of 20mm with rising UGM thicknesses was not as dominant as for other wearing course thicknesses, although still significant. The increase in pavement life for 20mm thick wearing course by increasing the UGM thickness from 20 to 60mm was up to 70% with respect to the baseline. The minimum increase in pavement life observed was 15.3% by increasing the UGM thickness from 35 to 50mm at a constant AC thickness of 20mm. So, it can be concluded that an increase in UGM thickness at any given AC thickness improves the pavement response significantly, although it is not parallel for all AC thicknesses.

The analysis of the results by varying the asphalt thickness for a constant unbound thickness exposed interesting pavement behaviour under load as shown in Figure 5.29. For lower unbound thicknesses of 20 and 35mm, the pavement response improved significantly by increasing the asphalt thickness from 15 to 20mm whereas a further increment of 5mm in asphalt thickness keeping all other parameters same didn’t increase the response as significantly. However, the reverse is observed in the case of thick unbound layers i.e.50 and 60mm. The increase in asphalt layer thickness from 15 to 20mm for 50 and 60mm thick UGM layer increases the pavement response but this is not as significant as in the case of a further increase of 5mm in AC layer thickness. This may be explained as quick propagation of a reflective crack in the case of a thin UGM layer. The propagation of cracks

in thin specimen, 15mm AC and 20mm UGM, is also aided by the thin asphalt having higher tensile strains at the bottom causing the crack to initiate swiftly. An increase in asphalt thickness, 20mm AC and 20mm UGM, causes less tensile strains at the bottom for the same thickness unbound layer resulting in a delayed crack initiation. Although the number of load cycles to initiate cracks in specimen having 25mm AC and 20mm UGM increased as compared to the specimen with 20mm AC, but it is not very significant. This can't be explained by just mentioning a decreased tensile strain with an increase in AC thickness. So, the hurried crack initiation in specimen, 25mm AC and 20mm UGM, as compared to 20mm AC could be due to a very thin unbound granular layer alone. A very analogous trend was observed by increasing the AC thickness by keeping the UGM thickness to 35mm. The only difference observed in the case of 35mm UGM as compared to 20mm was the percentage increase in pavement life by increasing the AC thickness from 20 to 25mm. An increase of 36% in pavement life was observed by increasing the AC thickness from 20 to 25mm for specimens having 35mm UGM as compared to only 6% improvement for 20mm UGM. So, it can be stated that the crack propagation in an inverted pavement depended on a combination of UGM and AC thickness.

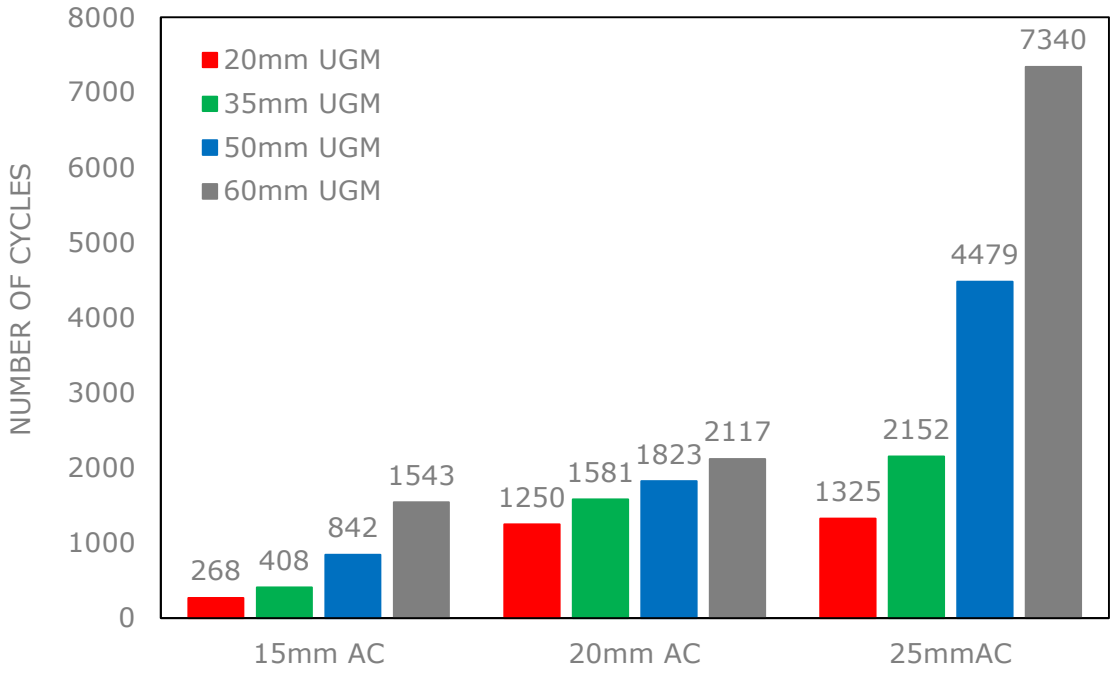


Figure 5.29: Effect of individual layers to initiate the cracks

The reverse can be observed in the case of thick unbound granular layers where crack propagation is mostly governed by the tensile strains at the bottom of the asphalt layer. As the UGM layer thickness increases, it acts as a medium to prevent the crack in the brittle cemented slab to move upwards or slow down its propagation. This results in the cracks initiating due to the tensile strains at the bottom of the asphalt layer, hence the pavement response improves significantly by increasing the asphalt layer thickness under the same test conditions. In case of specimens with thick UGMs, an increase in AC thickness improved the pavement performance significantly for an increment from 20 to 25mm as compared to the one from 15 to 20mm. It can be concluded that, although the pavement life increased by increasing the individual layer thicknesses, but the effect of this increase depended on the respective layer thicknesses. For example, an increase in AC thickness from 15 to 20mm improved the pavement life significantly for thin UGMs (20 and 35mm) as compared to its reverse effect for thicker UGMs (50 and 60mm). It can be commented that both the layers, AC and UGM, increase the pavement resistance with a combined effect from each. An increase in AC thickness generally results in reduced bending which causes increased pavement life by reducing the cracking tendency. Similarly, an increase in UGM thickness will reduce the concentrated bending above the crack in CTB resulting in improved pavement performance.

Figure 5.30 shows the number of cycles at the end of each test. Tests were stopped on visual inspection of the cracked specimen; an example is shown in Figure 5.25. The criterion to stop the test was similar for all the specimens, where at least one crack was developed throughout the width of the specimen. It may be termed as failure for the specimens tested.

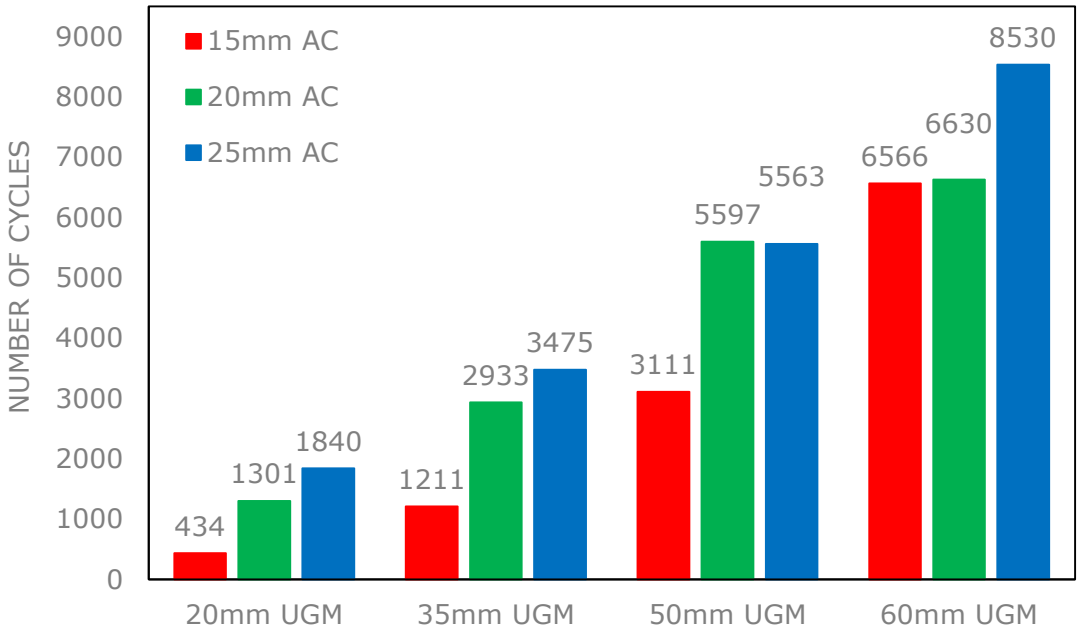


Figure 5.30: Cycles to end the test on visual inspection

5.4 Conclusions

This chapter documented all the results obtained from the simulative testing performed on wheel tracking equipment in the laboratory. The following are the findings from the study;

- The pavement resistance to both permanent deformation and reflective cracking increased by increasing the pavement thickness.
- An increase in individual layer thickness increased the pavement resistance. The pavement response improved with respect to both the criteria under study i.e. permanent deformation and reflective cracking. An increase in the layer thickness of any of the under-study materials i.e. AC and UGM resulted in an increased pavement resistance.
- For any given thickness of one layer, the increase in other layer thickness decreased the permanent deformation, although the increase in asphalt layer while keeping the unbound layer thickness constant has the most significant effect on pavement performance. Based on the trends observed by increasing the wearing course thicknesses in increments, it can be stated that the best performing thickness of asphalt layer can be reported under a given load.

- Similarly, the number of cycles to initiate the cracks in the pavement depended on the layer thicknesses and combinations. An increase in unbound thickness while keeping the asphalt thickness constant increased the pavement response significantly for cracking. It increased the pavement resistance to cracking by as much as 475%.
- The response of the pavement to an increase in asphalt layer while keeping the unbound layer thickness constant depended on the unbound layer thickness. For thin unbound layers, asphalt thickness increase enhanced the pavement response up to 20mm whereas further increase didn't affect it much. This was due to the combined effect of unbound thickness and asphalt bottom tensile strains on crack propagation. For thick unbound layers, an increase in asphalt from 20 to 25mm increased the pavement resistance to cracking significantly.

6 Predicting Permanent Deformation in Inverted Pavement

6.1 Introduction

Pavement engineers have been putting their utmost effort for decades to improve pavement durability and performance. This has involved various approaches including materials improvement by adding admixtures, optimizing material usage in a pavement, developing new testing equipment and upgraded methodologies, emerging new pavement types, new mechanistic design practises and improved scientific analysis and prediction techniques. Out of all these tactics, improved scientific analysis and prediction techniques enable a pavement engineer to study a pavement's performance using software under the different environmental and loading conditions it must endure during its lifetime. The analysis thus results in a reliable estimate of the pavement performance life. It also helps in amending the materials or testing methodology before the actual construction of the pavement based on the analysis results. Different prediction and analysis techniques have been developed by pavement researchers over the years, some of which have been described in the "Literature Review" chapter. It is obvious from the literature that these prediction procedures have involved several different loading, traffic and environmental conditions applied to different pavement layers. However, not much of research has been carried out to predict the permanent deformation over a full-depth pavement. Therefore, this chapter documents a scientific technique developed for predicting the permanent deformation in a full-depth inverted pavement. Different methods established previously have been combined and discussed in detail in this chapter to develop a new method to predict the permanent deformation in a pavement under load.

6.2 Linear Viscous Approach

Linear viscous approach is a type of analysis which employs a material's viscosity as elastic modulus in multi-layer linear elastic analysis to predict

the permanent deformation in a pavement. The permanent deformation in asphalt mixtures is caused by the movement between adjacent aggregate particles, coated with a thin bitumen layer and is governed by the rheological properties of this thin binder film (Hills et al. 1974). So, the principle of linear viscous analysis is analogous to linear elastic, except that the elastic parameter (Young's modulus) is replaced by the equivalent viscous parameter (viscosity) (Thrower 1977). Such an approach was reported by Nunn (1986) for predicting the permanent deformation in asphalt mixtures in which a uniaxial creep test was performed at 30°C and a constant stress of 100 kPa. He used only the viscous part of the materials behaviour in predicting the permanent deformation in asphalt mixtures by following these steps as mentioned below;

1. The creep test was performed to develop a plot of mixture stiffness $S_m(t)$ against loading time.
2. Similarly, a plot of binder (bitumen) stiffness $S_b(t)$ against loading time was generated by its properties such as softening point and penetration values.
3. A general plot was, then, constructed representing $S_m(t)$ versus $S_b(t)$.
4. An equivalent loading time for a given number of commercial vehicle passes was then calculated at an effective temperature and used to derive the $S_m(t)$, and then the axial viscosity.
5. The axial viscosity was then utilised in a multi-layer linear viscous analysis to calculate the permanent deformation accumulated in each increment of the number of commercial vehicle passes (new loading time).

The equation to determine the axial viscosity of the mixture (λ) was as follows:

$$\lambda_m(t) = \frac{\sigma}{\dot{\varepsilon}} = \frac{1}{\frac{d}{dt}\left(\frac{1}{S_m(t)}\right)}$$

The axial viscosity was used with the deformational Poisson's ratio in a multi-layer linear viscous analysis to determine the average rate of permanent strain and the accumulated permanent deformation in the whole

pavement layer. The predicted results showed an accuracy of ±30% compared to the measured deformation.

6.3 Methodology

The prediction of permanent deformation in an inverted pavement involves various steps. As the pavement consists of various layers and this project involves the effect of varying the asphalt and unbound thickness on the overall performance, so the prediction also involves these two layers. Two different methods have been employed for the two layers to input the parameters required for the prediction of full pavement behaviour.

The permanent deformation in an inverted pavement is predicted by following a pseudo-viscous approach in the current study as explained below. The methodology involves assigning viscosity values to all the individual layers within the pavement and finding the deformation rate under load. The procedure is carried out in a loop until the desired deformation is reached. For assigning the pseudo-viscosity to the layers, different methodologies have been developed. For assigning viscosities to the HMA layer, laboratory tests for deformation were carried out in the laboratory under same controlled stress conditions, whereas an already developed stress-strain model corresponding to the multistage stress conditions in the PUMA was adopted to find pseudo-viscosities for the Unbound Granular Base layer. Both approaches have been applied to find the appropriate input parameters i.e. viscosity of each layer and analysed under the given load in a multi-layer linear viscous system. Multi-layer analysis software like KENLAYER was used to find the strain rates and thus permanent deformation rates in the pavement. The predicted permanent deformation rate has, then, been compared with laboratory measured values and very reasonable comparison has been observed based on a few assumptions. The prediction procedure is described in detail in the following paragraphs both individually as well as combined.

6.3.1 Pseudo-Viscosity in Asphalt Mixtures

Various prediction procedures have been developed historically to predict the permanent deformation in HMA wearing course. The details have been documented in the literature review chapter. Out of the various procedures

mentioned, the linear viscous procedure has been used for predicting deformation in HMA wearing courses. The linear viscous approach involves the following steps.

- Laboratory wheel tracking tests were performed as mentioned in Chapter 5 to find the permanent deformation in different inverted pavements. The test data comprised laboratory determined rut depth curves for all the specimens.
- Another slab with the same density was prepared in the laboratory and cores were taken out of it as shown in Figure 6.1. The cores were then trimmed to the thicknesses used in the wheel tracking test. All the cores were then tested in Repeated Load Axial Test (RLAT) under different stress levels including the values corresponding to those applied during the laboratory wheel tracking test.

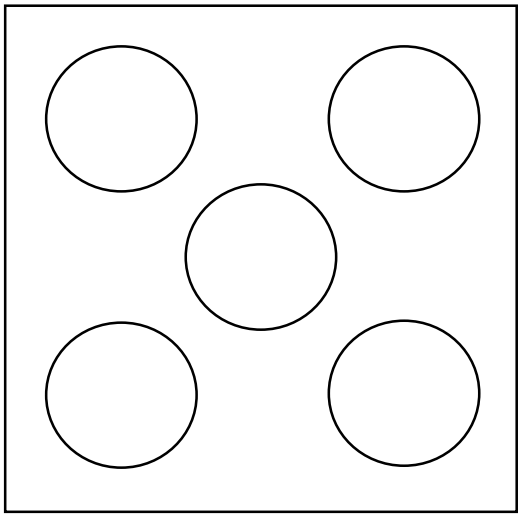


Figure 6.1: Cores taken from slab

- The strain rate for each loading cycle applied in the RLAT is calculated by the following equation;

$$\varepsilon' = \frac{\varepsilon 2 - \varepsilon 1}{t2 - t1} \qquad (1)$$

  where t2 and t1 are the time (in seconds = number of cycles) corresponding to the strains
- In the next step, the pseudo-viscosity ('pseudo' because it relates to repeated rather than steady load) of the mixture is determined as a function of strain and is calculated by dividing the axial stress in MPa by the strain rate already computed. (Nunn, 1986)

$$\eta = \frac{\sigma}{\varepsilon'} \qquad (2)$$

- The mixture pseudo-viscosity is then plotted against the strain. The plot is then used to establish the material's viscous properties for permanent deformation prediction. A typical plot representing a mixture showing all three stages of creep (primary, secondary, and tertiary) is shown in Figure 6.2.

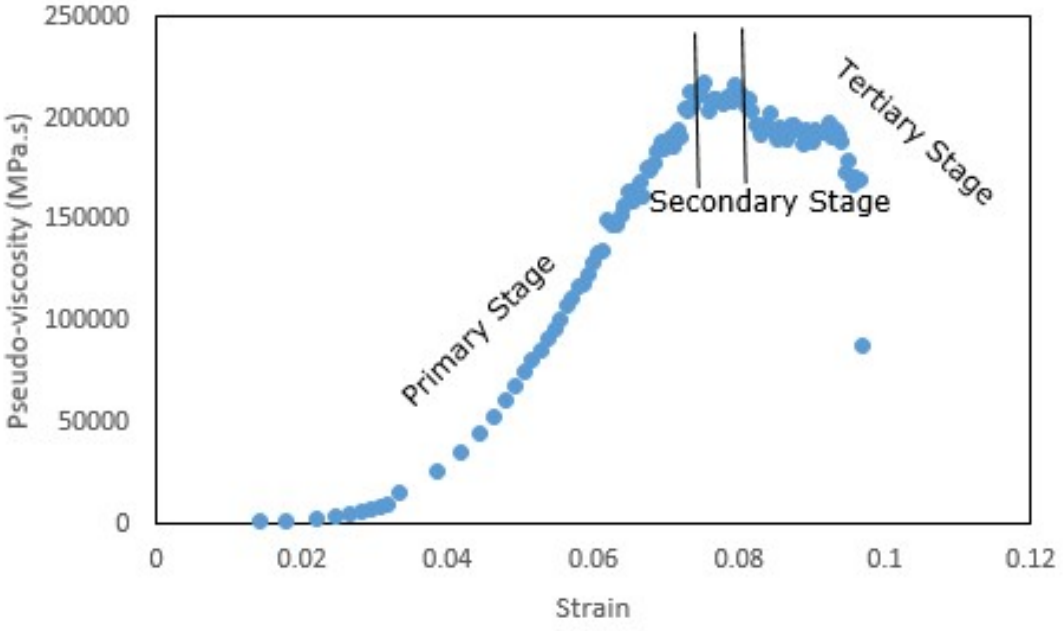


Figure 6.2: Viscosity vs Strain (Stages)

- After that, an initial material viscosity is determined from the viscosity-strain curve by extrapolating to zero strain. This initial value is then used in the 1st deformation analysis increment.
- The results obtained for all the thicknesses are presented below in Figures 6.3 - 6.5. The plot equations were used to extrapolate to zero strain as mentioned in the previous point.

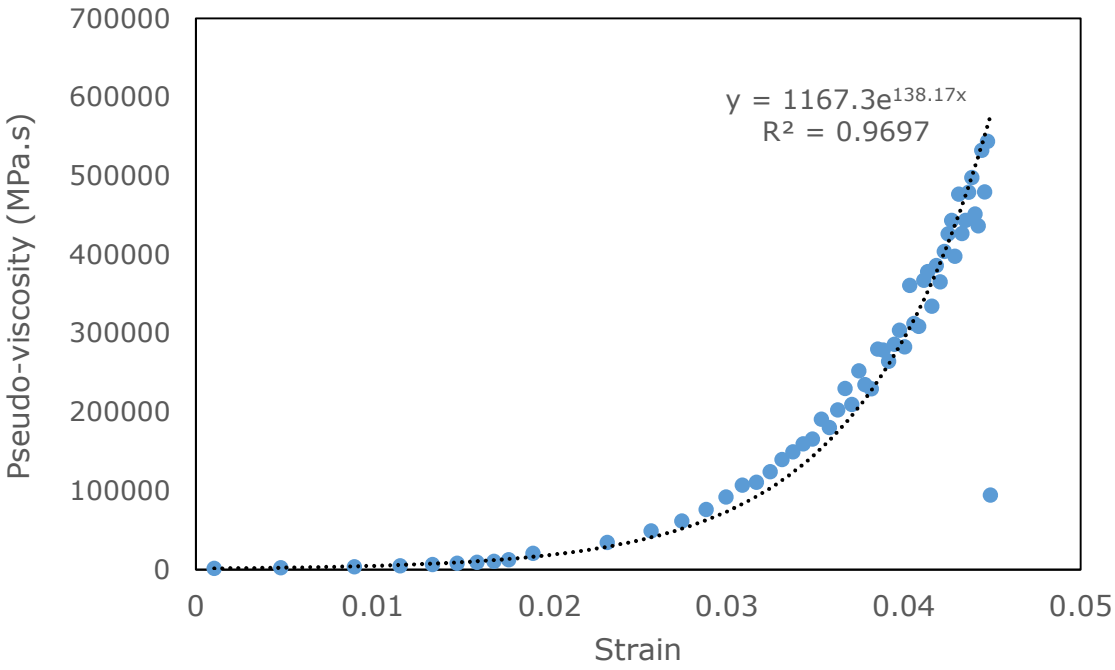


Figure 6.3: RLAT plot for 15mm AC

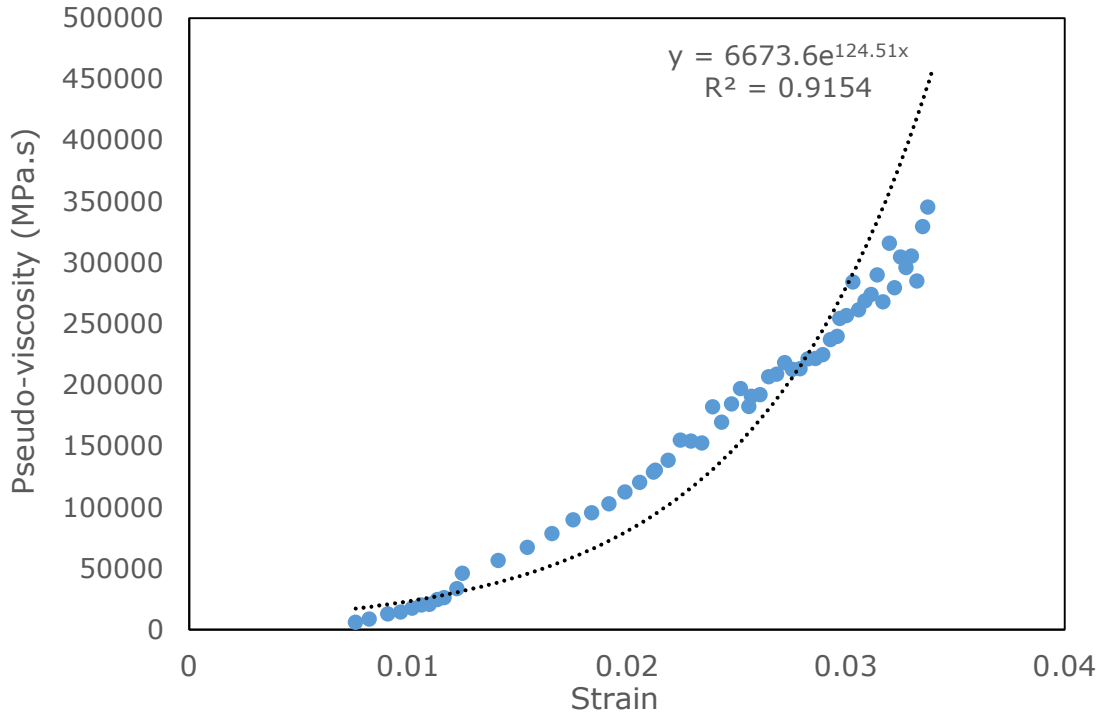


Figure 6.4: RLAT plot for 20mm AC

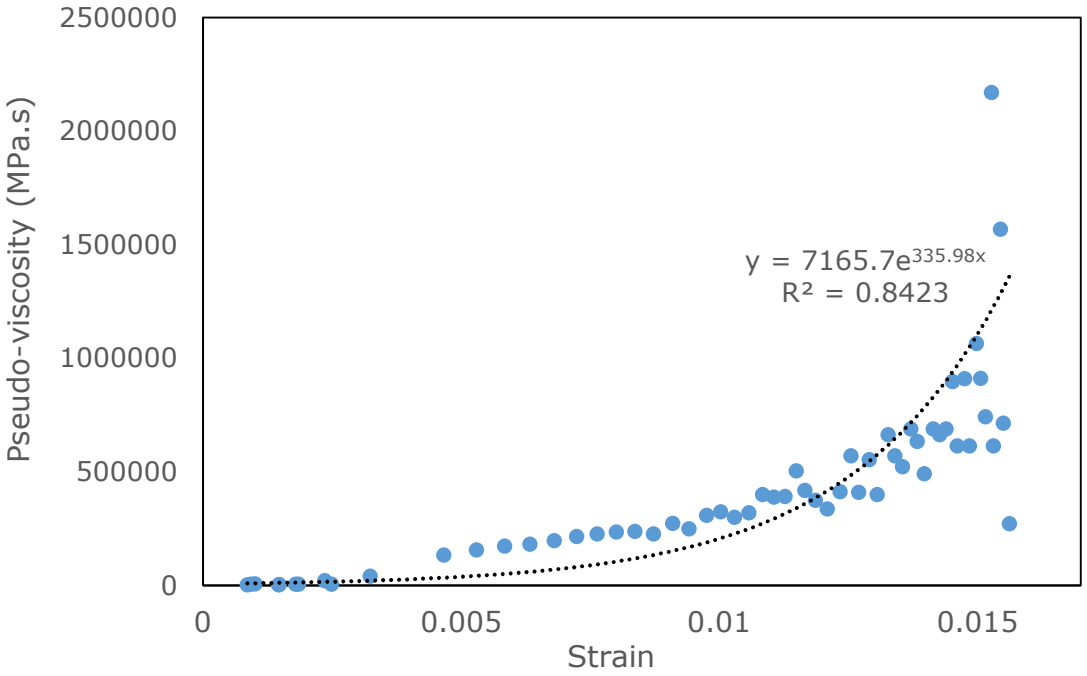


Figure 6.5: RLAT plot for 25mm AC

6.3.2 Pseudo-Viscosity in Unbound Granular Base Layer

A stress-strain model developed by Rahman and Erlingsson to predict permanent strain based on stress ratio and number of load applications was used as shown by the following equation;

$$\hat{\varepsilon}_p\,(N) = a\,N^{bS_f}\,S_f$$

where $\hat{\varepsilon}_p(N)$ is the accumulated permanent strain after N load cycles and a and b are regression parameters related to the material. The term S_f describes the effect of stress condition on the development of deformation which is expressed as

$$S_f = \frac{(q/p_a)}{(p/p_a)^{\alpha}}$$

where q is the deviator stress, p is the hydrostatic stress (one-third of the sum of the principal stresses) and α is a parameter determined using regression analysis. The term p_a =100 kPa (reference stress taken equal to the atmospheric pressure) was used to make the expression non-dimensional.

The Rahman-Erlingsson model was differentiated to get the strain rate and subsequently pseudo-viscosity by dividing the strain rate by the stress in MPa.

$$\frac{d\hat{\varepsilon}_p}{dN} = ab\ {S_f}^2 \left[\left(\frac{\hat{\varepsilon}_p}{a\ S_f}\right)^{\frac{1}{bS_f}}\right]^{(bS_f - 1)}$$

Therefore, the pseudo-viscosity can be calculated by dividing the strain rate into the axial stress as shown in the equation below;

$$\eta = \frac{q}{d\hat{\varepsilon}_p/dN}$$

where S_f was calculated by putting the p and q values from the KENLAYER data output file. The strains were also calculated against 0.1mm increments in each layer individually. The regression parameters "a and b" were calculated for all the materials containing different fines contents (4.1, 6.7, 13.5 and 7.4%) used in this research as stated in Chapter 3. The same parameters were used throughout the prediction exercise for all the specimens since the material containing 7.4% fines content was used in wheel tracking tests to find the laboratory measured deformation. One of the assumptions during the prediction process have been the value of parameter b which was not taken from the PUMA data as the very low values of parameter 'b' decreased the strain rate to hundreds and hence increased pseudo-viscosity. The increased pseudo-viscosity resulted in the improved stiffness of the material which resulted in very low permanent deformation. Another assumption was the value of S_f during the prediction process. The same value of S_f was used in any increment as the previous value if the current value decreased the material's pseudo-viscosity. It was assumed to increase the pseudo-viscosity values in every increment in order to be able to predict the permanent deformation without reaching the failure during the load applications similar to the laboratory measured deformations.

6.4 Permanent Deformation Prediction in Inverted Pavement

Permanent deformation in an inverted pavement was predicted by using pavement analysis software. For the purpose of this study, KENLAYER was used to determine the strains and hence deformations in the pavements by assigning the calculated pseudo-viscosity in place of stiffness modulus and applying wheel tracking load. After calculating the pseudo-viscosities as stated in the previous sections, the pavement was modelled in the software and full-depth pavement analysis was performed resulting in strain rates in all the layers. The step by step procedure is described below;

- The individual layer pseudo-viscosities were calculated by the already mentioned procedures for asphalt and unbound granular materials.
- The inverted pavements were modelled in KENLAYER with varying thicknesses of the layers. All the 12 different thickness combinations as mentioned in previous chapters were modelled. The following are the data to be input into the software for slab modelling;
  - Vertical Stress: 850 kPa corresponding to the stress in the wheel tracking test
  - Radius (m): 0.0236
- The number of layers (usually two for wearing course and two to three for the unbound granular layer) were assigned pseudo-viscosity values; for the first time step the same pseudo-viscosity was used for all layers in a given material. The initial pseudo-viscosity for wearing course asphalt mix was calculated by extrapolation to zero strain as stated previously, whereas a very small permanent strain value was assumed in the equation to get the initial viscosity of the unbound layer. It must be noted that as the same material and gradation was used for all the specimens, so the same initial viscosity was assigned to the unbound layer in all the specimens. Similarly, same initial pseudo-viscosity was assigned to the HMA layer for any given thickness i.e. 15, 20 and 25mm as calculated from Figure 6.3 -Figure 6.5.
- The cement-treated layer was not considered in the analysis due to its rigidity. It meant that the asphalt mix and unbound layer

contributed to the permanent deformation, hence only those two layers were involved in the analysis.

- A very stiff subgrade layer was added having effectively infinite viscosity. All the layers were assumed to be incompressible (Poisson's ratio of 0.5) to ensure that the deformation was due to shear flow, not densification, and full friction between layers was adopted.
- The analysis was performed and the strain rate (strain/second = strain/cycle) in the middle of each layer under the centre of the load was used in further calculations.
- A surface deformation increment of 0.1-0.5mm depending on the anticipated permanent deformation was applied and the layer strains and the number of cycles to cause this increment were determined.
- The new layer strains required new corresponding pseudo-viscosities from the strain viscosity curves (Figure 6.2 -Figure 6.5) established earlier in the process giving new pseudo-viscosities for each layer; these were used in KENLAYER for the following deformation increment.

  It is to be noted that the first deformation increment was always 0.1mm as the initial pseudo-viscosity in the unbound granular layer was based on the supposed deformation values. Further stages of the analysis were performed at different increment levels for the different specimens depending on the measured deformation values.
- This loop was continued until a specified deformation was reached. The methodology flow diagram is shown in Figure 6.6.

No adjustment was made to the loading time because it was similar in both cases (RLAT and wheel track). In the RLAT the stress was applied for 1 second and in the wheel tracking tests, the rate of loading was 26.5 cycles/minute and each cycle consisted of two passes.

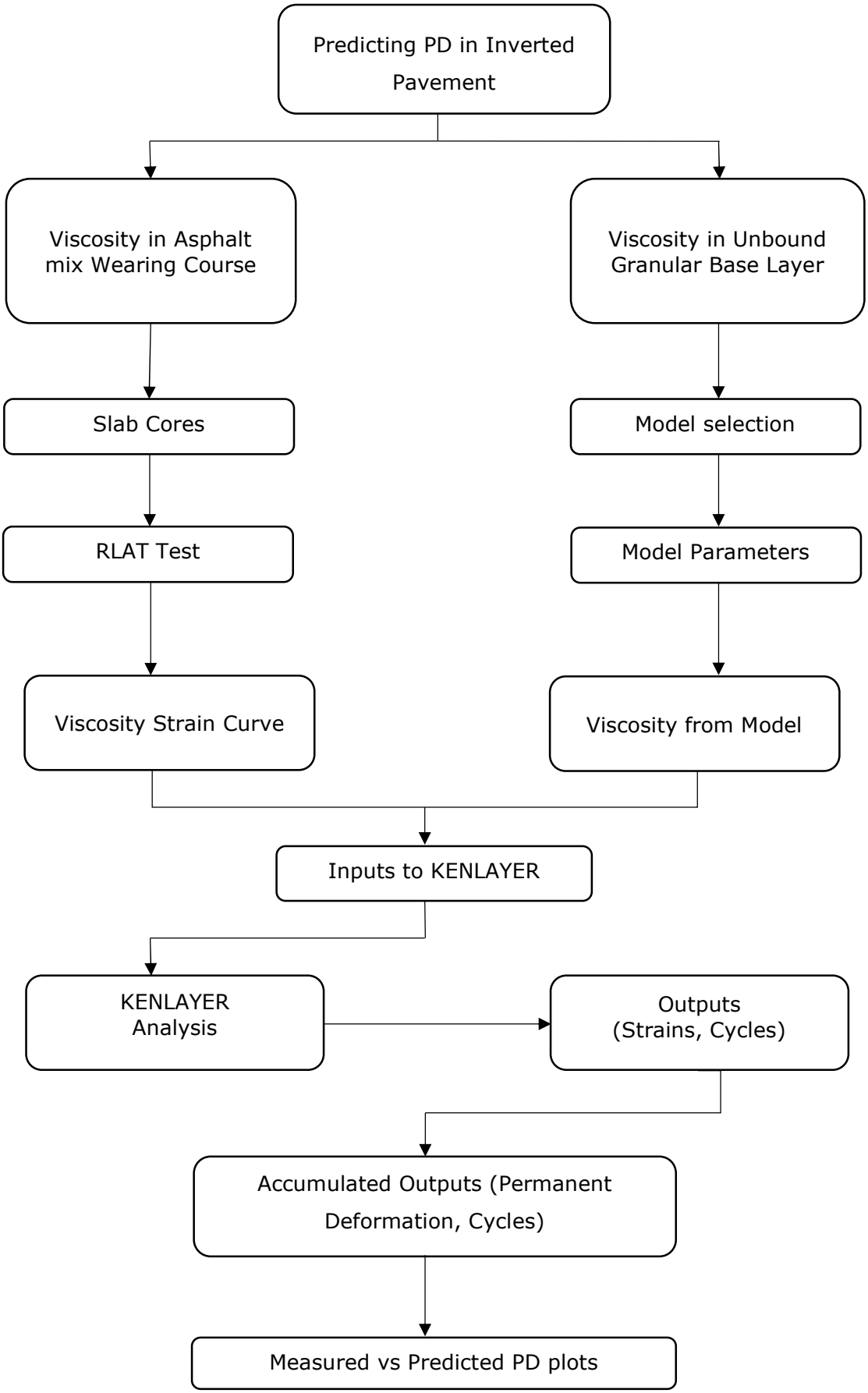


Figure 6.6: Flow chart for permanent deformation prediction

6.4.1 Assumptions

For the prediction exercise, a few assumptions have had to be made to get the optimum results. The assumptions have been mentioned in the previous sections, the following is a summary.

1. The same values for parameter "b" were used during the prediction process for all the specimens. The value of "b" was found to be 3.5.
2. It was assumed that the stress ratio does not decrease during the prediction process. This was assumed to accommodate the general trend of increasing permanent deformation for increased number of load applications. In case of reduced S_f values in any increment, the value from the previous increment was used in order to predict the permanent deformation in the current and subsequent increments.

6.4.2 Results

Permanent deformation in inverted pavements was predicted by following the procedure already mentioned. The results are presented and discussed in this section. Figure 6.7 -Figure 6.18 show the results obtained from the prediction exercise. It is very evident from the figures that the methodology developed in this study to predict the permanent deformation in inverted pavements has worked successfully.

Although the prediction approach functioned smoothly and effectively, it didn't work equally for all the different thickness combinations under study. Although it is very evident from the results that permanent deformation was either under-predicted or over-predicted, it was always within a reasonably close range. For thin pavements, the permanent deformation was over-predicted generally. It was observed only for the two thinnest pavements that the predicted deformation overlapped the measured one. The predicted values were greater than the measured ones at the start whereas they ended in under-prediction at the end of approx. 10,000 cycles. This was due to the fact that the prediction was based on the concept of increasing pseudo-viscosity in each increment which decreases the deformation, whereas the measured deformation values kept on increasing throughout the test. The thin pavement layers deformed with each load application and never settled. In the case of pavements with medium

thickness asphalt layer, 20mm, the permanent deformation was generally over-predicted with the exception being the one with the thinnest unbound layer. Similarly, in the case of pavements with the thickest asphalt layer, 25mm, the permanent deformation was under-predicted except WT-18 (25AC + 20UGM). Even for WT-18, the prediction was comparable to the measured values.

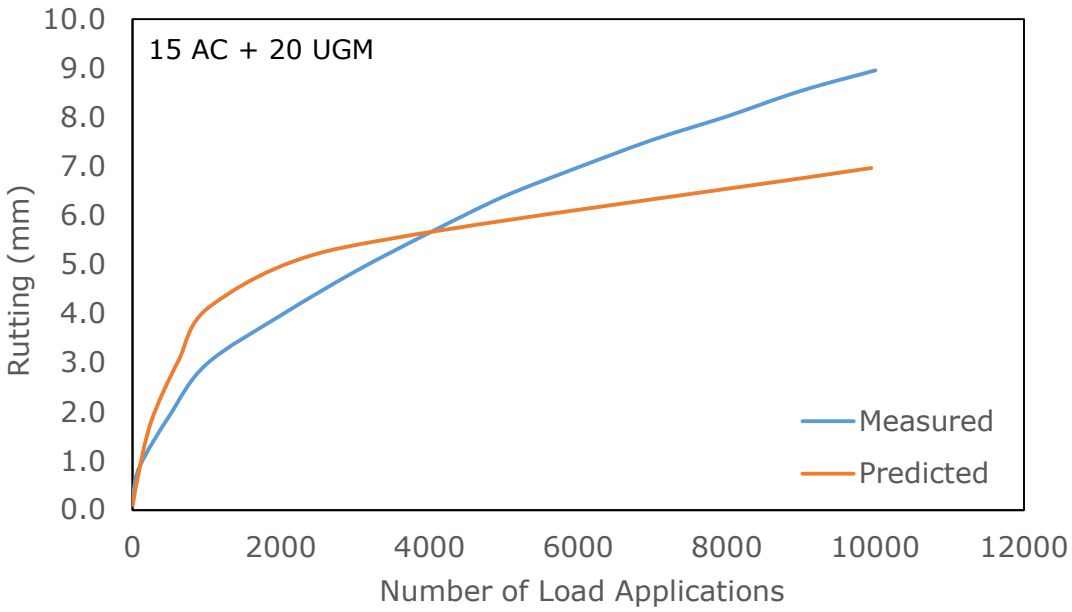


Figure 6.7: Measured vs Prediction Deformation in specimens having 15mm AC and 20mm UGM

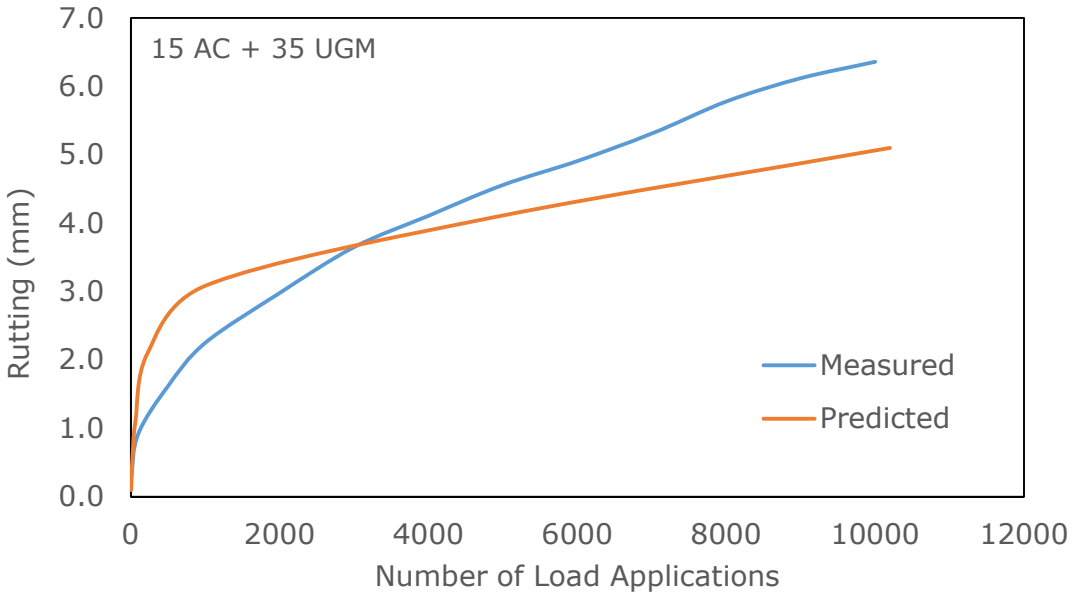


Figure 6.8: Measured vs Prediction Deformation in specimens having 15mm AC and 35mm UGM

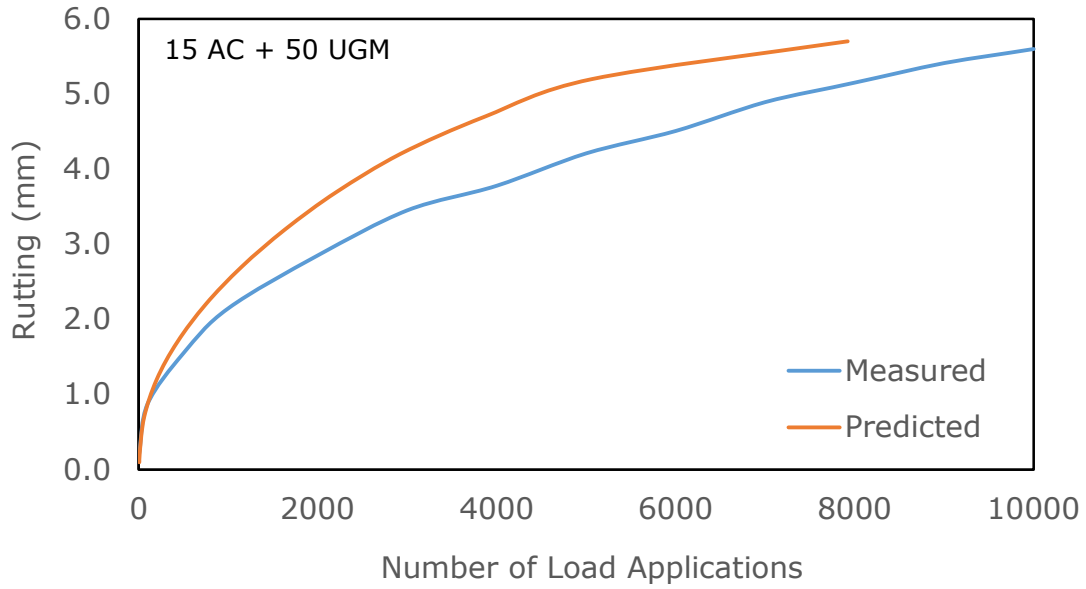


Figure 6.9: Measured vs Prediction Deformation in specimens having 15mm AC and 50mm UGM

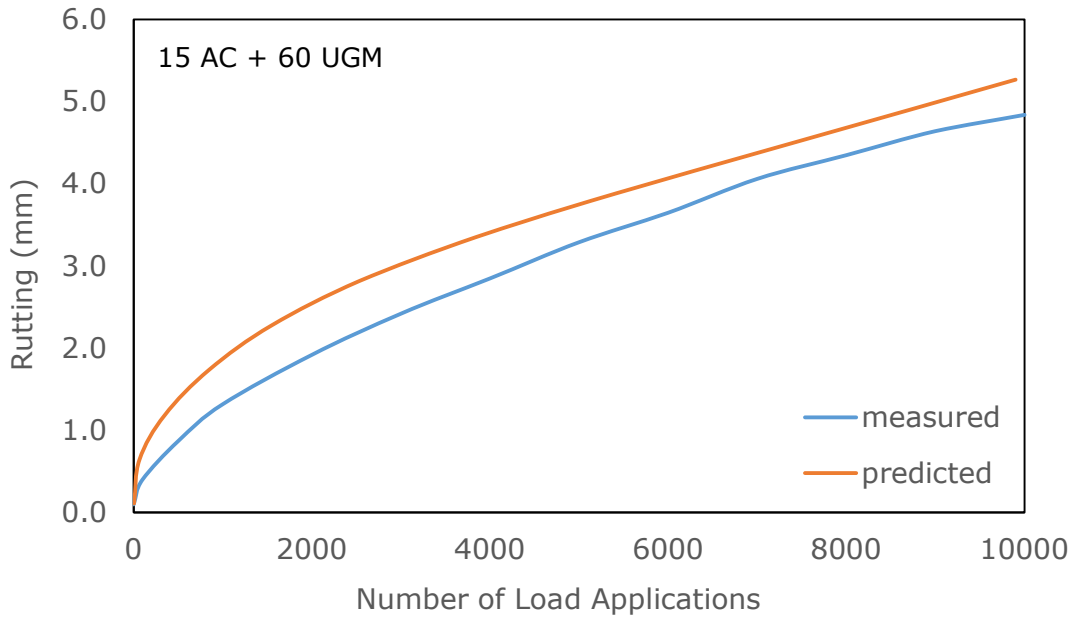


Figure 6.10: Measured vs Prediction Deformation in specimens having 15mm AC and 60mm UGM

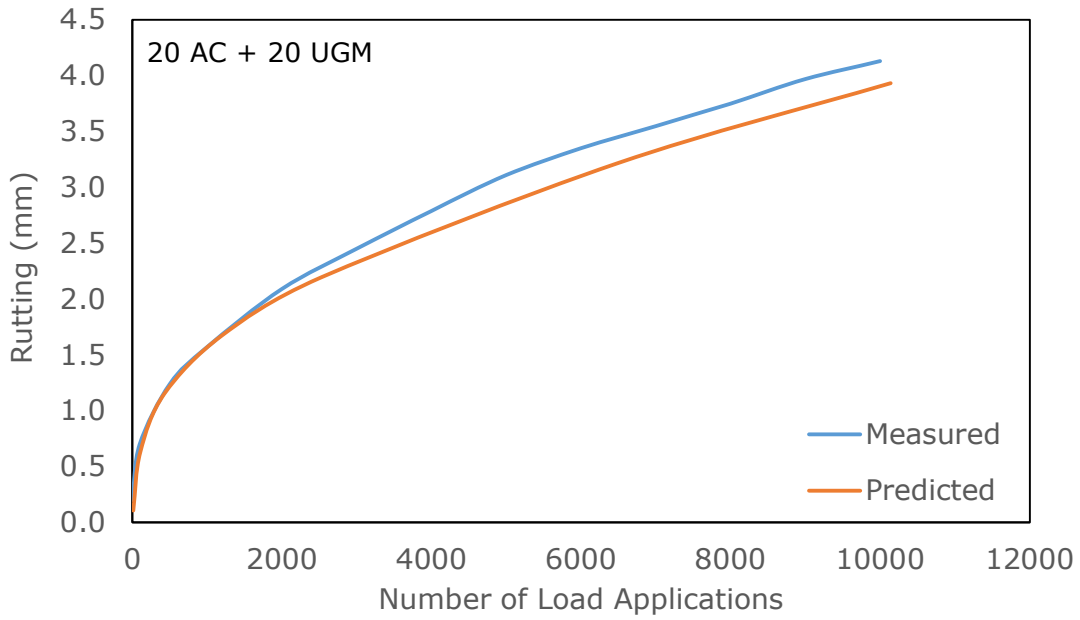


Figure 6.11: Measured vs Prediction Deformation in specimens having 20mm AC and 20mm UGM

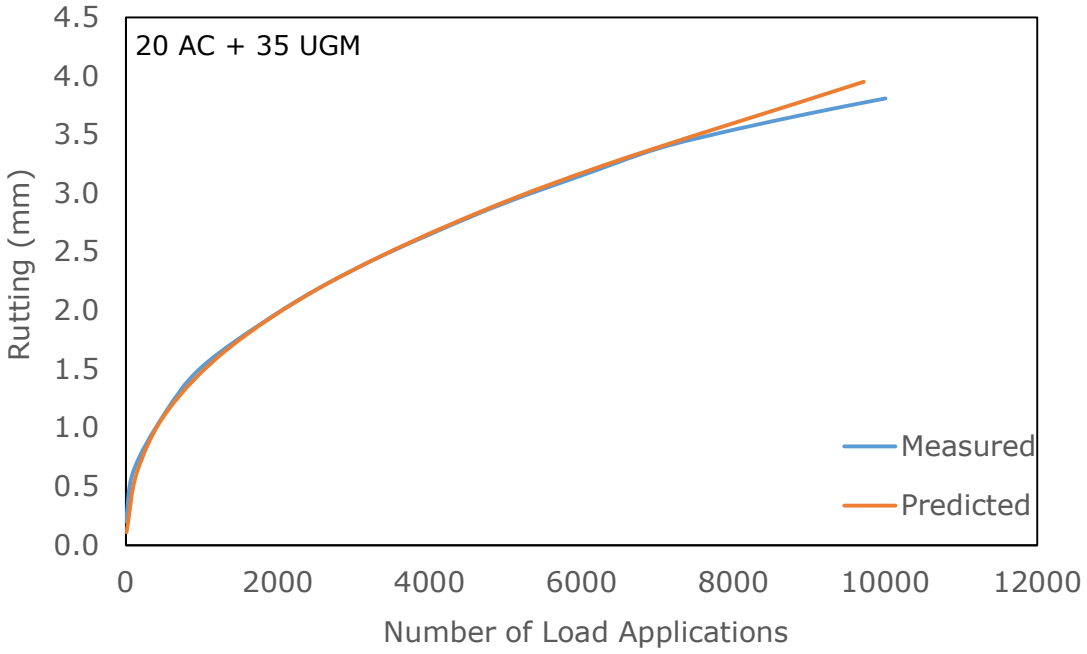


Figure 6.12: Measured vs Prediction Deformation in specimens having 20mm AC and 35mm UGM

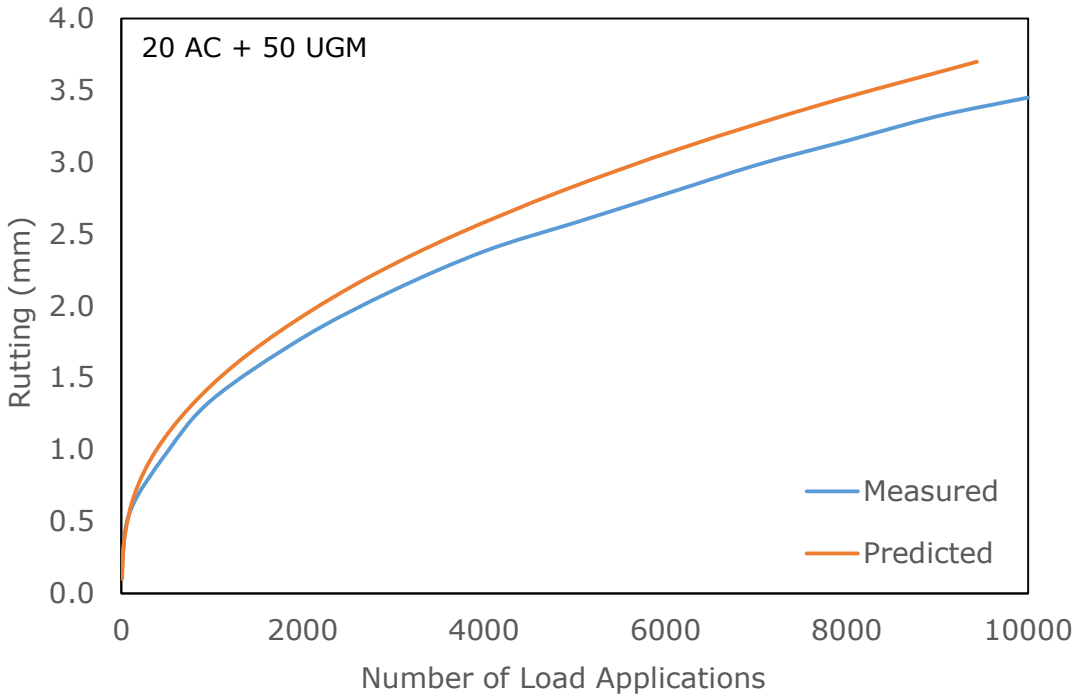


Figure 6.13: Measured vs Prediction Deformation in specimens having 20mm AC and 50mm UGM

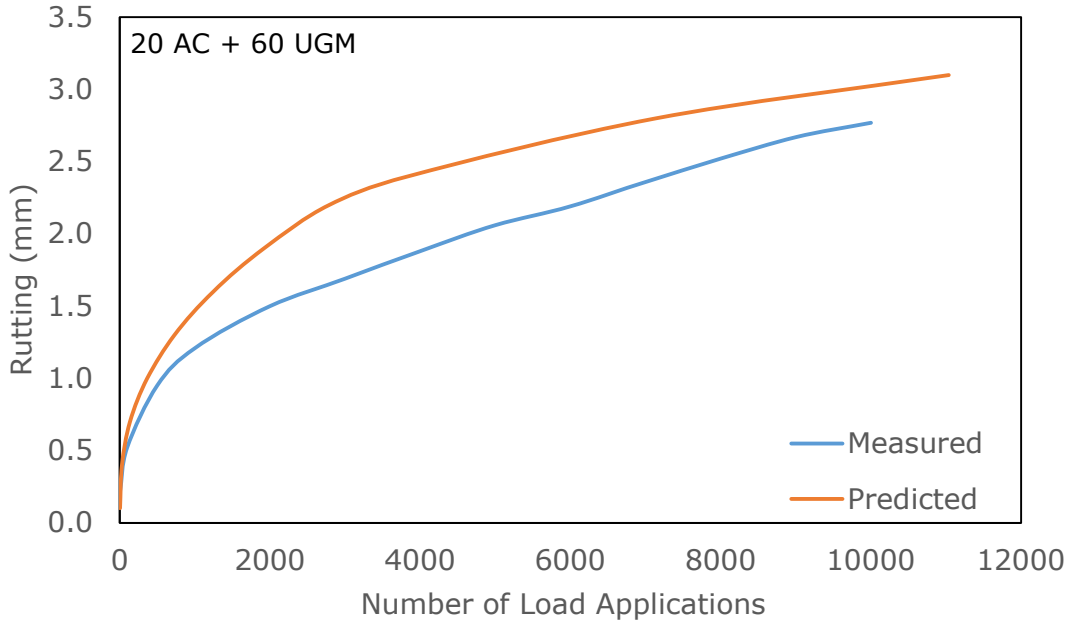


Figure 6.14: Measured vs Prediction Deformation in specimens having 20mm AC and 60mm UGM

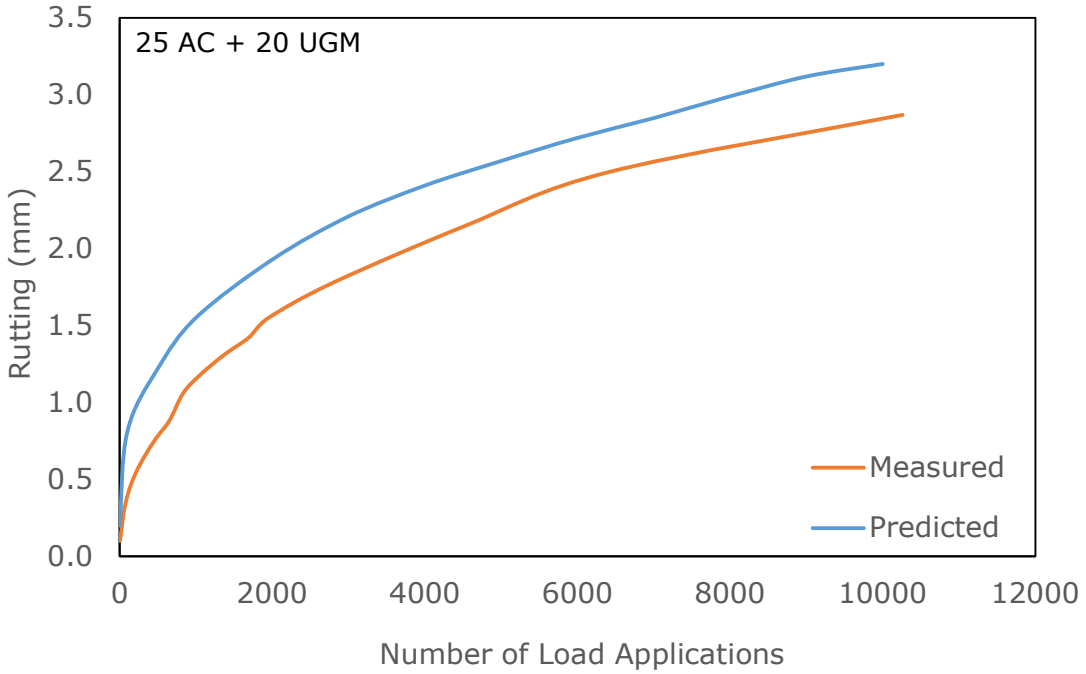


Figure 6.15: Measured vs Prediction Deformation in specimens having 25mm AC and 20mm UGM

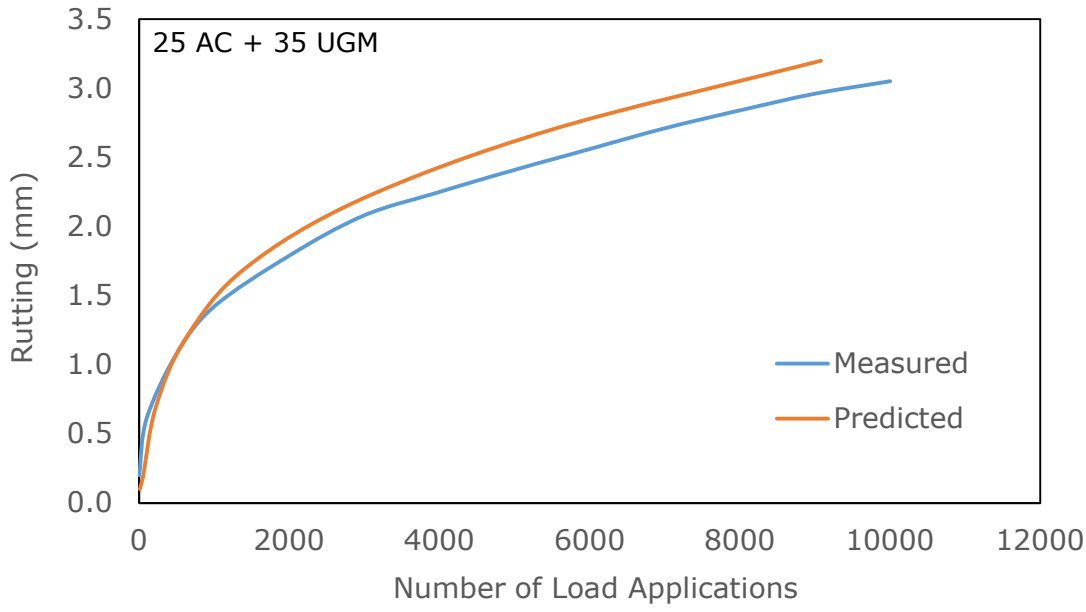


Figure 6.16: Measured vs Prediction Deformation in specimens having 25mm AC and 35mm UGM

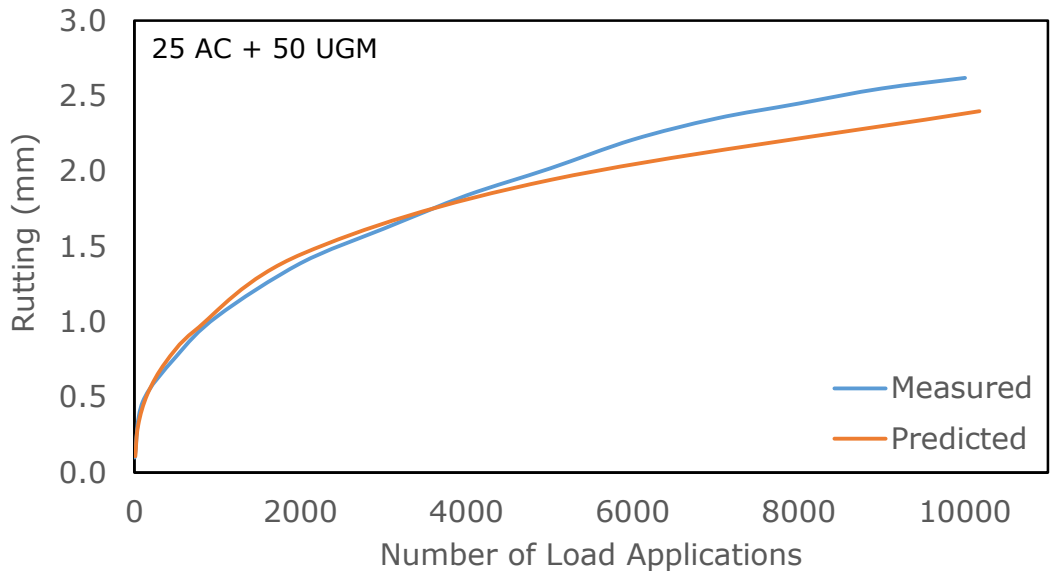


Figure 6.17: Measured vs Prediction Deformation in specimens having 25mm AC and 50mm UGM

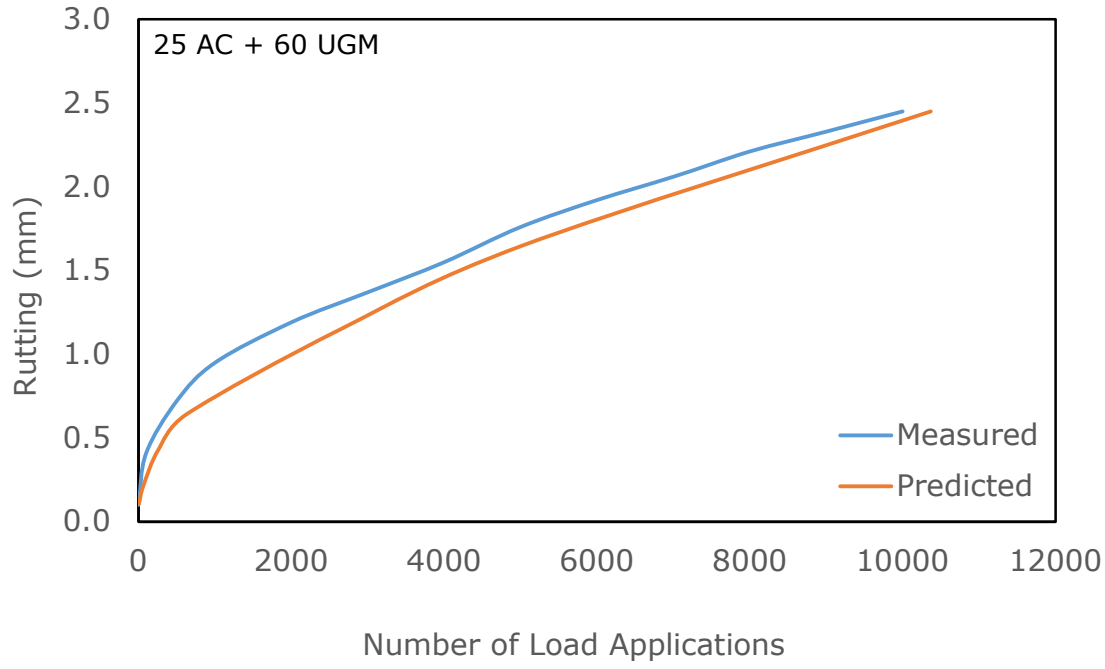


Figure 6.18: Measured vs Prediction Deformation in specimens having 25mm AC and 60mm UGM

6.5 Conclusions

The following are the conclusions from the permanent deformation prediction approach developed in this study.

- The already developed pseudo-viscous approach and stress-strain models can be combined to predict the permanent deformation in full depth pavement comprising asphalt mix and unbound granular layers.
- The prediction approach developed produced very reasonable and realistic results once a few key assumptions were made.
- The prediction results were affected by the thickness of the layers as a whole and asphalt mix layer particularly. From thin to thick asphalt layers, the permanent deformation prediction went from over-predicted to under-predicted, although almost all the predicted values were comparable to the measured ones.
- For very thin pavements, the prediction approach was not as reliable as for others but overall it predicted effectively for all the inverted pavement layer thickness combinations.

7 Predicting Fatigue Life in Inverted Pavements

7.1 Introduction

As mentioned in previous chapters, many different measures have been taken by researchers over the years to improve pavement performance under load. These measures include improving the material performance by adding different admixtures, improving design technologies, optimum usage of materials, and advancement in testing equipment as well as new scientific prediction techniques enabling engineers to predict pavement performance prior to construction. The pavement performance prediction techniques result in reasonable approximation of pavement performance under traffic and environmental attack with the ability to suggest the need for any amendments in materials and testing methodologies. Many techniques to predict crack initiation and propagation in pavements have been described in the literature review. But, the need to develop a methodology to predict reflective cracking and fatigue life in inverted pavements is very evident. This chapter represents a mechanics-based methodology to predict the fatigue life of inverted pavements.

7.2 Analysis of Wheel Tracker tests

Reflective crack propagation in inverted pavements has been predicted by following the laws of mechanics. The procedure involves equating forces and thus moments within a pavement structure. Moments generated bending in the asphalt and the strains were calculated at the bottom of asphalt. The strains were then plotted against the number of load cycles from the laboratory testing and a fatigue line was obtained. The detailed procedure along with labelled figures and equations is explained below.

Inverted pavements were constructed in the laboratory and the number of cycles to initiate the cracks as well as failure were calculated. The pavement structure and construction are explained in Chapter 5 and shown in Figure 7.1.

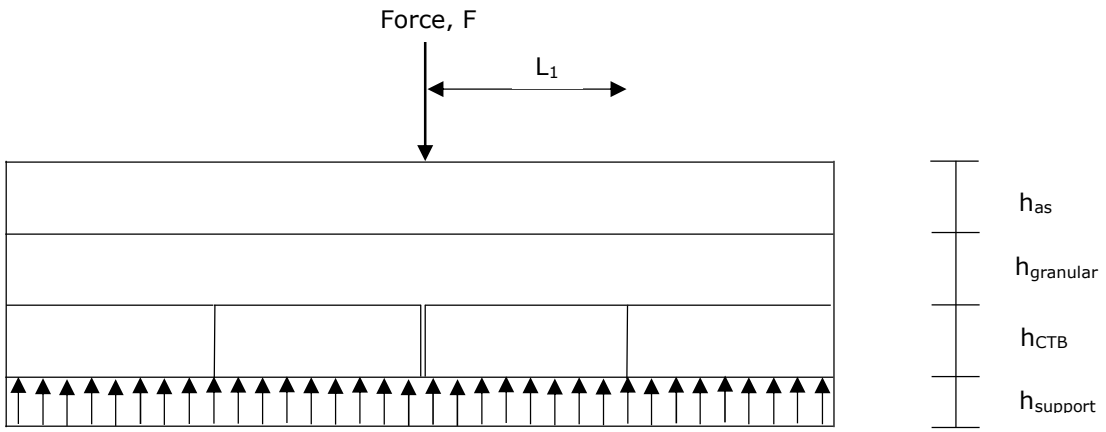


Figure 7.1: A typical inverted pavement with cracks in CTB under load

As explained in chapter 5, Figure 7.1 shows an induced crack midway along the cement treated base and two more cracks that developed while compacting the top-layers, i.e. unbound granular layer and AC wearing course respectively. The analysis was started considering a pavement without an unbound granular layer, with a cracked cemented layer just underneath the AC wearing course as shown in Figure 7.2.

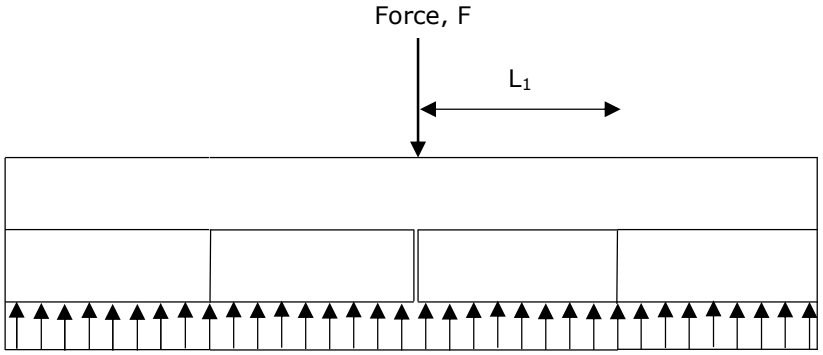


Figure 7.2: A pavement structure without unbound granular layer

For purposes of simplicity, only the middle severe crack is considered and the beam span is reduced considering only the two middle blocks as shown in Figure 7.3. This shows the deformed shape of the AC as well as the angle developed in the cracked cemented layer due to load application.

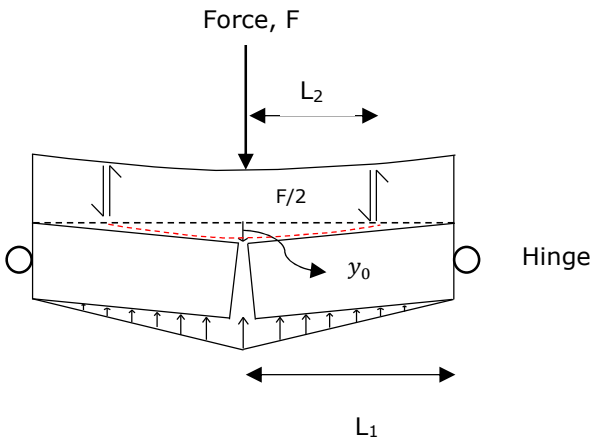


Figure 7.3: Pavement deformed shape under load showing forces and deflection

The shear force as shown by F/2 acts at a distance L_2 with the asphalt bending as shown by the red dotted line. The reaction as shown can be represented by "ky" with k being the modulus of subgrade reaction and y the deflection.

Taking moments about the 'hinge' i.e. the intermediate crack,

$$\frac{F}{2} \times (L_1 - L_2) = \int_0^{L_1} ky\, dx\, (L_1 - x)$$

But

$$y = y_0 \left(\frac{x}{L_1}\right)$$

Putting values, we get

$$\frac{F}{2} \times (L_1 - L_2) = \int_0^{L_1} ky_0 \left(x - \frac{x^2}{L_1}\right) dx$$

$$\frac{F}{2} \times (L_1 - L_2) = ky_0 \left[\frac{x^2}{2} - \frac{x^3}{3L_1}\right]_0^{L_1}$$

$$\frac{F}{2} \times (L_1 - L_2) = ky_0 \frac{L_1^2}{6}$$

So

$$Slope = \frac{4FL_2^2}{16EI} = \frac{y_0}{L_1}$$

$$F\,(L_1 - L_2) = ky_0 \frac{L_1^2}{3}$$

$$y_0 = \frac{F\,L_1 L_2^2}{4\,EI}$$

$$F\,(L_1 - L_2) = \frac{kFL_1^3 L_2^2}{12\,EI}$$

$$L_1 = \frac{kL_1^3 L_2^2}{12\,EI} + L_2$$

$$L_1 = L_2\left(\frac{kL_1^3 L_2}{12\,EI} + 1\right)$$

$$L_1 = \frac{kL_1^3 L_2^2}{12\,EI} + L_2$$

$$L_1 = \frac{kL_1^3 L_2^2 + 12\,EIL_2}{12\,EI}$$

$$12\,EIL_1 = kL_1^3 L_2^2 + 12\,EIL_2$$

$$kL_1^3.L_2^2 + 12\,EI.L_2 - 12\,EIL_1 = 0$$

This can then be solved to obtain L_2. Similarly, a deformed shape and calculations can be made for a pavement including an unbound granular layer as shown in Figure 7.4.

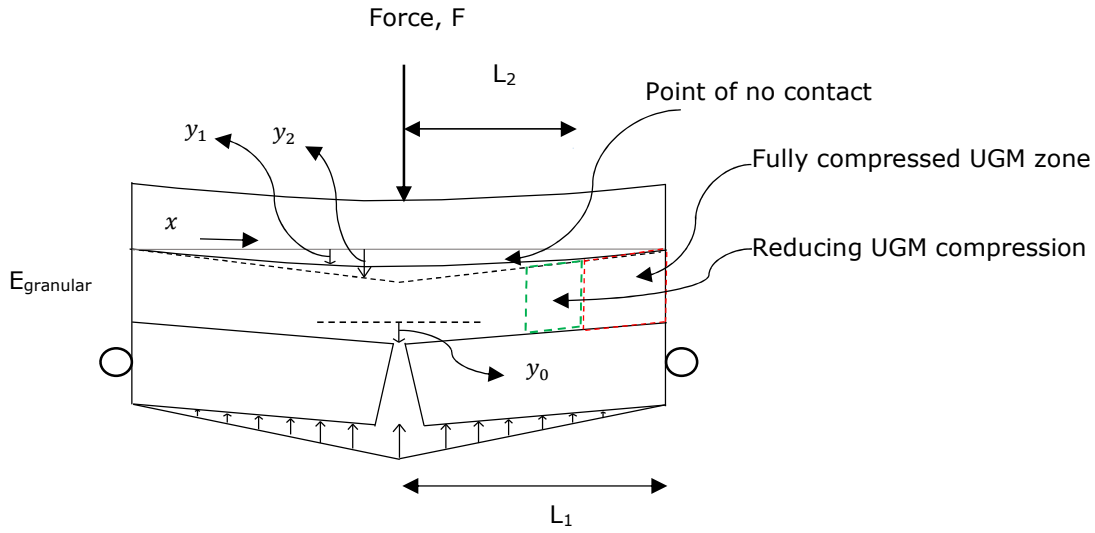


Figure 7.4: Inverted pavement deformed shape under load

Considering Figure 7.4, the granular material under the bent asphalt will be in compression due to the application of the Force F. First considering only the fully compressed UGM zone, as shown by the red dotted rectangle, the stress can be given by;

$$\text{Stress in remaining granular} = \frac{F/2}{(L_1 - L_2) \times z}$$

where 'z' is the out-of-plane thickness of the unbound granular layer. The compression on the unbound granular material can be expressed by the following expression.

$$\text{Compression} = \frac{F.h}{2(L_1 - L_2)\, z\, E_g}$$

To find the deflection y_1, we can take moments at any distance "x" whereas y_2 can be found by slope of the line.

$$M = \frac{F}{2}.x = EI\,\frac{d^2y}{dx^2}$$

$$\frac{d^2y}{dx^2} = \frac{Fx}{2EI}$$

$$\frac{dy}{dx} = \frac{Fx^2}{4EI}$$

$$y_1 = \frac{Fx^3}{12EI}$$

$$y_2 = \frac{x}{L_1}.y_0$$

Under the influence of the applied force and angle created by the deformed cement treated base, the unbound granular layer would lose contact with the AC surfacing resulting in a point of no contact between the two layers i.e. zero compression of the unbound granular layer. The deformed shape of the AC layer in the presence of the unbound granular layer can, therefore, be analysed to find this point of no contact "x" between AC and unbound granular layer as demonstrated in Figure 7.4. To find the point "x" where the granular layer loses contact with the AC layer, the compression can be related to deflections as shown by the following equation.

$$\frac{F.h}{2(L_1 - L_2)\, z\, E_g} = \frac{x\, y_0}{L_1} - \frac{Fx^3}{12EI}$$

$$\frac{Fx^3}{12EI} = \frac{xy_0}{L_1} - \frac{F.h}{2\,(L_1 - L_2)\, z\, E_g}$$

$$\frac{Fx^3}{12EI} = \frac{2xy_0\left\{(L_1 - L_2)\, z\, E_g\right\} - Fh\, L_1}{2L_1(L_1 - L_2)\, z\, E_g}$$

$$Fx^3.2L_1(L_1 - L_2)\,z\,E_g = 24\,xy_0\{(L_1 - L_2)\,z\,E_g\}EI - 12Fh\,L_1EI$$

$$\{2FL_1(L_1 - L_2)\,z\,E_g\}x^3 - \{24\,y_0zE_g\,(L_1 - L_2)EI\}x + 12Fh\,L_1EI = 0$$

$$2zE_g(L_1 - L_2)\left\{FL_1x^3 - 12\,y_0EI\;x + \frac{6Fh\,L_1EI}{zE_g(L_1 - L_2)}\right\} = 0$$

$$FL_1x^3 - 12\,y_0EI\;x + \frac{6Fh\,L_1EI}{zE_g(L_1 - L_2)} = 0$$

The expression takes the form of a cubic equation as shown below;

$$ax^3 + bx^2 + cx + d = 0$$

So,

$a = FL_1$ $\qquad$ $b = 0$

$c = 12\,y_0EI$ $\qquad$ $d = \frac{6Fh\,L_1EI}{zE_g(L_1 - L_2)}$

The cubic equation can be solved for the value of "x".

The compression in the unbound granular layer can be used in a simple mathematical analysis to find the effective length. From a careful analysis of "x" and "L_2" calculated for a specimen of 25mm thick AC and 60mm thick UGM, full compression of UGM at L_2" and 35% of this at the centre can be found respectively. The 35% compressed UGM at the centre shows that the layers are always in contact in this case which is also shown in Figure 7.5. Although in reality the compression would decrease towards the middle of the beam in a non-linear manner, a straight line is assumed for calculation. The effective length as shown in Figure 7.5 can be calculated by equating the area under the deformed shape to an approximately equivalent rectangular area shown by the dotted line.

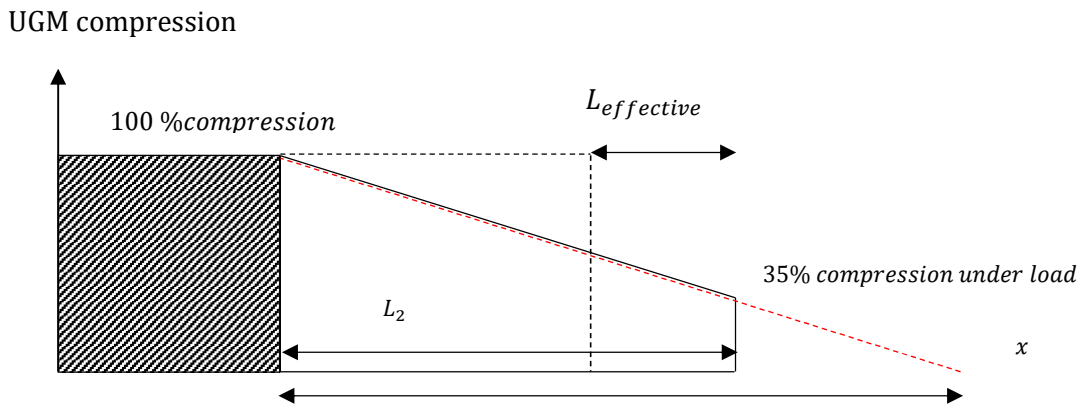


Figure 7.5: Explanation of effective length

The red dotted line shows the distance to a point of zero compression on the unbound granular layer. The Figure 7.5 is shown for a case where the distance to a point of zero compression is more than L_2 i.e. there is always some contact between AC and unbound granular layers. $L_{effective}$ can, then, be found by the following equation. In cases where the point of no contact was less than L_2, the difference $L_2 - x$ was added to find $L_{effective}$ in further calculations.

$$L_2 - L_{effective} = L_2 \times \frac{1}{2}\left\{1 + \left(\frac{x - L_2}{x}\right)\right\}$$

$$L_{effective} = L_2 \left\{1 - \frac{1}{2}\left(1 + \left(\frac{x - L_2}{x}\right)\right)\right\}$$

The curvature of the deformed AC beam without any unbound granular layer can be found by the following expression.

$$K = \frac{F}{2} \times \frac{L_2}{EI} = \frac{1}{R}$$

The curvature can also be calculated with the presence of the unbound granular layer. The difference will only be that the length to be considered for calculations becomes $L_{effective}$. The curvature calculated can then be related to the strains in the asphalt layer by the following expression.

$$\varepsilon = \frac{1/2 \; h_{asphalt}}{R}$$

The above methodology represents an approximate estimate of the strains at the bottom of the AC layer. The significance of the methodology

developed can be understood in the next section by analysing the results obtained from wheel tracking tests.

7.3 Results

All the calculated parameters i.e. lengths and strains are summarised in Table 7.1. The table also contains the strains at the bottom of the AC layer calculated by adopting the above methodology. As mentioned in chapter 5, a force of 1.5kN was applied in the tests; AC, unbound granular base and rubber subgrade were assigned moduli values of 9180, 350 and 414 MPa respectively. The AC modulus value at 10°C was calculated by extrapolating an ITSM stiffness at 20°C using 2 point bending (2PB) stiffness values for a similar mix at 10 and 20°C. The UGM modulus was approximated based on PUMA data and the rubber modulus was assigned based on the assumption of full friction between the rubber and the CTB and a Poisson's Ratio of 0.5. The beam thickness was 50mm.

Table 7.1: Calculations from the prediction exercise

Layer Thickness AC+UGM (mm)	Lengths (mm)			Strain
	L_2	x	$L_{effective}$	
15+20	34.36	33.33	18.74	5.3E-04
15+35	34.36	40.87	14.44	4.1E-04
15+50	34.36	46.40	12.72	3.6E-04
15+60	34.36	49.47	11.93	3.4E-04
20+20	45.79	45.53	23.28	3.7E-04
20+35	45.79	55.39	18.92	3.0E-04
20+50	45.79	62.66	16.73	2.7E-04
20+60	45.80	66.72	15.72	2.5E-04
25+20	54.83	57.54	26.12	2.6E-04
25+35	54.83	69.76	21.54	2.2E-04
25+50	54.83	78.80	19.07	1.9E-04
25+60	54.83	83.84	17.93	1.8E-04

The strains values obtained were used to establish a fatigue characteristic as shown in Figure 7.6. This was also compared with fatigue line already

developed for the same control hot mix asphalt (HMA) by Abed (Ahmed Abed 2019).

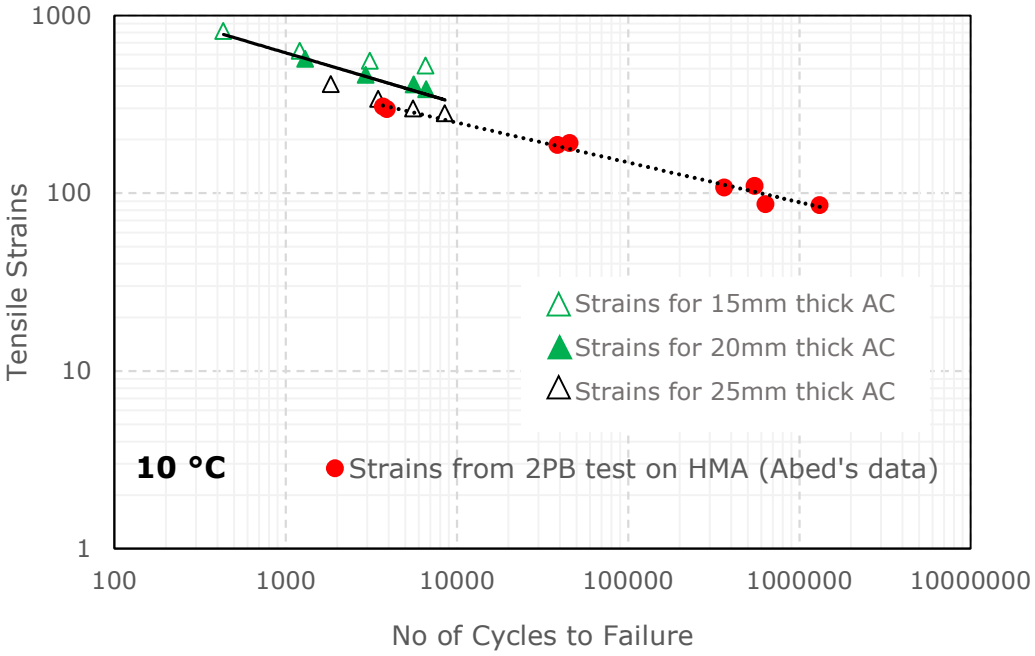


Figure 7.6: Fatigue characteristic

From a careful analysis of the fatigue line, it is very clear that the thicker AC layer showed least strains and the strains increased with a decrease in thickness as shown by differently labelled data points in Figure 7.6. The fatigue line developed from the wheel tracking test compared well with control specimen data from Abed. For a given number of load cycles, relatively higher strain values for the wheel tracker based fatigue line could be attributed to the lower frequency of applied load in the wheel tracking test as compared to the 2PB test.

The strain values were calculated for both cases i.e. with and without the presence of unbound granular layer as explained in the methodology. Three strain values were obtained for the three different AC thicknesses without considering the unbound granular layer and these are shown by the dotted lines in Figure 7.7. The calculated strains can then be extended to the already developed fatigue line and the number of cycles to reach those strains can then be computed as demonstrated in the figure. It is clear from the figure that for any given AC thickness without the presence of unbound granular layer, a significantly lower number of cycles are required to reach

the calculated strain values. This finding supports the inclusion of the unbound granular layer to reduce the tensile strains at the bottom of AC layer and hence increase the pavement's fatigue life significantly.

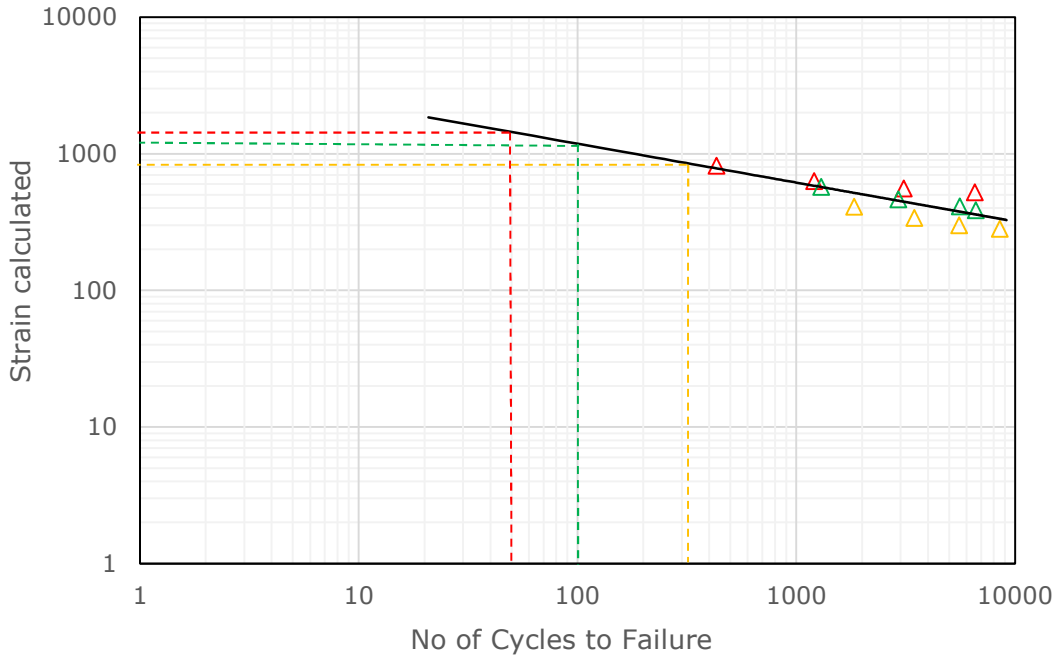


Figure 7.7: Fatigue life prediction with and without unbound granular layer

The calculated number of cycles for different AC thicknesses with and without the unbound granular layer are plotted in Figure 7.8. The green lines represent the number of cycles without unbound granular layer for 15, 20 and 25mm thick AC layers as computed from Figure 7.7. The findings clearly show a significant effect of increasing unbound granular layers from zero thickness on the number of cycles to failure. This effect becomes even more significant in the case of a thin AC layer. The presence of even the thinnest unbound granular layer, 20mm, improves the pavement performance significantly as compared to the instance without it for thicker AC layers i.e. 20 and 25mm. But a further increase in the unbound granular layer thickness doesn't improve the pavement performance as significantly.

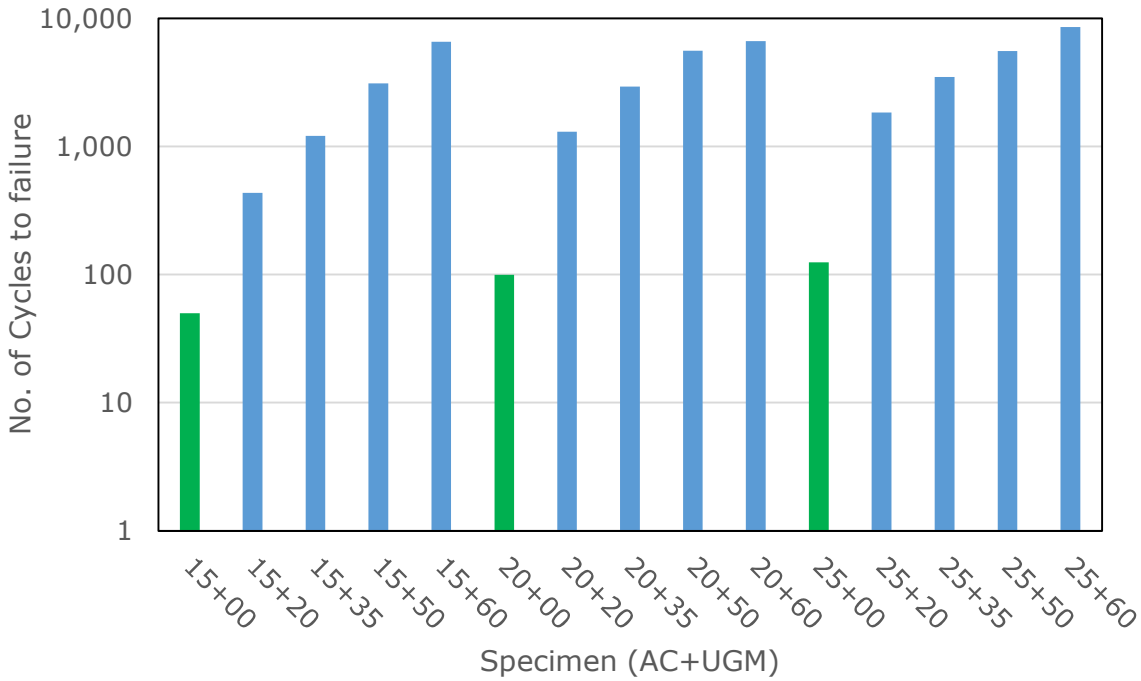


Figure 7.8: Measured and predicted number of cycles with and without UGM layer

7.4 Application to Real Pavements

The methodology adopted was applied to a real pavement to study its effectiveness. Different thickness combinations were analysed for this purpose. AC layer thicknesses of 60, 80 and 100mm were analysed with unbound granular layer thicknesses of 100, 120 and 150mm. A cement treated base layer of 200mm was considered for analysis having cracks at 2m spacing. AC, unbound granular and subgrade layer moduli of 9180, 350 and 50 MPa were taken in the analysis along with a load of 40kN. The results obtained are plotted in Figure 7.9. It is clear from the figure that an increase in the unbound granular layer thickness at the same thickness of AC reduces strains at the bottom of the asphalt and hence increases a pavement's fatigue life. Similarly, an increase in AC thickness for any given unbound layer thickness also reduces the strain values significantly.

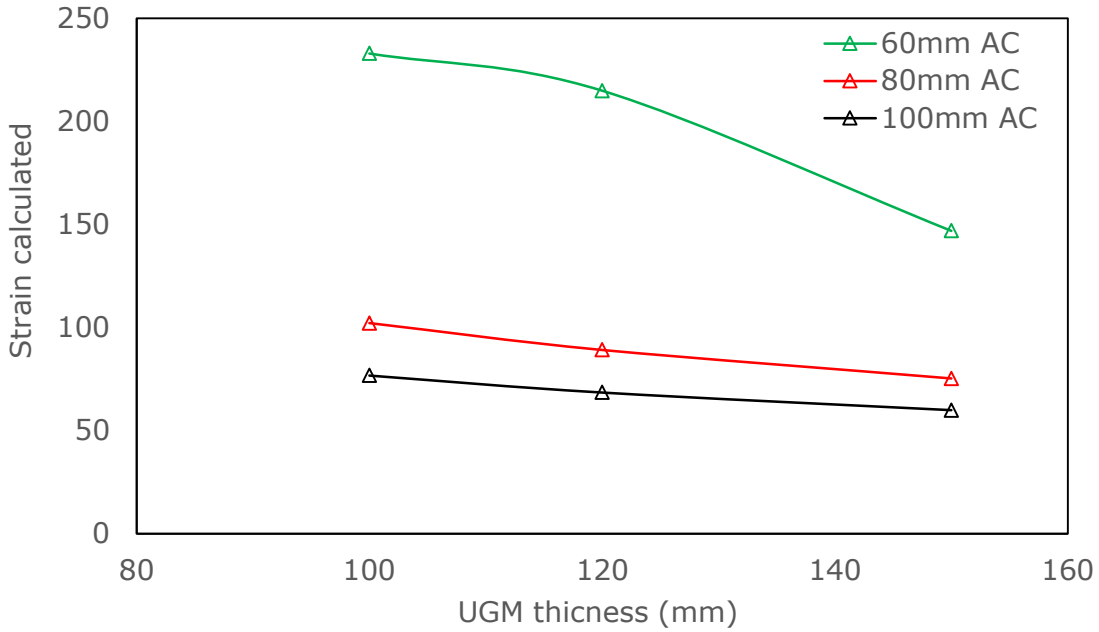


Figure 7.9: Effect of UGM thickness on strains calculated

The strains were also calculated for AC thicknesses of 60, 80 and 100mm without considering the unbound granular layer and plotted along with different unbound thicknesses as shown in Figure 7.10. The strains reduced with the increase in the unbound granular layer thickness as expected.

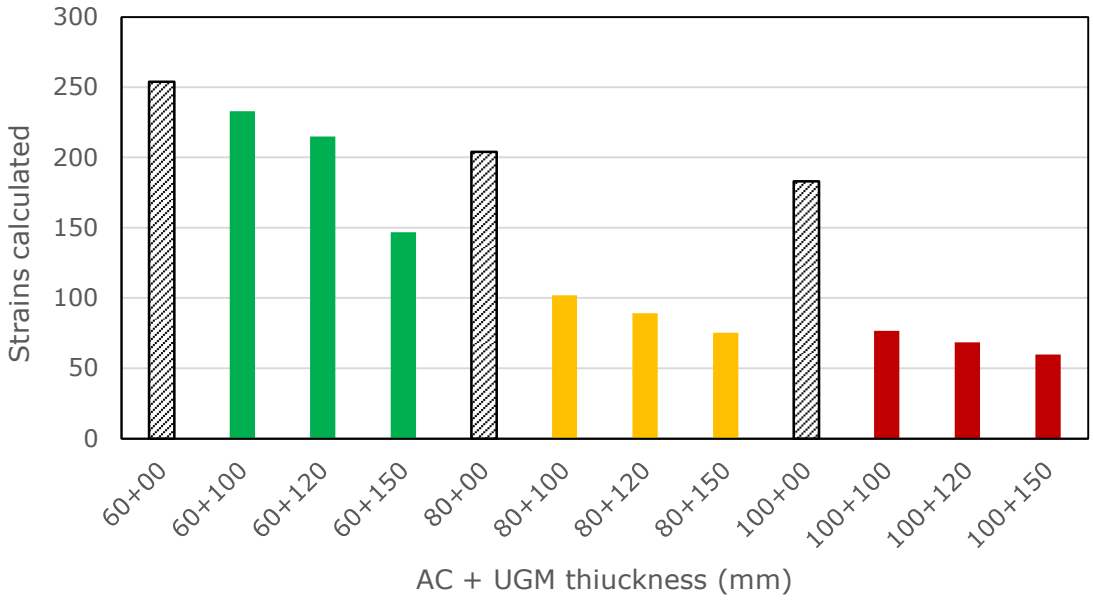


Figure 7.10: Strains calculated for different thickness combinations

The number of cycles to failure for the corresponding strains were also predicted the following universal model (Mathew and Rao 2009) and are

presented in Figure 7.11. The constants f_1 , f_2 and f_3 were obtained from Transportation and Road Research Laboratory (TRRL) who recommended values of 2E-10, 4.32 and 0 respectively (Huang 2004).

$$N_f = f_1 \, \varepsilon_t^{-f_2} E_1^{-f_3}$$

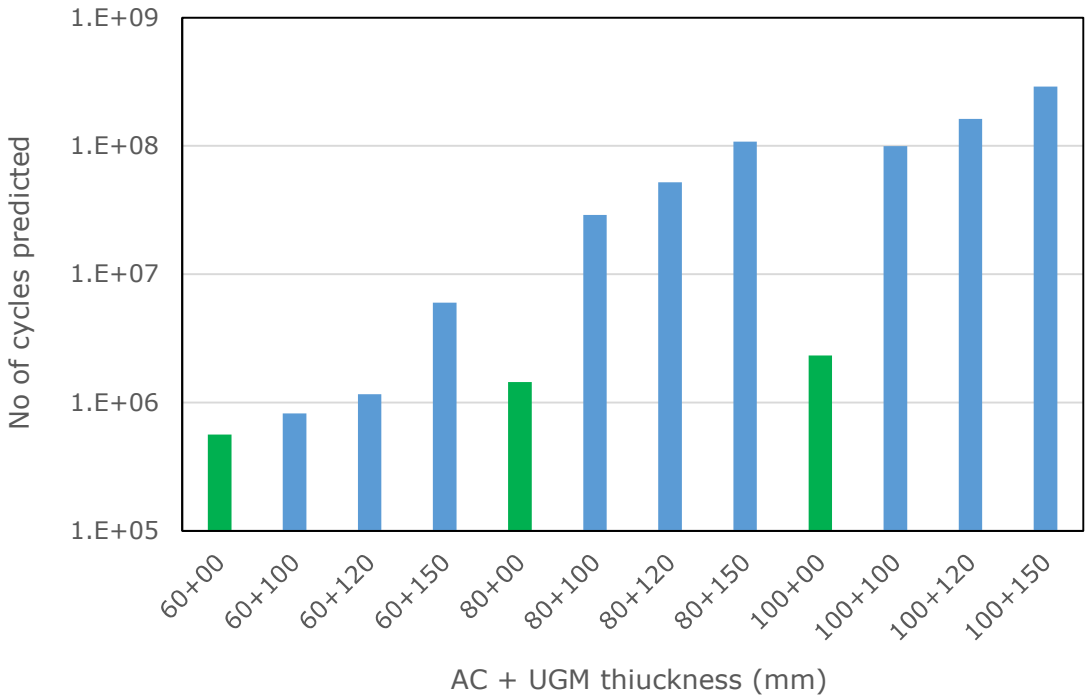


Figure 7.11: Number of predicted cycles to failure (TRRL)

An increase in the unbound granular layer thickness from zero to 150mm for AC thicknesses of 60, 80 and 100mm increased the pavement life by 11, 75 and 125 times respectively. Similarly, Figure 7.11 could be used to evaluate an AC replacing the unbound granular layer to give equal fatigue life, for example, the 60+150 specimen showed approximately 2.6 times more fatigue life as compared to a 100mm thick AC specimen without the unbound granular layer. In this case, the additional 40mm thick AC could be replaced by 150mm thick unbound granular thickness for 2.6 times higher fatigue life. The effect of the presence of an unbound granular layer became significantly higher for higher layer thicknesses. Although the methodology developed is based on a number of simplifications, it still is capable of providing reasonable strains at the bottom of the AC layer and hence predicting its life to failure as shown in Figure 7.11.

7.5 Conclusions

The chapter has explained the methodology developed to predict pavement fatigue life in inverted pavements. The following are the conclusions from the chapter.

- The methodology developed to obtain the strains at the bottom of the AC layer provided very reasonable values.
- The fatigue line developed from the calculated strains compared well with the control AC fatigue line obtained from Abed's data.
- The number of cycles to cause the corresponding strains for pavements without the unbound granular layer were also computed from the developed fatigue line.
- A very reasonable application of the methodology developed to predict fatigue life was made for thin beam-sections of real pavements under controlled test and environmental conditions.

8 Design Guide for Inverted Pavements

8.1 Introduction

This chapter attempts to present a general design guide for constructing inverted pavements based on the methodologies developed during this research project. As the project was started with an aim to design inverted pavements being capable to carry heavy load at warm temperatures, so a general guideline for designing such pavements must be presented. The general steps of the design are as represented and followed in South Africa, USA and any other countries following this rather innovative pavement construction technology.

8.2 Design approach

T This project proposes a design methodology for inverted pavements in response to the applied wheel load and environmental conditions. The basic steps proposed are the same as those presented as Figure 2.26 by Theyse et al. (1996). The design involves selecting appropriate materials for the pavement; the details of the gradations and subsequently desired elastic modulus values of all the individual layers are all tabulated in the "literature review". As has been mentioned earlier as well, the proximity of the unbound granular material layer to the applied load makes it a critical structural layer in an inverted pavement; it is , therefore, suggested from a design point of view to never compromise the quality and compaction properties of the base layer. The structural analysis involves finding the critical performance values (stresses and strains) for all the layers at the critical layer depths. The newly developed methodologies in this research project to predict the pavement rutting and fatigue properties are to be used to find the critical pavement responses for different performance parameters i.e. permanent deformation and cracking. The predicted pavement responses, then, could be correlated with the pavement life prediction for the applied vehicular loads.

8.3 Summary

This chapter represents a very short description of the guidelines for designing an inverted pavement by combining the South African design method with the methodologies developed in this project. The basic aim of the chapter is to combine the South African design metholdogy for constructing an inverted pavement with the methodologies developed during this research project to calculate the pavement's critical responses.

9 Conclusions and Recommendations

This chapter encompasses the findings from the research project. All the conclusions from the current study are documented along with recommendations for future studies.

9.1 Conclusions

The research project was carried out in different phases so the conclusions are also listed in different groups as follows;

9.1.1 Characterization of Unbound Granular Materials

- It was found through this research project that the performance of Granite for unbound base layer in an inverted pavement was affected significantly by varying the moisture and fines content. The performance was evaluated by both deformation parameters i.e. resilient and permanent by using a Precision Unbound Material Analyser (PUMA) device.
- The research study revealed an increase in unbound material deformation (both resilient and permanent) by increasing the fines content for gradations having same maximum particle size. The results were not the same for gradations with relatively smaller maximum particle size. It was also observed that the theoretically targeted results i.e. less deformation at optimum moisture content, were obtained for smaller maximum particle size.
- The most complicated results were observed for specimens having given fines content gradation tested at different moisture contents. The effect of moisture content on evaluation of deformation performance of unbound granular materials was quite contrasting for different variations. Of all the findings, one was the observance of highest permanent deformation and resilient modulus values for the specimens tested at suction point for all the gradations. The reasons have been mentioned in detail in the relevant chapters. Another noteworthy point was the increase in UGM permanent

deformation by increasing the moisture content from suction to optimum moisture content.

- The further extension of the research project to the application of shakedown theory for characterising the permanent deformation behaviour of unbound granular materials revealed the performance to be purely elastic to plastic creep which responds to the Range A and B as defined in literature with none of the specimen observing incremental collapse stage which is termed as Range C and stated to be an un-allowable condition in a pavement.

9.1.2 Simulative Testing

- The simulative laboratory testing in wheel tracking environment to study the effect of layer thickness combinations on rutting (permanent deformation) and fatigue (cracking) performance of an inverted pavement showed a linear relationship between performance and an increase in overall pavement thickness. It is also to be noted that enhanced pavement performance response under loading were also observed by increasing the thickness of any single layer, asphalt wearing course and unbound granular base, while keeping the other layer' thickness constant.
- The simulative laboratory testing was performed for both the performance criteria in different testing environment as stated in the relevant chapter, so the conclusions are also summarised separately for each parameter. In case of permanent deformation as performance criteria, an increase in thickness of any layer, AC and UGM, decreased pavement rutting while keeping the other layer thickness constant. This observance was even more profoundly significant with an increase in AC layer while keeping the UGM thickness constant. In general, the pavement's resistance to permanent deformation increased manifold by increasing the layer thicknesses, individual as well as overall.
- The laboratory results upon analysis represented another way to look and summarise the results. By a somewhat simple method of measuring the rutting in individual layers of the tested specimens, the rutting in the individual layers was computed. Based on the

individual rutting percentages, the rutting in unbound granular layers at different intervals was calculated which was then analysed based on shakedown limits and it was concluded that the unbound layer in six thinnest combinations performed in Range C which could not be allowed whereas the rest of thickness combinations performed in Range B whereas the thickest specimen was in Range A. The results were reported to be slightly different than PUMA results due to the simplicity of the method and chance of personal errors associated with it.

- The similar improvements were also observed for laboratory tests involving different pavement layer thickness combinations to resist crack development under the influence of the applied wheel load. Like permanent deformation, the resistance to crack development increased in all the specimens by increasing the overall pavement thickness. An increase in individual layer thickness also augmented the pavement resistance to cracking while keeping the other layer thickness constant. The resistance to cracking increased very significantly in case of an increment in the unbound granular base thickness while keeping the AC thickness constant. In one of the increments, it increased the pavement' resistance to cracking as much as 475%.
- The effect of an increase in AC thickness while keeping the UGM thickness constant on the resistance to cracking within an inverted pavement was not as simple as otherwise and it depended on UGM thickness. An increase in resistance to cracking was observed by increasing the AC thickness from 15mm to 20mm for thin UGM layers of 20 and 35mm. A further increase in AC layer thickness form 20 to 25mm in case of thin UGM layers of 20 and 35mm didn't show any significant improvement, although it increased the pavement resistance to cracking. The simulative laboratory pavements comprising of thicker UGM layers of 50 and 60mm thickness depicted opposite results to that of thin ones. In case of thicker UGM layers, an increase in AC thickness from 15 to 20mm didn't improve the pavement response as significantly as it did for an increase in AC layer from 20 to 25mm.

9.1.3 Predicting Rutting in inverted pavements

- A novel linear viscous approach is developed capable of predicting the permanent deformation in an inverted pavement. The methodology involved assigning the viscosity (pseudo-viscosity) values to the pavement layers and modelling in a pavement analysis software resulting in strains in different sublayers which were then worked out to get the permanent deformation in the pavements. The approach shows its suitability by observing very good comparisons between measured and predicted results for the simulative laboratory specimens. The viscosities were assigned based on an already developed pseudo-viscous approach for AC layer whereas a stress-strain based model was selected and used for it in case of UGM layer.
- Based on a few key assumptions related to the regression parameters in the selected models and stress ratio values, very reasonable and realistic predictions of the permanent deformation in inverted pavements were made. The assumptions involved assigning a specific value to the parameters in the model for all the specimens and not allowing the stress ratio to increase during the increments based on the anticipated predictions.
- Permanent deformation prediction results were affected by the thickness of the layers as a whole and AC layer particularly. From thin to thick asphalt layers, the permanent deformation prediction went from over-predicted to under-predicted, although almost all the predicted values were comparable with the measured ones.
- For very thin pavements, the permanent deformation prediction approach was not as reliable as for others but overall, it predicted effectively for all the inverted pavement layer thickness combinations.

9.1.4 Predicting Fatigue life in inverted pavements

- A very simplified methodology was developed to predict the pavement fatigue life with and without the presence of an unbound granular layer. The methodology involved balancing the forces and moments in an inverted pavement under the influence of the applied

wheel load. Based on this mechanics-centred approach, the strains were computed at the bottom of the AC layer which was then correlated to the pavement fatigue life.

- The approach was also expanded to the pavements with and without an unbound granular layer thereby pointing towards the benefits associated with the presence of an unbound granular later between cemented and asphalt layer. This presence is, theoretically, expected to improve the pavement fatigue life significantly. During this studies, similar results were reported i.e. very high fatigue lives were observed for the pavements with unbound granular layers as compared to pavements without them.
- In the next phase, the methodology was expected to perform well for the real pavements which was carried out with very positive results. Different thickness combinations of the pavements were modelled under the influence of more realistic loading and environmental conditions by following the developed methodology and it was found out that the methodology developed to predict a pavement's fatigue life successfully predicted the fatigue life of the real pavements.
- The thesis also encompasses the general design procedures adopted in South Africa and used in USA. It is therefore suggested that the same pavement design procedure could be followed for constructing any test sections for introducing this innovative pavement construction technology in the UK.

9.2 Recommendations

The following are the recommendations for future studies for better understanding and developing of usefulness of inverted pavements under different environmental conditions.

- A project may be carried out to study the effect of different ranges of moisture and fines contents along with more realistically representative stress conditions on resilient and permanent deformation of UGMs in the PUMA. The maximum particle size should

be varied up to the South African G1 base gradation suggested size of 50mm.

- The effect of the South African base construction technique called slushing should be studied in order to find the improvements in UGMs density and hence pavement performance.
- The influence of compaction and density of the layers can be studied in the wheel tracker to evaluate their effect on permanent deformation performance of inverted pavements.
- The effect of moisture infiltration on overall structural performance of inverted pavements due to the presence of thin HMA layers needs to be evaluated in the laboratory.
- Inverted pavement testing under heavy loading and high temperatures in the laboratory can be a good project to study the inverted pavement's significance under these severe environmental conditions.
- The inverted pavement performance can be studied in a simulative environment involving 3D finite element analysis techniques.
- The developed technique to predict permanent deformation can be improved to constitute a program capable of predicting permanent defromation in inverted pavement.
- A range of pavements and pavement combinations are needed to be modelled for PD prediction in order to suggest constant values of parameters "a" and "b" in the Rahman-Erlingsson model.
- As the PD prediction exercise involved assuming a constant or decreasing value of stress ratio, Sf, it is suggested that a range of stress ratios may be employed in the prediction process in order to study its effect on predicting the permanent deformation of the pavement.
- The fatigue life prediction methodology may be studied for different environmental conditions.

10 References

AASHTO. (2002). Guide for Mechanistic-empirical design of new and rehabilitated pavement structure, Washington, DC.

AASHTO, Mechanistic-empirical pavement design guide: a manual of practice, AASHTO Designation: MEPDG-1, Washington, DC, 2008.

AASHTO Guide for Design of Pavement Structures 1993, American Association of State Highway and Transportation Officials, Washington, D.C., 1993.

AASHO Road Test Report 2 Materials and Construction, Highway Research Board Special Report 61B, National Academy of Sciences – National Research Council Publication 951, Washington, D.C., 1962.

Abdullah, G.M.S.; (2019) 3D finite element modelling to predict the foamed sulfur asphalt marlsoil mixes rutting behaviour, Ain Shams Engineering Journal, Accepted 26 march 2019

Ahmed Abed (2019), Investigation of Warm Mix Asphalt Performance with Incorporation of Reclaimed Asphalt Pavement, PhD thesis, University of Nottingham, UK.

ARA, Inc. (2004). Guide for mechanistic-empirical design of new and rehabilitated pavement structures (NCHRP 1–37 A, Transportation Research Record, pp. 45–55). Washington, DC.

Ahlvin, R. G., Turnbull, W. J., Sale, J. P., and Maxwell, A. A. (1971). "Multiple-Wheel Heavy Gear Load Pavement Tests. Volume I. Basic Report." A. F. W. Laboratory, ed., U.S. Army Engineer Waterways Experiment Station, Vicksburg, Mississippi.

Al-Khateeb, G., Basheer, I., (2009) A three-stage rutting model utilising rutting performance data from the Hamburg Wheel-Tracking Device (WTD), Road Transp. Res. 18; 12–25.

Al-Khateeb, L.A.; Saoud, A.; Al-Msouti, M.F.; (2011) Rutting prediction of flexible pavements using finite element modeling, Jordan J. Civil Eng. 5 (2); 173–190.

ALARM (2016). "Annual Local Authority Road Maintenance Survey ", Asphalt Industry Alliance, www.asphaltindustryalliance.com/alarm.asp.

Allen, J.J. (1973). The effects of non-constant lateral pressures on the resilient response of granular materials. Ph.D. Dissertation, Department of Civil Engineering, University of Illinois, Urbana, IL, May.

Allou, F., Chazallon, C., Hornych, P.; (2007) A numerical model for flexible pavements rut depth evolution with time. Int J Numer Anal Methods Geomech; 31: 1–22.

Allou, F., Petit, C., Chazallon, C., Hornych, P.; (2009) Influence Of The Macroscopic Cohesion On The 3D FE Modeling Of A Flexible Pavement Rut Depth. In: In Bearing Capacity of Roads, Railways and Airfields. 8th International Conference (BCR2A'09).

Al-Qadi IL, Wang H, Tutumluer E. (2010). Dynamic analysis of thin asphalt pavements utilizing cross-anisotropic stress-dependent properties for granular layer. Transportation Research Record: Transportation Research Board; 2154: 1-17.

Anderson, T. L.; (1994) Fracture mechanics: fundamentals and applications (Second edition), CRC Press, Boca Raton, FL.

Ansell, P.; Brown, S. F.; (1978) ''Cyclic simple shear apparatus for dry granular material.'' Geotech. Testing J., 1(2), 82–91.

Archilla, A. R.; Medanat, S.; (2000) Development of asphalt pavement rutting model from experimental data. 79th annual TBR meeting, Transportation Research Record. Washington, DC

Arnold, G.; Alabaster, D.; Steven, B.; de Pont, J.; (2003) Effect on Pavement Wear of an Increase in Mass Limits for Heavy Vehicles – Stage 3. Transfund New Zealand, Wellington, New Zealand.

Arnold, G.K.; (2004) Rutting of granular pavements. Thesis (PhD). University of Nottingham, England

Baek, J.; (2010) Modeling Reflective Cracking Development in Hot-Mix Asphalt Overlays and Quantification of Control Techniques, PhD Thesis, University of Illinois at Urbana-Champaign, IL

Barker, W. R., Brabston, W. N., and Townsend, F. C. (1973). "An Investigation of the Structural Properties of Stabilized Layers in Flexible Pavement Systems." US Army Engineers Waterways Experiment Station.

Barksdale, R. D.; (1972) ‘‘Laboratory evaluation of rutting in base course materials.’’ Proc., 3rd Int. Conf. on Struct. Des. of Asphalt Pavements, 161–174.

Barksdale, R. D. (1984). "Performance of Crushed-Stone Base Courses." Transportation Research Record, 954, 78-87.

Barksdale, R. D., and Todres, H. A. (1983). "A study of factors affecting crushed stone base performance." Georgia Institute of Technology, 639.

Barksdale, R. D.; Itani, S.; (1989) Influence of Aggregate Shape on Base Behavior, Transportation Research Record, 1227, 173-182

Barksdale, R. D.; (1991) The aggregate handbook. National Stone Association, Washington, D.C.

Bastos, J.; Babadopulos, L.; Soares, J.; (2017) Relationship between multiple stress creep recovery (MSCR) binder test results and asphalt concrete rutting resistance in Brazilian roadways, Constr. Build. Mater. 145; 20–27.

Battiato, G.; Ronca, G.; Verga, C.; (1977) Moving loads on a viscoelastic double layer: Prediction of recoverable and permanent deformations, in: Volume I of proceedings of 4th International Conference on Structural Design of Asphalt Pavements, Ann Arbor, Michigan, August 22–26,

Bonaquist RF, Witczak MW. A comprehensive constitutive model for granular materials in flexible pavement structures. In: Proceedings of the fourth international conference on asphalt pavements, Seattle, Washington, USA; 1997. p. 783–802.

Boulbibane M, Collins IF, Ponter ARS, Weichert D. Shakedown of unbound pavements. Int J Road Mater Pave Des 2005;6(1):81–96.

Boyce, H.R. (1980). “A nonlinear model for the elastic behavior of granular materials under repeated loading.” International Symposium on Soils under Cyclic and Transient Loading. Balkema, Rotterdam, The Netherlands, 285-294.

Brown, S. F., and Pell, P. S. (1967). ‘‘An experimental investigation of the stresses, strains and deflections in a layered pavement structure subjected to dynamic loads.’’ Proc., 2nd Int. Conf. Struct. Des. of Asphalt Pavements, 487–504.

Brown, S. F.; Hyde, A. F. L.; (1975) ‘‘Significance of cyclic confining stress in repeated-load triaxial testing of granular material.’’ Transp. Res. Rec. 537, Transportation Research Board, Washington, D.C., 49–58.

Brown, S. F.; Pappin, J.W.; (1981) Analysis of Pavements with Granular Bases. In Transportation Research Record 810, TRB, National Research Council, Washington, D.C., pp. 17–23.

Buchanan, S. (2011) “Inverted Pavement Economics.” Presentation to Georgia Department of Transportation.

Buchanan, S. (2010). "Inverted Pavement Systems." AGG1.

Buchanan. M.S., Inverted Pavements: What, Why, and How, AFTRE Webinar Presentation, National Stone, Sand and Gravel Association (NSSGA), June 1, 2010.

Cardosa, J., Inverted Pavements: Georgia Experience, National Aggregate Base Conference Presentation, National Stone, Sand and Gravel Association (NSSGA), 2008.

Carvalho, R.; (2012) Prediction of permanent deformation in asphalt Concrete Ph.D. thesis, University of Maryland, College Park

Castell, M. A., Ingraffea, A. R., and Irwin, L. H.; (2000) “Fatigue crack growth in pavements,” *Journal of Transportation Engineering*; 126 (4); 283–290

CCA, (2005) Road Rehabilitation Energy Reduction Guide for Canadian Road Builders, Canadian Construction Association (CCA), 2005.

CEN-European Committee for Standardization, 2004a. Cyclic load triaxial test for unbound mixtures. Brussels: European Standard. EN 13286-7.

Cerni, G.; Cardone, F,; Virgili, A.; Camilli, S.; (2012) Characterisation of permanent deformation behaviour of unbound granular materials under repeated triaxial loading. Construction and Building Materials, 28, 79–87.

Chan, F. W. K.; (1990) ‘‘Permanent deformation resistance of granular layers in pavements,’’ PhD thesis, Dept. of Civ. Engrg., University of Nottingham, Nottingham, England.

Chazallon, C., Hornych, P., Mouhoubi, S.; (2006) An elastoplastic model for the long-term behaviour modelling of unbound granular materials in flexible pavements. Int J Geomech ASCE; 6(4): 279–89.

Chazallon, C., Allou, F., Hornych, P., Mouhoubi, S.; (2009) Finite elements modelling of the long-term behaviour of a full-scale flexible pavement with the shakedown theory. Int J Numer Anal Meth Geomech;3 3 (1): 45–70.

Cheng, D., Little, D.N., Lytton, R.L., Holste, J.C., (2002), Surface energy measurement of asphalt and its application to predicting fatigue and healing in asphalt mixtures, Transp. Res. Rec. 1810, 44–53.

Choi, Y.; Kim, Y. R.; (2013) Development of characterisation models for incremental permanent deformation model for asphalt concrete in confined compression. Road Materials and Pavement Design, 14, 266–288

Chow, L., Mishra, D., and Tutumluer, E.; (2014) “Framework for development of an improved unbound aggregate base rutting model for mechanistic-empirical pavement design.” Transp. Res. Rec.; 2401(1); 11–21

Collins, I.F., Wang, A.P., Saunders, L.R.; (1993) Shakedown in layered pavements under moving surface loads. Int J Numer Anal Methods Geomech; 17(3): 165–74.

Collins, I.F., Boulbibane, M.; (1998) The application of shakedown theory to pavement design. Met Mater; 4(4): 832–7.

Collop, A.; Cebon, D.; Hardy, M.; (1995) Viscoelastic approach to rutting in flexible pavements, J. Transp. Eng. 121 (1); 82–93.

Corté, J., and Goux, M. (1996). "Design of pavement structures: the French technical guide." Transportation Research Record: Journal of the Transportation Research Board, 1539(1), 116-124.

Cortes, D. D., and Santamarina, J. C. (2013). "The LaGrange case history: inverted pavement system characterisation and preliminary numerical analyses." International Journal of Pavement Engineering, 14(5), 463-471

Cortes, D.D., Shin, H., and Santamarina, J.C., 2012. Numerical simulation of inverted pavement systems. Journal of Transportation Engineering, 138 (12), 1507–1519.

Cortes, D. D. (2010). "Inverted Base Pavement Structures." Ph.D., Georgia Institute of Technology, Atlanta, GA.

Crockford, W.W., Bendana, L.J., Yang, W.S., Rhee, S.K., and Senadheera, S.P. (1990). Modelling stress and strain states in pavement structures incorporating thick granular layers. Final Report, Contract F08635-87-C-0039, the Texas Transportation Institute, The Texas A&M University, College Station, Texas, April

CRONEY, D. (1977), 'The design and performance of road pavements', HMSO.

CRONEY, D., COLEMAN, J.D. and BLACK, W.P.M. (1958), 'Movement and distribution of water in soil in relation to highway design and performance', Highway Research Board, Special Report No. 40.

Dawson, A. R.; Thom, N. H.; Paute, J. L.; (1996) "Mechanical characteristics of unbound granular materials as a function of condition." Flexible Pavements, Proc., Eur. Symp. Euroflex 1993, A. G. Correia, ed., Balkema, Rotterdam, The Netherlands, 35–44.

Dawson, A.R.; Wellner, F.; (1999) Plastic Behaviour of granular materials. Nottingham: The University of Nottingham. Reference PRG99014, April, 1999, Final report ARC Project 933.

De Beer, M. Aspects of the Design and Behavior of Road Structures Incorporating Lightly Cementituous Layers. Ph.D. thesis. University of Pretoria, Pretoria, South Africa.

De Bondt, A. H.; (1998) "Anti-Reflective Cracking Design of (Reinforced) Asphalt Overlays," *Ph.D. Dissertation*, Department of Civil Engineering, Delft University of Technology, Delft, The Netherlands.

Desai CS. Mechanistic pavement analysis and design using unified material and computer models. In: Third international symposium on 3D finite elements for pavement analysis, Amsterdam. The Netherlands: Balkema; 2002. p. 1–63.

Dobry, R, Ng, T.T., and Petrakis, E. (1989). "Deformation characteristics of granular soil in the light of particulate mechanics." Proceedings, 14th Conference on Geotechnics, Italian Geotechnical Association, Torino, November 28-30

Dodds, A.; Logan, T.; McLachlan, M.; Patrick, J.; (1999) Dynamic Load Properties of New Zealand Basecourse, Transfund New Zealand, Wellington, New Zealand

Domingos, M.; Faxina, A.L.; Bernucci, L.; (2017) Characterization of the rutting potential of modified asphalt binders and its correlation with the mixture's rut resistance, Constr. Build. Mater. 144; 207–213.

Dormon, G. M.; (1962) The extension to practice of a fundamental procedure for the design of flexible pavements. Proceedings of the first international conference on the structural design of asphalt pavements, Ann Arbor, MI, USA, pp. 785–793

Du Plessis, L., Coetzee, N. F., Hoover, T. P., Harvey, J. T., and Monismith, C. L. (2006) "Three decades of development and achievements: The Heavy Vehicle Simulator in accelerated pavement testing." Proc., GeoShanghai International Conference, ASCE.

Dunlap, W. A. (1963). ''A report on a mathematical model describing the deformation characteristics of granular materials.'' Tech. Rep. No. 1, Proj. 2-8-62-27, Texas Transp. Inst., Texas A&M University, College Station, Tex.

Dunlap, W. A.; (1966) ''Deformation characteristics of granular materials subjected to rapid repetitive loading,'' PhD thesis, Texas A&M University, College Station, Tex.

Eisenmann, J., and Hilmer, A., (1987), Influence of wheel load and inflation pressure on the rutting effect at asphalt-pavements – experiments and theoretical investigations, in: Sixth International Conference on the Structural Design of Asphalt Pavements, Ann Arbor,

El-Basyouny, M.M.; Witczak, M.; Kaloush, K.; (2005) Development of the permanent deformation models for the 2002 design guide. In: Compendium of papers of the annual meeting of the transportation research board of the national academies, Washington, DC.

Elliot, R. P., and Lourdesnathan, D. (1989). ‘‘Improved characterization model for granular bases.’’ Transp. Res. Rec. 1227, Transportation Research Board, Washington, D.C., 128–133.

Epps, J.; Sebesta, S.; Hewes, B.; Sahin, H.; Luo, R.; Button, J.; Lytton, R.; Herrera, C.A.; Hatcher, R.; Gu, F.; (2014). “Development of a specification for flexible base construction.” Final Rep. No. FHWA/TX-13/0-6621, College Station, TX, 414.

Erlingsson, S.; Magnusdottir, B.; (2002) Dynamic Triaxial testing of unbound granular base course materials. In: Proceedings of the 6th international conference on bearing capacity of roads and airfields, BCRA ’02, Lisbon, Portugal, Lisse, Netherlands: Balkema, 989–1000

Erlingsson, S.; Rahman, M.S.; (2013) Evaluation of Permanent Deformation Characteristics of Unbound Granular Materials by Means of Multistage Repeated-Load Triaxial Tests. Transportation Research Record: Journal of the Transportation Research Board, Transportation Research Board of the National Academies, Washington, D.C., No. 2369, 11-19. DOI: 10.3141/2369-02.

FHWA, (1996). Resilient modulus of unbound granular base/subbase materials and subgrade soils long-term pavement performance protocol 46. Federal Highway Administration Pavement Performance Division

Finn, F.; Saraf, C.; Kulkarni, R.; Nair, K.; Smith, W.; Abdullah, A.; (1977) The use of distress prediction subsystems for the design of pavement structures. Proceedings of the fourth international conference on the structural design of asphalt pavements, Ann Arbor, MI, USA, pp. 3–37

Fleming, P.R., Frost, M.W., and Lambert, J.P., (2007). Review of lightweight deflectometer for routine in situ assessment of pavement material stiffness. Transportation Research Record: Journal of the Transportation Research Board, (1), 80–87. doi:10.3141/2004-09.

Fleming, P.R., Frost, M.W., and Rogers, C.D.F., (2000). A comparison of devices for measuring stiffness in situ. Unbound aggregates in road construction: Proceedings of the Fifth International Symposium on Unbound Aggregates in Roads, UNBAR 5, Nottingham, UK. pp. 193–200.

Francken, L.; (1977) Pavement deformation law of bituminous road mixes in repeated triaxial compression. Proc., 4th international conference on the structural design of asphalt pavements, Volume I, University of Michigan, Ann Arbor, Aug

Freeme, C. R., Otte, E., and Mitchell, M. F. (1980). Economics of Pavement Type Selection for Major Roads, Pavement type selection committee for the National Transport Commission, Pretoria.

Freeme, C. R., Maree, J. H., and Viljoen, A. W. (1982). Mechanistic design of asphalt pavements and verification using the heavy vehicle simulator, National Institute for Transport and Road Research.

Garg, N., and Thompson, M. R. (1997). ''Triaxial characterization of Minnesota road research project granular materials.'' Transp. Res. Rec. 1577, Transportation Research Board, Washington, D.C., 27–36.

Garg, N., Tutumluer, E., and Thompson, M.R. (1998). "Structural modeling concepts for the design of airport pavements for heavy aircraft," Proceedings, 5th International Conference on the Bearing Capacity of Roads and Airfields, Trondheim, Norway, July, 115-124.

Ghadimi, B., Nega, A., Nikraz, H.; (2014) Simulation of shakedown behavior in pavement's granular layer. Int J Eng Technol; 7

Gidel, G., et al., 2001. A new approach for investigating the permanent deformation behaviour of unbound granular material using the repeated load triaxial apparatus. Bulletin de Liaison des Laboratoires des Ponts et Chausse´es, 233, 5–21.

Gladkikh, V.; Korolev, E.; Smirnov, V.; Sukhachev, I.; (2016), Modeling the rutting kinetics of the sulfur-extended asphalt, Proced. Eng. 165; 1417–1423

Goh, W., You, Z., Williams, R., Li, X., (2011) Preliminary dynamic modulus criteria of HMA for field rutting of asphalt pavements: Michigan's experience, J. Transp. Eng. 1; 37–45.

Gong, H., Sun, Y., Mei, Z., Huang, B.; (2018) Improving accuracy of rutting prediction for mechanistic-empirical pavement design guide with deep neural networks, Construction and Building Materials; 190; 710-718

Gu, F., Zhang, Y., Droddy, C.V., Luo, R., Lytton, R.L.; (2016) Development of a New Mechanistic Empirical Rutting Model for Unbound Granular Material, ASCE J. Mater. Civ. Eng.; 28(8); 04016051

Gu, F., Zhang, Y., Luo, X., Sahin, H., Lytton, R.L.; (2017) Characterization and prediction of permanent deformation properties of unbound granular materials for Pavement ME Design, Construction and Building Materials; 155; 584–592

Grau, R. W. (1973). "Evaluation of Structural Layers in Flexible Pavement." U.S. Army Engineer Warterways Experiment Station, Vicksburg, Mississippi

Habiballah, T.M., Chazallon, C.; (2005) Cyclic plasticity based model for the unbound granular materials permanent strains modelling of flexible pavements. Int J Numer Anal Methods Geomech; 29:577–96.

Hand, A. J.; Epps, J. A.; Sebaaly, P. E.; (1999) Development of APT based permanent deformation prediction models translatable to other environments. Accelerated pavement testing international conference, Reno, NV

Haynes, J. G.; Yoder, E. J.; (1963) ‘‘Effects of repeated loading on gravel and crushed stone base course materials used in the AASHO road test.’’ Hwy. Res. Rec. 39

Heukelom, W., and A. J. G. Klomp. Dynamic Testing as a Means of Controlling Pavements During and After Construction. Proc., International Conference on the Structural Design of Asphalt Pavements, Ann Arbor, Mich., 1962.

Hicks, R.G. and Monismith, C.L., (1971). Factors influencing the resilient response of granular materials. Highway Research Record (345), 15–31

Hicks, R.G. (1970). Factors influencing the resilient properties of granular materials. Ph.D. Dissertation, Institute of Transportation and Traffic Engineering, University of California, Berkeley, May.

Holubec, I.; (1969) ‘‘Cyclic creep of granular materials.’’ Rep. No. RR147, Department of Highways, Ontario, Canada

Horne, D., Belancio, G., Carradine Jr, S. A., Gaj, S., Hallin, J., Jackson, N., Jordan, C., Lucas, D., and Zink, R. (1997). "FHWA Study of South African Pavement and Other Highway Technologies and Practices." FHWA, ed.

Hornych, P.; Absamad, A.E.; (2004) Selection and evaluation of models for prediction of permanent deformations of unbound granular materials in road pavements. Competitive and Sustainable Growth (GROWTH) Programme, SAM-05-DE10.

Hua, J.; (2000) Finite element modeling and analysis of accelerated pavement testing devices and rutting phenomenon (Ph.D. thesis), Civil Engineering, Purdue University

Huang, Y.H.; (2004) Pavement analysis and design. 2nd ed. Upper Saddle River, NJ: Pearson Education

Huurman, M.; (1997) Permanent deformation in concrete block pavements Ph.D. thesis, Delft University of Technology

Javilla, B., Mo, L., Hao, F., Shu, B., Wu, S., (2017) Multi-stress loading effect on rutting performance of asphalt mixtures based on wheel tracking testing, Constr. Build. Mater. 148; 1–9.

Jayawickrama, P. W., Smith, R. E., Lytton, R. L., Tirado, M. R.; (1987) "Development of asphalt concrete overlay design equations," *Final Report*, Texas Transportation Institute, TX.

Jayawickrama, P. W., Smith, R. E., Lytton, R. L., Tirado, M. R.; (1989) "Development of asphalt overlay design program for reflective cracking," *Proceedings of RILEM Conference on Reflective Cracking in Pavements*, (R. Degeimbre, L. Francken, and J. M. Rigo, eds.), Liege, Belgium; 164 – 169

Johnson, C. W. (1961). "Comparative Studies of Combinations of Treated and Untreated Bases and Subbases for Flexible Pavements." Highway Research Board Bulletin, 289, 44-61.

Johnson, T. C., Berg, R. L., and Dimillio, A. (1986). ''Frost action predictive techniques: An overview of research results.'' Transp. Res. Rec. 1089, Transportation Research Board, Washington, D.C., 147–161.

Jooste, F., and Sampson, L. (2005). "The Economic Benefits of HVS Development Work on G1 Pavements." Department of Public Transport, Roads and Works

Jordaan, G. J. Towards Improved Procedures for the Mechanistic Analysis of Cement-treated Layers in Pavements. Proc., 7th International Conference on the Structural Design of Asphalt Pavements, Nottingham, England, 1992.

Kamal, M. A.; Dawson, A. R.; Farouki, O. T.; Hughes, D. A. B.; Sha'at, A. A.; (1993) ''Field and laboratory evaluation of the mechanical behaviour of unbound granular materials in pavements.'' Transp. Res. Rec. 1406, Transportation Research Board, Washington, D.C., 88–97.

Kenis, W. J.; (1977) Predictive design procedure, VESYS user's manual: Interim design method for flexible pavement using the vesys structural subsystem (Final Report No. FHWA-RD-77-154). Washington, DC: FHWA.

Kenis, W. J.; Wang, W.; (1997) Calibrating mechanistic flexible pavement rutting models from full scale accelerated tests. Proceedings of the 8th international conference on asphalt pavements, University of Washington, Vol. 1, pp. 663–672.

Khanzada, S.; (2000) Permanent deformation in bituminous mixtures (Ph.D. thesis), Civil Engineering, The University of Nottingham

Khodaii, A., Mehrara, A., (2009) Evaluation of permanent deformation of unmodified and SBS modified asphalt mixtures using dynamic creep test, Constr. Build. Mater. 23; 2586–2592.

Kim, I.T. and Tutumluer, E., (2005). Unbound aggregate rutting models for stress rotations and effects of moving wheel loads. Transportation Research Record: Journal of the Transportation Research Board, 1913 (1), 41–49. doi:10.3141/1913-05.

Kim, S.H., Little, D.N., and Masad, E., (2005). Simple methods to estimate inherent and stress-induced anisotropy of aggregate base. Transportation Research Record: Journal of the Transportation Research Board, 1913 (1), 24–31. doi:10.3141/1913-03

Kim, W.J., Le, V.P., Lee, H.J., Phan, H.T.; (2017) Calibration and validation of a rutting model based on shear stress to strength ratio for asphalt pavements, Construction and Building Materials, 149; 327-337

Kim, Y.; (2009) Modeling of Asphalt Concrete, ASCE Press, McGraw-Hill.

Kinchen, R. W., and Temple, W. H. (1980). "Asphaltic concrete overlays of rigid and flexible pavements." L. D. o. T. a. Development, ed. Baton Rouge.

Kleyn, E. G. (2012). "Successful G1 Crushed Stone Basecourse Construction." 31st Southern African Transport Conference

Kolisoja, P. (1997). ‘‘Resilient deformation characteristics of granular materials,’’ PhD thesis, Tampere University of Technology, Publ. No. 223, Tampere, Finland.

Kolisoja, P.; (1998) ‘‘Large scale dynamic triaxial tests.’’ III. Delprosjektrapport 20, Arbeidsfelleskapet KPG, Oslo, Norway.

Konishi, J. (1978). Microscopic model studies on the mechanical behavior of granular materials. Proc. of the US-Japan Seminar on Continuum Mechanics and Statistical Approaches in Mechanics of Granular Materials, Sendai, Japan, June, pp. 27-45.

Kopperman, S.E., Stokoe, K.H., and Knox, D.P., (1982). Effect of state of stress on velocity of low-amplitude compression waves propagating along principal stress directions in dry sand. Technical report, US Air Force Office of Scientific Research

Korkiala-Tanttu, L.; (2005), A new material model for permanent deformations in pavements, Proceedings of the 7th International conference on bearing capacity of roads and airfields, BCRRA ’05, Trondheim, Norway

KRAHN, J. and FREDLUND, D.G. (1972), 'On total, matric and osmotic suction, Soil Science, Vol 114, Pt 5.

Kuo, C.M., Hsu, T.R.; (2003) “Traffic induced reflective cracking on pavements with geogrid-reinforced asphalt concrete overlay,” *Proceedings of the 82th Annual Meeting at the Transportation Research Board (CD-ROM),* Washington, D.C

Lade, P.V. and Nelson, R.B. (1987). "Modeling the elastic behavior of granular materials." International Journal for Numerical and Analytical Methods in Geomechanics, Vol. 11, 521-542.

Lashine, A. K.; Brown, S. F.; Pell, P. S.; (1971) ''Dynamic properties of soils.'' Rep. No. 2, Submitted to Koninklijke/Shell Laboratorium, Dept. of Civ. Engrg., University of Nottingham, Nottingham, England

Lekarp, F.; (1997) ''Permanent deformation behaviour of unbound granular materials,'' Licentiate thesis, Royal Institute of Technology, Stockholm.

Lekarp, F.; Dawson, A.; (1998) ''Modelling permanent deformation behaviour of unbound granular materials.'' Constr. and Build. Mat., 12(1), 9–18.

Lekarp, F.; (1999) Resilient and permanent deformation behavior of unbound aggregates under repeated loading. Thesis (PhD). Royal Institute of Technology (KTH), Stockholm, Sweden.

Lekarp, F.; Isacsson, U.; Dawson, A. (2000) State of the art. I: Resilient response of unbound aggregates. Journal of Transportation Engineering. 126(1): 66-75

Lewis, D. E.; Ledford, K.; Georges, T.; Jared, D. M. (2012). "Construction and Performance of Inverted Pavements in Georgia." TRB 91st Annual meeting.

Lo, S.C.R. and Lee, I.K. (1990) Response of granular soil along constant stress increment ratio path. J Geotechnical Engineering. Vol. 116, No. 3, March, pp. 355-376.

Lu, Q., Harvey, J.T., (2006), Evaluation of Hamburg wheel tracking device test with laboratory and field performance data, Transp. Res. Rec. 1970 (2006) 25–44.

Lu, Z. L.; Sun, L. J.; (2007) Research on rutting prediction of asphalt pavement. Journal of Tongji University (Natural Science), 35(2), 1476–1480.

Lytton, R. L.; (1989) "Use of geotextile for reinforcement and strain relief in asphalt concrete," *Journal of Geotextile and Geomembranes*; 8; 217 – 237

Majidzadeh, K.; Khedr, S.; EI-Mojarrush, M.; (1978) Evaluation of permanent deformation in asphalt concrete pavements (Transportation Research Record, Transportation Research Board, pp. 21–31). Washington, DC.

Maree, J.H.; (1978) Ontwerpparameters vir Klipslag in Plaveisels. (Design Aspects for Crushed Stone in Pavements). M Eng. Thesis, University of Pretoria, Republic of South Africa.

Maree, J. H., Van Zyl, N. J. W., and Freeme, C. R. (1981). "Effective Moduli and Stress Dependence of Pavement Materials as Measured in Some Heavy-Vehicle Simulator Tests." Transportation Research Record, 852, 52-60

Maree, J. H.; Freeme, C. R.; Van Zyl, N. J.; Savage, P. F.; (1982) ''The permanent deformation of pavements with untreated crushed stone bases as measured in heavy vehicle simulator tests.'' Proc., 11th ARRB Conf., Part 2, 16–28.

Marek, C. R.; (1977) ''Compaction of graded aggregate bases and subbases.'' Transp. Engrg. J. of ASCE, 103(1), 103–113.

Masad, E.; Tashman, L.; Somedavan, N.; Little, D.; (2002) Micromechanics-based analysis of stiffness anisotropy in asphalt mixtures. Journal of Materials in Civil Engineering. 14(5):374-383.

Mathew, T. V.; Rao K. K.; (2009) Introduction to transportation engineering. pp. 27.1–8 (National Programme on Technology Enhanced Learning, India, May, 2009, chapter 27)

May, R. W., and Witczak, M. W. (1981). ''Effective granular modulus to model pavement responses.'' Transp. Res. Rec. 810, Transportation Research Board, Washington, D.C., 1–9.

McLean, V., and Lytton, R. L.; (1993) "Development and validation of performance prediction models and specifications for asphalt binders and paving mixes." SHRP-A-357, Strategic Highway Research Program, Washington, DC.

Metcalf, J. B., Romanoschi, S. A., Li, Y., Rasoulian, M. (1999). The first full-scale accelerated pavement test in Louisiana: Developments and findings. Minnesota DoT.

Metcalf, J. B. NCHRP Synthesis of Highway Practice 235. (1996). Application of Full-Scale Accelerated Pavement Testing. TRB, National Research Council, Washington D.C.

Mitchell, M. F., and Walker, R. N. (1985) "The economics of pavement type selection." Proc., 3rd international conference on concrete pavement design and rehabilitation

Mirzahosseini, M.; Aghaeifar, A.; Alavi, A.; Gandomi, A.; Seyednour, R.; (2011) Permanent deformation analysis of asphalt mixtures using soft computing techniques, Expert Syst. Appl. 38 (5); 6081–6100

Moavenzadeh, F.; Carnaghi, R.; (1966) Viscoelastic response of sand asphalt beams on elastic foundations under repeated loading, Proc. Assoc. Asphalt Pour. Technol. 35; 514–528.

Moghaddam, T.B.; Soltani, M.; Karim, M.R.; (2014) Evaluation of permanent deformation characteristics of unmodified and Polyethylene Terephthalate modified asphalt mixtures using dynamic creep test, Mater. Design 53; 317–324.

Monismith, C.L.; Secor, K.E.; (1962) Viscoelastic behavior of asphalt concrete pavements, in: International Conference on the Structural Design of Asphalt Pavements, vol. 203

Monismith, C. L., Seed, H. B., Mitry, F. G., and Chan, C. K. (1967). ‘‘Prediction of pavement deflections from laboratory tests.’’ Proc., 2nd Int. Conf. Struct. Des. of Asphalt Pavements, 109–140.

Monismith, C.L.; Ogawa, N.; Freeme, C.R.; (1975) Permanent deformation characteristics of subgrade soils due to repeated loading, Transport. Res. Rec. 537.

Monismith, C.L.; Inkabi, K.; Freeme, C.; McLean, D.; (1977) A subsystem to predict rutting in asphalt concrete pavement structures, in: Volume I of proceedings of 4th International Conference on Structural Design of Asphalt Pavements, Ann Arbor, Michigan, August 22–26,

Monismith, C. L.; Hicks, R. G.; Finn, F. N.; Sousa, J.; Harvey, J.; Weissman, S.; Paulsen, G.; (1994) Permanent deformation response of asphalt

aggregate mixes (SHRP-A-415, Asphalt Research Program Institute of Transportation Studies, pp. 313–334). Berkeley: University of California

Morgan, J. R. (1966). "The response of granular materials to repeated loading." Australian Road Research Board Proc.

Motola Y, Uzan J. (2007). Anisotropy of field-compacted asphalt concrete material. Journal of Testing and Evaluation. 35(1):1-3.

Morris, J.; Haas, R.; Reilly, P.; Hignell, E.; (1974) Permanent deformation in asphalt pavements can be predicted, in: Proc. AAPT, vol. 43.

MOU, C.H and CHU, T.Y. (1981), 'Soil-suction approach for evaluation of swelling potential'. Transport Research Record 790

Mukhtar, M. T., Dempsey, B. J.; (1996) "Interlayer stress absorbing composite for mitigating reflective cracking in asphalt concrete overlays," *Transportation Engineering Series*, No. 94, University of Illinois at Urbana-Champaign, Urbana, IL.

Nahi, M.H., Kamaruddin, K., Ismail, A., Al-Ezzi Al-Mansob, R.; (2014) Finite Element Model for Rutting Prediction in Asphalt Mixes in Various Air Void Contents, Journal of Applied Sciences, Volume 14 (21): 2730-2737

Nataatmadja, A., and Parkin, A. K. (1989). ''Characterization of granular materials for pavements.'' Can. Geotech. J., Ottawa, 26, 725–730

Nataatmadja, A. (1992). ''Resilient modulus of granular materials under repeated loading.'' Proc., 7th Int. Conf. on Asphalt Pavements, Vol. 1, 172–185.

Nazarian, S., Baker, M.R., and Crain, K., (1993). Development and testing of a seismic pavement analyzer. Report, Strategic Highway Research Program, National Academy of Sciences

NCHRP, (2008). NCHRP synthesis 381: falling weight Deflectometer usage. Washington, DC: U.S. Department of the Interior

NCHRP, (2002). Recommended standard method for routine resilient modulus testing of unbound granular base/subbase materials and subgrade soils, protocol 1-28a. National Cooperative Highway Research Program, Washington, DC

Nesnas, K., Nunn, M.; (2004) "A model for top-down reflection cracking in composite pavements," *Proceedings of the 5th International RILEM Conference–Cracking in Pavements*: *Mitigation, Risk Assessment, and Preservation*, (C. Petit, I. L. Al-Qadi, and A. Millien, eds.), Limoges, France; 409 – 416

Nguyen, A.D., Hachemi, A., Weichert, D.; (2008) Application of the interior-point method to shakedown analysis of pavements. Int J Numer Methods Eng; 75(4):414–39.

Nunn, M.; (1986) Prediction of permanent deformation in bituminous pavement layers, in: Transport and Road Research Laboratory (TRRL), RESEARCH REPORT 26

Nunn M. E.; (1989) "An investigation into reflection cracking in composite pavement," *Proceedings of RILEM Conference on Reflective Cracking in Pavements*, (R. Degeimbre, L. Francken, and J. M. Rigo, eds.), Liege, Belgium.

Nur Hossain, E.I., Singh, D., Zaman, M.; (2013) Dynamic Modulus-based Field Rut Prediction Model from an Instrumented Pavement Section, Procedia - Social and Behavioral Sciences; 104; 129-138

Oscarsson, E.; (2011) Evaluation of the Mechanistic-Empirical Pavement Design Guide model for permanent deformations in asphalt concrete, Int. J. Pavement Eng. 12 (1); 1–12

Pagen, C.A.; (1972) Dynamic structural properties of asphalt pavement mixtures, in: Intl Conf Structural Design Proc, vol. 1.

"Pavements Constructed with Processed (Graded) Crushed Stone (Aggregate) Bases on Stabilized Subbases," (video script), South African Roads Board, (1998).

Papadopoulos, E.; Santamarina, J.C.; (2016) Analysis of inverted base pavements with thin-asphalt layers, International Journal of Pavement Engineering, 17:7, 590-601

Papadopoulos, E. and Santamarina, J.C., (2015). Analysis of inverted base pavements with thin asphalt layers. International Journal of Pavement Engineering. Online published. doi:10.1080/10298436.2015.1007232.

Papadopoulos, E. and Santamarina, J.C., (2014). Optimization of inverted base pavement designs with thin asphalt surfacing. In: Geo-congress 2014 technical papers. Atlanta, GA: ASCE, 2996–3004.

Pappin, J. W.; (1979) ''Characteristics of granular material for pavement analysis,'' PhD thesis, Dept. of Civ. Engrg., University of Nottingham, Nottingham, England.

Park, D.W.; Seo, W.J.; Kim, J.; Vo, H.V.; (2017) Evaluation of moisture susceptibility of asphalt mixture using liquid anti-stripping agents, Constr. Build. Mater. 144; 399–405.

Paute, J. L.; Hornych, P.; Benaben, J. P.; (1996) ''Repeated load triaxial testing of granular materials in the French network of Laboratoires des Ponts et Chausse´es.'' Flexible Pavements, Proc., Eur. Symp. Euroflex 1993, A. G. Correia, ed., Balkema, Rotterdam, The Netherlands, 53–64.

Pavement Preservation Technology in France, South Africa, and Australia. International Technology Exchange Program. Publication No. FHWA-PL-03-001, FHWA, U.S. Department of Transportation, October 2002.

Pavements Constructed with Processed (Graded) Crushed Stone (Aggregate) Bases on Stabilized Subbases, (video script), South African Roads Board, 1998.

Pérez, I., Gallego, J.; (2010) Rutting prediction of a granular material for base layers of low-traffic roads, Constr. Build. Mater. 24; 340–345

Pezo, R. F. (1993). ''A general method of reporting resilient modulus tests of soils—A pavement engineer's point of view.'' 72nd Annual Meeting of the TRB.

Puppala, A.J., (2008). Estimating stiffness of subgrade and unbound materials for pavement design. Washington, DC: Transportation Research Board

Rahman M.S., Erlingsson, S.; (2015) Predicting permanent deformation behaviour of unbound granular materials, International Journal of Pavement Engineering; 16(7); 587-601

Rahman M.S., Erlingsson, S.; (2015) Moisture influence on the resilient deformation behaviour of unbound granular materials, International Journal of Pavement Engineering. DOI: 10.1080/10298436.2015.1019497

Rahman M.S., Erlingsson, S.; (2016) Modelling the Moisture Dependent Permanent Deformation Behavior of Unbound Granular Materials, Advances in Transportation Geotechnics 3. The 3rd International Conference on Transportation Geotechnics (ICTG 2016), published in Procedia Engineering; 143; 921–928

Rasoulian, M. (2004). Stone Interlayer Pavements. Presentation at Louisiana Pavement Conference.

Rasoulian, M., Becnel, B., and Keel, G. (2000). "Stone interlayer pavement design." Transportation Research Record, 1709, 60-68.

Rauhut, J. B.; (1980) Permanent deformation characterization of bituminous mixtures for pavement rutting predictions (Transportation Research Record 777, Transportation Research Board). Washington, DC: National Research Council.

Raymond, G. P.; Williams, D. R.; (1978) ‘‘Repeated load triaxial tests on a dolomite ballast.’’ J. Geotech. Engrg. Div., ASCE, 104(7), 1013–1029.

Roesler, S.K., (1979). Anisotropic shear modulus due to stress anisotropy. Journal of the Geotechnical Engineering Division, 105 (7), 871–880.

Romain, J.; (1972) Rut depth prediction in asphalt pavements, in: Presented at the Third International Conference on the Structural Design of Asphalt Pavements, Grosvenor House, Park Lane, London, England, Sept. 11–15, vol. 1,

Rushing, J.; Little, D.; (2014) Static Creep and Repeated Load as Rutting Performance Tests for Airport HMA Mix Design, J. Mater. Civ. Eng. 26 (9); 04014055.

RUSSELL, E.R. and MICKLE, J.L. (1970), 'Liquid limit by soil moisture tension', Proc. ASCE, Vol 96, SM3

Rust, F.C., J.P. Mahoney and J.B. Sorenson, An International View of Pavement Engineering, Bearing Capacity of Roads and Airfields Conference, Trondheim, Norway, 1998.

Saberian, M., Li, J.; (2019) Long-term permanent deformation behaviour of recycled concrete aggregate with addition of crumb rubber in base and sub-base applications, Soil Dynamics and Earthquake Engineering; 121; 436–441

Saberian, M., Li, J., Setunge, S.; (2019) Evaluation of permanent deformation of a new pavement base and subbase containing unbound granular materials, crumb rubber and crushed glass, Journal of Cleaner Production; 230; 38-45

Sadrossadat, E., Ghorbani, B., Oskooei, P.R., Sheikhkanloo, M.H.M.; (2018) A New Model for Estimating the Resilient Modulus of Silt-Clay Subgrade Soils, International Conference of Modern Research in Civil Engineering, Architecture, Urban Management and Environment At Karaj, Iran

SANRA (1998), High Performance Crushed Stone Based (G1) Used on South African Highways, South African National Roads Agency (SANRA), Pretoria, South Africa, October 1998.

Santamarina, J.C. and Cascante, G., (1996). Stress anisotropy and wave propagation: A micromechanical view. Canadian Geotechnical Journal, 33 (5), 770–782.

Schuettpelz, C.C., Fratta, D., Edil, T.B., (2010). Mechanistic corrections for determining the resilient modulus of base course materials based on elastic wave measurements. Journal of Geotechnical and Geo-environmental Engineering, 136 (8), 1086–1094.

Seed, H. B., Mitry, F. G., Monismith, C. L., and Chan, C. K. (1967). "Prediction of flexible pavement deflections from laboratory repeated load tests." NCHRP Rep. No. 35, National Cooperative Highway Research Program.

Seyhan, U., Tutumluer, E., and Yesilyurt, H. (2005). "Anisotropic aggregate base inputs for mechanistic pavement analysis considering effects of moving wheel loads." ASCE Journal of Materials in Civil Engineering, Vol. 17, No. 5, October, 505-512.

Seyhan, U.; Tutumluer, E. (2002). Anisotropic Modular Ratios as Unbound Aggregate Performance Indicators. Journal of Materials in Civil Engineering. 14(5): 409-416

Sha, Q. L.; (1993) "Two kinds of mechanism of reflective cracking, reflective Cracking in pavements: state of the art and design recommendations," *Proceedings of the Second International RILEM Conference–Reflective Cracking in Pavements: State of the Art and Design Recommendations*, (J. M. Rigo, R. Degeimbre, and L. Francken, eds.), Liege, Belgium; 441 – 448.

SHACKEL, B. (1973), 'Changes in soil suction in a sand-clay subjected to repeated triaxial loading', Highway Research Record No. 429.

Shafabakhsh, G.H., Ani, O.J., Talebsafa, M.; (2015) Artificial neural network modelling (ANN) for predicting ruttingperformance of nano-modified hot-mix asphalt mixtures containingsteel slag aggregates, Construction and Building Materials; 85; 136-143

Sharp, R; Booker, J.; (1984) Shakedown of pavements under moving surface loads. Journal of Transportation Engineering, 110 (1), 1–14.

Sharp, R.; (1985) Pavement design based on shakedown analysis. Transport Research Record: Journal of the Transportation Research Board, 1022, 99–107.

Shell Pavement Design Manual—Asphalt Pavements and Overlays for Road Traffic. Shell International Petroleum Company Limited, London, England, 1978.

Simpson, A.L., Daleiden, J.F., Hadley, W.O.; (1995) Rutting Analysis from a Different Perspective, Transportation Research Record; 1473

Siripun, K., Jitsangiam, P., Nikraz, H.; (2010) Permanent deformation behaviour and model of crushed rock base. Aust J Civil Eng;8 (1)

SNETHEN, D.R. and JOHNSON, L.D. (1977), 'Characterisation of expansive soil subgrades using soil suction data', U.S. Army Engineer, Waterways Experiment Station, Vicksburg, Mississippi. Conf of TRB Comm. A2L06.

Song, S. H.; (2006) "Fracture of asphalt concrete: a cohesive zone modeling approach considering viscoelastic effects," *Ph.D. Dissertation*, University of Illinois at Urbana- Champaign, Urbana, IL.

Song, S. H., Paulino, G. H., Buttlar, W. G. (2006). "A bilinear cohesive zone model tailored for fracture of asphalt concrete considering viscoelastic bulk material," *Engineering Fracture Mechanics*; 73 (18); 2829–2849

Sousa, J.B.; Craus, J.; and Monismith, C.L. (1991), Summary report on permanent deformation in asphalt concrete, SHRP-A/lr-91 104.

Sweere, G. T. H.; (1990) "Unbound granular bases for roads," PhD thesis, University of Delft, Delft, The Netherlands.

Tam, W. A., and Brown, S. F. (1988). "Use of the falling weight deflectometer for in situ evaluation of granular materials in pavements." Proc., 14th ARRB Conf., Vol. 14, Part 5, 155–163.

Tao, M.; Mohammad, L.N.; Nazzal, M. D.; Zhang, Z.; (2010) Application of shakedown theory in characterizing traditional and recycled pavement base materials. Journal of Transportation Engineering, 136 (3), 214–222.

Tapkın, S., Cßevik, A., Usßar, U.; (2009) Accumulated strain prediction of polypropylene modified Marshall Specimens in repeated creep test using artificial neural networks, Expert Systems with Applications, 36; 11186-11197

Tarefder, R.A.; (2003) Laboratory and model prediction of permanent deformation in asphalt concrete Ph.D. thesis, University of Oklahoma

Tarefder, R.A.; Zaman, M.; Hobson, K.; (2003) A laboratory and statistical evaluation of factors affecting rutting, Int. J. Pavement Eng. 4 (1); 59–68.

Tarefder, R.A.; Ahmed, M.U.; Rahman, A.; (2016). Effects of cross-anisotropy and stress-dependency of pavement layers on pavement responses under dynamic truck loading. Journal of Rock Mechanics and Geotechnical Engineering. 8:366-377.

Technical Recommendations for Highways (TRH) 4, Department of Transport, Republic of South Africa, Pretoria, South Africa, 1996.

Terrell, R. G., Cox, B. R., Stokoe, K. H., Allen, J. J., and Lewis, D. (2003). "Field evaluation of the stiffness of unbound aggregate base layers in inverted flexible pavements." *Transportation Research Record*, 1837(2003), 50-60.

Theyse, H.L., M. de Beer, F.C. Rust, Overview of the South African Mechanistic Pavement Design Analysis Method. Transportation Research Record: Flexible Pavement Design and Rehabilitation Issues, No. 1539, Transportation Research Board of the National Academies, Washington, D.C., 1996, pp. 6-17.

Theyse, H.; (2000) The development of mechanistic-empirical permanent deformation design models for unbound pavement materials from laboratory and accelerated pavement test data, UNBAR 5; 285–293

Theyse, H. L.; (2002) "Stiffness, strength, and performance of unbound aggregate materials: application of South African HVS and laboratory results to California flexible pavements." Report produced under the auspices of the California Partnered Pavement Research Program for the California Department of Transportation. University of California, 76

Tholen, O.; (1980) Falling weight deflectometer: a device for bearing capacity measurements: properties and performance. Stockholm: Department of Highway Engineering, Royal Institute of Technology (KTH). Degree project

Thom, N. H. (2014), Principles of Pavement Engineering, 2nd Edition.

Thom, N. H.; Brown, S. F.; (1987) ‘‘Effect of moisture on the structural performance of a crushed-limestone road base.’’ Transp. Res. Rec. 1121, Transportation Research Board, Washington, D.C., 50–56

Thom, N. H.; (1988) ‘‘Design of road foundations,’’ PhD thesis, Dept. of Civ. Engrg., University of Nottingham, Nottingham, England.

Thom, N. H.; Brown, S. F.; (1988) ‘‘The effect of grading and density on the mechanical properties of a crushed dolomitic limestone.’’ Proc., 14th ARRB Conf., Part 7, 94–100

Thom, N. H.; Dawson, A.R.; (1996) The permanent deformation of a granular material modelled using hollow cylinder testing. Flexible Pavements, Gomes Correia (ed.). 1996 Balkema, Rotterdam

Thompson, M. R.; Elliott, R.P.; (1985) ILLI-PAVE-Based Response Algorithms for Design of Conventional Flexible Pavements. In

Transportation Research Record 1043, TRB, National Research Council, Washington, D.C., pp. 50–57.

Thrower, E.; (1977) Methods of predicting deformation in road pavements, in: Volume I of proceedings of 4th International Conference on Structural Design of Asphalt Pavements, Ann Arbor, Michigan, August 22–26

Titi, H., Rasoulian, M., Martinez, M., Becnel, B., and Keel, G. (2003). "Long-term performance of stone interlayer pavement." *Journal of Transportation Engineering*, 129(2), 118-126.

Tseng, K.H., Lytton, R.L.; (1989) Prediction of permanent deformation in flexible pavement materials. In: H.G. Schrauders and C.R. Marek, eds. Implication of aggregates in design, construction, and performance of flexible pavements. Philadelphia, PA: American Society for Testing and Materials, 154–172. ASTM STP 1016

Tutumluer, E.; Thompson, M.R.; "Anisotropic Modeling of Granular Bases in Flexible Pavements" Paper No. 970539, Transportation Research Record: 1577

Tutumluer, E. (1995) Predicting Behavior of Flexible Pavements with Granular Bases. Ph.D. dissertation. School of Civil and Environmental Engineering, Georgia Institute of Technology, Atlanta,

Uthus, L.; (2007) Deformation Properties of Unbound Granular Aggregates. Thesis (PhD). Norwegian University of Science and Technology, Trondheim.

Uzan, J.; (1983) Prediction of rut depth performance in flexible highway pavements. Association of asphalt paving technologists proceedings, Association of Asphalt Paving Technologists, Netherlands, pp. 489–507.

Uzan, J.; (2004) Permanent deformation in flexible pavements. Journal of Transportation Engineering, 130 (1), 6–13.

Van de Loo, P. J.; (1976) A practical approach to the prediction of rutting in asphalt pavements-the SHELL method (Transportation Research Record 616, Transportation Research Record, pp. 15–21). Washington, DC.

Von Quintus, H.L.; (1994) Performance Prediction Models in the Superpave Mix Design System, vol. 699, Strategic Highway Research Program, National Research Council, Washington, DC, USA.

Von Quintus, H. L.; Mallela, J.; Bonaquist, R.; Schwartz, C. W.; Carvalho, R. L.; (2012) Calibration of rutting models for structural and mix design (NCHRP Report 719, Transportation Research Record). Washington, DC

Wang, J., Yu, H.S.; (2013) Shakedown analysis and design of layered road pavements under three-dimensional moving surface loads. Road Mater Pavements Des; 14: 703–22.

Wang, Y., Lu, Y.J., Si, C.D., Sun, T.C.; (2017) Finite Element Analysis for Rutting Prediction of Asphalt Concrete Pavement under Moving Wheel Load, Int j simul model, 16 (2); 229-240

Weingart, R., Inverted Pavements: Virginia Experience, AFTRE Webinar Presentation, National Stone, Sand and Gravel Association (NSSGA), June 1, 2010.

Werkmeister, S.; Dawson, A.R.; Wellner, F.; (2001) Permanent deformation behavior of granular materials and the shakedown concept. Transport Research Record: Journal of the Transportation Research Board, 1757, 75–81.

Werkmeister, S.; Dawson, A.R.; Wellner, F.; (2004) Pavement design model for unbound granular materials. Journal of Transportation Engineering, 130 (5), 665–674.

Werkmeister, S.; (2006) Shakedown analysis of unbound granular materials using accelerated pavement test results from New Zealand's CAPTIF facility. Pavement Mechanics and Performance, 154, 220–228.

Whiffin, A. C.; Lister, N. W.; (1962) The application of elastic theory to flexible pavements. Proceedings of the first international conference on the structural design of asphalt pavements, Ann Arbor, MI, pp. 499–521.

Wijeratne, A.; Sargious, M.; (1987) Prediction of rutting in virgin and recycled asphalt mixtures for pavement using triaxial tests. Association of asphalt paving technologists proceedings, Association of Asphalt Paving Technologists, USA, pp. 111–129

Witzcak, M.W.; (2002) Simple Performance Test for Superpave Mix Design, National Academy Press, Washington, D.C.

Wolff, H.; (1992) Elasto-plastic behavior of granular pavement layers in South Africa (Ph.D. Thesis), University of Pretoria, South Africa

Wolff, H., Visser, A.T.; (1994) Incorporating elasto-plasticity in granular layer pavement design. In: Proceedings of the Institution of Civil Engineers Transport, vol. 105; 259–72.

Wood, D.M.; (1990) Soil behaviour and critical state soil mechanics. Cambridge: Cambridge University Press.

Xie, J., Li, H., Gao, L., Liu, M.; (2017) Laboratory investigation of rutting performance for multilayer pavement with fiber Bragg gratings, Construction and Building Materials, 154; 331-339

Ye, Y.; Yang, X.; Chen, C.; (2009) Experimental researches on visco-elastoplastic constitutive model of asphalt mastic, Constr. Build. Mater. 23; 3161–3165.

Yildirim, Y., Jayawickrama, P.W., Hossain, M.S., Alhabshi, A., Yildirim, C., Smit, A.F., Little, D., (2007) Hamburg Wheel Tracking Database Analysis, Texas Department of Transportation, Austin, Texas, FHWA/TX-05/0-1707-7.

Youd, T. L.; (1972) ‘‘Compaction of sands by repeated shear straining.’’ J. Soil Mech. and Found. Div., ASCE, 98(7), 709–725.

Yu, H.S., Hossain, M.Z.; (1998) Lower bound shakedown analysis of layered pavements using discontinuous stress fields. Comput Method Appl Mech Eng; 167: 209–22.

Zarka, J., Casier, J.; (1979) Elastic plastic response of structure to cyclic loading: practical rules. Mech Today; 6: 93–198.

Zeng, G.; Yang, X.; Bai, F.; Gao, H.; (2014) Visco-elastoplastic damage constitutive model for compressed asphalt mastic, J. Cent. South Univ. 21; 4007–4013

Zhang, D. L.; Li, J.; (1995) Prediction of rutting in asphalt pavement. China Journal of Highway and Transport, 8(1), 23–29.

Zhang, J.; Pei, J.; Zhang, Z.; (2012) Development and validation of viscoelastic-damage model for three-phase permanent deformation of dense asphalt mixture, J. Mater. Civ. Eng. 24 (7); 842–850.

Zhang, J.; Fan, Z.; Fang, K.; Pei, J.; Xu, L.; (2016) Development and validation of nonlinear viscoelastic damage (NLVED) model for three-stage permanent deformation of asphalt concrete, Constr. Build. Mater. 102; 384–392

Zhao, J., Sloan, S.W., Lyamin, A.V., Krabbenhoft, K.; (2008) Bounds for shakedown of cohesive frictional materials under moving surface loads. Int J Solids Struct; 45(11): 3290–312.

Zhao, Y., Zhang, J., (2009) A mechanical model for three-phase permanent deformation of asphalt mixture under repeated load, J. Wuhan Univ. Technol. 24; 1001–1003.

Zheng, N. X.; Niu, S. S.; Xu, X. Q.; (2009) Temperature, axle load and axle load frequency model of rutting prediction of heavy-duty asphalt pavement. China Journal of Highway and Transport, 22(3), 7–13.

Zhou, F., Sun, L.; (2002) "Reflective cracking in asphalt overlay on existing PCC," *Proceedings of the 9th International Conference on Asphalt Pavements* (CD-ROM), Copenhagen, Denmark.

Zhou, F., Scullion, T.; (2005) "Overlay tester: a simple performance test for thermal reflective cracking," *Journal of the Association of Asphalt Paving Technologists*. Vol. 74, pp. 443 – 484

Zhu, L.y.; Fwa, P.T.; (2006) Rutting potential evaluation of asphalt mixtures by repeated-load creep test, Int. J. Highway Eng. 8 (3); 21–28.